K-625-65-1

FIRST QUARTERLY REPORT FOR MILLIMETER COMMUNICATION PROPAGATION PROGRAM

(1 NOV., 1964 - 1 FEB., 1965)

Contract No. NAS5-9523

Prepared by
RAYTHEON COMPANY
SPACE AND INFORMATION SYSTEMS DIVISION
Sudbury, Massachusetts

Raytheon Report No. FR-65-40

for

GODDARD SPACE FLIGHT CENTER
SPACECRAFT SYSTEMS AND PROJECTS DIVISION
COMMUNICATIONS SATELLITE RESEARCH BRANCH
Greenbelt, Maryland

RAYTHEON COMPANY
SPACE AND INFORMATION SYSTEMS DIVISION

K-625-65-1

First Quarterly Report

for

Millimeter Communication

Propagation Program

(1 Nov., 1964 - 1 Feb., 1965)

Contract No.: NAS5-9523

Prepared by

RAYTHEON COMPANY

SPACE AND INFORMATION SYSTEMS DIVISION

Sudbury, Massachusetts

Raytheon Report No. FR-65-40

for

GODDARD SPACE FLIGHT CENTER

SPACE CRAFT SYSTEMS AND PROJECTS DIVISION

COMMUNICATIONS SATELLITE RESEARCH BRANCH

Code 625

Greenbelt, Maryland

SUMMARY

This document is the first quarterly report for the Millimeter Communication Propagation Program being performed under Contract No. NAS5-9523 by Raytheon's Space and Information Systems Division for Goddard Space Flight Center. This program is an eight-month study to design experiments which will determine the effects of the propagating medium on millimeter-wave (10 to 100 gigacycles) space-earth communications.

This report describes the effects of the propagation medium as it is known today and recommends a one-year space-earth experiment program to be performed approximately within calendar year 1967. This program represents the best balance between quality and quantity of new scientific propagation data it will produce, degree of required development in instrumentation hardware, and utilization of existing experimental millimeter-wave ground facilities.

The main area of uncertainty relating to millimeter space-earth communication links is the influence of the condition of the media (rain, gases, temperature, wind, etc.) on millimeter wave propagation. A well controlled scientific one-year propagation experiment, using a medium altitude orbit satellite, is needed for an increased understanding of the various physical phenomena which occur and to develop meaningful statistics. Some millimeter-wave propagation data has been obtained from spectroscopic laboratory measurements, link measurements along the surface of the earth, vertical measurements with balloons, and measurements using aircraft. This data verifies, to some extent, the propagation theory which has been developed. However, no amount of extrapolition and interpolation of the available measured data will satisfactorily assess the impact of these variations on future space-earth communication channels. While reliable

absorption data for a specified water density profile along a communication path can be derived, there is not enough known about the variation in the profile itself during inclement weather. Furthermore, there is a lack of statistical knowledge on the effects of multipathing on flat frequency fading at low elevation angles, especially in bad weather. Finally, there is not enough known about the wideband selective frequency fading characteristics of the medium (i. e., what is the maximum coherent bandwidth that the medium will support?).

The proposed experiment is the next logical step in providing new information about millimeter propagation as it relates to space-earth channels. The recommended experiment is really a package of experimental links, certain combinations of which can be selected for final implementation.

The primary segment of the experiment consists of a 35 Gc transmitter in a 6000 mile altitude satellite. This transmitter radiates a simple amplitude modulated waveform which can be received by all or some combination of the existing millimeter wave ground facilities at Aerospace Corporation, University of Texas, Air Force Cambridge Research Labs, and Lincoln Laboratory, plus the facility planned for Goddard Space Flight Center. Each ground facility receiver would be equipped with identical signal processors and tape recorders to minimize data processing expense. Each receiver would share its RF head with a 35 Gc radiometer in order to make sensitive sky temperature measurements.

The second segment of the experiment employs a 94 Gc transmitter, presently being developed for the Aerospace Facility, which would transmit a amplitude modulated waveform to a 94 Gc receiver piggybacked upon the 35 Gc satellite transmitter. The signal processor in the receiver would function like those in the ground facilities except that the processed signals would be transmitted to earth via telemetry before being recorded. It should be noted that the Aerospace facility might be best instrumented by using a 6 foot

auxiliary dish to receive 35 Gc while the existing 16 foot antenna is transmitting 94 Gc. It should also be noted that all boresight installations at each of these ground facilities must be equipped, for calibration and check-out purposes, with the appropriate transmitters and/or receivers which function like those aboard the satellite.

Initially, a third portion of the experiment was under consideration which consisted of a dual reflector, variable base-length interferometer receiver configuration to receive the 35 Gc waveform transmitted from the satellite and measure phase and amplitude decorrelation as a function of distance. At present, however, it appears that the only requirement is to instrument a monopulse type dish configuration to measure wave front tilt and use the resulting data as the basis for design of a future interferometer type of experiment.

Well planned correlative measurements are essential to the propagation program in order to classify the particular weather model involved in each test and to explain why certain things are happening to the received test signals. In addition to basic meteorological surface measurements, sky temperature measurements with radiometers at 35 Gc and 94 Gc in the ground terminals are a necessity. Use of weather radar is being considered for one or more sites in order to provide a condensed water profile so that, in conjunction with the radiometer measurements, the attenuation attributed to water vapor can be identified. Under certain measurement conditions, ground terminal cloud cover photography and weather satellite infrared and optical data are expected to be of some value.

These millimeter experiments are designed to determine the effects of the propagation medium on space-earth channels. Of necessity, therefore, consideration for the water vapor and oxygen absorption regions around 22 Gc and 60 Gc have been excluded. The analytical portion of the study was based on four frequencies (16 Gc, 35 Gc, 70 Gc and 94 Gc) which were representative

of the atmospheric medium from 10 to 100 Gc. From these frequencies, the fundamental frequency for the experiment was chosen to be 35 Gc because it represents the useful atmospheric window between 22 Gc and 60 Gc bands. In addition, most of the ground facilities being considered are easiest to instrument with receivers at 35 Gc than at any other frequency. A down-link using a 35 Gc satellite transmitter was chosen principally because: instrumenting the ground facilities with transmitters is extremely difficult; simultaneous reception by several ground facilities can conserve payload resources; a closed loop between satellite and ground terminal is not needed for acquisition and tracking; and experiments using monopulse receiver configurations are possible.

The secondary frequency was chosen to be 94 Gc because it represents the useful atmospheric window above the 60 Gc band. Unfortunately, a down-link could not be recommended because of the risk in developing a spaceworthy transmitter of adequate power within a two year time period. The 94 Gc link was therefore conceived taking advantage of the 10 watt and possibly the 100 watt transmitters being developed for the Aerospace facility. The 94 Gc satellite receiver can be piggybacked upon the 35 Gc transmitter at small additional expense in payload weight, volume and prime power. Proper pointing of the Aerospace 94 Gc antenna can be confirmed with the 35 Gc auxiliary antenna.

A medium altitude satellite (typically 6000 nautical miles) is most desirable as the space platform for the experimental propagation link. The behavior of the millimeter channel with varying elevation angle is vitally important because the minimum useful horizon for a given radiated power, channel bandwidth and receiver sensitivity is a key factor in the design of profitable space-earth communications links whether they be employed in satellite communication systems or employed as spacecraft-to-earth data links. The angular elevation velocity of medium altitude satellites is slow enough to permit ample viewing time per pass with sufficient data samples

per degree of elevation. On the other hand, the elevation angular velocity is fast enough to complete a full elevation cycle profile before significant weather changes can occur. The altitude of this satellite is sufficiently high to permit simultaneous observation by many ground stations. It passes over a given ground station three or more times per day, permitting considerable flexibility in planning data collection schedules which are compatible with other mission schedules that may involve the satellite. The resulting propagation data from the medium altitude satellite can be directly applied or extrapolated to the design of communication systems using satellites at any altitude, even as low as 100 miles.

Within the next two years, synchronous stationary satellites may be the only satellites available for instrumenting suitable propagation experiments. Although it is felt that synchronous stationary satellites are less desirable as a space platform for basic scientific propagation experiments, a fresh look, from a slightly different set of ground rules, will be taken during the next quarter. Considerable operational expense is saved by not having to generate precise and timely ephemeris data for acquiring and tracking 6000 nautical mile satellites with narrow millimeter-wave beams. In addition, all of the existing millimeter-wave facilities will no longer require costly modifications to the present tracking equipment. The position of the satellite is critical in that the right combination of elevation angles from two or more existing ground stations may not be possible. Under these circumstances, it is reasonable to consider addition of inexpensive semi-fixed non-tracking antenna installations at locations, other than those of the existing millimeter facilities, to provide a suitable elevation angle profile for measuring signal fading statistics.

The basic measurement waveform to be transmitted is a simple one, that is, a carrier and one pair of AM sidebands, yet it will provide ample information on the propagation channel. Although other more sophisticated waveforms are discussed, these are left for use in future experiments which are based on the results of this initial experiment. A choice between an unmodulated

carrier and a modulated carrier will be provided with the modulating frequency being variable in several discrete steps up to at least 50 megacycles.

The experiment equipment design is conservative in order to guarantee complete ground instrumentation and a reliable payload within 18-24 months. It represents the minimum capability that can realistically be achieved within this time period and still justify the experiment in terms of the propagation data it will produce. As the equipment design phases progress throughout the remaining five months, it is expected that this minimum capability (presented in Section 7) can be exceeded. Since the launch date for a suitable satellite could be later than the first quarter of CY 1967, this basic experiment can be expanded accordingly as will be shown in succeeding quarterly reports.

BLANK PAGE

TABLE OF CONTENTS

CONTENTS (continued)

CONTENTS (continued)

CONTENTS (continued)

CONTENTS (continued)

CONTENTS (continued)

LIST OF ILLUSTRATIONS

ILLUSTRATIONS (continued)

ILLUSTRATIONS (continued)

ILLUSTRATIONS (continued)

ILLUSTRATIONS (continued)

ILLUSTRATIONS (continued)

LIST OF TABLES

TABLES (Continued)

1. INTRODUCTION

This document is the First Quarterly Report for the Millimeter Communication Propagation Program being performed under Contract No. NAS5-9523 by Raytheon's Space and Information Systems Division for Goddard Space Flight Center. This program is an eight month study to design experiments which will determine the effects of the propagating medium on millimeter wave space-earth communications.

The objective of this experiment design study is to design a series of carefully chosen experiments on a spacecraft availability and cost effectiveness basis which will show how the objectives of the experiment can be met. Wherever design problems cannot be solved, courses of action in the form of component tests and breadboard design will be recommended. This objective includes development of experiment cost estimates and time schedules, including that for data processing and analysis. Results of the study will also include equipment design, source of key components, definition of basic measurements and description of how these basic measurements can be used to meet the objectives of the experiment.

This quarterly document, which is a report of work accomplished during the period 1 November, 1964 to 1 February, 1965, describes the effects of the propagation media as they are known today and recommends a one-year space-earth experiment to be performed approximately within calendar year 1967. This basic experiment will provide new and useful qualitative and quantitative propagation data, yet the experimental equipment is of conservative design, thus insuring that operational dates can be met.

The recommended experiment design can be conveniently broken down into segments and experimental links, certain combinations of which can be chosen for implementation depending on the limitation of financial resources, urgency for the scientific information, and payload allocations aboard available satellites. Other follow-on experiments are discussed, but in much less detail since complete experiment formulation must await initial results of the first experiment.

Section 2 of this report, "Objectives of the Propagation Program", describes the objective of the propagation experiments and the general system applications for millimeter wave communications that are used as guidelines.

Section 3, "Propagation of Millimeter Waves", discusses the effects of water vapor and rain on absorption of millimeter waves, flat fading and selective frequency fading, time-bandwidth product, and antenna aperture limitations. A brief introduction to the effects of rain on antennas and radomes is given, plus a review of the satellite tracking problems due to atmospheric refraction. Also given in Section 3 is a review of available literature on propagation through a plasma, as a convenience to the reader interested in evaluating millimeter waves for communication with vehicles re-entering the earth's atmosphere.

For the basic signal measurements required, various waveforms are discussed from an analytical point of view in Section 4, "Definition of Basic Measurements."[1] It is explained how the basic measurements can be used to determine performance of various modulation systems. Also discussed are the correlative meteorological and radiometric measurements required to establish the condition of the atmosphere at the time the propagation measurements are made.

Section 5, "Formulation of Experiments", deals with candidate satellite evaluation, up-links versus down-links, signal level analysis and hardware implementation of waveforms.

Section 6, "Ground Facilities Evaluation", describes the capabilities and limitations of experimental millimeter facilities which are candidates for ground terminals in the propagation experiments. Weather descriptions are given for the geographical areas in which the ground terminals are located.

In Section 7, "Recommended Equipment for Experiments", the recommended experiment is defined in terms of block diagrams, and weight, volume and power estimates. The most significant work to be accomplished during the remaining five months of study is to: a) broaden the scope of material given in Section 4 of this quarterly report; b) design the experiment hardware needed to perform the experiment recommended in Section 7, as approved by GSFC; and c) define the data processing requirements for a one-year propagation data collection program. The details of work to be accomplished during the next quarter are given in Section 8.

Section 9 is a bibliography of reports referenced in the other sections of this report. A complete descriptive bibliography will be furnished in the next quarterly report.

The scope of work for this eight month study program was defined in Exhibit "A" of NASA Contract NAS5-9523 and supplemented by Raytheon Proposal, "A Millimeter Communication Propagation Program", BR-3011, 3 June 1964. Certain technical sections of the latter document are attached as appendices to the quarterly report to eliminate the need for the reader to have a copy of the proposal.

Another report which supplements Exhibit "A" of the NASA contract is "Program Definition Plan for Millimeter Communication Propagation Program", FR-4-498-B, January 29, 1965 (Revision of FR-4-498-A dated December 15, 1964). It defines the objectives of the program, lists the task to be performed, and describes the various work activities under each task, including their time relationships with one another.

2. OBJECTIVES OF STUDY

The objectives of the propagation experiments are to improve the scientist's understanding of the physical structure of the atmosphere as it relates to millimeter wave atmospheric absorption, flat frequency and selective frequency fading, channel time-bandwidth product, and aperture size limitations. Equally important are the objectives to provide the communication system designer with an engineering handbook which contains the necessary quantitative knowledge to accurately assess the effects of the propagating medium on millimeter wave space-earth communication channels in the 10 to 100 Gc frequency range. For a given frequency of operation, modulation scheme, meteorological profile and communication path, this millimeter wave propagation data handbook will allow one to determine: a) required effective radiated power and effective receiver sensitivity to achieve given nominal data transmission capacities; b) the signal fidelity or error rate probability of transmitted signals after propagation through the channel; and c) the reliability or percentage of time the quantities of a) and the qualities of b) can be expected to prevail.

The first and foremost incentive for determining the effects of the propagation medium on millimeter wave signals is to develop new communication bands to relieve the overcrowding of the lower frequency bands. Establishment of ten percent frequency bands for space-earth communications at 35 Gc and 94 Gc would represent an order of magnitude more capacity than all the lower frequency bands presently assigned. This increase in available bandwidth is necessary if future aerospace communication links are to handle the steadily increasing quantities of information which must be transmitted from space vehicles. Use of millimeter waves

is inevitable, the principal question being when. Propagation data is required to guide the development of millimeter wave component technology and to indicate to space communication planners when millimeter systems will be technically and economically competitive.

Another very important reason for learning more about millimeter wave propagation is the wide bandwidth offered by millimeter wave components. If the propagation medium does not severely limit the coherent bandwidth of signals transmitted through it, then real-time transmission of information from high altitude sophisticated space-borne sensors is possible. For low altitude spacecraft (100 to 300 miles altitude), where data acquisition time by a ground facility or aircraft is restricted to short intervals (2-10 minutes at each site two or three times per day), the wide bandwidth offers fast read-out of stored sensor data.

As the orbital altitude of the spacecraft decreases, effective utilization of millimeter waves becomes more dependent upon the effects of the propagation medium. The decreasing data acquisition time in number of satellite passes and in amount of time per pass forces one to consider foul weather operation at very low elevation angles. The increasing angular velocities of the space-earth communications path with respect to the ground station could further limit the channel time-bandwidth product under turbulent atmospheric conditions.

Turbulent atmospheric conditions, as well as antenna surface errors, seriously limit the maximum receiving aperture size, especially in the power-starved space-to-earth communication links. If suitable propagation data is available, it may be possible to design millimeter wave multiple reflector antenna systems which avoid the large reflector mechanical problems and automatically restore loss in antenna gain due to wavefront distortion from atmospheric inhomogeneities. These antenna arrays would

employ self-adaptive techniques which would compensate for random phase fluctuations.

Millimeter wave antennas with very narrow beams offer a certain degree of communication privacy in space-earth links at the expense of the antenna pointing problem. Other forms of privacy are offered by millimeter waves, but these involve the operation of space-space and space-aircraft data links in the 22 Gc water vapor and 60 Gc oxygen absorption regions. The propagation experiments being designed in this program do not support future applications in these regions.

A vehicle which re-enters the earth's atmosphere at hypersonic velocities becomes enveloped in an ionized plasma of compressed and heated air. This plasma severely attenuates communication to and from the vehicle, increases the effective noise temperature of the vehicle antenna thus degrading receiver sensitivity, and limits the amount of power that can be radiated from the vehicle. Because of the uncertanties in the plasma parameters for a typical re-entry condition, it is evident that the use of millimeter-wave signals holds considerable promise. This study is not directly related to the problem of propagating through a plasma; however, it must be pointed out that one must determine the effects of propagating through the atmosphere before an optimum re-entry communications frequency can be chosen which represents the best trade-off between plasma effects and propagation effects.

Potential applications of millimeter communications systems, especially space-earth systems, cannot be fully assessed until a basic propagation measurements program is performed.

In communication systems, where medium of synchronous altitude satellites are used to relay information from one point on the earth's

surface to another, several hardware areas also require concentrated attention. Directional millimeter wave satellite antennas are needed to provide increased receiving aperture and increased transmitting gain to overcome the penalties of atmospheric attenuation and fading. Likewise, more investigation into larger receiving apertures for the ground terminals are required. Unlike radio telescope antenna systems which operate only in good weather, the communications systems must have an all weather capability.

For all applications, of course, more stable, efficient and spaceworthy millimeter wave sources are required. For satellite communication systems, millimeter wave ground transmitters must be developed which are comparable in output power level to that of present lower frequency systems. Since radio telescopes have requirements for low noise receivers, it appears that this area of hardware technology has received attention for some time and therefore is not as critical as the other areas.

3. PROPAGATION OF MILLIMETER-WAVES

This section describes the effects of the propagating medium on millimeter wave transmission. It discusses the effects of water vapor and rain on absorption of millimeter waves and the effects of atmospheric turbulence on flat fading, selective frequency fading, coherent bandwidth, integration time limitations and antenna aperture limitations. A review of available literature is given on tracking errors due to atmospheric refraction effects, effects of rain on radomes and antennas, and the propagation of millimeter waves through plasma.

3.1 Atmospheric Attenuation

The typical atmospheric attenuation curves for water vapor, rain and oxygen are given in Appendix I. The purpose of this portion of the study was to determine how weather conditions might affect the design and conduct of the communication propagation experiments. Four possible sites were considered: Boston; Washington, D.C.; Austin, Texas; and Los Angeles. Computed values of apparent sky temperature and atmospheric transmission factors for the range of weather conditions expected at these four sites showed no significant variation between sites or for weather changes at a particular site. Based on the obvious factors of rainfall rate, temperature, and relative humidity, certain generalizations can be made about the design and conduct of the communication experiment. For example, measurements made during a one month period in the Boston area seem to give all the necessary data about atmospheric and weather effects. This portion of the study is continuing to determine whether there is a less obvious factor such as size and movement of bubbles or globs of air masses which could affect the experiment.

Basic data was obtained from the U.S. Weather Bureau (References 1 and 2) from which profiles of surface temperature, relative humidity, rainfall rates, and rainfall intensity/duration were generated. Some of

this data is tabulated in Table 3-I. Climatological summaries are given for each area in Section 4 under Geographical and Meterological Profiles. The water vapor content (ρ) data was obtained from equation (3-1).

$$\rho = \frac{2.17\, e \times 10^2}{T} \quad f, \text{ grams meter}^{-3} \qquad (3\text{-}1)$$

where

e is the saturated water vapor pressure in millibars from a standard Characteristic Diagram (Reference 3).

T is air temperature in ^{o}Kelvin, and

f is relative humidity in percent

Using the above weather data and a program for the Raytheon IBM-7044 digital computer (described in Appendix II), values of atmospheric transmission factor versus antenna zenith angle were computed for the four frequencies 16, 35, 70, and 94 Gc for the cases shown in Table 3-II. Standard meteorological lapse rates for temperature and pressure versus altitude were used.

This investigation was intended to cover a representative range of seasonal and diurnal conditions with more detailed calculations to be done after the first set was analyzed. It was discovered, upon analyzing the resulting data, that there was no significant variation, as can be seen from Table 3-III. The tabulated data is for an elevation angle of 60 degrees and is representative of data at other angles and other frequences.

The importance of this data is that it shows that there is no apparent effect on the design or conduct of the experiment due to weather differences between ground stations.

After completing the above calculations, consultation with Dr. David Atlas of AFCRL Weather Branch revealed that the weather model being used was not a realistic one. From the discussion with Dr. Atlas, and from studying one of his published papers (Reference 4), a revised weather model was developed.

Dr. Atlas and his associates have worked for years on the radar analysis of weather systems. As a result of this work they have developed curves which show how water vapor and rainfall rate vary with altitude.

TABLE 3-I

LOCAL WEATHER DATA FOR FOUR SITES

Weather Factor (3)	Boston	Washington, D.C.	Baltimore (1)	Los Angeles	Austin
Temperature (^{o}F)					
High	82	87	87	83	96
Low	23	30	30	46	40
Relative Humidity (%)					
High (2)	54	52	52	53	43
Low (2)	69	67	72	45	73
Annual Rain (inches)	42.8	40.8	44.2	14.7	32.6
Mean Days					
Clear	99	105	121	185	119
Partly Cloudy	106	105	123	107	113
Cloudy	160	155	121	73	133
Heavy Fog	24	14	15	17	23
Rain (4)	130	114	123	35	81
Sleet, Snow (5)	11	5	6	0	0
Thunderstorms	20	30	32	6	40
Water Vapor Content (g/m^3)					
High	11.5	19.1	18.8	14.7	18.8
Low	1.65	3.3	3.2	5.2	4.8

(1) Baltimore is included to help describe GSFC.
(2) Relative Humidity figures are associated with high and low temperature data. That is, high relative humidity number occurred at high temperature reading.
(3) All data based on 30 year records.
(4) Days on which .01 inch or more was recorded.
(5) Days on which 1.0 inch or more was recorded.

TABLE 3-II

WEATHER MODELS USED TO INVESTIGATE ATMOSPHERIC ATTENUATION

Case	Surface Temperature (°Kelvin)	Water Density (g/m^3)	Surface Pressure (millimeters)	Rainfall Rate (inches/hr)
1	265	1.65	760	0.22
2	302	18.0	760	0.22
3	288	5.5	760	0.22
4	294	8.25	760	0.22
5	299	11.5	760	0.22
6	286	9.6	760	0.16

TABLE 3-III

COMPARISON OF WEATHER EFFECTS ON ATMOSPHERIC TRANSMISSION FACTOR

Case	70 Gc			94 Gc		
	Clear	Cloud	Rain	Clear	Cloud	Rain
1	.509	.209	.109	.878	.184	.094
2	.560	.230	.120	.791	.166	.085
3	.560	.230	.120	.867	.182	.093
4	.565	.230	.121	.852	.179	.092
5	.570	.235	.122	.834	.175	.089
6	.550	.225	.124	.830	.174	.089

Their results are based on a dependence between updraft velocity and raindrop fall velocity and the moisture holding ability of the atmosphere at a given temperature and pressure. Based on their results and the surface conditions estimated for our work, the curves in Figure 3-1 were developed to serve as a revised weather model. The cloud condition represents a heavy cloud cover for a temperature zone area, and the rainfall rate corresponds to a surface rate of 0.2 inches per hour. The major difference between candidate ground stations is expected to be the number of days of heavy cloud cover and days of rain, as indicated in Table 3-I.

This revised weather model was incorporated into the computer program and Case 2 was computed again. The results of these calculations are given in Figure 3-2 through 3-5. Associated curves for apparent antenna temperature are given in Figures 3-6 through 3-9. (Note: $T_A = T_{S\phi}$ which is given in Equation II-3 in Appendix II). These data show the expected result that atmospheric attenuation increases with increasing

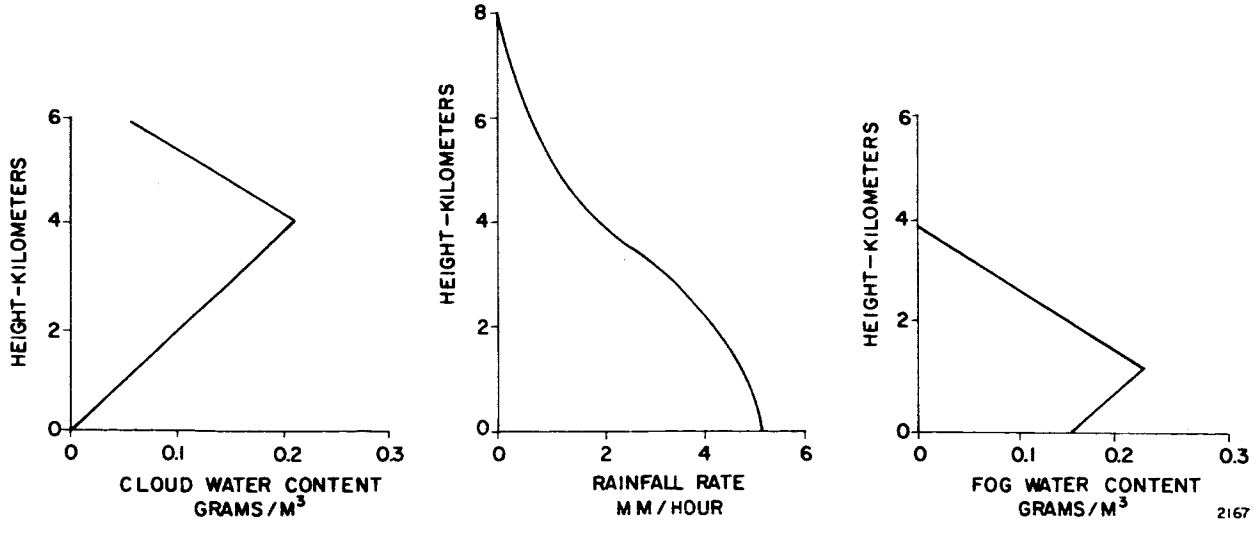

Figure 3-1 - Revised Weather Model

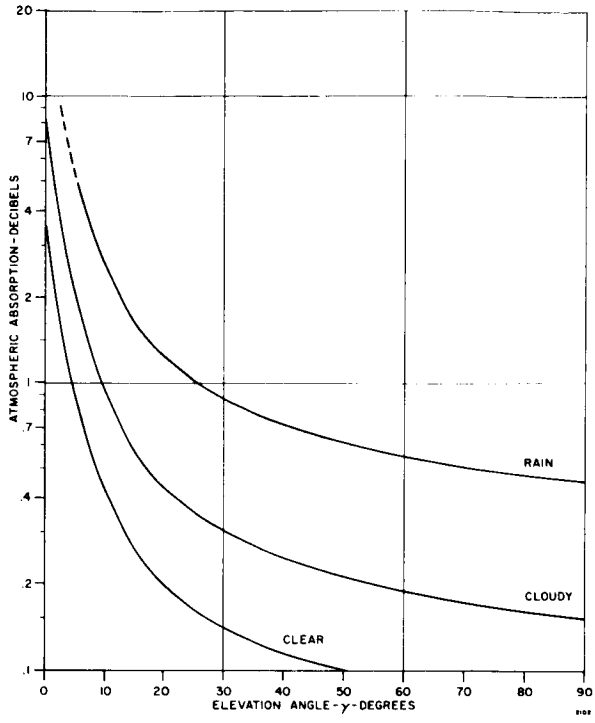

Figure 3-2 - Atmospheric Absorption at 16 Gc

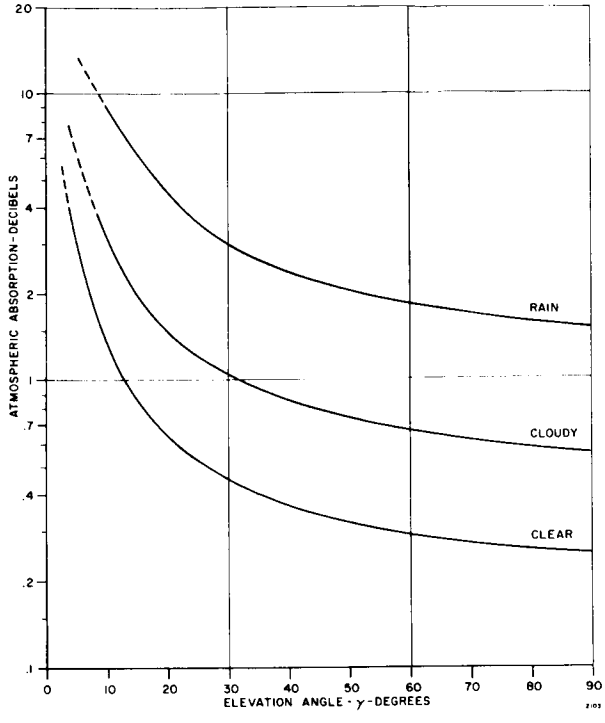

Figure 3-3 - Atmospheric Absorption at 35 Gc

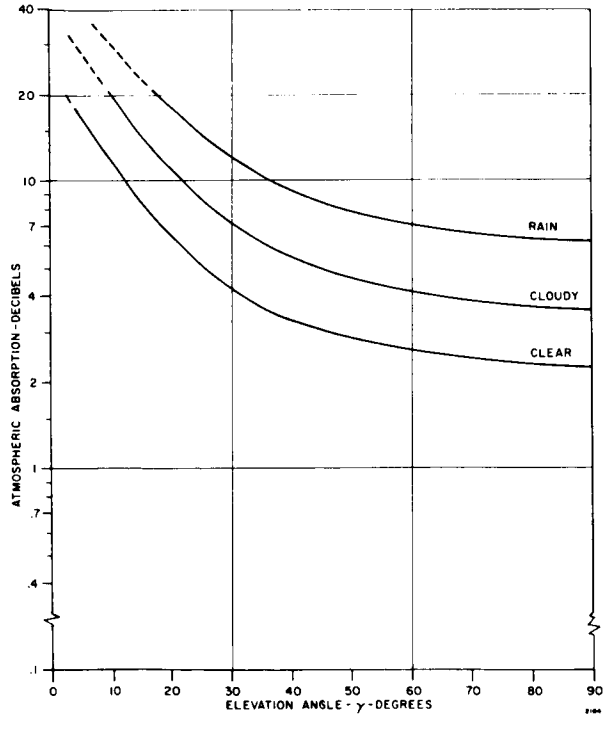

Figure 3-4 - Atmospheric Absorption at 70 Gc

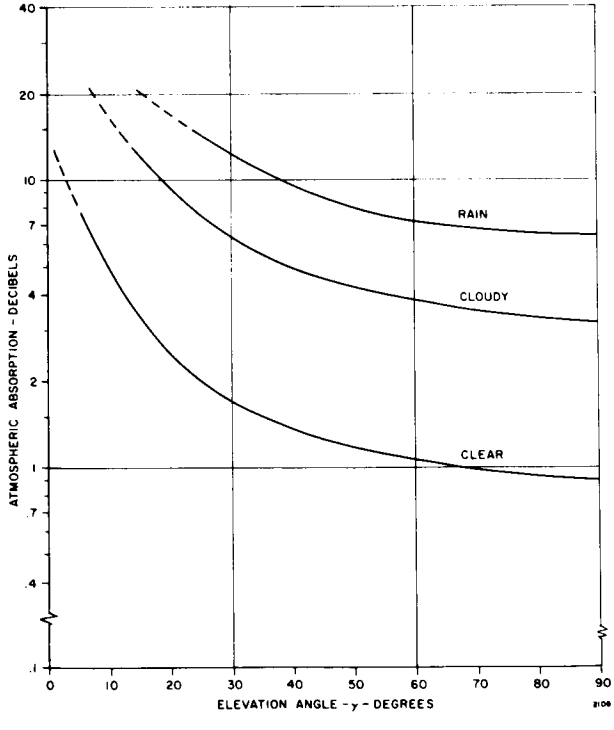

Figure 3-5 - Atmospheric Absorption at 94 Gc

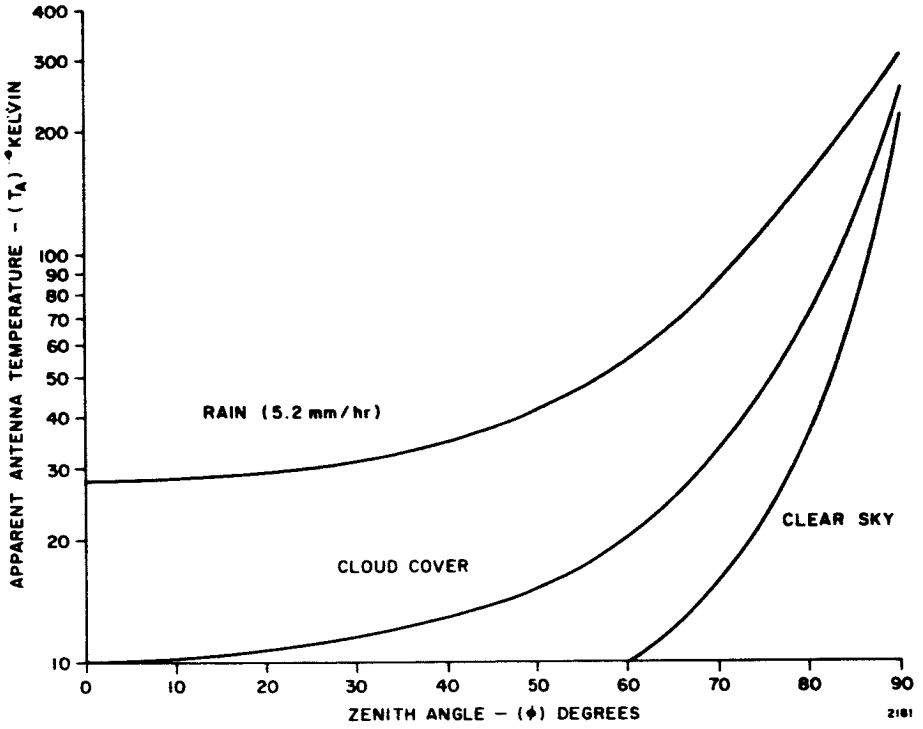

Figure 3-6 - Apparent Temperature of the Atmosphere at 16 Gc

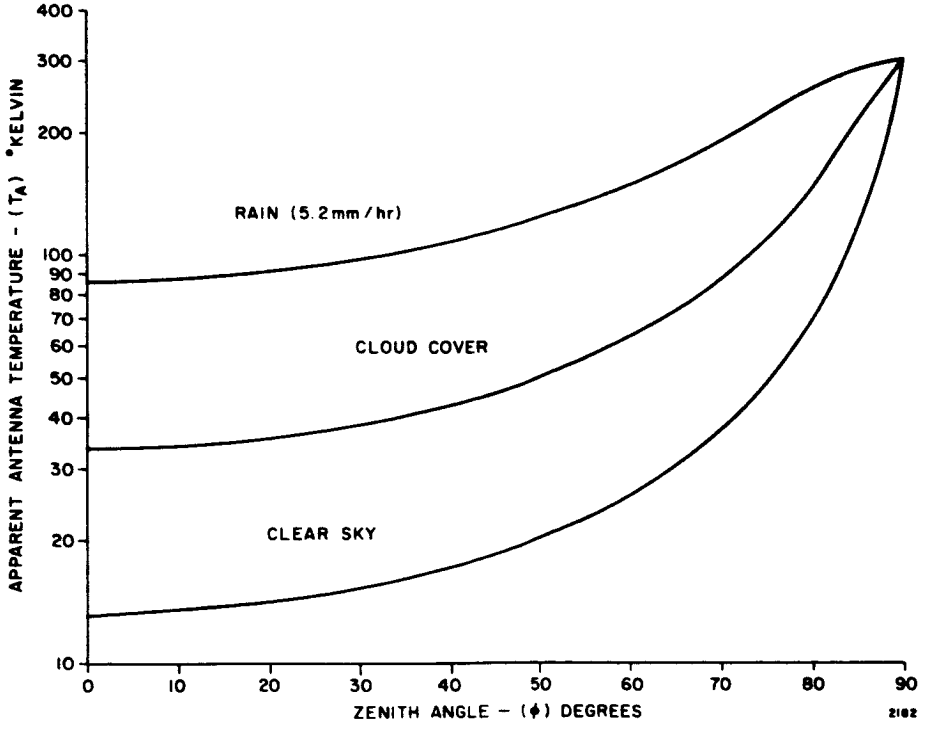

Figure 3-7 - Apparent Temperature of the Atmosphere at 35 Gc

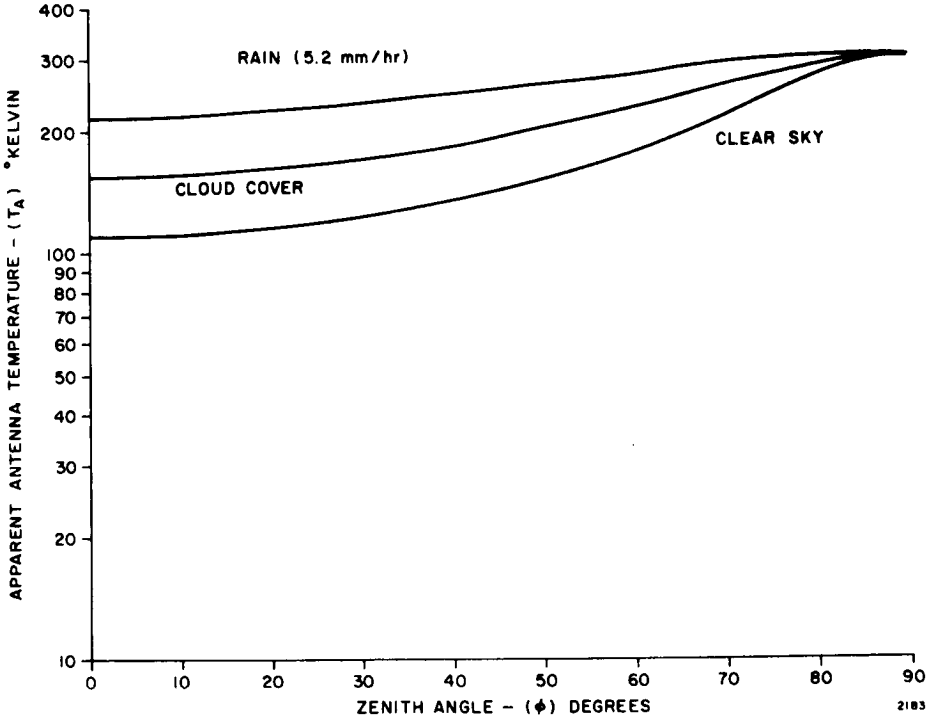

Figure 3-8 - Apparent Temperature of the Atmosphere at 70 Gc

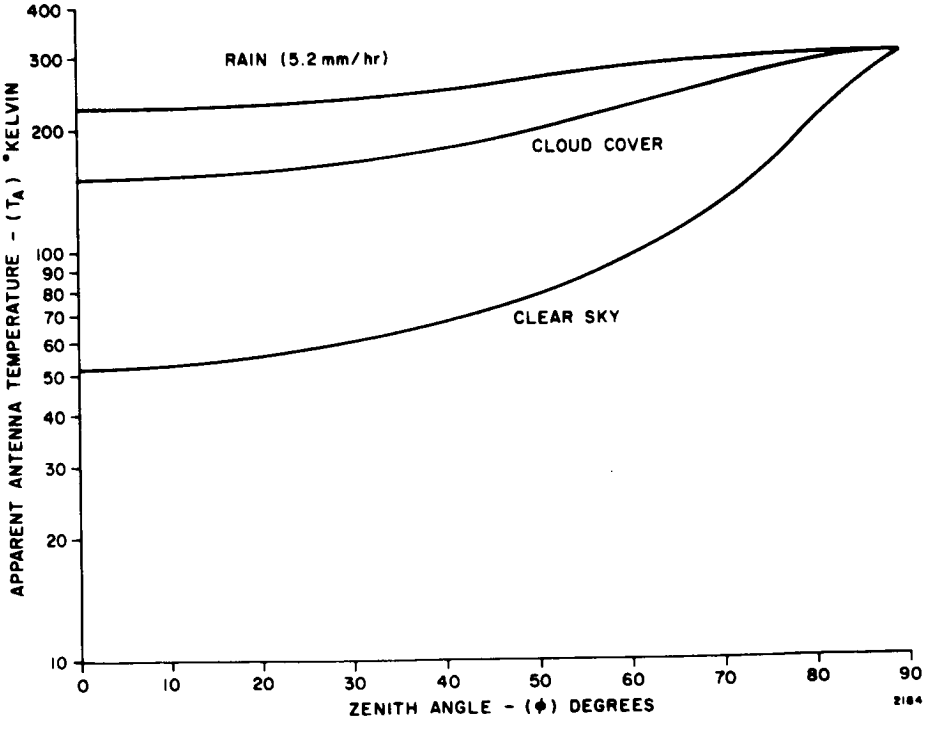

Figure 3-9 - Apparent Temperature of the Atmosphere at 94 Gc

frequency and that there is a superimposed attenuation peak at frequencies near the oxygen absorption peak at 60 Gc.

U.S. Weather Bureau Technical Paper 40 (Reference 2) contains maps of the continental United States with iso-pluvial lines for rainfall duration from 30 minutes to 24 hours from data gathered over 1, 2, 5, 10, 25, 50, and 100 year periods. Data from these maps was extracted for the candidate ground station sites and is tabulated in Table 3-IV. Each entry in the table represents a maximum rainfall recorded for that duration and period. This data was used in conjunction with data from Table 3-I and the method given in Reference (5) to develop the curves of Figure 3-10. A surface rainfall rate of 0.2 inches per hour was chosen from these curves as a design point. This is a rate which will be exceeded only about 45 hours per year (0.5 percent) at any of the four candidate sites.

Figure 3-11, taken from Reference (5), shows the percentage time for exceeding a precipitation rate for rates of .06 in/hour, .12 in/hour, and .18 in/hour. The average daily rain is derived from Table 3-I where values

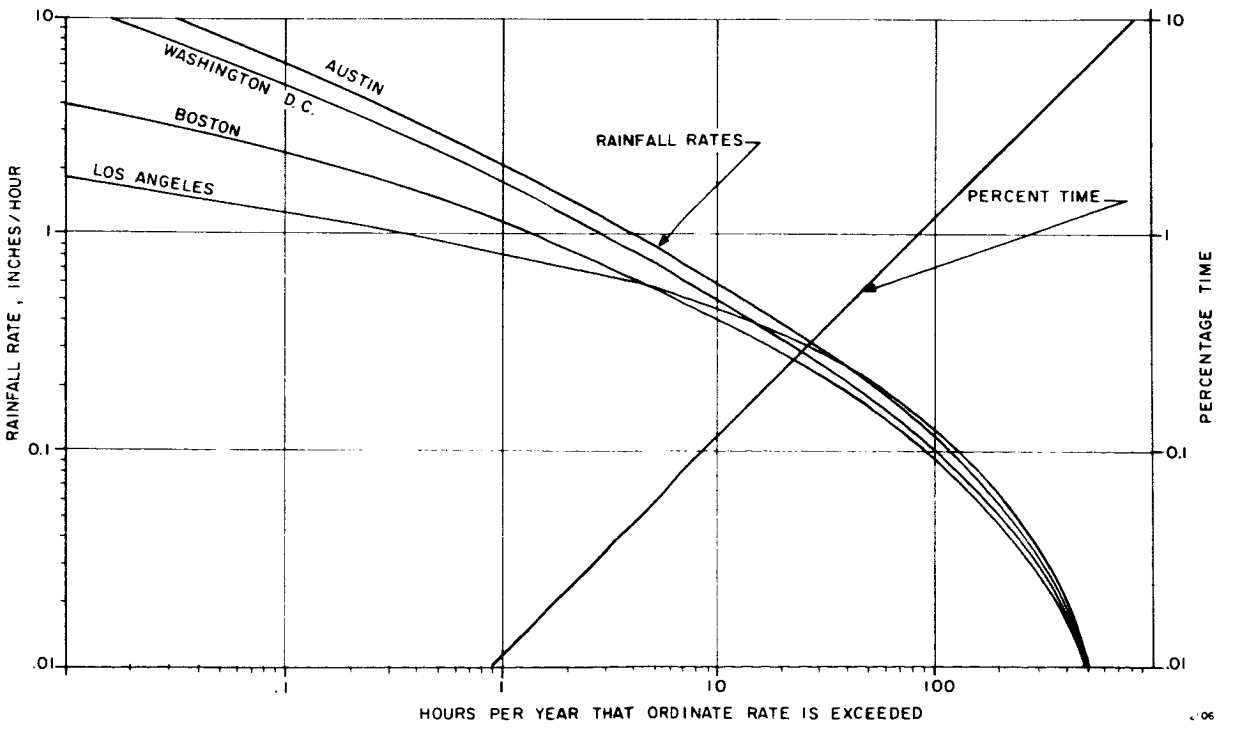

Figure 3-10 - Frequency of Occurrence of Rainfall of a Given Intensity

TABLE 3-IV

RAINFALL DURATION-INTENSITY DATA

Rainfall Duration	Return Period	Maximum Rainfall - Inches					
		Boston	Washington	Baltimore	Austin	Los Angeles	Ottawa
30 min	1 year	.8	1.0	1.0	1.4	.4	.6
	2	1.0	1.4	1.3	1.7	.6	.8
	5	1.3	1.8	1.7	2.1	.8	1.0
	10	1.5	2.0	1.9	2.4	1.0	1.2
	25	1.7	2.4	2.2	2.8	1.2	1.4
	50	1.9	2.8	2.6	3.1	1.4	1.6
	100	2.2	3.0	2.8	3.4	1.5	1.7
1 hour	1	1.0	1.4	1.3	1.7	.6	.8
	2	1.2	1.8	1.7	2.1	.8	1.0
	5	1.5	2.2	2.0	2.6	1.0	1.2
	10	1.8	2.6	2.6	3.0	1.2	1.4
	25	2.1	3.0	2.8	3.5	1.4	1.8
	50	2.4	3.4	3.2	3.9	1.8	2.0
	100	2.7	4.0	3.7	4.4	2.0	2.2
2 hours	1	1.3	1.6	1.6	2.0	.8	1.0
	2	1.5	2.0	2.0	2.4	1.1	1.2
	5	2.0	2.6	2.5	3.2	1.5	1.7
	10	2.3	3.1	3.0	3.7	1.8	1.8
	25	2.7	3.6	3.5	4.4	2.1	2.2
	50	3.0	4.1	4.0	4.9	2.5	2.3
	100	3.3	4.5	4.5	5.5	2.8	2.7
3 hours	1	1.4	1.8	1.7	2.2	1.1	1.0
	2	1.7	2.1	2.1	2.7	1.5	1.3
	5	2.3	2.7	2.7	3.5	1.8	1.5
	10	2.6	3.2	3.2	4.1	2.3	2.0
	25	3.0	3.7	3.7	4.8	2.8	2.3
	50	3.4	4.4	4.3	5.5	3.2	2.7
	100	3.7	5.0	4.7	6.1	3.7	3.0

TABLE 3-IV (Continued)

Rainfall Duration	Return Period	Maximum Rainfall - Inches					
		Boston	Washington	Baltimore	Austin	Los Angeles	Ottawa
6 hours	1 year	1.8	2.1	2.1	2.5	1.6	1.3
	2	2.2	2.6	2.5	3.2	2.2	1.5
	5	2.8	3.2	3.1	4.2	3.0	2.0
	10	3.3	3.8	3.7	5.0	3.5	2.9
	25	3.8	4.3	4.2	5.9	4.5	2.8
	50	4.3	5.1	4.9	6.6	5.0	3.0
	100	4.8	5.4	5.3	7.3	6.0	3.5
12 hours	1	2.3	2.4	2.3	2.9	2.5	1.5
	2	2.7	3.0	2.9	3.6	2.8	2.0
	5	3.4	3.7	3.6	5.0	4.0	2.5
	10	4.0	4.6	4.4	5.9	4.8	2.8
	25	4.7	5.3	5.1	7.0	5.8	3.3
	50	5.1	5.7	5.5	8.0	6.5	3.6
	100	5.8	6.4	6.2	8.9	7.0	4.0
24 hours	1	2.7	2.7	2.6	3.2	2.6	2.0
	2	3.2	3.3	3.2	4.2	3.6	2.3
	5	4.0	4.3	4.2	5.7	5.0	2.9
	10	4.7	5.2	5.1	6.9	6.0	3.4
	25	5.5	5.8	5.7	8.1	7.0	3.8
	50	6.0	6.5	6.4	9.1	8.0	4.2
	100	6.8	7.3	7.2	10.5	8.0	4.5

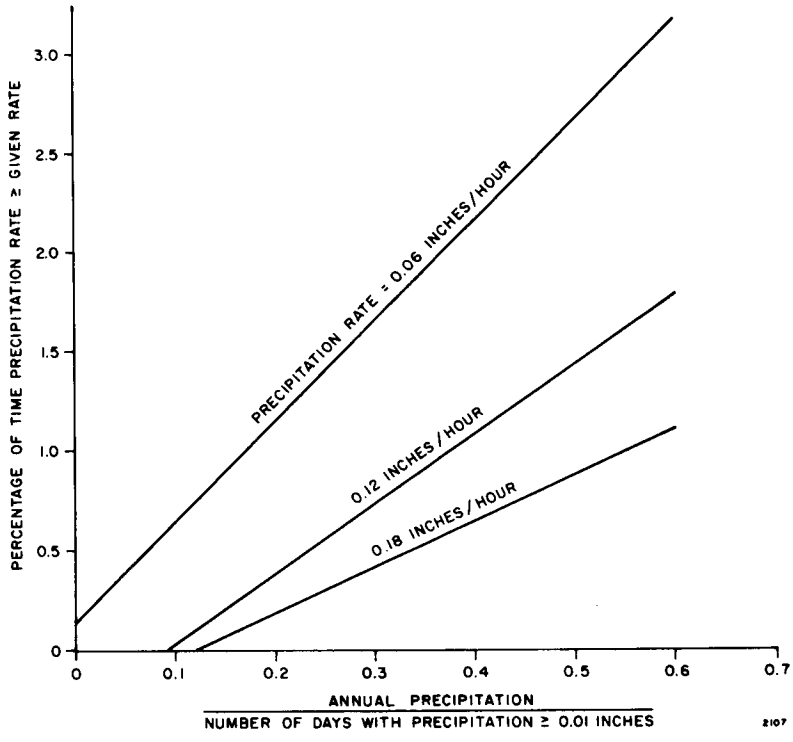

Figure 3-11 - Precipitation Rate Occurrence Based on Annual Precipitation

of annual precipitation and number of days with precipitation exceeding .01 inch are given for each site. The curves of Figure 3-1 then are used to find the percentage of time that the given rates will be exceeded. This gives three points on each curve of Figure 3-10. A fourth point was established for the one hour position on each curve from the data in Table 3-IV in the 1 hour 2 year set of data. This means that the curves in Figure 3-10 are subject to some error to the left of the 10 hour line, but in the area of the 40 hour line the error is negligible.

3.2 Effects of Rain on Radomes and Antenna Reflecting Surfaces

Considerable attention has been given to the effects of water vapor and rain in the propagation medium between the earth terminal and the satellite. In millimeter wave communication systems, all weather operational capability is required and consideration of the effects of rain on the ground antenna installation itself is necessary. Up till now these

effects of rain have been overlooked. This section reviews Blevis' recent work (Reference 6) on this subject and relates it to the problems it presents to the propagation experiment design and to the ultimate application of millimeter wave communication channels. The next phase of this study will deal with this problem in more detail.

In this report only the effects on radomes will be discussed, since they are easier to analyze. Under normal operating conditions the effect on systems with radomes is much worse than that on antennas without radomes, providing, of course, that the antenna feeds are adequately protected. Only the transmission losses and reflection losses of the water film on a radome are discussed here. The effects of increase in antenna noise temperature and degradation of antenna gain have not yet been considered.

Blevis used values for complex relative dielectic constant of water obtained by Grant, Buchanan and Cook (Reference 7) and certain mathematical treatments by Leaderman and Turner (Reference 8) to derive the transmission and reflection losses. According to Gibble's (Reference 9) approximation for water film thickness as a function of rainfall rate over a spherical radome:

$$d^3 = \frac{3}{2} \frac{\mu r R}{W}$$

where μ - viscosity of water
W - weight density of water
r - radius of the radome
R - rainfall rate

the water film is 5×10^{-3} inches thick over the upper hemisphere of a 25 foot radius radome under a 0.2 inch per hour rainfall in the absence of wind. According to curves in Reference (6) the transmission and reflection losses total 5.3 db for a frequency of 16.0 Gc and it appears that they might be 2 or 3 db more for a frequency of 35.0 Gc.

Since a rainfall rate of 0.2 inch per hour occurs 50 hours per year, more than 0.5 percent of the time, in most regions of the United States (see Figure 3-10 in Section 3.1), then the effects of rain on antennas and radomes is of definite concern in the design of the propagation experiments

and the use of the experimental results in designing communication systems.

3.3 Refraction Effects on Maximum Integration Time and Maximum Antenna Size

Propagation of millimeter waves through a turbulent atmosphere at low elevation angles has an effect upon the maximum useful receiver signal integration time and the maximum useful receiving antenna size. Variations in index of refraction along a propagation path are caused by changes in the inhomogeneous atmosphere by wind and the angular movement of a satellite with respect to the ground terminal. These variations in index of refraction, which are a function of wind velocity and satellite angular velocity, degrade the spectral purity of the transmitted signal, thus affecting the maximum useful integration time. This useful integration time increases with aperture size. These effects upon integration time are of particular significance in the design of phase-lock receivers for ground communication terminals which receive millimeter signals from low altitude spacecraft.

The gain of large millimeter antennas might also be affected by the turbulent atmosphere. As the antenna becomes larger, the wavefront of the received signal incident upon the aperture becomes less and less planar. The resulting effects upon antenna performance are very similar to those effects caused by reflector mechanical errors. The relative motion between the atmosphere and the propagation path does not have an effect upon the gain of the antenna.

Data taken from National Bureau of Standards experiments are analyzed to estimate the magnitude and spectra of fluctuations in earth-satellite radio paths. Range fluctuations over a period of a day can be expected to reach a level of about 25 cm (rms) at a 6^{o} elevation angle under poor weather conditions. The corresponding fluctuation over a period of one minute would be about 0.4 cm. For the case of the 100 nmi satellite, the rms velocity fluctuation could be as great as 72.5 cm/sec for an antenna of 6 inch diameter at 94 Gc, corresponding to a frequency fluctuation of 228 cps. The rms velocity fluctuation for a 15 foot diameter paraboloid at a frequency of 94 Gc (considered to be the maximum useful antenna size

at this frequency) would be 7.1 cm/sec, corresponding to a frequency fluctuation of 22 cps. For the 6000 nmi satellite, and the 15 foot diameter paraboloid at 94 Gc, the rms velocity fluctuation would be .06 cm/sec, corresponding to a frequency fluctuation of less than one cps. Range fluctuations over a 15 foot aperture will be of the order of .01 cm, indicating little beam broadening or loss of gain at a frequency of 94 Gc.

3.3.1 Spectrum of Fluctuation

The influence of the troposphere on the apparent lengths of fixed radio paths has been investigated for several years by the National Bureau of Standards at Boulder, Colorado. The best statistical summary of voluminous results takes the form of a composite power spectrum, extending from 10^{-8} to 10 cps. Such curves have been published for paths in Colorado, Hawaii, and Florida (References 10, 11, and 12). In each case, the path considered is about 15 miles long and leaves a flat surface at an angle of about 6 degrees. Considerable variation in amplitude can be expected from site to site and from time to time, but a typical spectrum for an atmosphere containing cumulus clouds can be expressed as:

$$W(f) = W_o \qquad f < f_a$$

$$W(f) = W_o \left(\frac{f_a}{f}\right)^{8/3} \qquad f > f_a$$

$$W_o = 10^7 \text{ (ppm)}^2/\text{cps}$$

$$f_a = 10^{-5} \text{ cps}$$

The spectral density is expressed here in units of (parts per million)^2 per cps. For a path length of 36 km (120,000 feet), the low-frequency spectral density W_o would correspond to 1.3×10^8 cm^2/cps. The spectrum given above may be applied to path lengths from about 20 to 40 km at altitudes below 5 km without modification. A plot of this spectrum is given in Figure 3-12. For convenience in interpretation, the spectrum may be replotted as in Figure 3-13, where the ordinate represents the weighted

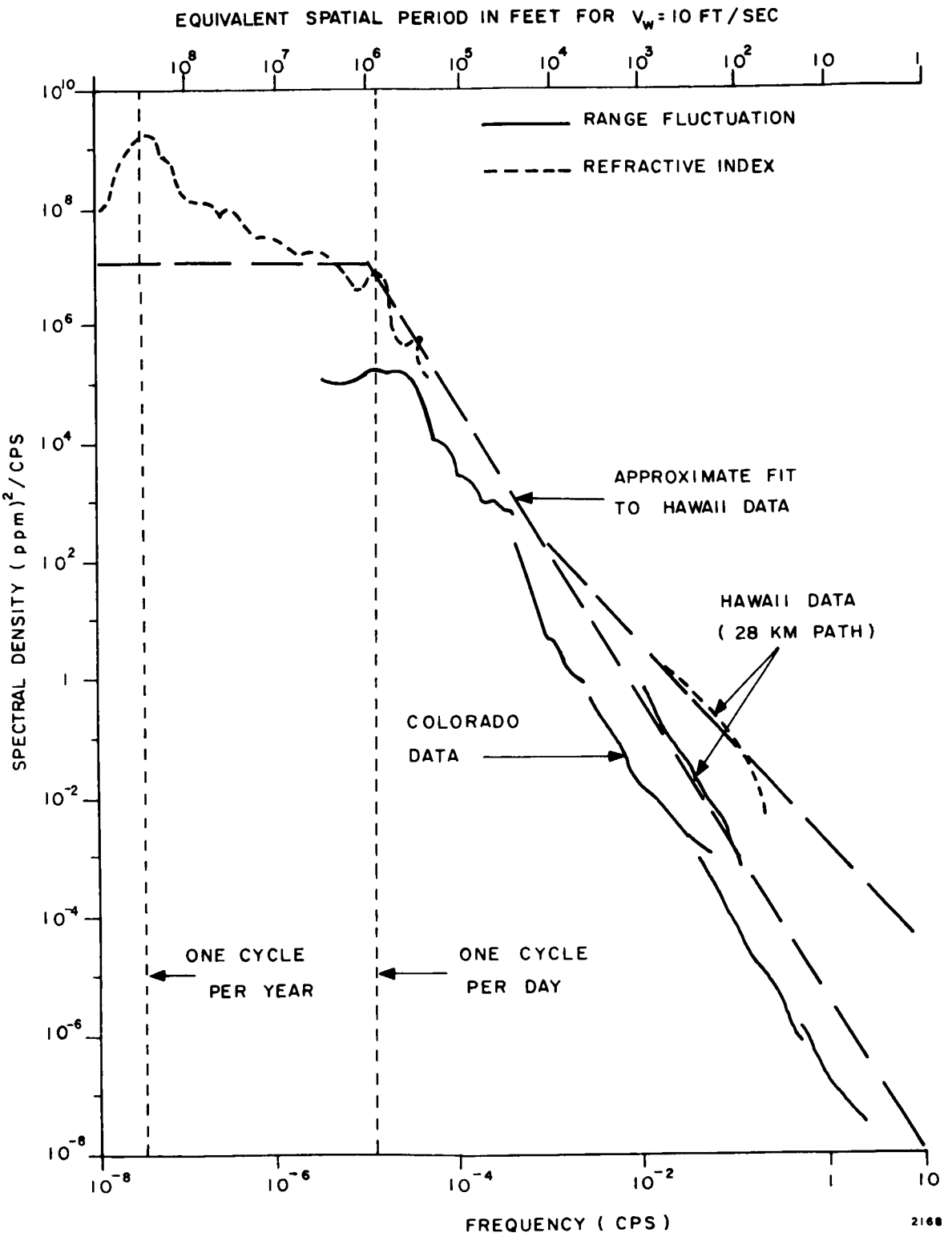

Figure 3-12 - Spectra of Refractivity and Range Fluctuation (NBS Data)

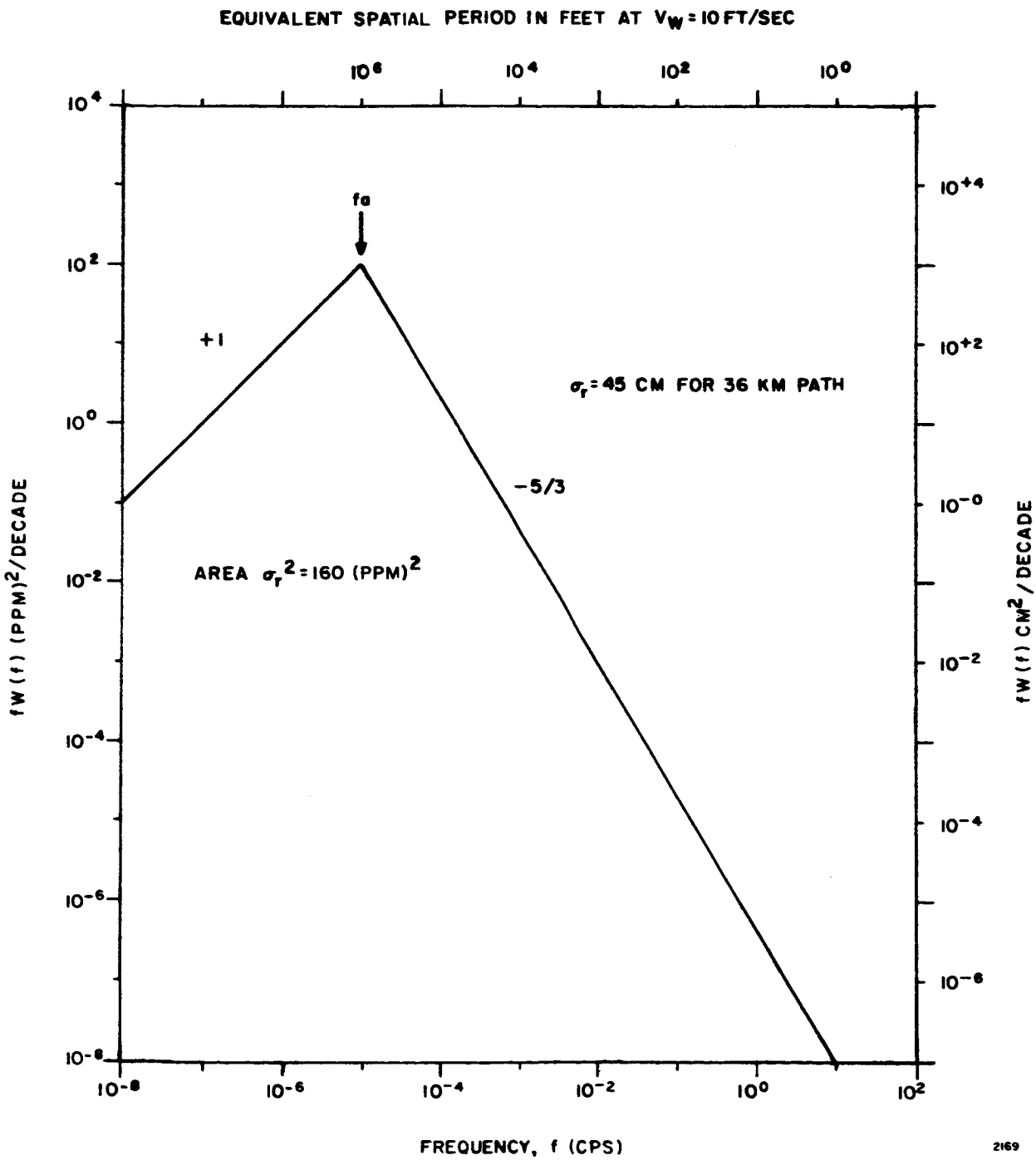

Figure 3-13 - Modified Plot of Range Fluctuation Spectrum

spectral density f W(f). The effect of the weighting is to show the relative contribution to the total area of each octave or decade in the spectrum. Thus it is seen that the predominant frequency components in the fluctuation spectrum will lie between 10^{-6} and 10^{-4} cps.

3.3.2 Magnitude of Fluctuation

The magnitude of range fluctuation observed over a given time interval t_1 may be estimated by integrating the product of the spectral density times a filter function $G_1(f)$ which expresses the effect of the finite observation interval (Reference 11):

$$\sigma_r^2 = \int_0^\infty G_1(f)\, W(f)\, df$$

$$G_1(f) = (f\, t_1/2)^2 \qquad f < 2/t_1$$

$$G_1(f) = 1 \qquad f > 2/t_1$$

The filter functions for observation periods of one day and one minute are applied to the basic spectrum in Figure 3-14. The predominant frequencies of fluctuation are in the region near $f_1 = 2/t_1$, and lower frequency components are lost, appearing as "trends" of greatly reduced amplitude in the short samples of data. The rms fluctuations will be about 23 cm over a day, and 0.1 cm over a minute (for periods shorter than a day, the rms fluctuation will vary as the 5/6 power of the observation period).

3.3.3 Velocity (or Frequency) Fluctuation

The rate of change of fluctuation in range gives the velocity fluctuation, and this quantity, divided by the wavelength, gives the frequency fluctuation in cps. The spectral density of velocity fluctuation is just $(2\pi f)^2$ times that of range fluctuation (Figure 3-15). The rms velocity fluctuation is the integral of this spectrum. Since the predominant frequencies are near the high end of the spectrum, the observation time is no longer of great importance. However, the upper limit of the -8/3

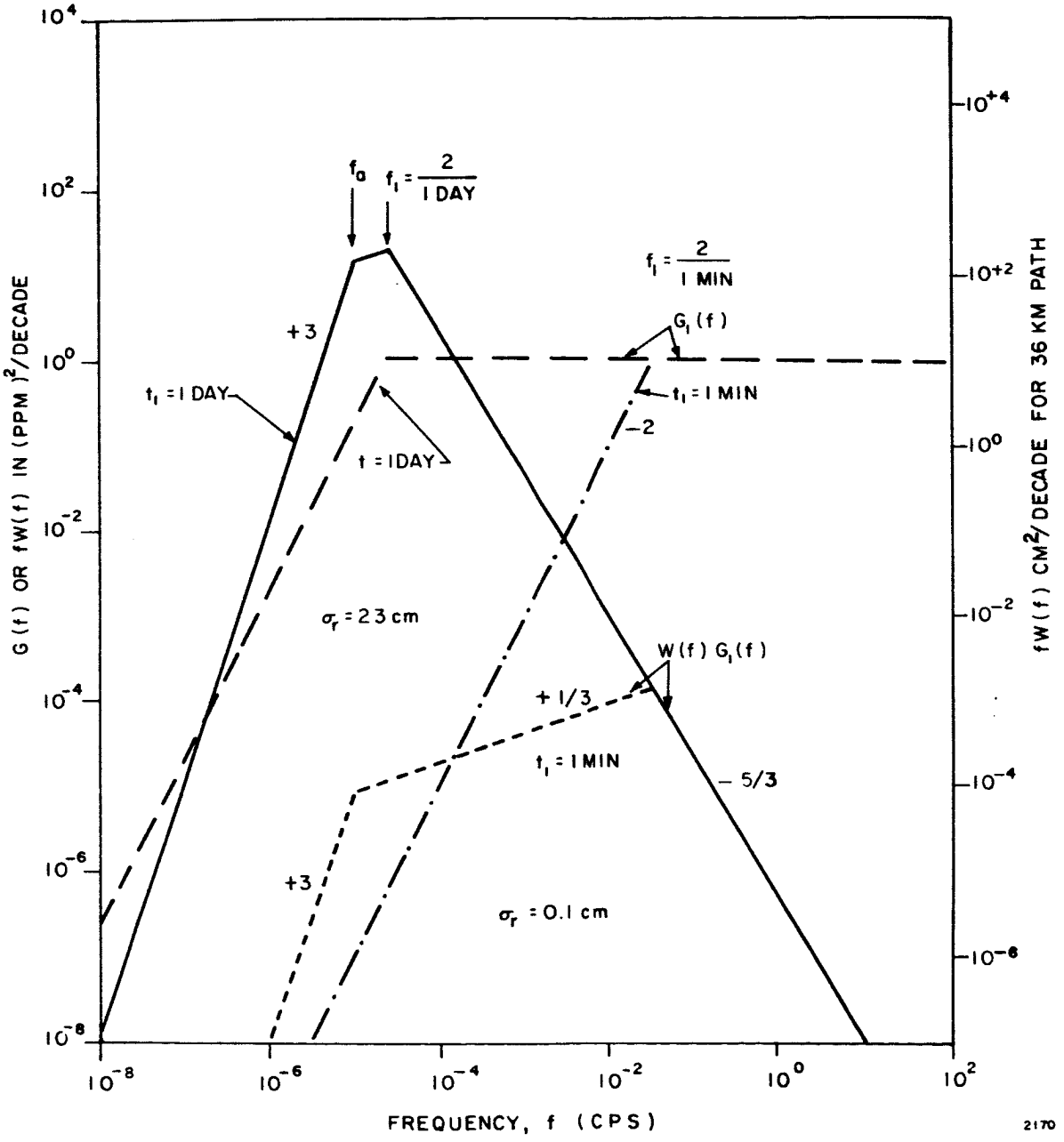

Figure 3-14 - Range Fluctuation Spectra for Finite Observation Periods

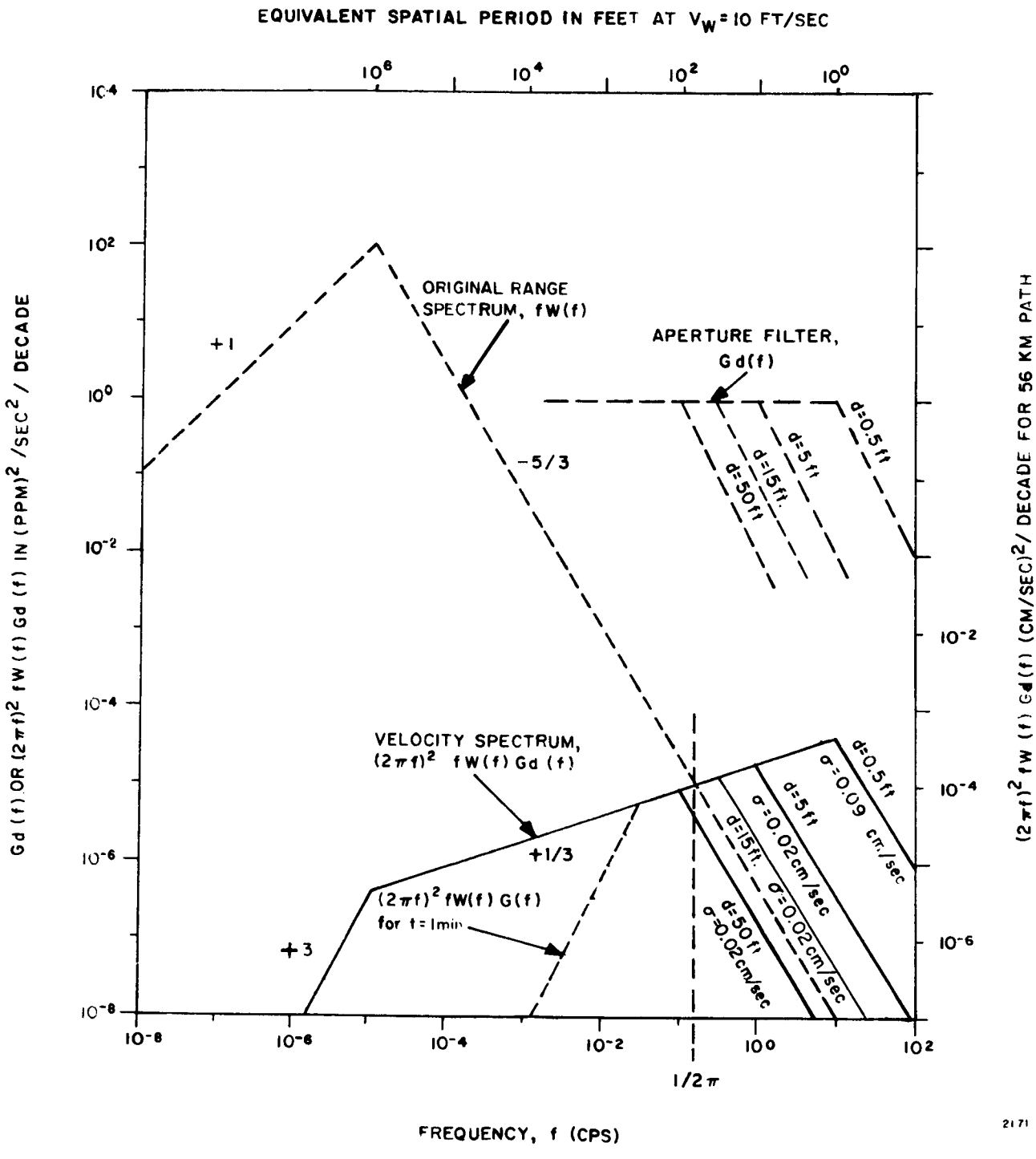

Figure 3-15 - Velocity Fluctuation Spectrum for Different Aperture Diameters

portion of the spectrum will be important in establishing velocity fluctuation. This limit, set either by aperture size or by physical properties of the atmosphere, will lie between 0.1 and 10 cps for the case of the fixed path. An aperture of diameter d will tend to filter out fluctuations lying above a frequency $f_d = V_w/2d$, where V_w is the wind velocity component normal to the antenna axis. The equivalent aperture filter function is

$$G_d(f) = \left(\frac{f_d}{f}\right)^2 \qquad f > f_d$$

$$G_d(f) = 1 \qquad f < f_d$$

This function is shown in Figure 3-15, superimposed on the velocity spectrum, for d = 50, 15, 5 and 0.5 feet.

The velocity fluctuation may now be computed from:

$$\sigma_f^2 = (2\pi)^2 \int_o^\infty f^2 W(f)\, G_1(f)\, G_d(f)\, df$$

$$(2\pi)^2 \int_o^\infty f^2 W(f)\, G_d(f)\, df$$

Expected values for the fixed path will run from 0.02 to 0.09 cm/sec, depending on aperture. This corresponds to an rms frequency deviation of 0.02 to 0.09 cps at f_o = 30 Gc (λ = 1 cm).

3.3.4 Fluctuation on Moving Paths

The preceding results may be applied directly to communication paths to a synchronous satellite, where the fluctuations result entirely from atmospheric drift across the path and temporal variations in the refractivity along the path. If the satellite moves, relative to the ground terminal, a further effect is introduced by angular motion of the radio path through the atmosphere. Although this angular motion cannot be simulated exactly in fixed-path experiments, its effect can be estimated with reasonable accuracy by considering an average velocity of the antenna

beam relative to the tropospheric features which cause fluctuation. This velocity is used to modify the spectrum of Figures 3-12 and 3-13, by assuming that the tropospheric features are "frozen" in the air mass and pass through the beam at a frequency proportional to the total velocity of the air relative to the beam. The following analysis will assume that this relative velocity at an altitude of 12,000 feet is an appropriate weighted average for tropospheric effects. At an elevation angle of 6 degrees, the path from a terminal at sea level to this point will be about 120,000 feet in length. The "apparent" wind velocities as determined from Figure 3-16 for 100 nmi and 6000 nmi satellites are 813 and 25 ft/sec., respectively. Addition of the typical wind velocity to the "apparent" wind velocity (actually the velocity of the satellite) yields values of 823 and 35 ft/sec for v_b used in the computations.

The range and velocity fluctuation spectra for the moving beam case will be as shown in Figures 3-17 and 3-18. The frequency scale has been multiplied by the factor v_b/v_w, and the density scale in W(f)

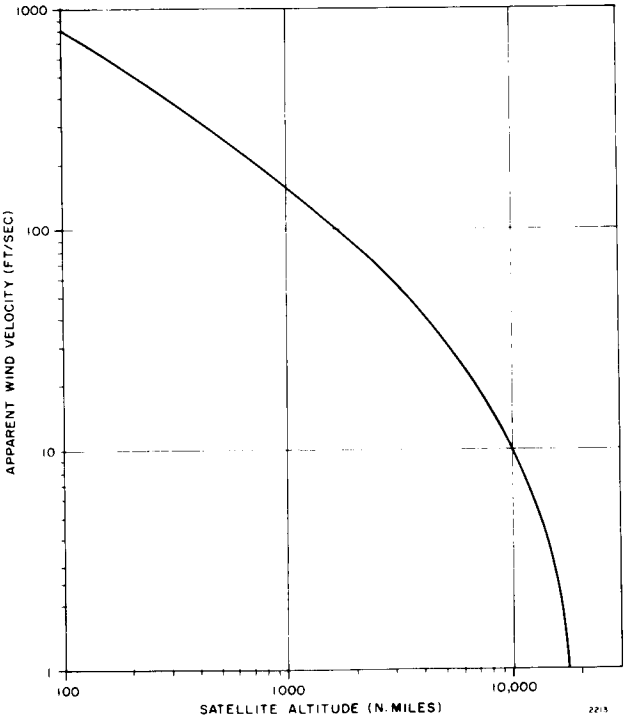

Figure 3-16 - Apparent Wind Velocity vs Satellite Altitude

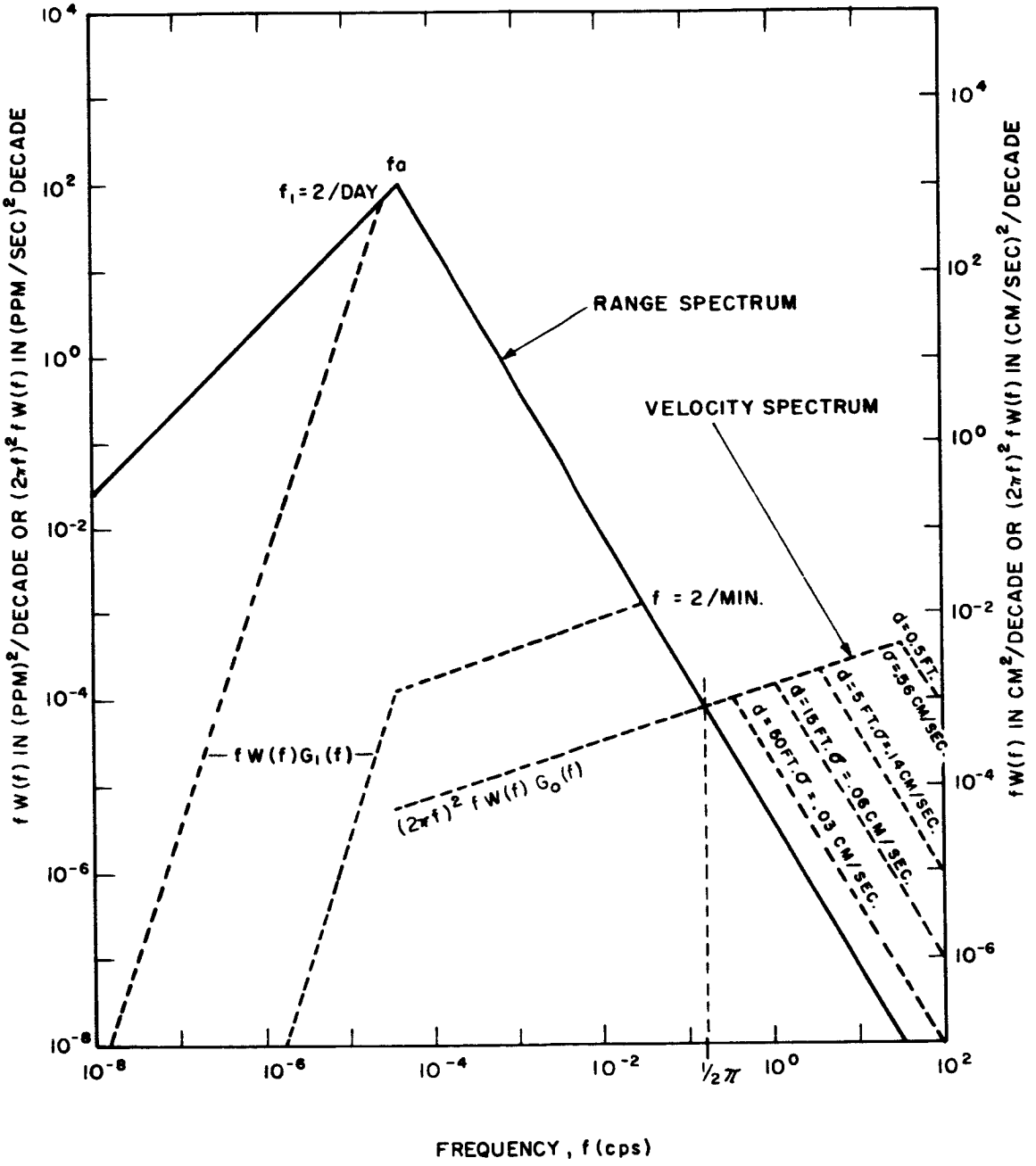

Figure 3-17 - Range and Velocity Spectra for Moving Path, 6000 nmi Satellite

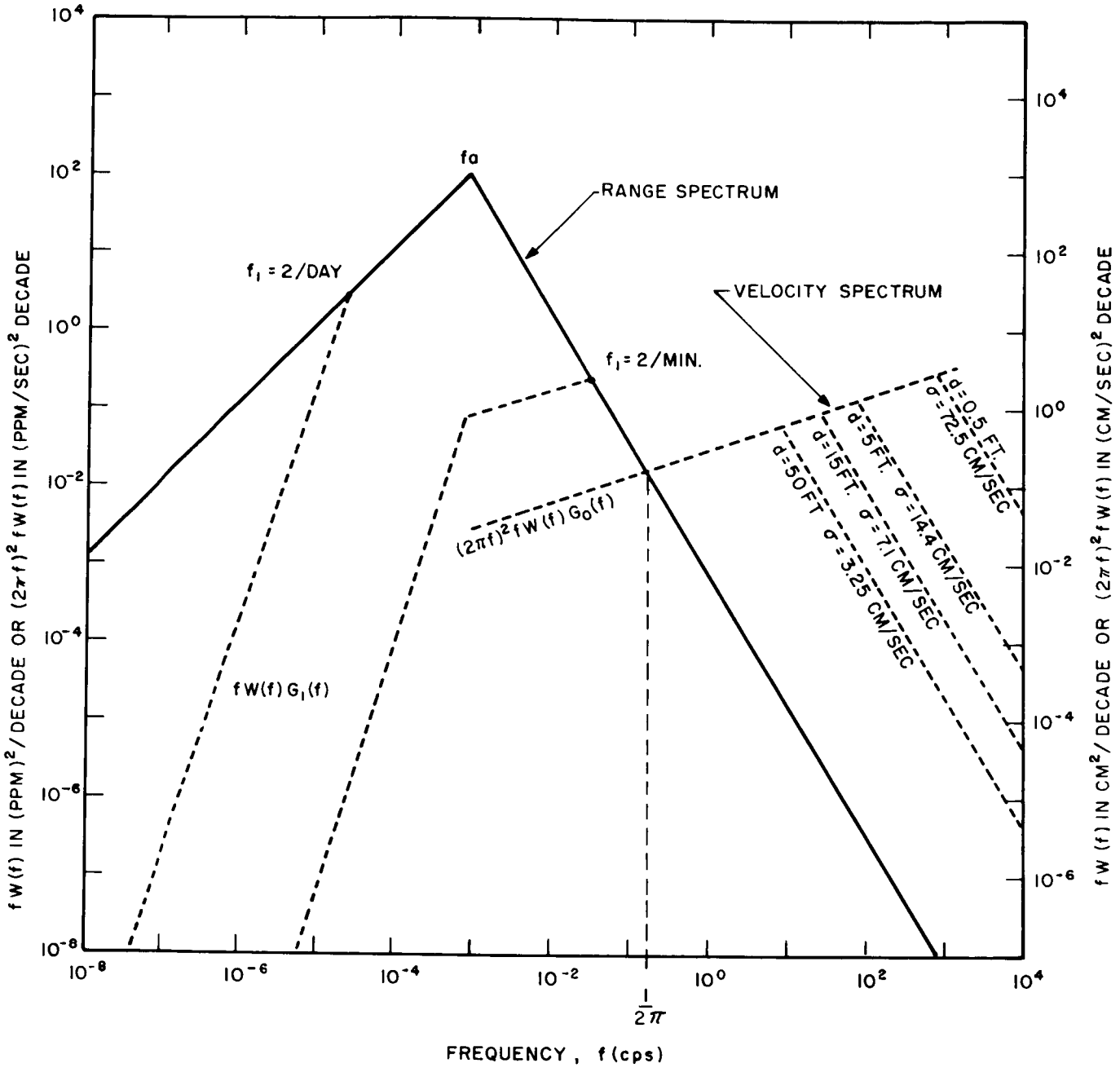

Figure 3-18 - Range and Velocity Spectra for Moving Path, 100 nmi Satellite

divided by the same quantity preserving the area under the curve. However, the variances observed in short time periods will be increased approximately by the factor $(v_b/v_w)^{5/3}$. The fluctuations for fixed and moving beams are compared in Table 3-V. Table 3-VI gives the resulting frequency fluctuations at 94 Gc for a 100 nmi satellite.

3.3.5 Phase-Difference Fluctuations

Information on the magnitude of phase-difference fluctuations across a large aperture can also be obtained from the NBS data. If we assume that the "frozen" model of the atmosphere is valid, at least for tropospheric features whose dimensions are smaller than several aperture widths, the rms range-difference fluctuations between two points separated by a distance b are found by applying the following transfer function (Ref. 11) to the basic spectrum:

$$G_b(f) = 2\,(f/f_b)^2 \qquad f < f_b$$

$$G_b(f) = 2 \qquad f > f_b$$

$$f_b = 0.22\, v_w/b$$

This is a "high-pass" filter function, as shown in Figure 3-19. Fluctuations at frequencies below f_b will introduce linear variations in phase across an aperture of width b, changing the apparent angle of arrival. Frequencies near f_b will cause broadening of the antenna beam, while those above f_b will increase sidelobes. The number of sidelobes affected will be proportional to the increase in frequency beyond f_b. The amount of broadening or sidelobe increase will depend on the rms phase-difference contributed by the corresponding portion of the error spectrum $w(f)\, G_b(f)$. Significant reduction in gain will occur when the rms phase error across the aperture exceeds about 0.3 radian (or when the rms range difference fluctuation exceeds $\lambda/20$).

Figures for range-difference fluctuations shown on Figure 3-19 indicate fluctuations of less than 0.1 cm for a 50 foot aperture and of the order of 0.01 cm for a 15 foot aperture. At a frequency of 94 Gc, .01 cm

TABLE 3-V

FLUCTUATIONS FOR FIXED AND MOVING BEAMS

	Fixed Path (v_n=10 ft/sec)	Moving Path 6000 nmi satellite (v_b=35 ft/sec)	Moving Path 100 nmi satellite (v_b=823 ft/sec)
Total range fluctuation	45 cm	45 cm	45 cm
Fluctuation in one day	23 cm	23 cm	23 cm
Fluctuation in one minute	0.1 cm	.36 cm	
Velocity fluctuation(d=50 ft)cm/sec	.02 cm/sec	.03 cm/sec	3.3 cm/sec
Velocity fluctuation(d=15 ft) cm/sec	.02 cm/sec	.06 cm/sec	7.1 cm/sec
Velocity fluctuation(d=5 ft)cm/sec	.02 cm/sec	.14 cm/sec	14.4 cm/sec
Velocity fluctuation (d=0.5 ft)cm/sec	.09 cm/sec	.56 cm/sec	72.5 cm/sec

TABLE 3-VI

FREQUENCY FLUCTUATIONS AT 94 Gc FOR A 100 nmi SATELLITE

Antenna Diameter (ft)	Frequency Fluctuation (cps)
15.0	22
5.0	45
0.5	228

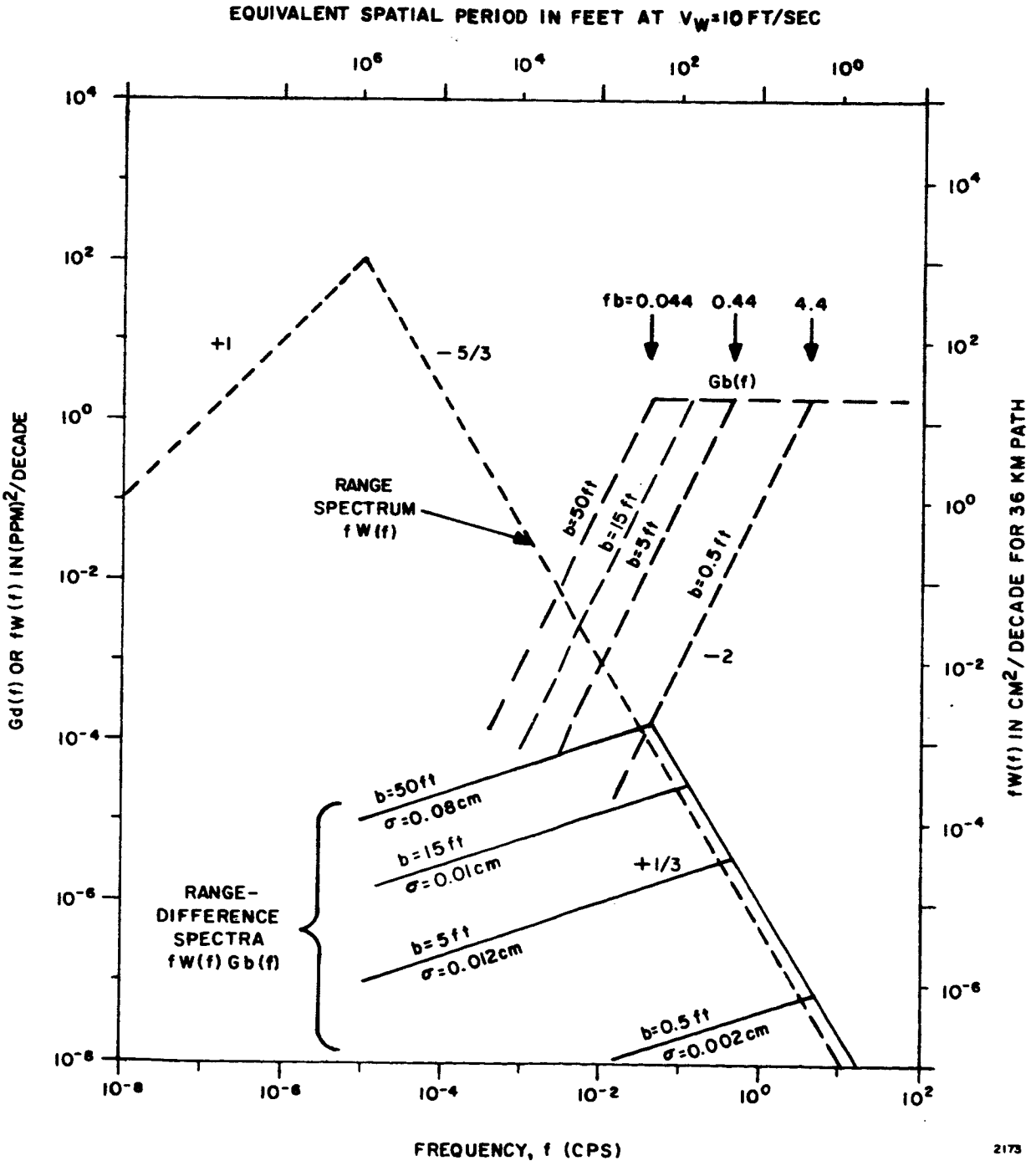

Figure 3-19 - Range-Difference Spectra for Separations From 0.5 to 50 Feet

is equivalent to .03 λ, indicating no appreciable deterioration in gain.

3.4 Refraction Effects on Satellite Angle Tracking

The objectives of this section* are several: 1) to outline those atmospheric effects which can lead to tracking errors; 2) to obtain estimates of the relative magnitudes of these errors; 3) to summarize briefly those methods used for the correction of these errors; 4) to obtain estimates on the accuracy of the corrected measurements; 5) to determine the effects of the atmosphere on the accuracy of the instrumentation.

3.4.1 Classification and Description of Atmospheric Errors

Classification of Atmospheric Errors by Type

Atmospheric errors can be conveniently classified according to Table 3-VII.

TABLE 3-VII
CLASSIFICATION OF ATMOSPHERIC ERRORS

a.	Source of Error
	Tropospheric
	Ionospheric
b.	Measured Quantity
	Angle of arrival or phase difference
	Range delay or signal phase
c.	Spatial Correlation
	Across radar aperture (5 to 100 feet)
	Across short baseline (100 to 1,000 feet)
	Across long baseline (1,000 to 100,000 feet)
d.	Temporal Correlation of Error
	Bias (fixed during one track)
	Fluctuation (periods of seconds or minutes)

* This section is a synopsis of References 13 and 14.

The error should be known for each combination of the above characteristics as a function of frequency, target altitude, elevation angle, and state of the atmosphere.

Effects of the Lower Atmosphere

The real part of the index of refraction of the gaseous atmosphere is given by:

$$(n - 1) \cdot 10^6 = N = \frac{77.6}{T} \left(P + \frac{4810\, p}{T}\right), \qquad (3\text{-}2)$$

where T represents the atmospheric temperature in degrees Kelvin; P represents the total pressure of the atmosphere in millibars (there are 1013.25 millibars in an atmosphere); p represents the partial water vapor pressure in millibars; and N is defined as the refractivity. The refractivity for the usual range of atmospheric variables and for radio frequencies less than 30 Gc can be computed from Equation (3-2) with an accuracy of 0.5 percent.

If it is assumed that the refractivity decreases exponentially with height, i.e.,

$$N(z) = N_o\, e^{-z/H}, \qquad (3\text{-}3)$$

where N_o is the refractivity at the radar, H is a scale height, and z is the height above the radar, then the expression for the range error becomes:

$$\Delta R_e = N_o\, H \csc \theta_o \cdot 10^{-6} \cdot (1 - e^{-h/H}) \qquad (3\text{-}4)$$

where ΔR_e is the range error, and θ_o is the elevation angle.

For a typical case, let $N_o = 313$; $H = 7$ km; $h = 30$ km; $\theta_o = 20^o$. The range error for this case turns out to be 6.4 meters. It can be seen from (3-4) that the range error increases as the path length through the atmosphere increases, or as the initial elevation angle decreases.

The error in elevation angle for a tracker can be shown to be

$$\delta = N_o \cot \theta_o \cdot 10^{-6}, \qquad (3\text{-}5)$$

if it is assumed that the refractivity decreases exponentially with increasing height and if the initial elevation angle is not too small. It can be seen from (3-5) that the error in angle for a tracker can be as great as 300 microradians at an elevation angle of 45 degrees.

An excellent compilation of geographical, seasonal, and diurnal variations in refractive data has been published by Bean, et al (Reference 15). The standard deviation of the surface refractivity has been estimated approximately from that data and appears in Table 3-VIII. The elevation angle is assumed to be 20^o and the height of the target exceeds 32 km.

The standard deviation of the refractivity which is measured one hour prior to track is based on the fact that the refractivity can be measured with an accuracy of 4 N-units and will change 3 N units, typically, during one hour.

The lower atmosphere is not quite spherically stratified, and its refractivity is constantly changing. Hence, the propagation errors are actually larger than have been given for a spherically stratified atmosphere. In general, these errors will be quite small.

3.4.2 Effects of the Ionophere

The index of refraction of the ionosphere is given by

$$n = \left[1 - \frac{N_e e^2}{m \epsilon_o \omega^2} \right]^{1/2} \qquad (3\text{-}6)$$

where N_e is the electron density, e is the electron charge, m is the electron mass, ω is 2π times the frequency, and ϵ_o is the permittivity of

TABLE 3-VIII

AIR REFRACTIVITY AND RANGE ERRORS

Standard Deviation	N_o measured one hour before guidance time	Diurnal (Summer)	Seasonal	Annual	Geographical for the U.S. at sea level	
					summer	winter
N_o	5	10	15	20	30	20
ΔR_e	0.1 m	0.2 m	0.3 m	0.4 m	0.6 m	0.4 m

free space. Equation (3-6) may be rewritten as

$$n = \left[1 - \frac{\omega_p^2}{\omega^2} \right]^{1/2} \qquad (3\text{-}7)$$

where $\omega_p^2 = \frac{N_e e^2}{m \epsilon_o}$, and ω_p is the plasma angular frequency.

The maximum value of ω_p^2 for the ionosphere (assuming a maximum electron density of $10^6/cm^3$) is 3.18×10^{15}. When the signal frequency is much greater than the plasma frequency, Equation (3-7) may be rewritten as

$$n = \left[1 - \left(\frac{\omega_p}{\omega} \right)^2 \right]^{1/2} \approx 1 - \frac{1}{2} \left(\frac{\omega_p}{\omega} \right)^2 \qquad (3\text{-}8)$$

Expressing (3-8) in terms of the refractivity,

$$N = (n - 1) \cdot 10^6 = -\frac{1}{2} \left(\frac{\omega_p}{\omega} \right)^2 \cdot 10^6 \qquad (3\text{-}9)$$

At a frequency of 10 Gc, N = - 0.4 units. Consequently, the ionosphere will introduce negligible refraction at frequencies of 10 Gc and higher.

3.4.3 Atmospheric Sounding for Correction of Tracking Data

Methods of Measuring and Estimating Tropospheric Profiles

The index of refraction profile may be obtained indirectly through the use of radiosonde or dropsonde instruments. Carried aloft on free balloons, or jettisoned by parachute from aircraft or rockets, the device samples the absolute values of dry bulb temperature, relative humidity, and atmospheric pressure. The measurements are transmitted as

modulation of an RF carrier signal. A switching device alternately switches circuits to the transmitter, thereby providing a sequence of the samples being measured, one at a time. The refractivity is then computed as a function of the measured variables.

A more accurate method of making refractivity measurements is to use a microwave refractometer. This is a direct measurement in that the deviation in the resonant frequency of a microwave cavity from its initial condition of resonance is directly related to the refractivity. The lag of a refractometer is dictated by the speed of its carrier and the time required to flush the air sample from the instrument.

Estimated Accuracy of Corrected Measurements

The accuracy of atmospheric refractivity measurements has been discussed by McGavin (Reference 16) who states:

"Meteorological sensing is limited mainly by the inaccuracy in measuring humidity which under ideal conditions appears to limit the accuracy to $\pm$ 1.0 N-units. Gradient measurements using radiosondes reflect an accuracy no better than $\pm$ 3N units. Radio frequency refractometers are capable of accuracies as much as an order of magnitude better than that achieved by meteorological sensors. Lightweight refractometers have been devised for balloon-borne and dropsonde measurements reflecting accuracies inferior to the conventional refractometer but superior to the radiosonde."

Since surface refractivity is on the order of 330 N-units, the range corrections resulting from the use of complete profiles with the above accuracies will be in error by 0.3 to 1 percent. Angle corrections, which depend upon gradients of refractive index and are more sensitive to variations in the profile, will have a larger error, usually between 2 and 4 percent of the initial value of error. The accuracy of the angle correction will be better for long range targets than for those which lie within the troposphere, since the elevation error approaches the total bending in the long range case.

Experience at the test ranges confirms the feasibility of correcting tracker data to about 50 microradians.

3.4.4 Conclusions

Using surface refractometer measurements made at the ground terminal just before an earth-space propagation test will permit the modification of predicted satellite elevation data to adjust for tropospheric bias errors to within 100 microradians down to 2 or 3 degrees elevation. Since bias errors can be of the same order of magnitude as the antenna beamwidth, refraction corrections are essential for satellite acquisition and programmed tracking. The task of obtaining correlative data becomes doubly important since it is used for angle corrections as well as being used to classify the weather during the propagation test.

Tropospheric fluctuation errors are not correctable using any known procedure and will amount to a few tenths of a foot in range, and to 10 to 50 microradians in angle.

In range instrumentation applications where the beam is not fixed, the residual bias and long term error components will change as the beam is moved, and additional atmospheric rate errors will be generated. These errors will be proportional to the tangential velocity of the satellite, and will typically be five to fifty times the errors measured for a fixed beam.

The uncertainty in tropospheric path leads to errors equivalent to motion of the instrument on the ground. The motion of the virtual source amounts, typically, to several feet normal to the path and a few tenths of a foot along the path.

Ionospheric errors are essentially unpredictable, and will exceed the residual tropospheric errors when frequencies below 3 Gc are used. Even in the 5 to 6 Gc range, ionospheric errors will contribute to overall atmospheric error during daytime operation.

3.5 Coherence Bandwidth

In this section consideration is given to how the atmosphere limits the coherence bandwidth of the communications channel. The size of the coherence bandwidth is limited by the multipath spread arising in the channel. Roughly speaking, the coherence bandwidth is equal to the reciprocal of the multipath spread in the channel. A number of atmospheric

phenomena give rise to multipathing in the millimeter link under consideration. These are" 1) scattering from random inhomogeneities in the atmosphere; 2) refraction resulting from non-random inhomogeneities (that is, clouds, vortex columns, etc.); and 3) inhomogeneities having a size smaller than the transmitter or receiver antenna size. Consideration of multipathing arising from small scale inhomogeneities will be given in Section 4.2

3.5.1 Scattering

Multipathing arising from scattering from blobs is treated separately here as single scattering (first order Born approximation) and multiple scattering (higher order Born approximation).

In single scattering, propagation is considered to be along a single ray path and additional small contributions come from atmospheric irregularities near the path. The contributions are calculated from the first Born approximation (Reference 17). By hypothesis there is a very dominant single ray path so that not much fading, either flat or at selective frequencies, can occur from this cause. Whatever effects do occur are proportional to the rms fluctuation level $< \sqrt{(\Delta n)^2} >$ and to the path length L. Muchmore and Wheelon have shown that the limitation from this type of effect on coherence bandwidth is negligible.

In a turbulent medium a single ray is inadequate to represent the behavior of a transmitted short pulse, and a bundle of rays (or, equivalently, multiple scattering) of slightly different lengths must be considered. The presence of multiple rays gives rise to a limit on coherence bandwidth or, equivalently, to flat frequency fading.

For short paths, these effects are all second order (though not necessarily small) in the sense that they are proportional not to the rms fluctuation level but to its square. For long paths, the dependence becomes more complicated.

The coherence bandwidth limit is proportional to the reciprocal of the spread in arrival time associated with the various rays of the bundle. So long as the wavelength is much smaller than the scale of atmospheric irregularities, this time spread depends merely on the spread in path

lengths. Thus this limit on coherence bandwidth is frequency independent.

The coherence bandwidth determines the character of the fading to be expected from random inhomogeneities. If the coherence bandwidth is greater than the carrier frequency, then fading is impossible. Once the carrier frequency is raised well above the coherence bandwidth, the paths of the rays of the bundle have the potential to be grouped into pairs which have a half-wavelength separation so that cancellation of the signal occurs. Fading will then be expected to depend on signal frequency away from the carrier in a random manner, that is, frequency selective fading. The depth of fading will presumably oscillate as the carrier frequency is further raised, while the rate of fading would be expected to be proportional to signal frequency, since the higher the signal frequency the greater phase changes in the path lengths. All that can be said at this time is that the dependence is not linear with path lengths, nor is it linear with the refractive index fluctuation level.

3.5.2 Non-Random Inhomogeneities

Atmospheric fluctuations of a non-random character, such as distinct clouds, vortex columns, etc., make a third kind of contribution which must be evaluated for the situation at hand, and which must be evaluated from direct experiments.

While it might be possible to calculate the effect of a cloud of specified shape and droplet density, the character of real weather is not known in enough detail to be able to predict the frequency of clouds of various sizes, shapes and densities. The associated vortex columns and other completely transparent structured (that is, non-random) irregularities which abound in the atmosphere are even less predictable.

3.5.3 Projected Comparison with Surface Propagation

The dependence of multiple ray effects on path lengths and fluctuation level is under study. If the expected results are obtained, it will be possible to determine a path length on the surface of the earth that would be expected to have the same correlation bandwidth as any given

earth-space path. The known surface data could be used to estimate the multiple ray effects.

3.6 Propagation Through a Plasma

A vehicle which re-enters the earth's atmosphere while travelling at hypersonic velocities becomes enveloped in a shock layer of compressed and heated air. As the vehicle descends into the atmosphere, the air temperature in the shock rises to several thousand degrees Kelvin. While in the region of elevated temperatures, the air in the shock layer becomes thermally ionized, and consequently, electrically conducting. This phenomenon can affect communications in several ways: 1) telemetry signals can be severaly attenuated; 2) the plasma can have an effect on the effective noise temperature of an antenna and consequently degrade receiver sensitivity; 3) the plasma can lower the breakdown power level of the antenna. It is the purpose of this section to discuss these effects.

3.6.1 Electromagnetic Properties of a Uniform Plasma

Complex Dielectric Constant

The complex dielectric constant of an infinite, uniform plasma can be deduced from Maxwell's fourth equations. Assuming a harmonic field variation and the permittivity of the plasma to be the same as that of free-space, Maxwell's fourth equation can be written as

$$\nabla \times \vec{H} = \vec{J} + \frac{\delta}{\partial t}(\epsilon_o \vec{E}) \tag{3-10a}$$

$$= \sigma \vec{E} + j\omega\epsilon_o \vec{E} \tag{3-10b}$$

$$= j\omega K \epsilon_o \vec{E} \tag{3-10c}$$

where $\vec{H}$ and $\vec{E}$ are the magnetic and electric field vectors, respectively of an electromagnetic wave incident on the plasma; $\vec{J}$ is the current density; σ is the conductivity of the plasma; ω is the angular frequency of the electromagnetic wave; $j = \sqrt{-1}$ and K is the complex dielectric constant given by

$$K = 1 + \frac{\sigma}{j \omega \epsilon_o} \tag{3-11}$$

If it is assumed that the collision frequency of the electrons is independent of the velocity distribution, it can be shown that the conductivity of the plasma may be expressed by

$$\sigma = \frac{n e^2}{m(\nu + j \omega)} \tag{3-12}$$

where e is the electronic charge = 1.602×10^{-19} coulomb; m is the electron mass = 9.108×10^{-31} kilogram; n is the number of electrons per unit volume, and ν is the effective collision frequency of the electrons.

Substituting (3-12) into (3-11) and separating the right side of (3-11) into its real and imaginary parts,

$$K = K_r + j K_i = \left\{ 1 - \left(\frac{\omega_p}{\omega}\right)^2 \frac{1}{1 + \left(\frac{\nu}{\omega}\right)^2} \right\} - j \left\{ \left(\frac{\omega_p}{\omega}\right)^2 \frac{\frac{\nu}{\omega}}{1 + \left(\frac{\nu}{\omega}\right)^2} \right\} \tag{3-13}$$

where $\omega_p^2 = \frac{n e^2}{m \epsilon_o}$ and ω_p is defined as the "plasma frequency."

Propagation Constant

Having described the plasma by its "plasma frequency" and "collision frequency" and expressing the complex dielectric constant in terms of these frequencies, it is necessary to relate the propagation

constant to the complex dielectric constant. The complex dielectric constant can be expressed as

$$\gamma = \alpha + j\beta \tag{3-14}$$

where γ is the complex propagation constant; α is the attenuation constant, and β is the phase constant.

In a uniform plasma, assumed to be neutral there is no net charge. Hence, the divergence of E is 0. Maxwell's third and fourth equations can be manipulated to yield

$$\nabla^2 \vec{E} + k^2 K \vec{E} = 0 \tag{3-15}$$

$$\nabla^2 \vec{H} + k^2 K \vec{H} = 0$$

where $k = \frac{\omega}{c} = \frac{2\pi}{\lambda}$, c = velocity of light, and λ = wavelength in free-space. Equations (3-15), when written in terms of the propagation constant, become

$$\left.\begin{aligned} \nabla^2 \vec{E} - \gamma^2 \vec{E} &= 0 \\ \nabla^2 \vec{H} - \gamma^2 \vec{H} &= 0 \end{aligned}\right\} \tag{3-16}$$

Equating the coefficients of E (or H) in (3-15) and (3-16)

$$\gamma = j k K^{1/2} \tag{3-17}$$

Equating the real and imaginary parts of (3-17), expressions for

the attenuation and phase constants are obtained.

$$\frac{\alpha}{K} = \sqrt{\frac{|K| - K_r}{2}} = A \tag{3-18}$$

$$\frac{\beta}{k} = \sqrt{\frac{|K| + K_r}{2}} = B \tag{3-19}$$

In deriving Equations (3-13), (3-18), and (3-19) several simplifying assumptions were made: 1) a wave solution to Maxwell's equations does not consider near field effects in the plasma; 2) the wave solution used requires that the medium be linear, which means that the electron velocity distribution in the plasma must not be significantly affected by the presence of the RF fields; 3) the electromagnetic wave radiated from the vehicle cannot usually be described in terms of a plane wave; 4) in general, the medium is inhomogeneous during re-entry since the temperature and density vary considerably through the shock layer.

In order to satisfy the second requirement of the preceding paragraph, the electric field strength for signals above UHF frequencies must satisfy (Reference 18)

$$\vec{E} \leq 1.5 \times 10^{-5} \; f \sqrt{T} \quad \frac{\text{volts}}{\text{centimeter}} \tag{3-20}$$

where $f = \omega/2\pi$ = the signal frequency in megacycles; T = gas temperature in degrees Kelvin.

Universal Representation of Electromagnetic Parameters

Following the procedure of Bachynski (Reference 19) one can construct a universal chart for mapping the properties of the plasma. Normalization is made with respect to frequency or to plasma frequency.

1) Normalizing with respect to frequency:
   $S = \nu/\omega$ = normalized scattering frequency
   $N = (\omega_p/\omega)^2$ = normalized electron density
2) Normalizing with respect to plasma frequency
   $C = \nu/\omega_p$ = normalized collision parameter
   $F = \omega/\omega_p$ = normalized RF frequency

Use of these relationships permits the mapping of loci of constant scattering frequency S, constant electron density N, constant collision parameter C, or constant RF frequency F on the complex dielectric constant plane as on the complex propagation constant plane.

For the case of the complex dielectric constant plane, it can be shown that the loci of constant S are a series of straight lines with slope -S and K_r intercept of 1. Similarly the loci of constant N are a series of circles with center at $[(1 - N/2), 0]$ and radius N/2. The loci of constant F are circles with centers located at $[(1 - 1/(2F)^2), 0]$. Loci of constant C must be determined from the rather complicated expression

$$K_i = (1 - K_r)\left(\frac{1}{C^2(1 - K_r)} - 1\right)^{-1/2} \qquad (3\text{-}21)$$

Families of curves of constant scattering frequency and constant electron density are shown in Figure 3-20, while curves of constant collision parameter and constant RF frequency are shown in Figure 3-21.

Representation of the normalized parameters can be accomplished in the complex propagation plane. It can be shown that the defining equations for such representations are:

$$S = \frac{2AB}{1 - (B^2 - A^2)}, \qquad (3\text{-}22a)$$

or

$$B^2 - A^2 + \frac{2AB}{S} = 1 \qquad (3\text{-}22b)$$

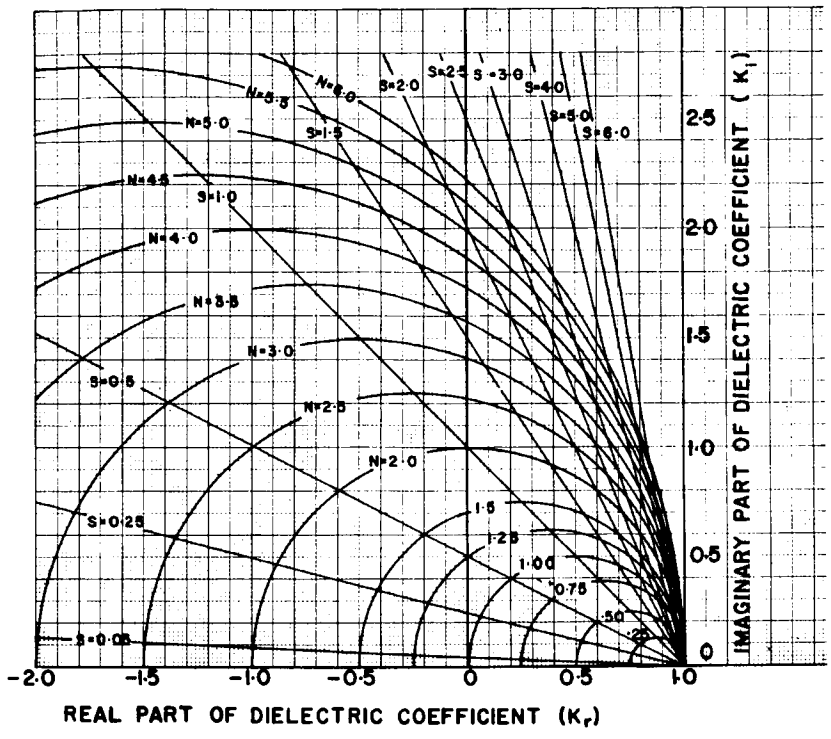

Figure 3-20 - Variation of Normalized Scattering Frequency and Electron Density in Complex Dielectric Coefficient Plane

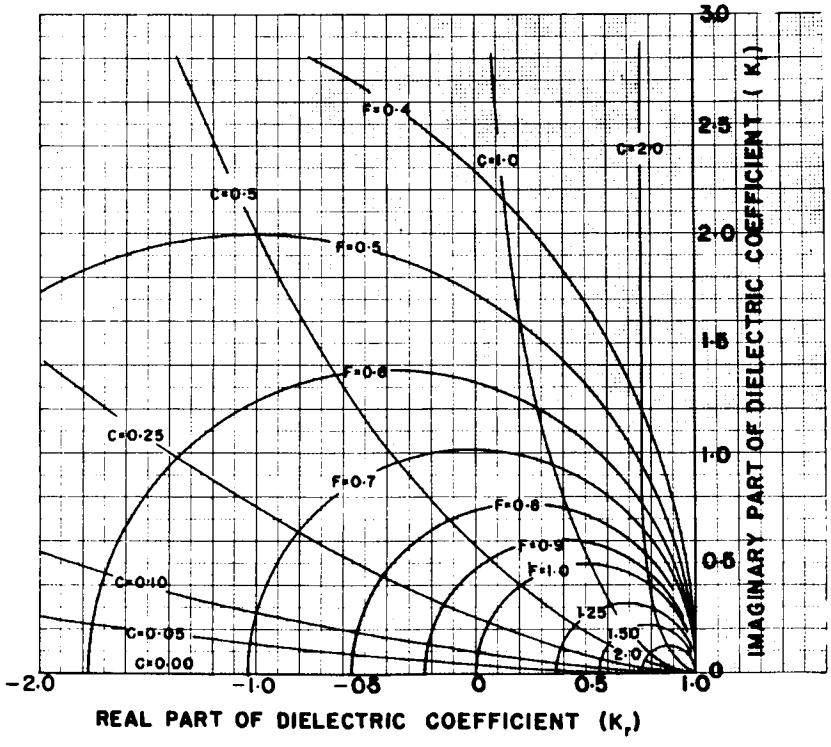

Figure 3-21 - Variation of Normalized Collision Parameter and RF in Complex Dielectric Coefficient Plane

$$N = 1 + A^2 - B^2 + 4A^2 B^2/(1 + A^2 - B^2), \tag{3-23a}$$

or

$$(A^2 + B^2)^2 - (2-N)(B^2 - A^2) + (1 - N) = 0 \tag{3-23b}$$

Since $C^2 = S^2/N$, Eqs. (3-22a) and (3-23a) are used to obtain an expression for C in terms of A and B (A and B being defined by Eqs. (3-18) and (3-19)). Also since $F = N^{-1/2}$, Eq. (3-23a) can be used to define F in terms of A and B.

Contours of constant S and constant N in the complex propagation constant plane are shown in Figure 3-22, and plots of constant C and F in Figure 3-23. Extended values of these parameters are shown plotted on a logarithmic scale in Figures 3-24 and 3-25.

Once the collision, plasma, and signal frequencies are specified it is a simple matter to determine the attenuation and phase constants from the graphs of Figure 3-22 through 3-25. Usually the quantities of interest, however, are the reflection and transmission coefficients, which are functions of the attenuation and phase constants and the depth of the plasma.

In terms of previously defined quantities, the complex reflection coefficient is given by

$$R = \frac{(K^{-1/2} - K^{1/2}) \sinh \gamma d}{2 \cosh \gamma d + (K^{-1/2} + K^{1/2}) \sinh \gamma d} \tag{3-24}$$

where d is the thickness of the plasma sheath, and R is the complex reflection coefficient.

Similarly, the complex transmission coefficient is given by

$$T = \frac{2}{2 \cosh \gamma d + (K^{-1/2} + K^{1/2}) \sinh \gamma d} \tag{3-25}$$

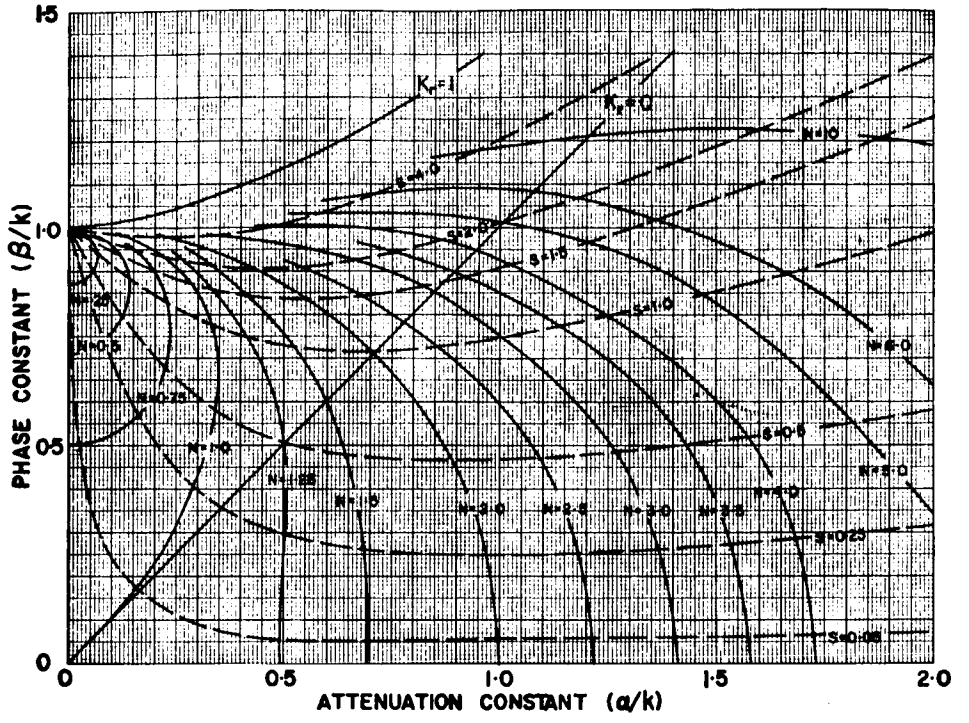

Figure 3-22 - Variation of Normalized Scattering Frequency and Electron Density in Complex Propagation Constant Phase

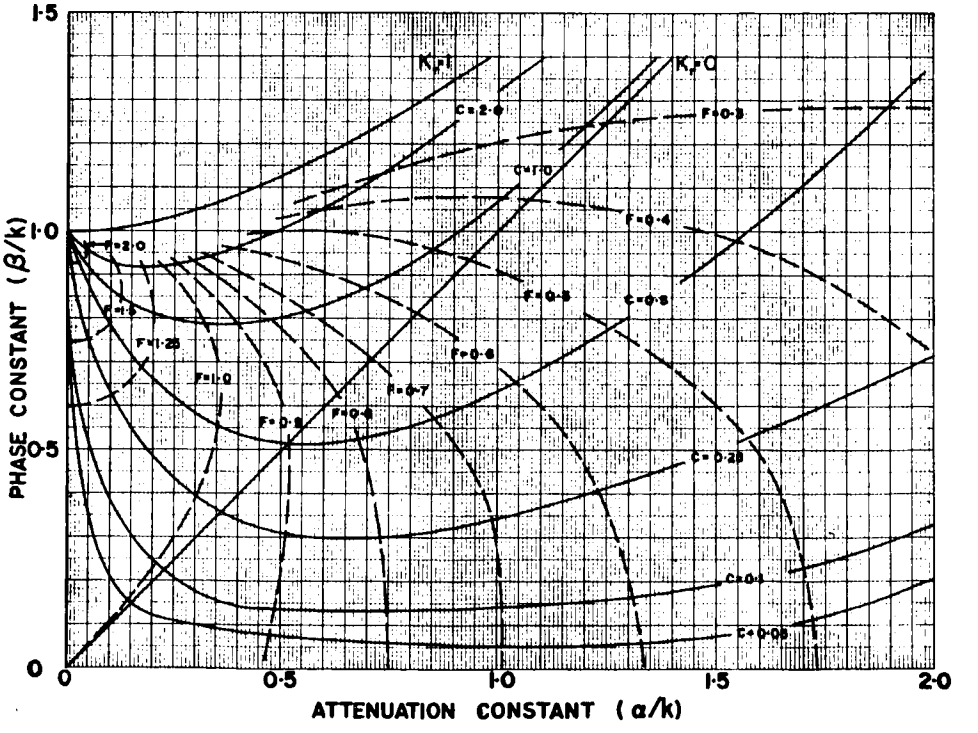

Figure 3-23 - Variation of Normalized Collision Parameter and RF in Complex Propagation Constant Plane

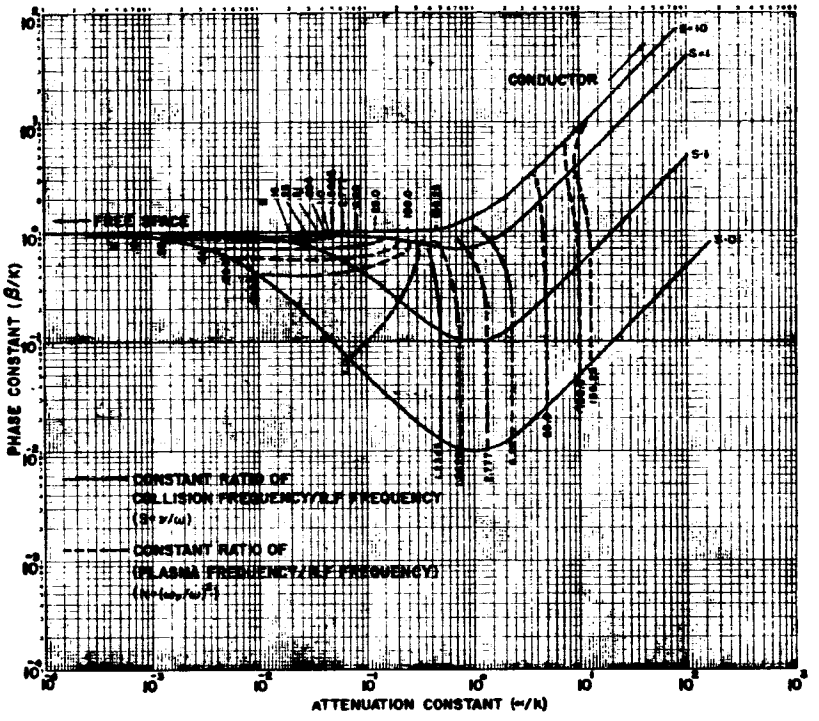

Figure 3-24 - Variation of Normalized Scattering Frequency and Electron Density in Complex Propagation Constant Plane (Extended)

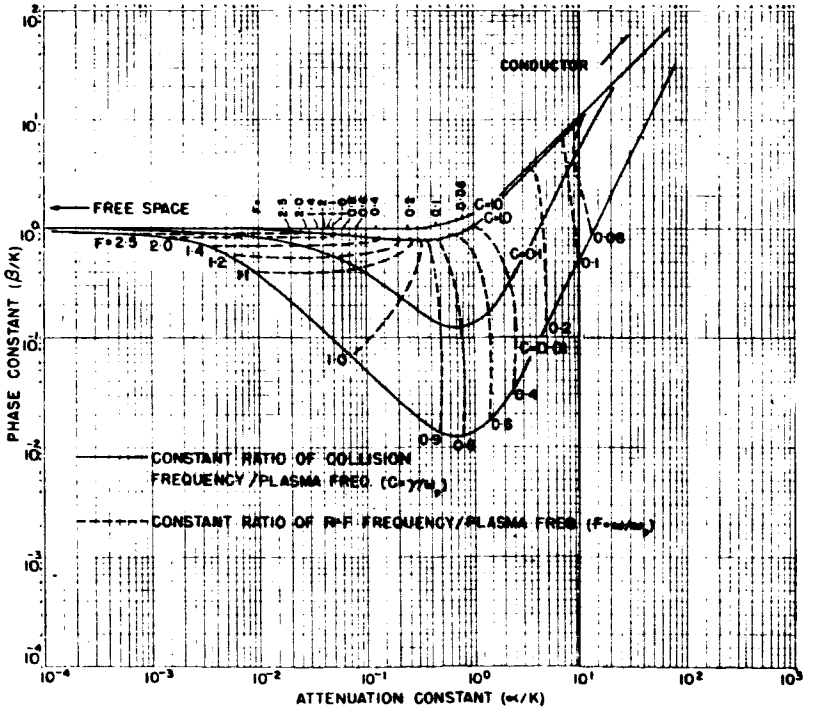

Figure 3-25 - Variation of Normalized Collison Parameter and RF in Complex Propagation Constant Plane (Extended)

where T is the complex transmission coefficient.

The fraction of the incident power which is reflected from the plasma is obtained by taking the magnitude of R and squaring it. Similarly, the fraction of the incident power which is transmitted is obtained by taking the magnitude of T and squaring it.

If K in (3-24) and (3-25) is expressed as a function of α and β, (3-24) and (3-25) can be simplified to yield (Reference 20)

$$|R|^2 = (L^2 + M^2)\,(\sinh^2 \alpha\, d + \sin^2 \beta\, d)\;|T|^2 \tag{3-26}$$

and

$$|T|^2 = \Big[(P^2 + Q^2)\,(\sinh^2 \alpha\, d + \sin^2 \beta\, d) + P \sinh^2 \alpha\, d + \sinh^2 \alpha\, d + \cos^2 \beta\, d - Q \sin \alpha\, \beta\, d \Big] \tag{3-27}$$

where

$$P = \frac{\beta}{2k} \cdot \frac{(k^2 + \alpha^2 + \beta^2)}{(\alpha^2 + \beta^2)}$$

$$L = \frac{\beta}{2k} \cdot \frac{(k^2 - \alpha^2 - \beta^2)}{(\alpha^2 + \beta^2)}$$

$$Q = \frac{\alpha}{2k} \cdot \frac{(k^2 - \alpha^2 - \beta^2)}{(\alpha^2 + \beta^2)}$$

$$M = \frac{\alpha}{2k} \cdot \frac{(k^2 + \alpha^2 + \beta^2)}{(\alpha^2 + \beta^2)}$$

Determination of the Plasma and Collision Frequencies

In the previous section expressions for the attenuation and phase constants were given at a function of the plasma, collision and signal frequencies. In addition, expressions for the transmission and reflection coefficients of a plasma were given in terms of the attenuation and phase constants. All of these calculations hinge upon the determination of the plasma and collision frequencies. The purpose of this section is to outline the method used to obtain these properties as a function of temperature for air at different densities.

The method of constant free path (Reference 21) which assumes the mean free path of electrons to be independent of electron velocity is used here to calculate the collision frequency. Making this assumption, the collision frequency for a Maxwellian distribution of electron velocities at high RF frequencies becomes (Reference 22)

$$\nu = \bar{C} \sum n \quad Q \tag{3-28}$$

where n = number density of the nth specie; Q = Maxwell-averaged total electron collision cross-section of the specie; $\bar{C} = \frac{4}{3}\sqrt{\frac{8KT}{\pi m}}$; K = Boltzmann's constant.

With the collection cross-sections of the neutral species as given by Massey and Burhop (Reference 23) and calculating the conductivity due to electron-ion collisions (References 24 and 25) from

$$\sigma_{ion} = \frac{1.1632\, m}{\ell n\left(\frac{h}{b_o}\right)} \left(\frac{4\pi\epsilon_o}{e}\right)^2 \left(\frac{2KT}{\pi m}\right)^{3/2} \tag{3-29}$$

where

$$h = \left(\frac{KT\, 4\pi\epsilon_o}{8\pi n e^2}\right)^{1/2}, \quad b_o = \frac{e^2}{(4\pi\epsilon_o)(3KT)}$$

The variation of collision frequency with temperature and density were calculated using (3-28). The results appear in Figure 3-26.

Attenuation and Phase Constants

The normalized attenuation and phase constants for air in thermal equilibrium are shown as a function of temperature and density for RF frequencies of 1, 10, and 100 Gc in Figures 3-27 and 3-28 respectively.

The frequency dependence of the normalized attenuation and phase constants is illustrated in Figures 3-29 and 3-30 for gas temperatures of three thousand, six thousand, and twelve thousand degrees Kelvin and for air densities of 10^{-4}, 10^{-3}, 10^{-2}, and 10^{-1} that of atmospheric, as well as air at its normal density.

Variation of Electron Density and Collision Frequency at the Stagnation Point of a Re-entry Vehicle as a Function of Velocity with Altitude as a Parameter

The electron density and collision frequency of a plasma are determined by the temperature and density of the ionized shock layer which are both functions of the vehicle ballistic coefficient and re-entry angle. In an attempt to maintain reliable communication during re-entry the antenna or antennas are located in a relatively "cool" region of the vehicle i.e., a location away from the stagnation region.

An analysis of the electron density and collision frequency distributions in a region other than the stagnation region is made difficult by the fact that the temperature and density distributions of the shock are not very well-known. However, it may be instructive to determine the propagation characteristics of an electromagnetic wave in the stagnation region of the vehicle for two reasons: 1) assuming thermal equilibrium the thermodynamic properties in this region can be deduced from aerodynamic considerations; 2) this is the region of most dense plasma and hence the most critical condition for penetration of an electromagnetic wave.

Figure 3-31 shows the variation of plasma frequency and collision frequency at the stagnation point of a hypersonic re-entry vehicle with velocity at various altitudes above the earth. The ARDC model of the

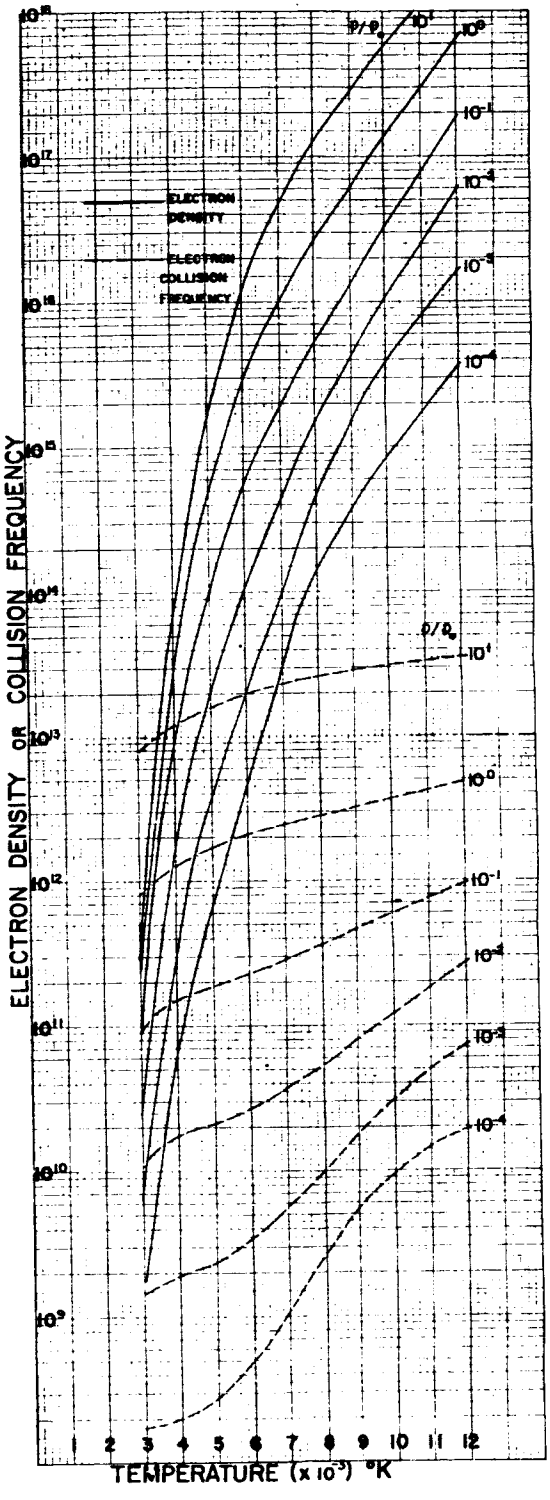

Figure 3-26 - Variation of Electron Density and Collision Frequency with Air Temperature

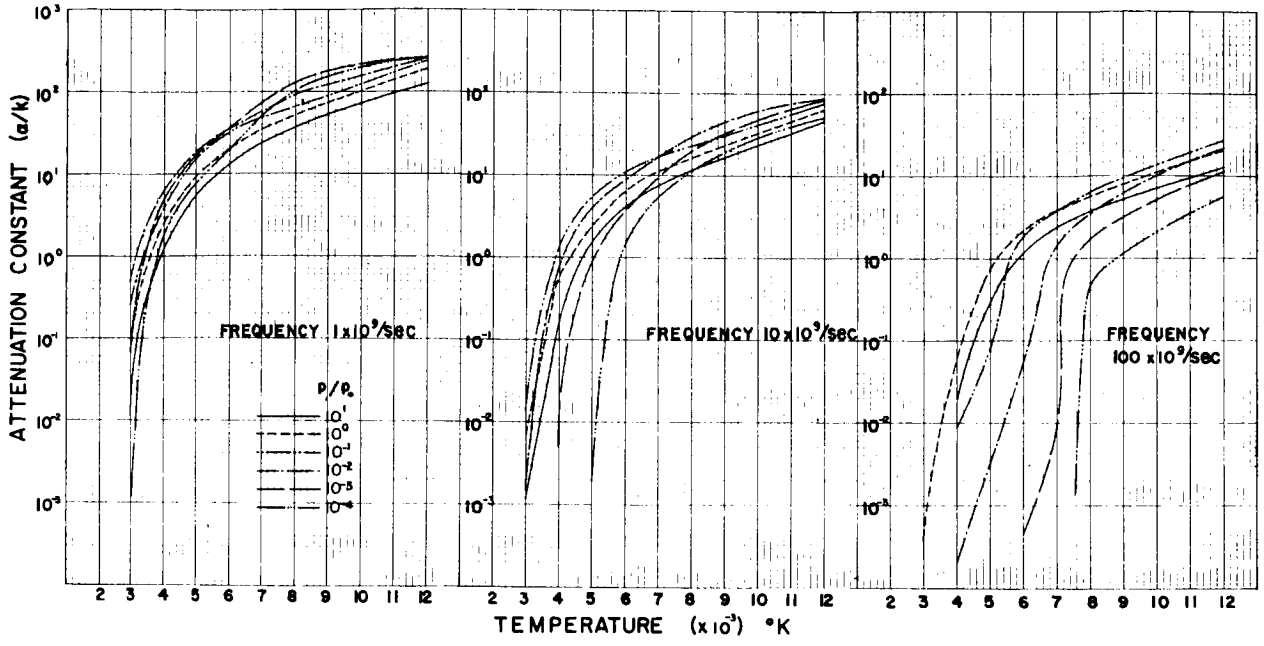

Figure 3-27 - Dependence of Attenuation Constant on Temperature and Density of Air

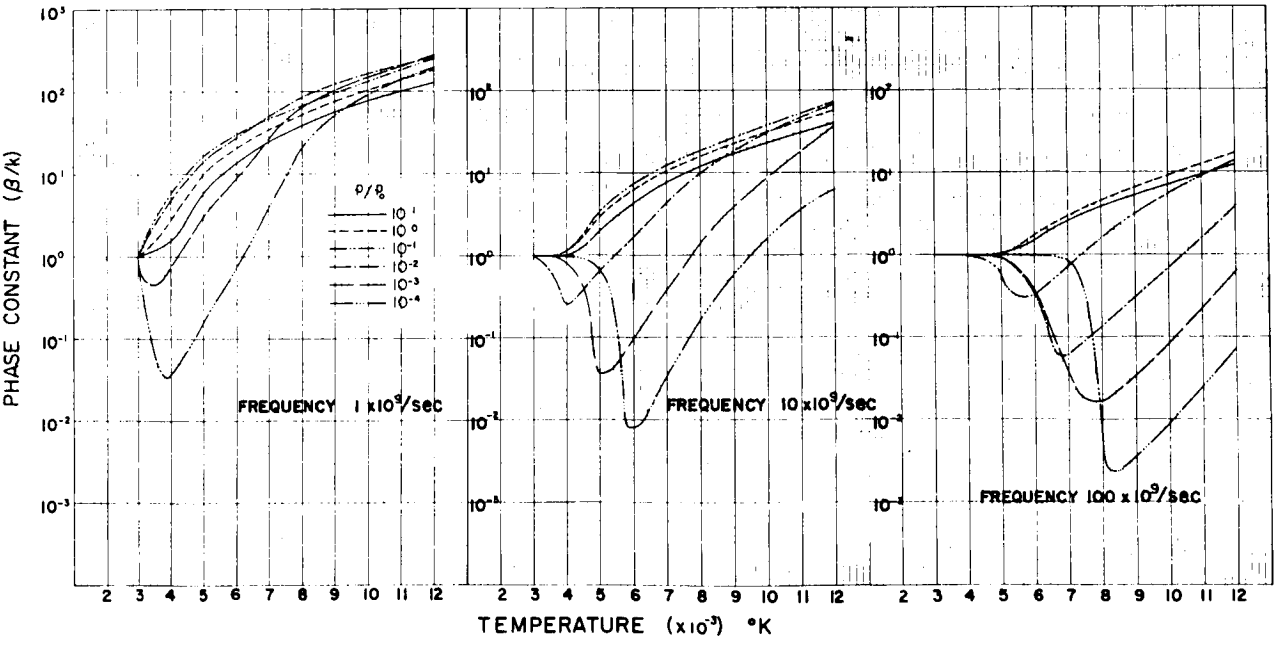

Figure 3-28 - Dependence of Phase Constant on Temperature and Density of Air

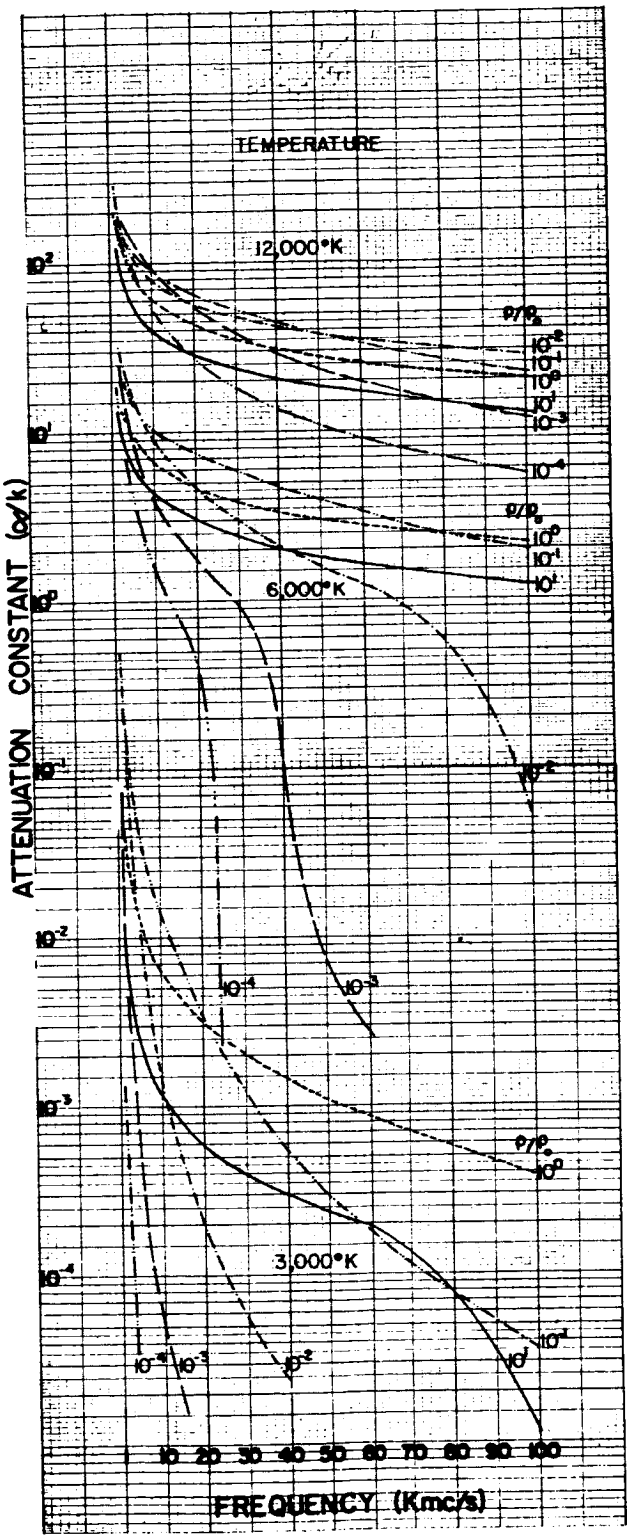

Figure 3-29 - Dependence of Attenuation Constant on Frequency for High Temperature Air

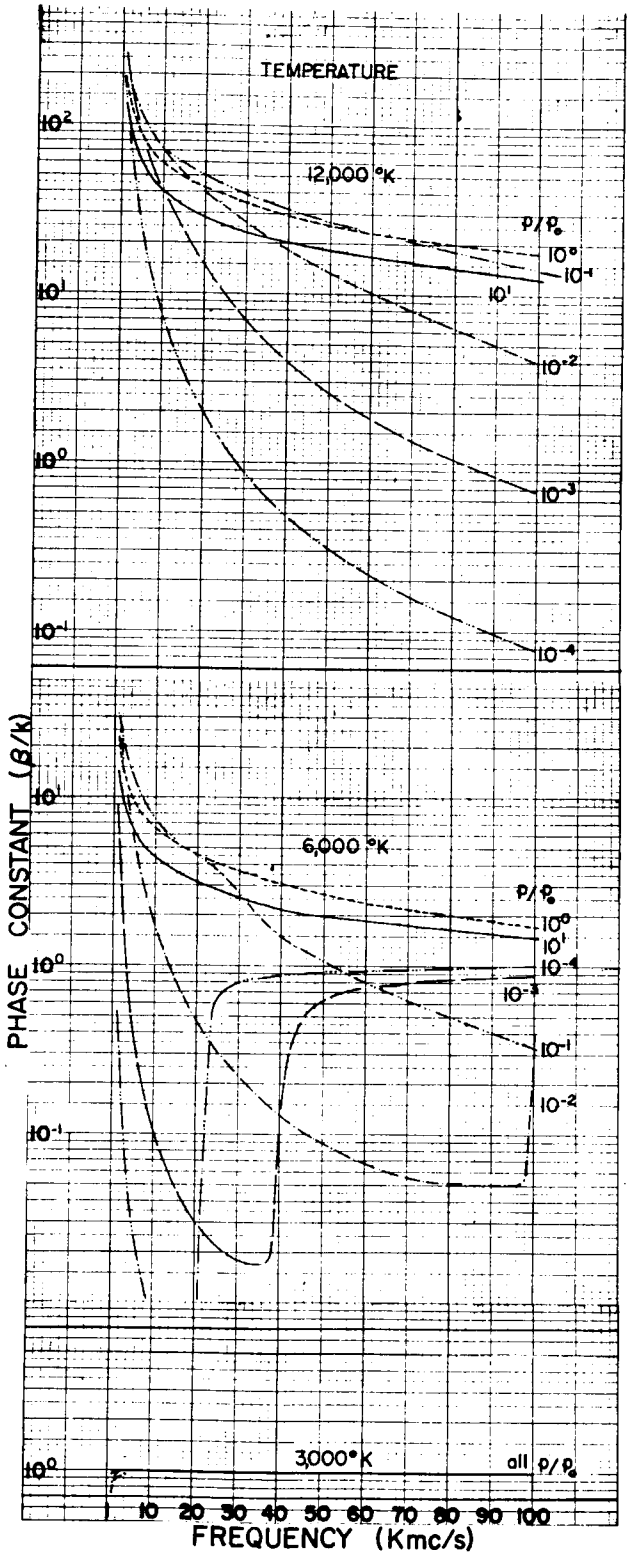

Figure 3-30 - Dependence of Phase Constant on Frequency for High Temperature Air

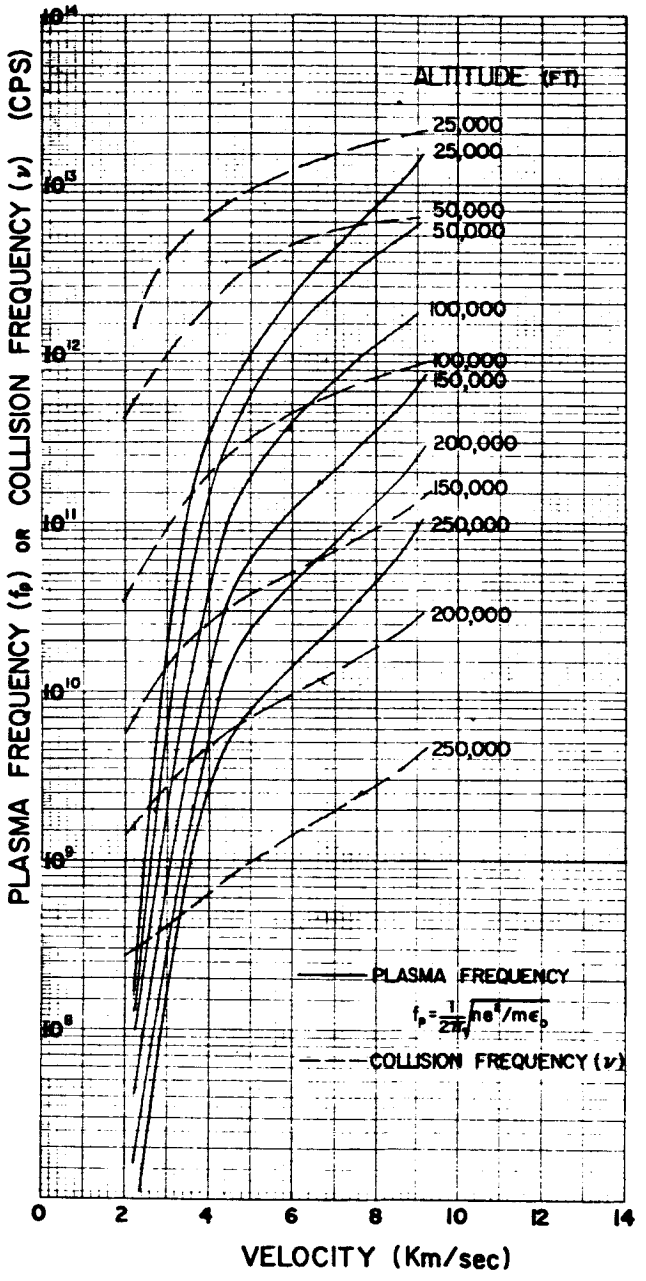

Figure 3-31 - Variation of Plasma Frequency and Electron Collision Frequency with Velocity at the Stagnation Point of a Hypersonic Vehicle

atmosphere was used in the aerodynamic considerations (Reference 26).

In order to determine the maximum plasma and collision frequencies from Figure 3-31 it is necessary to know the variation in velocity with altitude for the re-entry vehicle. The velocity of the vehicle is a function of: 1) its initial velocity at some reference altitude; 2) its ballistic coefficient; 3) re-entry angle.

Making several simplifying assumptions it can be shown that the re-entry vehicle velocity as a function of altitude is given, approximately, by

$$v = v_o e^{\frac{\rho_o \csc \psi \, e^{-\mu h_o}}{2 \mu \phi}} \quad e^{\frac{\rho_o \csc \psi \, e^{-\mu h}}{2 \mu \psi}} \qquad (3\text{-}30)$$

where v_o = vehicle velocity at altitude h_o; ρ_o = density of air = .081 lb/ft^3; ψ = re-entry angle; μ = air density gradient = 4.15 x 10^{-5}/ft; ϕ = ballistic coefficient.

As an example, assume a re-entry vehicle velocity of 22,000 feet per second at an altitude of 200,000 feet, a re-entry angle of 15 degrees, and a ballistic coefficient of 500. Eq. (3-30) can be rewritten as

$$v = 22{,}000\, e^{-7.53\, e^{-4.15 \times 10^{-5} h} \cdot \left(e^{\frac{\rho_o \csc \psi \, e^{-\mu h_o}}{2 \mu \phi}} \approx 1 \right)} \qquad (3\text{-}31)$$

The velocity as a function of altitude is given in Table 3-IX.

Table 3-X contains data on the plasma and collision frequencies for these conditions

It is obvious from Table 3-X that if one attempted to propagate directly through the stagnation region an extremely high rate of attenuation

TABLE 3-IX

VELOCITY AS A FUNCTION OF ALTITUDE

Altitude (feet)	Velocity (ft/sec)	Velocity (km/sec)
150,000	21,650	6.6
100,000	19,300	5.87
50.000	8,550	2.61

TABLE 3-X

FREQUENCY OF PLASMA AND COLLISION

Altitude (ft)	Velocity (km/sec)	Plasma Frequency (fp)	Collision Frequency ($\nu/2\pi$)
200,000	6.7	7×10^{10} cps	1.2×10^{10} cps
150,000	6.6	1.8×10^{11} cps	6×10^{10} cps
100,000	5.87	4×10^{11} cps	4.8×10^{11} cps
50,000	2.61	2×10^{9} cps	7×10^{11} cps

would occur. Usually, the antenna will be located in a region well aft of the stagnation region where the electron density will be considerably lower. Unfortunately, it is difficult to determine the plasma and collision frequencies at a point other than the stagnation region because, as was pointed out earlier, the temperature and density distributions of the shock are not well-known. The plasma and collision frequencies are functions of the velocity and altitude, as is the thickness of the plasma. Furthermore, the plasma is not of uniform density, which further complicates the determination of attenuation.

In principle, if one knows the signal, plasma, and collision frequencies and the thickness of the plasma (assuming it to be of uniform density), it is relatively simple to determine the reflection and transmission coefficient for the altitudes specified. Once the plasma and collision frequencies are normalized to the signal frequency, the attenuation and phase constants can be read from the graphs of Figure 3-22 through 3-25. Eqs. (3-26) and (3-27) can then be used to compute the reflective loss and total insertion loss (dissipative and reflective).

Because of the difficulty of specifying the plasma parameters no attempt will be made to make a computation of the losses involved. It is to be noted however, that for RF frequencies above the plasma frequency the plasma behaves more or less like a dielectric, the lossiness of which is determined by the collision frequency. At frequencies well below the plasma frequency, the plasma behaves like a very good conductor, while at frequencies around the plasma frequency, cutoff or very high attenuation and reflection occur so that the wave cannot penetrate the plasma to any great extent.

Because of the uncertainties in the plasma parameters for a typical re-entry condition, it is evident that the use of extremely high frequency signal transmission is desirable, emphasizing the importance of millimeter waves in communications, particularly during re-entry.

3.6.2 Other Factors Affecting Microwave Communications

Antenna Noise Temperature in Plasma Environment (Reference 20)

A receiving antenna in a space vehicle is subjected to three main sources of external noise on re-entry, namely, RF emission from the plasma sheath, noise emission from the hot surface of the vehicle which finds its way into the receiving antenna and noise sources external to both the vehicle and the plasma.

An illustrative example is worked out in Reference 20. In the example it is assumed that the plasma possesses the following properties:

Electron density - n - 4×10^{12} electrons/cm^3

Collision frequency - 1.12×10^9/sec

Plasma thickness - 4.18 cm

Plasma temperature - 5,000°K

Re-entry vehicle temperature - 500°K

Earth Temperature - 300°K.

The total effective noise temperature is shown to be

$$T_n = A_\omega T_p + R_\omega T_v + T_\omega T_{ex} \qquad (3\text{-}31)$$

where T_n = the effective noise temperature (°K); T_p = The plasma temperature (°K); T_{ex} = the temperature of any source external to the vehicle and the plasma, in this case the earth, in degrees Kelvin; A_ω = the absorptivity = $1 - |R|^2 - |T|^2$; R_ω = the reflectivity = $|R|^2$; T_ω = the transmissivity = $|T|^2$; R and T are defined by Eqs.(3-24) and (3-25).

The transmissivity, reflectivity, and absorptivity were computed for the parameters given, as a function of (ω/ω_p). Knowledge of these constants permitted the computation of the effective noise temperature as a function of (ω/ω_p). The results are shown graphically in Figure 3-32.

The important thing to note is the sudden rise in the effective antenna temperature in the vicinity of $\omega/\omega_p = 1$, which implies a degradation in receiver sensitivity when the plasma and signal frequencies

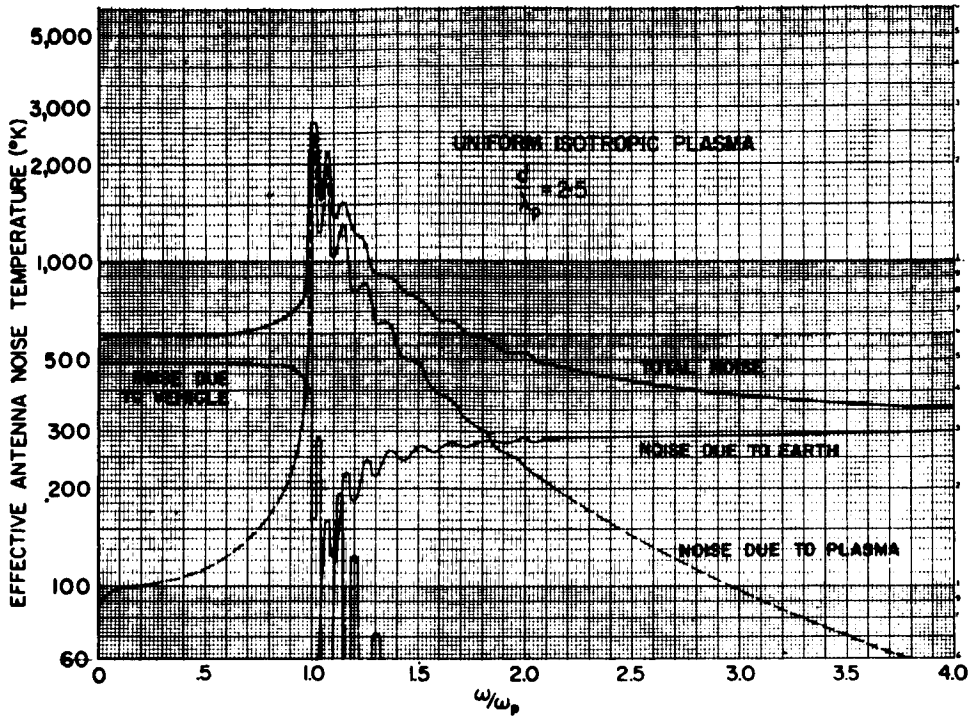

Figure 3-32 - Effective Noise Temperature for a Hypersonic Space Vehicle (Isotropic Plasma with $\nu/\omega_p = 10^{-2}$ and $d/\lambda_p = 2.5$)

are approximately equal. For this case, high attenuation and reflection both occur. Thus, there are two reasons for operation at a signal frequency much greater than the plasma frequency.

Antenna Breakdown at High Altitudes

Antenna breakdown in air at high altitudes has been computed by MacDonald and others. The results of MacDonald's calculations appear in Figure 3-33 (Reference 27). It is apparent from Figure 3-33 that there is an obvious advantage to transmission at the higher frequencies as far as the breakdown problems is concerned.

In computing the breakdown field strength as a function of altitude for the curves of Figure 3-33, the effects of external ionization were not taken into account. Whitmer and MacDonald (Reference 28) have calculated breakdown fields as a function of altitude under the influence of the ionization

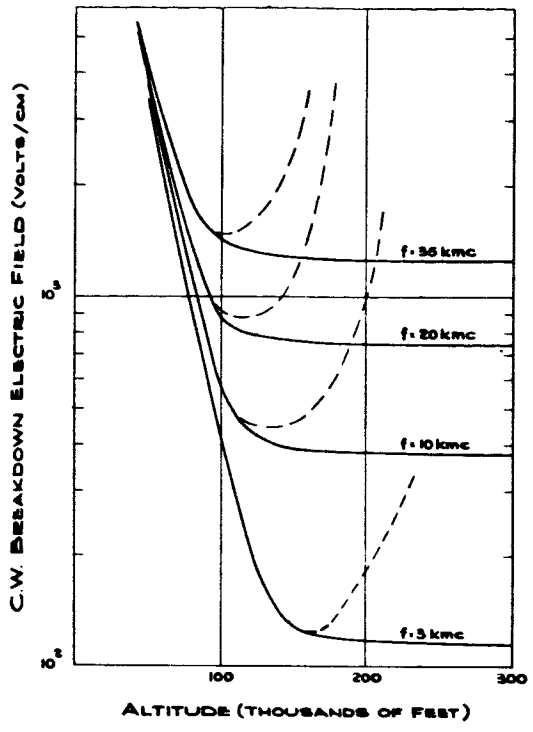

Figure 3-33 - CW Breakdown Threshold Electric Field vs Altitude (solid line, Λ very large; dashed line, $\Lambda = \lambda/2$)

produced by a shock wave, for various velocities, nose-cone angles and RF frequencies. The general conclusions of this study are: 1) the pressure increase due to the buildup of the shock wave tends to shift breakdown conditions to higher altitudes and to cause breakdown more readily; 2) breakdown fields increase as the frequency increases.

Scharfman and Morita (Reference 29) have investigated experimentally the effect of a plasma upon the breakdown characteristics of an antenna. In one experiment a slot antenna was excited with 373 mc radiation and a dc discharge was maintained at the antenna window. The equivalent electron densities were such as to yield plasma frequencies which were approximately 1/2 and 1 times the signal frequency.

For Figure 3-34 where the plasma frequency is approximately one-half the RF frequency, the attenuation is negligible and transmitted and reflected power increase directly with the incident power. Breakdown occurs at 4.5 watts. For Figure 3-35, where the plasma frequency is approximately

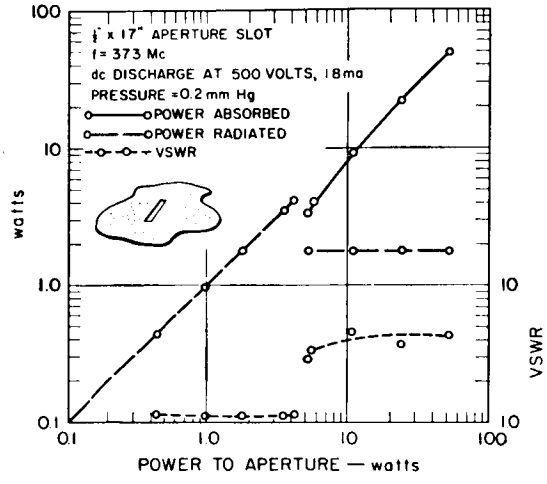

Figure 3-34 - Power Handling Characteristics of a Slot Antenna in the Presence of a 500 v dc Discharge

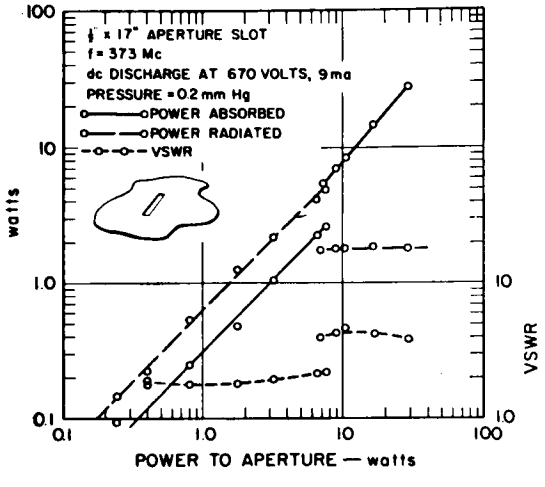

Figure 3-35 - Power Handling Characteristics of a Slot Antenna in the Presence of a 670 v dc Discharge

equal to the RF frequency, RF attenuation and an increase in the voltage standing wave ratio occur prior to breakdown which, in this case, is at 7 watts. The slot antenna dimensions are one-half inch and seventeen inches.

Similar measurements were made with pulsed power at 9.4 Gc with both a dc discharge and a 300 mc RF discharge used as sources of ambient ionization. An X-band waveguide 0.4 by 0.9 inch, with a dielectric window was used as the antenna. The electron density produced by either discharge was sufficiently low, so that negligible absorption occurred prior to breakdown. Without the plasma, a 2 kilowatt peak power level was required for breakdown. With the plasma, breakdown occurred at a peak power level of 1 kilowatt.

3.6.3 Summary

The effects of a plasma on communications have been discussed with regard to: 1) attenuation of signal; 2) degradation of receiver sensitivity; 3) maximum breakdown power level. It is concluded that the use of millimeter wave communications systems is optimum in that: 1) the attenuation of the plasma decreases with increasing frequency; 2) the degradation in receiver sensitivity is negligible when the signal frequency is greater than the plasma frequency; 3) the breakdown power level increases with increasing frequency. Experimental evidence indicates that antenna breakdown is not a problem for the satellite transmitter power levels contemplated in the millimeter wave communications program.

BLANK PAGE

4. DEFINITION OF BASIC MEASUREMENTS

In this section AM, PAM and PAM/FM test waveforms are discussed from an analytical point of view. It is explained how basic signal measurements, which are derived from the use of these waveforms can be used to infer performance of various modulation systems. Also discussed are the basic correlative measurements required to describe the condition of the atmosphere and explain why certain things are happening to the signals.

4.1 Measurement Waveforms

In order to determine the performance of the satellite-to-ground, ground-to-satellite link at millimeter wave frequencies when various types of analog and digital modulations are used, it is necessary to know the characteristics of the link. In order to know the characteristics of the link, or equivalently of the channel, it is desirable to obtain a reasonable model for the channel and, in turn, a measure of the parameters specifying the channel model. A somewhat detailed description of a general channel model that can represent any communications link was given in the Raytheon proposal (Reference 30) and is reprinted in Appendix III. A description of the anticipated channel model for the millimeter communication link is given in Section 4.2. Here we shall only summarize some of the pertinent characteristics which describe the channel. These are:

1) The multipath structure of the channel.
2) The dispersion introduced by each of the multipaths.
3) The time variations of gain and delay for each of the multipaths.

4) The amplitude and phase characteristics as a function of frequency for the overall channel.

5) The noise characteristics of the channel.

Knowledge of the above characteristics would give a fairly complete description of the channel. In particular, it would give the total coherence bandwidth, the selective fading, and the amplitude fading of the channel. Other factors, not included in the above model, which are also of interest are the spatial decorrelation distance, the polarization diversity exhibited by the channel, and any angle diversity introduced by the channel. Knowledge of all of the above characteristics, as a function of meteorological conditions, location of the ground system and the elevation and velocity of the satellite, would provide a basis for determining the performance of the communications system using various types of modulations.

Ideal waveforms can be specified which give a measurement of the first four characteristics listed above. Such a waveform would have an impulse-like characteristic which enables it to measure the scattering function of the channel. A detailed discussion of optimum test waveforms and their properties has been given in BR-3011 (Reference 30). In this section waveforms are presented which, although not optimum, provide information on the channel characteristics that apply for determining the system performance for most modulations of interest. Three types of test waveforms are considered. These are an AM waveform with two side bands, a PAM test waveform which is a time quantized pulse amplitude modulated waveform, and a PAM-FM test waveform, which involves modulating the FM carrier with a PAM waveform. Where possible it would be desirable to design the system so that it could transmit as many of these waveforms as possible in a programmed manner.

4.1.1 AM Test Waveform

The simplest waveform under consideration consists of an amplitude modulated carrier. The carrier is modulated by a single sinusoidal signal so as to produce two sidebands, one below and one above the carrier, each a distance away from the carrier equal to the modulation frequency. The modulation index is made as close to 100 percent as is deemed safe without risking the possiblility of distortion due to having a modulation greater than 100 percent.

This type of test waveform is most suitable when the processing is to be done aboard the satellite with the transmitter on the ground, as is expected to be the case for the 94 Gc experiment. For this situation the receiver in the satellite would filter out the carrier and phase lock a satellite signal to the incoming carrier waveform. The phase lock signal is used in order to enable measurements of the phase shift of each of the sidebands relative to the carrier signal. The phase shifts are measured in both magnitude and sign. In addition to measuring the phase shifts of the sidebands, the amplitudes of the sidebands as a function of time would be measured. The amplitude of the carrier as a function of time would also be measured. The time between samples would be determined by the coherence and the strength of the transmitted signal. It is expected that the integration time required in order to obtain a good signal-to-noise ratio for the receiver signal is from 0.01 to 0.1 seconds. Hence the time between the samples of the phase and amplitudes of the carrier and side bands would be in the same range.

The amplitude modulated test waveform just described has the advantage of providing a measure of the phase and amplitude transfer characteristics of the channel at three frequencies on one measurement. By using a different modulation frequency for different measurements,

the transfer characteristics can be obtained over different points in the channel bandwidth. Considerations are being given to modulating with various signals between 5 mc and 50 mc to measure the coherence bandwidth for high data rate systems and perhaps with a 5 kc signal to measure the characteristics for the channel for a telemetry signal. The University of Texas has proposed the use of a single sideband test waveform for measuring the coherence bandwidth of the atmosphere over a ground link of about 6 miles. Such a waveform would not be as desirable as amplitude modulation since it would only give a measure of the amplitude of the channel transfer characteristic at two frequencies after one measurement and would not give any phase information.

The circuitry by which the test waveform can be used to obtain the sum of the phase shifts introduced on each sideband is presented in Section 7.5. An alternate method involving the use of a frequency discriminator was also described in Appendix IV which gives a reprint of Section 3.5 of the Raytheon proposal. This information will provide data on the coherence bandwidth of the channel, the distribution of the fading of the channel and the time autocorrelation function of the fading.

It is important to point out that a measurement of the channel characteristics can be obtained almost as readily with the use of AM waveforms as with the optimum test waveform. That is, theoretically the same information can be obtained about the channel with measurements involving the use of AM test signals as with the ideal test waveforms. To show this, a calculation is made of the cross correlation of the sidebands of the return signal. Assume that the scintillation introduced by the j^{th} path is $n(t, \tau_j)$ where t is time and τ_j is the propagation delay time for the j^{th} path. (It is assumed that complex envelope function representation is being used - Reference 31). Then the received signal for the upper sideband of frequency $+\Delta f/2$ relative to the carrier is

$$s_+(t) = \sum_{i=1}^{m} n(t, \tau_i)\, e^{j\pi \Delta f(t - \tau_i)} \qquad (4\text{-}1)$$

The above can be approximated by an integral given by

$$s_+(t) = \int_0^T n(t, \lambda)\, e^{j\pi \Delta f(t - \lambda)}\, d\lambda. \qquad (4\text{-}2)$$

The parallel expression for the lower sideband is

$$s_-(t) = \int_0^T n(t, \lambda) e^{j\pi \Delta f(t - \lambda)} d\lambda. \qquad (4\text{-}3)$$

The two-frequency correlation function (Reference 32) for the channel is defined as

$$R(\Delta f, \tau) = \overline{s_+(t)\, s^*_-(t - \Delta)}.$$

From (4-2) and (4-3) it follows that

$$R(\Delta f, \tau) = \left[\int_0^T \phi(\tau_1, \lambda) e^{-j2\pi \Delta f \lambda} d\lambda\right] e^{j2\pi \Delta f t - j\pi \Delta f \tau} \qquad (4\text{-}4)$$

$$\phi(\tau, \lambda) = \overline{n(t, \lambda)\, n^*(t - \tau, \lambda)} \qquad (4\text{-}4a)$$

Physically $\phi(\tau, \lambda)$ represents the autocorrelation function of the component of the return from a path having a propagation delay of λ. In obtaining (4-4) it is assumed that the fluctuations introduced by separate paths are independent. For this assumption, $\phi(\tau, \lambda)$ completely describes the channel characteristics.

The exponential terms outside the brackets can be dropped to yield finally

$$R(\Delta f, \tau) = \int_0^T \phi(\tau, \lambda) e^{-j 2 \pi \Delta f \lambda} d\lambda \qquad ((4-5)$$

Hence obtaining several measures of $R(\Delta f, \tau)$ by using AM signals with different modulating frequencies gives us the autocorrelation function $\phi(\tau, \lambda)$, since $\phi(\tau, \lambda)$ is equal to the inverse transform of $R(\Delta f, \tau)$. The two-frequency correlation function can be shown to be also related to the scattering function and tap-gain correlation function for the channel (Reference 32).

A discussion of the data processing requirements centering around the use of the AM waveform is given in Appendix V.

4.1.2 PAM Test Waveform:

The AM test waveform described above has the advantage of providing the transfer characteristics of the channel as a function of frequency. The test waveform also provides information on selective frequency fading if such fading exists and information on the coherence bandwidth and multipath structure of the channel. From this information the performance of various modulations can be determined for the channel under consideration. However, rather than indirectly obtaining information on the performance of various modulations from transfer characteristic measurements it would be more desirable to measure the effects on the types of modulations to be used directly and from these obtain an indication of the performance of channel for these modulations. To do this, it is desired to use a test waveform which comes as close as possible to the actual types of modulations to be used. In particular, if a PAM/AM waveform is to be transmitted, then a test waveform which is similar to a PAM/AM waveform should be transmit-

ted. In this way it can be determined directly if the channel has sufficient bandwidth to carry the PAM/AM waveform under consideration by measuring the rise time, pulse width and increase in sidelobe level. Such a test waveform is suggested in this subsection. The PAM test waveform under consideration applies to other types of modulation as well as PAM/AM modulation. In particular, it would provide an indication of how well the system performs for PAM, PWM, PPM, PWM/AM, and PPM/AM. The test waveform involves the transmission of narrow pulses and at the same time permits transmission at the same power level as with the AM signal and to utilize the same integration time.

The waveform involves the transmission periodically of a narrow pulse. The pulsewidth is made as narrow as possible and the duty cycle for the pulse train is chosen to be about 0.1. At present the receiver appears to be limited to a bandwidth of about 100 mc. Hence, a reasonable pulsewidth appears to be about 10 nanoseconds and the time between pulses would be about 100 nanoseconds. Figure 4-1a shows the amplitude modulation on the carrier signal applied by the test waveform. The spectrum for the test waveform is shown in Figure 4-1b.

The question arises as to how to process the signal in order to remove the noise. In order to suppress the noise from the waveform, a processor is used in the receiver which is essentially a matched filter. It is noted from Figure 4-1b that the spectrum of the test waveform consists of a line spectrum. About 90 percent of the total signal energy is contained in the spectral lines within the band from -100 mc to +100 mc. Nearly all the energy would be contained within a bandwidth from -200 mc to +200 mc. Assume that a 10-cycle integration filter was required to process the received signal if no modulation were placed on the carrier, that is, if only the carrier were transmitted and all the energy were in the carrier. To process the modulated waveform, 10-cycle filters are

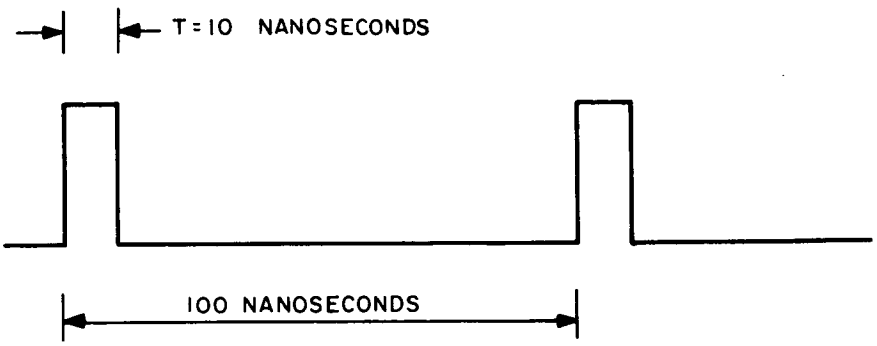

a. Amplitude Modulation

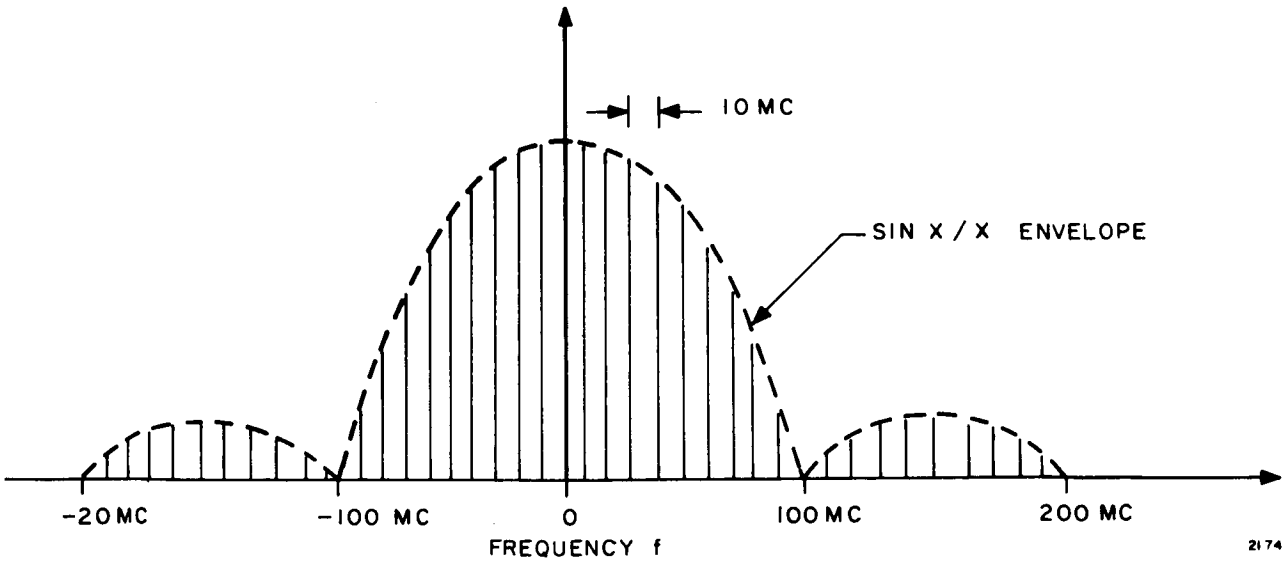

b. Line Spectrum

Figure 4-1. AM Test Waveform

placed at each line in the spectrum shown in Figure 4-1b. For the modulation specified about a total of 40 filters would be required in the receiver. By adding the outputs of these filters the received pulse train could be obtained without the noise, or at least with a low noise level. The outputs of the filters are weighted before adding. In particular, greater weight is given to the filters in which the signal-to-noise ratio is larger. In other words, the weights are in proportion to the signal-to-noise ratios anticipated for each of the filters. In an actual train of 10 nanosecond pulses, the line spectrum would not, of course, extend out as far as indicated. Instead, because of rounding of the pulses, the line spectrum would drop off faster so that fewer than 40 receiver filters would be required.

To determine how effective the receiver comb filter processor is in suppressing the noise, a comparison needs to be made of the signal-to-noise ratio obtained with the pulse amplitude modulation test waveform described above (and its receiver processing) with the signal-to-noise ratio achieved if only the carrier were transmitted and all the energy of the transmitted waveform were in the carrier and a 10-cycle integration filter were used for the carrier signal. To do this the $\frac{\sin x}{x}$ envelope for the line spectrum of the test waveform given in Figure 4-1b shall be approximated by a rectangular envelope extending from -50 mc to +50 mc. Hence, to process the signal in the receiver 11 filters would be required with signal-to-noise ratio in each filter being the same at the receiver. Since there are 11 filters, the noise at the output of the summer will be 11 times greater than the noise at the output of one filter or, in particular, 11 times greater than the noise for the CW system. The signal power at the output of the summer will be the same, however. Hence the average signal power-to-noise ratio at the output of the summer will be 1/11 that for the case where just the carrier is transmitted and all the energy is in the carrier. However, since the duty cycle is 0.1 during the time when

the signal peaks, the signal power-to-noise ratio will be 10 times greater than the average; hence, the signal power-to-noise ratio for the pulse amplitude modulated test waveform is about the same as for the case when just the carrier is transmitted.

Of course the above conclusion applies only if for a given prime power the same average output power can be achieved for the CW and pulse system. This would be the case if a hard tube or power line type modulation system is used for the generation of the pulse train. However, in the event that an RF line modulator is used to generate the train, the output power is reduced by the duty cycle of the pulse system.

Due to the complexity of the receiver processor for the pulse amplitude modulated test waveform, this waveform could be used only for down transmission from the satellite, where the processing would be done on the ground receiver. The parameters given above for the test waveform correspond to testing out the performance of the channel for a high data rate system, or for a time multiplex telemetry system. In order to check out the performance anticipated for one channel of a frequency multiplexed telemetry system, a modulation in which the pulse width is 200 microseconds and the time between pulses is 2 milliseconds would also be transmitted.

The data observed on the received signal would be the rise time, the pulsewidth, the sidelobe level, and the fading rate of the signal. Computations would be made of the probability distribution of the fading and the time autocorrelation function of the fading.

4.1.3 PAM/FM Test Waveform:

In many systems frequency modulation is used. For example in the Applications Technology Satellite (ATS) program the communications

system uses wide band 4 Gc and 6 Gc FM/FM TV links. Other types of FM considered for satellite applications are PAM/FM, PWM/FM, PCM/FM, and PPM/FM. A test waveform is described in this subsection which comes close in form to the type of FM to be considered in many of the satellite applications. As in the case of the PAM/AM test waveform it is possible with this test waveform to operate at the same transmitter power level and integrate between 0.01 and 0.1 seconds in order to suppress the background noise.

One of the frequency modulations for the carrier being considered is shown in Figure 4-2. The period T shown in the figure is made as narrow as possible. Due to the receiver limitations already mentioned, it appears that the minimum period, T, is about 40 nanoseconds to take advantage of the noise suppression characteristics of FM by using a modulation index of three and at the same time remains in a 100 mc bandwidth.

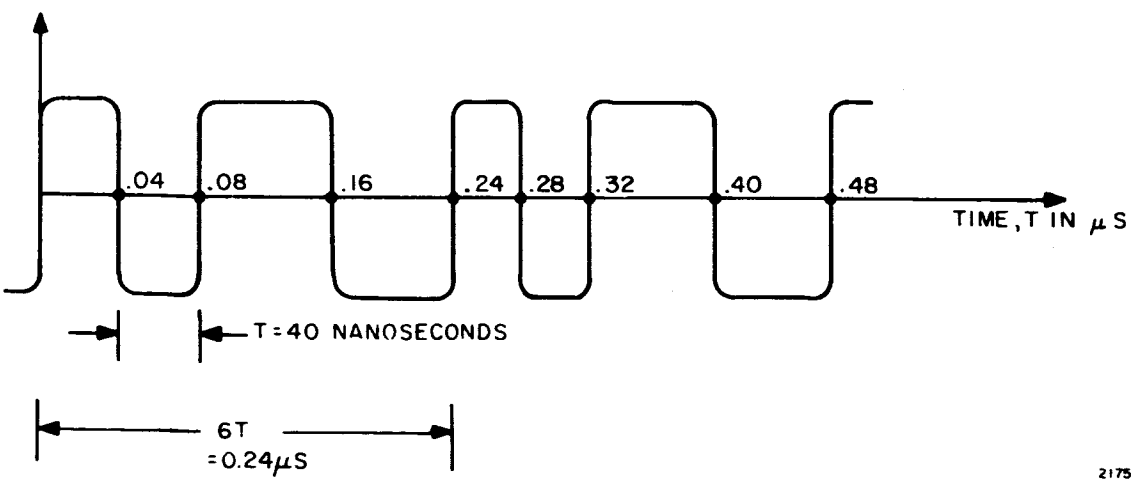

Figure 4-2 Frequency Modulation

For this modulation index and for the above mentioned pulsewidth of 40 nanoseconds, the signal bandwidth would be about 25 percent larger than the total deviation of 75 mc. To arrive at this anticipated bandwidth use is made of the results obtained by Corrington (Reference 33) as to the bandwidth for various modulations. In particular, the bandwidth is approximated to be equal to the bandwidth obtained for a triangular modulation, the results obtained for a triangular modulation being somewhat worse than for a sinusoidal modulation. Figure 4-3 shows the curve for the increase in bandwidth above the total deviation for the case where the carrier is modulated by a triangular waveform. The figure gives the signal bandwidth as a function of the modulation index. Three different types of signal bandwidths are given. These are indicated by curves A, B and C. Curve A gives the signal bandwidth occupied by the triangular wave modulated carrier which is defined as the distance between the two frequencies beyond which none of the side frequencies is greater than 1

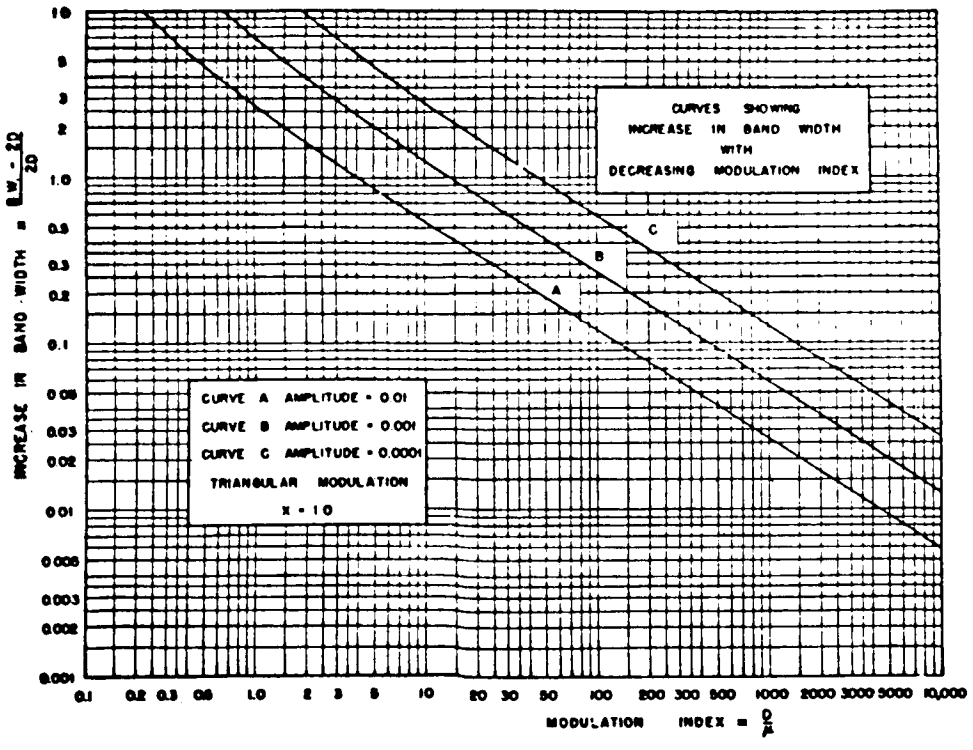

Figure 4-3. Variation of Bandwidth with Modulation Index

percent of the carrier amplitude obtained when the modulation is removed. Curves B and C give the bandwidth defined as the distance between two frequencies beyond which none of the side frequencies is greater than 0.1 and 0.01 percent, respectively. For 100 mc bandwidth receivers it is apparent from the figure that a bandwidth specified by curve A is being used in the system.

The receiver processor for the FM waveform would be similar to that used for the PAM test waveform. Figure 4-4 gives a rough sketch of the line spectrum for the FM test waveform. Most of the energy in the test waveform is anticipated to be centered about the frequencies ±25 mc away from the carrier frequency. The major portion of the energy should be in about 11 tones about the frequencies -25 mc and +25 mc away from the carrier. A total of about 80 filters would be required in the receiver in order to process essentially all the signal energy. Weightings would be

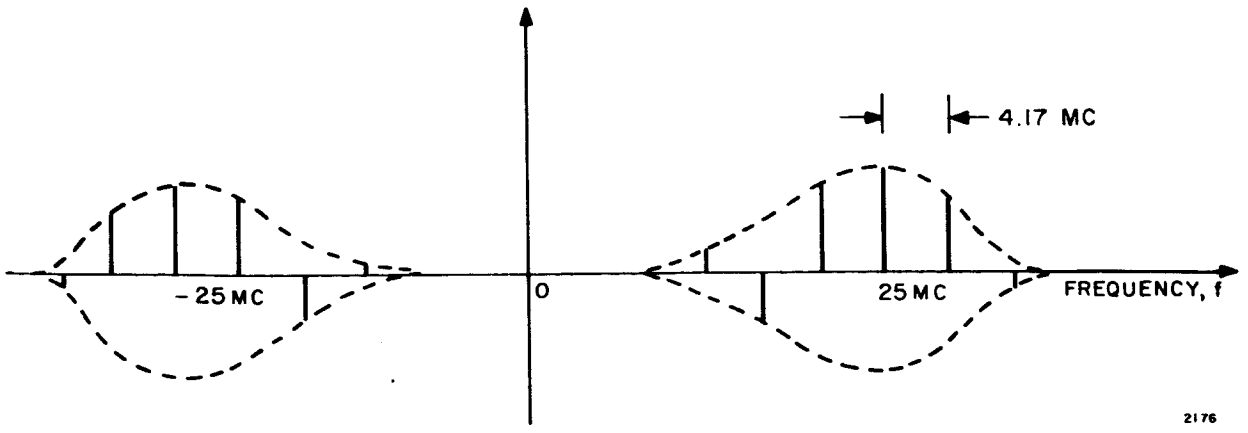

Figure 4-4. Line Spectrum of Frequency Modulation

used at the output of each filter before the summation takes place. The weightings would be proportional to the signal-to-noise ratios anticipated for each of the filter tones. The FM test waveform can be expected to yield a signal-to-noise ratio at the output of the processor not far below that obtained if a CW waveform were transmitted with the same energy contained in the FM test waveform. This arises from the noise suppression due to the comb filtering and the inherent noise suppression of an FM system.

The waveform parameters given above correspond to those that would be used to test out the channel for high data rate systems. For checking the performance of the channel for telemetry data transmitted on a PCM/FM or similar modulation, the period T would be made equal to 200 microseconds.

Other basic types of modulation waveforms for the FM carrier are possible. However, the one given in Figure 4-2 seems to be the most suitable. One reason for this is that as much of the energy as possible is placed at the frequencies with maximum deviation from the carrier, with as little energy as possible being placed at the carrier frequency. This is desirable since when the signal is at the carrier frequency, the output of the FM discriminator is zero, being at the carrier corresponding to having a zero modulation signal or a zero output so that all the energy at the carrier would be wasted as far as the modulation waveform is concerned. Since no phase locking is employed in the receiver when an FM test waveform is used, this does not offer any disadvantage because the receiver uses frequency locking.

As in the case of the PAM test waveform, measurements are made on the demodulated waveform of its rise time, pulse width, and sidelobe levels. Also, measurements are made of the fading of the signal.

These measurements would enable the determination of the distribution of the fading and its time autocorrelation function.

4.2 System Performance

Based on the measurements made with the test waveforms specified above, data on the characteristics of the channel will be determined from which the performance of the channel for various modulation can be inferred. Before giving these results, predictions of the channel fading and multipath characteristics will be given. The multipath structure of the channel shall be described and then the various parameters specifying the multipath structure predicted.

The multipath structure for the channel arises primarily from inhomogeneities (both random and non-random) in the atmosphere. For very low elevation angles, multipathing can arise from ground reflections. However, in the discussion that follows, this type of multipathing is neglected. At millimeter wavelengths the beamwidths and sidelobe levels of the antennas under consideration are such that multipathing from ground reflections will be small.

The multipathing represents the arrival of the signal at the receiver antenna via different propagation paths. These propagation paths will have different gains and different propagation times. Moreover, the gains and propagation times for these paths will vary with time in a random manner. As a result the signal at the summation point in the receiver will be formed from constructive and destructive interference of the signals from the various paths. The random variations of the propagation times will cause random fading of the sum signal.

4.2.1 Multipathing Phenomena

There are several phenomena which give rise to multipathing in the atmosphere. One phenomenon arises from scattering, in particular, scattering from blobs distributed randomly in the atmosphere. These scattered rays interfere with the direct rays. For large size antennas, a second phenomenon giving rise to multipathing results from the fact that there can exist two direct paths separated far enough from each other so that they see completely different inhomogeneities. Multipathing arising from non-random inhomogeneities in the atmosphere was discussed in Section 3.5. In the following, consideration is only given to the effects on system performance of multipathing arising from the first two phenomena mentioned above.

Figure 4-5, which illustrates the multipathing arising from scattering, indicates the direct ray and the scattered ray. The received signal

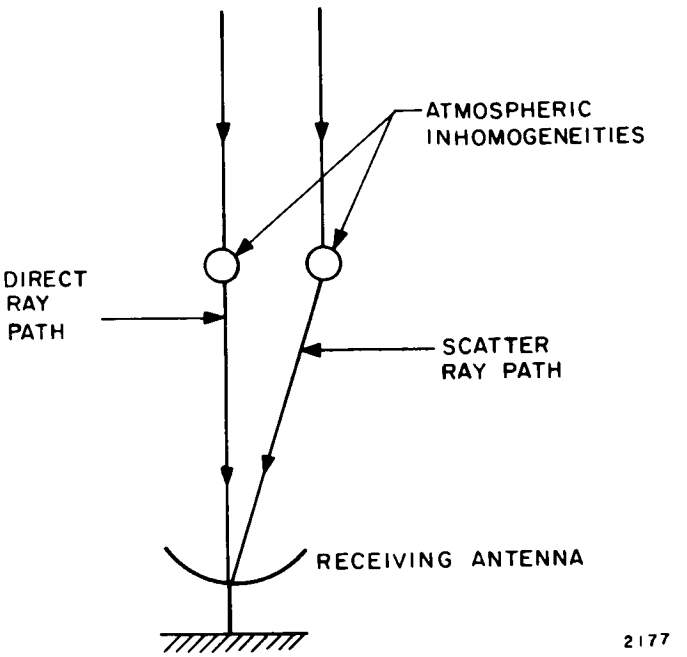

Figure 4-5. Scatter Paths

will consist in this case of the major return from the direct ray path plus the returns from the scatter paths. Generally, the scatter returns will arrive after the direct path return. Furthermore, the return via the direct path will be very much larger than that from the scatter paths in general and will not be scintillating. The difference in delay between the direct and scatter paths is very small. In particular, based on a first order Born approximation, Muchmore and Wheelon (Reference 17) to be much less than a nanosecond (the contribution resulting from higher order terms is not known).

It is convenient to total the contributions from the scatter paths. Due to the fact that there are many scatter paths and the returns from each scatter path will add up in random phase, the contribution from the scatter paths will consist of a randomly fluctuating term in the receiver. This randomly fluctuating term can be expected to have a Gaussian distribution as far as its instantaneous voltage is concerned and a Rayleigh distribution as far as its envelope is concerned. It follows from the above discussion that if only the multipathing due to scattering from inhomogeneities in the atmosphere is considered the return signal can be written as

$$e_r(t) = s(t - \tau)\left[\alpha\, e^{-j\delta} + \beta\, e^{-j\epsilon}\right] \qquad (4\text{-}6)$$

where

- $s(t)$ = the transmitted signal
- τ = the propagation time
- α = the amplitude of the return received over the direct path
- δ = the phase of the return received over the direct path
- β = the instantaneous amplitude of the sum of the scattered signals
- ϵ = the phase of the sum of the contributions from the scattered terms

The quantity α is non-random; δ will have a slow random variation which will be discussed later; β has a Rayleigh distribution; ϵ has a uniform distribution. The variance of β is designated here for convenience as 2σ. The ratio of the intensity of the direct term and the sum total of the scatter terms is dependent on the elevation angle of the satellite. Estimates of the ratios of these two terms can be obtained from the results of Bergmann (Reference 34).

These results were given in the Raytheon proposal and are repeated in Appendix V. It was shown that for vertical propagation, in which case the path length is about 10,000 yards, the rms intensity of the fluctuations of the received signal is only 0.05 db. This implies that the combinations from the scatter components is only about one-half percent of the contribution from the direct path. For low elevation angles the same theory predicts that the depth of the amplitude fading would be about 0.8 db. Hence for low elevation angles (elevation angles resulting in path lengths of about 60,000 yards), the contributions from the scattering in the atmosphere can be appreciable.

The multipathing from the second phenomenon is illustrated in Figure 4-6. Since the scale size for the inhomogeneities is of the order of 100, such multipathing would be observed for antennas having a size greater than 100 feet. Such an antenna is the Haystack antenna. If the antenna size is slightly over 100 feet, there will be more than one direct path, hence the return signal will have the form

$$e_r(t) = s(t-\tau)\left[\alpha_1 e^{-j\delta_1} + \alpha_2 e^{-j\delta_2} + \beta e^{-j\epsilon}\right] \qquad (4\text{-}7)$$

where the direct signal by two direct paths of intensities α_1 and α_2 and phase δ_1 and δ_2 have been approximated. Assuming that the satellite is at a low elevation angle such that the path through the atmosphere is

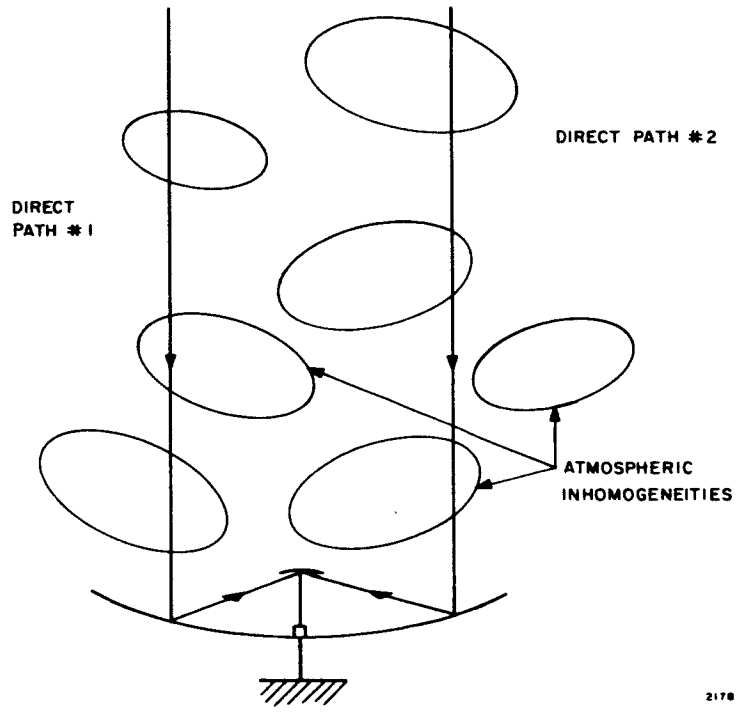

Figure 4-6. Direct Path Multipaths

100,000 feet and the scale size is 100 feet and that the intensity of the index fluctuations is of the order of 0.2 N units (this is a reasonable value based on results given by Crain, et al, Reference 35), it follows that the difference in delays between the two paths would be of the order of 0.6 nanoseconds.

The coherence bandwidth for the channel is determined by the multipath spread, that is, the maximum difference in delay between the earliest arriving signal and the latest arriving multipath signal. The analysis given by Muchmore and Wheelon (Reference 17) predicts that the multipath spread due to scattering should be less than a nanosecond. Although there is some question as to the validity of Muchmore and Wheelon's analysis, assume for the moment that their prediction is correct. As was pointed out above, the direct path multipath spread for

low elevation angles, where the path length is about 100,000 feet, can be expected to be of the order of 0.6 nanoseconds when very large antennas are used. Hence the expected coherence bandwidth with very large antennas can be 1500 megacycles at a minimum.

In addition to the amplitude variations mentioned above due to multipathing, there will be a variation of the direct path ray propagation time. The random variations of the direct ray propagation path will cause a random phase variation of the received signal carrier and a random doppler frequency variation of the received signal carrier. The results given in Section 3.3 indicate that the phase variation will be very slow and hence of no consequence. In particular, the phase variation is expected to be 120 degrees in one minute for a stationary beam due to a 10-foot per second wind velocity and not be much greater for beam tracking a satellite at an altitude of 6,000 miles. Such a slow variation in phase could easily be tracked by a phase lock receiver if need be. The doppler frequency introduced by the propagation path variations is expected to be about 1 cps based on results given in Section 3.3.

Consideration is now given to the effects of the channel performance on various modulations. First, consideration is given to the effect of fading on an FSK system. Next, the effects of large dispersions over the signal band on binary AM, PM and FM signals are given. Finally, the effects of multipathing on a wideband FM system are discussed.

4.2.2 Effects of Fading on FSK Systems

The results given by Turin (Reference 36) can be used to determine the performance of an FSK system in a fading channel, in particular, in a Rician channel which is characterized by the signal given by equation (4-6). The results are given in Figure 4-7. This figure gives the probability of error as a function of the average signal-to-noise ratio in the

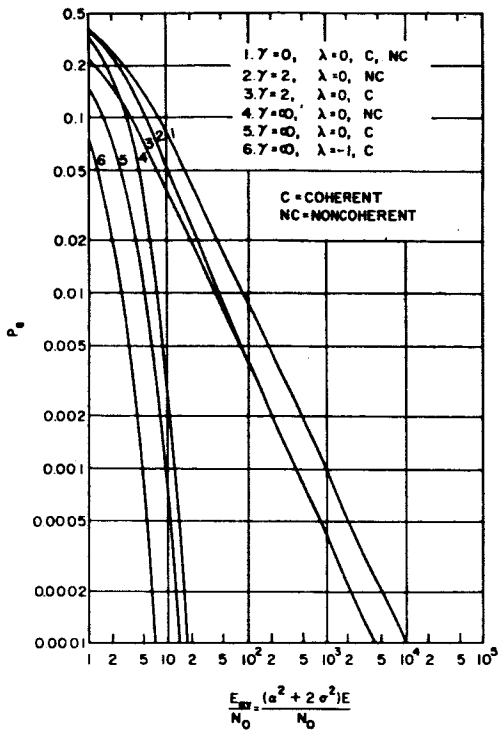

Figure 4-7. Comparison of Probability of Error Curves

receiver per binary received bit. The quantity γ represents the voltage ratio of the direct path term to the scattering term, in particular, $\gamma = \alpha/\sigma$. The quantity λ represents the complex cross-correlation coefficient between the two waveforms transmitted in a binary FSK system. $\lambda = 0$ corresponds to the case where the two signals are orthogonal, whereas $\lambda = -1$ corresponds to the case where the two signals are identical in form except that one is the negative of the other. The results are given in the figures for both cases of coherent and noncoherent receivers. The difference between the coherent and noncoherent receiver is that in the coherent receiver it is assumed that α and σ in equation (4-6) are known and that optimum use is made of the knowledge of these two parameters in the receiver processing. In the noncoherent receiver it is assumed that α and σ are not known and that the receiver processes the returned signal optimally on the basis of an unknown α and σ. Assume that it is desired

to design for a bit error rate of 10^{-3} when there is no random term, that is, when there is no scattering term so that $\gamma = \infty$. From Figure 4-7 it follows that the signal-to-noise ratio required in the receiver per bit is 5. For low elevation angles where γ might be assumed to be equal to 2, it is apparent from the curve that to maintain the same bit error rate, nearly a 100-fold increase in the transmitted power would be required.

The above discussion of course assumed that no diversity is used. If spatial diversity is used in the ground receiver system by the use of two antennas, then the increase in power required to maintain the same error rate would be considerably less. In particular, if two antennas are used having the same gain, instead of one, and maximum diversity ratio is used in the receiver, the results given by Lindsey (References 37 and 38) indicate that only a 2-fold increase in power is required to maintain the 10^{-3} error rate.

4.2.3 Effects of Large Delay Dispersion and Fading on Binary AM, and FM Systems

For a digital AM, PM, or FM system, the presence of multipathing or, equivalently, delay distortion will give rise to pulse distortion and resultant intersymbol interference. The same is true of time multiplexed systems such as PAM/AM and PAM/FM. In this section the distortion resulting from delay dispersion, as well as fading, on the error rate of binary AM, PM and FM systems is given.

Sunde (Reference 39) gives results on the increase in error rate for the above mentioned binary systems due to delay dispersion and fading. Sunde's results for assumptions on the channel do not apply completely to the mm channel under consideration. However, his results are close enough to serve as an estimate and in certain cases as a boundary to the error rates anticipated for the millimeter channel. He points out that the

error rate in the presence of fading, noise and delay dispersion is equal to the sum of the error rates when only delay dispersion is present, which he refers to as $P_e^{(1)}$, (no fading or noise is assumed present), plus the error rate due to the presence of fading and noise alone, which he refers to as $P_e^{(3)}$. The results are given by Sunde for the case where in the received signal there is only the fading term of Equation (4-6) that is, the signal is completely fading with $\gamma = 0$. Actually γ is expected to be slightly greater than zero hence, with respect to this assumption the results given by Sunde provide a lower bound on the error rates. For the results given, it is also assumed that all the multipath paths have equal gain and that there are an infinite number of multipaths having delays between the minimum and maximum delays.

Consider first the error due to delay dispersion. As a result of the linear delay dispersion shown in Figure 4-8, a pulse having a raised cosine spectrum will be distorted as indicated in the figure. In the figure, $\hat{B}$ equals the bandwidth of the pulse and $T = 1/\hat{B}$. The quantity d equals the delay dispersion at the edges of the signal band. The total delay dispersion, Δ, is equal to 2d. The resultant maximum reduction in tolerable noise (the noise margin reduction) is given in Figure 4-9 for a binary AM with envelope detection, binary FM with frequency discrimination detection, binary PM with synchronous detection. Using the results of Figures 4-8 and 4-9 and the distribution for Δ anticipated Sunde (Reference 39) obtains the following expressions for the error probability due to delay dispersion for binary AM, FM, PM (with a differential phase detection) systems.

$$P_e^{(1)} \doteq \frac{\Delta^2 \hat{B}^2}{6} \left[1 + \ell n \left(1 + \frac{3}{2\pi \Delta^2 \hat{B}^2} \right) \right] \qquad (4\text{-}8)$$

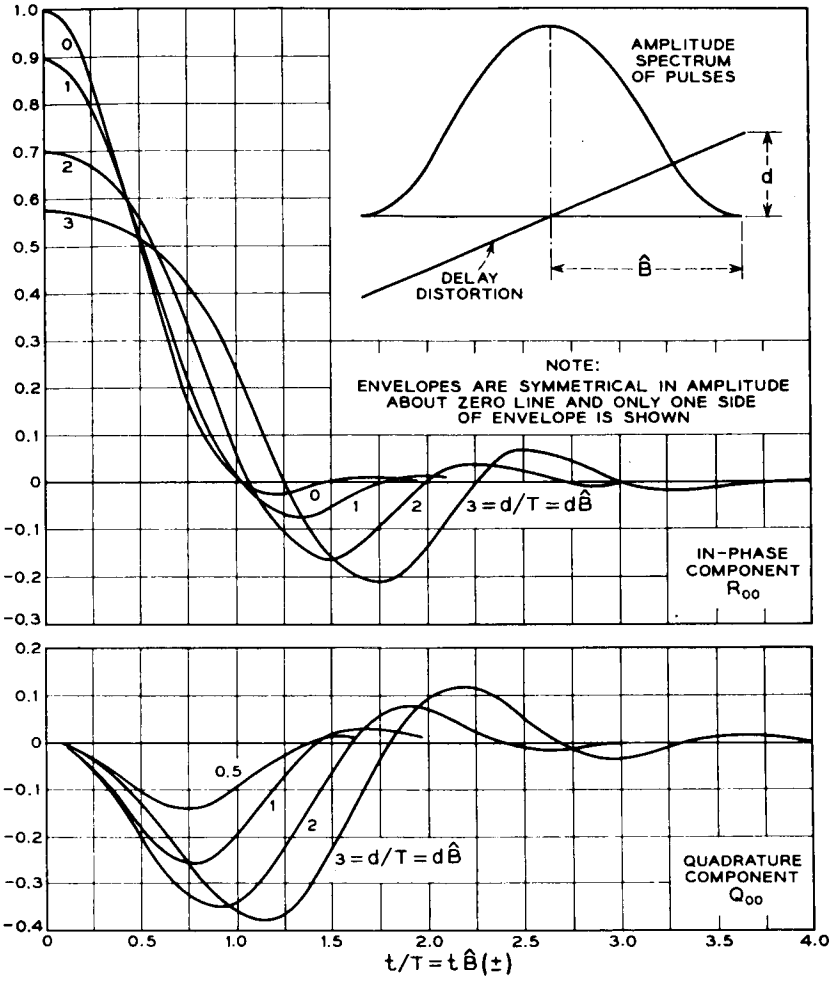

Figure 4-8. Pulse Distortion

For $\Delta = 1.0$ nanosecond and B = 100 mc equation (4-8) yields that $P_e^{(1)} = 8 \times 10^{-3}$.

The error due to Rayleigh fading and noise for the above AM, FM, and PM systems are, respectively

$$P_e^{(3)} \doteq \frac{1}{2}\left[\frac{\ell n\,\bar{\rho}}{\rho - 1} + \exp\left(-\ell n\,\rho\right)\right] \qquad (4\text{-}9)$$

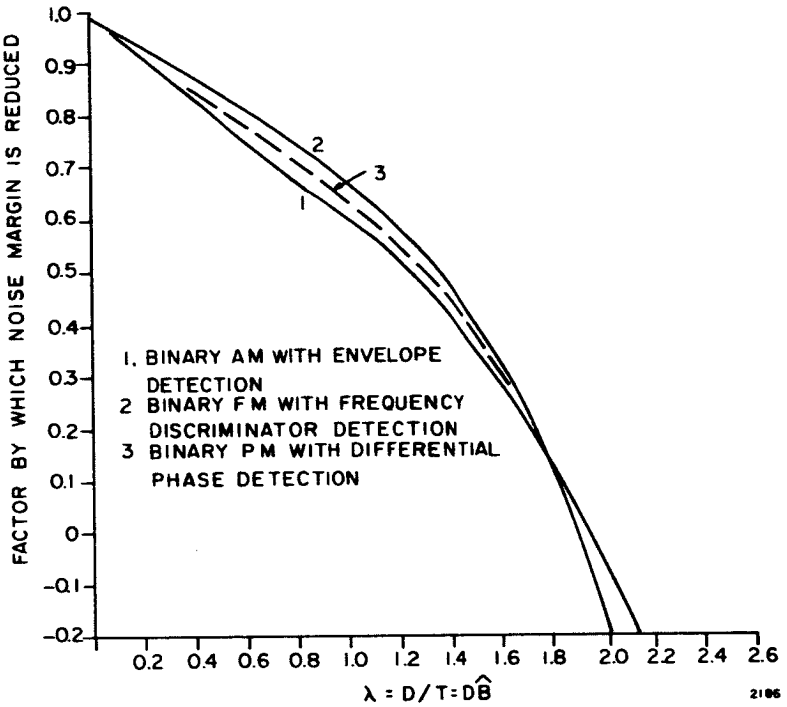

Figure 4-9. Maximum Reduction in Noise Margin Owing to Linear Delay Distortion

$$P_e^{(3)} \doteq 1/z\,\bar{\rho} \qquad (4\text{-}9a)$$

and $$P_e^{(3)} = 1/2\,(\bar{\rho} + 1)$$

where $\bar{\rho}$ = average power signal-to-noise ratio at the receiver.

For the AM system it was assumed in obtaining (4-9) that an optimum threshold which gives minimum error is used. Values for $P_e^{(3)}$ for FM and PM systems are tabulated below.

$P_e^{(3)}$	$\bar{\rho}$ db
$1/2 \times 10^{-2}$	20
$1/2 \times 10^{-3}$	30
$1/2 \times 10^{-4}$	40

$P_e^{(3)}$	$\bar{\rho}$ db
$1/2 \times 10^{-5}$	50

In many cases one used frequency devision multiplexing to avoid intersymbol interference of a time-multiplexed system. For a frequency multiplexed system one must be concerned with intermodulation distortion. Sunde (Reference 40) points out that intermodulation interference will cause less transmission impairment than does intersymbol interference in direct digital transmission if a cost of a two-fold increase in bandwidth and carrier power can be tolerated.

4.2.4 Effects of Multipathing on a Wide Band FM System

First, consider the case where the bandwidth of the signal is not large enough (that is, in wideband TV) so as to have the frequency dispersion and multipath spread affect the system performance. In this case only the fading introduced onto the signal would affect the fidelity of the transmission. The effect of fading in and FM system is to raise the threshold level required before system performance degrades.

Now consider the effects of multipath spread, Δ, when the signal bandwidth is large enough so that $B \geq 1/\Delta$. The discussion of the effects of multipathing on wideband FM systems in this case can be broken down into two cases. First, the case where there is only one main path component as indicated by equation (4-6). Second, the case where there are one or more main path components as represented by equation (4-7). For the first case, if the main path component is larger than the scatter components, then due to the capture phenomena of FM systems only the main path component would be observed and no distortion will result. The beat frequency interference is suppressed relative to the full signal by a ratio equal to the ratio of the deviation to the emphasis frequency.

In the case where there are two or more main path components (as would occur for a very large receiving antenna), and the one which dominates varies from one time to the next, then no one main component will be captured. Instead, alternately one main component and then another would be captured. This switching from one main component to another can introduce excessive noise and distortion into the system. Hence wide-band FM modulation would not be suitable in this situation.

4.3 Basic Correlative Measurements

Basic correlative measurements are required to classify the weather model existing in each test in order that the statistical propagation data can be translated to other geographical locations which experience similar meteorological conditions. Good correlative measurements will also help explain why certain things are happening to the test signals which are being propagated through the complex atmosphere. In addition to the usual surface meteorological data which must be collected at each ground terminal, radiometric measurements in coincidence with the basic signal measurements are a necessity. The apparent sky temperature, which is the result of these radiometric measurements, directly relates to the atmospheric attenuation due to the water and oxygen content of the atmosphere. Since the initial propagation experiments are conducted in atmospheric windows, the effects of oxygen absorption are considered negligible.

The test signals undergo fading due to multipathing as well as fading due to variations in water content within the receiving beam. The radiometric measurements should therefore help us to isolate these two fading effects. A weather radar, preferrably located right at the ground terminal, could provide another correlative input - a rainfall rate profile along the communication path. The total effect of rain absorption and scattering

could be deduced from the profile and, with the radiometric measurements, separate water vapor attenuation from condensed water attenuation.

4.3.1 Meteorological Measurements

Since weather effects will markedly influence the performance of communications channels in the 10 to 100 Gc frequency range, it is clear that correlative meteorological data should be taken to facilitate communications data analysis. Fortunately, the instrumentation required for this purpose is relatively inexpensive. A description of a low-cost system capable of recording wind speed, wind direction and temperature at the surface is given in Reference 41. Other sensors can be substituted for, or added to, those listed in the paper to cover pressure, relative humidity and precipitation rate.

Basically, the minimum requirement for meteorological data, to be used in communication channel performance evaluation, is as follows:

- -- Atmospheric temperature
- -- Atmospheric pressure
- -- Atmospheric relative humidity
- -- Precipitation rate
- -- Wind velocity and direction

These measurements should be made at least at ground level at the transmitter site and, if possible, at other points along the transmission path. If accurate data is available on pressure, temperature and relative humidity, it will be possible to compute the index of refraction. Knowledge of this parameter will assist in determining the reasons for signal fluctuations at a particular time.

Radiosonde correlative measurements would be highly useful since atmospheric temperature, pressure and relative humidity vary with height above the surface. Accurate measurements can be made of these parameters up to an altitude of approximately 50,000 feet; however, radiosondes are capable of rising to altitudes of 125,000 feet. The maximum errors involved in radiosonde measurements are as follows:

Temperature:	±1°C referred to surface temperature
Pressure:	±1.5 millibars, over a range of 100 - 1000 millibars ±4 millibars, over a range of 0 - 1000 millibars
Relative Humidity:	±5 percent up to 40°C, dry bulb reading 5-10 percent up to 30,000 feet altitude 20-50 percent above 30,000 feet.

The above performance figures apply to the AMT-4, MT-12 and AMG-9 radiosonde transmitters, except that the last-mentioned equipment does not measure pressure.

The surface and radiosonde measurements should be supplemented with Weather Bureau data during analysis of communications channel performance. This information includes surface, radiosonde, weather radar, and weather satellite data. The Weather Bureau can furnish the necessary information from central data collection and storage facilities.

4.3.2 Radiometric Measurements

A considerable amount of theoretical and experimental data is available on the absorptive properties of the atmosphere. However, for a proper analysis of the effects of various types of weather on the performance of a given ground-to-space communications channel, correlative measurements must be made at the test signal frequency by means of ground-based radiometers whose antenna beam coincides with and is equal in width to the communications beam. These measurements are particularly important in heavier weather conditions at lower elevation angles. Atmospheric absorption is directly proportional to water vapor content, length of path in the atmosphere and operating frequency.

The measurement of this absorption phenomena is a direct consequence of the second law of thermodynamics, which simply states: "In order for a body (the atmosphere) to remain in thermodynamic equilibrium, it must radiate an equal amount of energy as it absorbs." To fully appreciate this fact, an understanding of the concept of temperature as it applies to the radiometer is presented in Appendix VI.

Although a ground-based microwave radiometer, pointed at the sky, simply provides a reading of apparent sky temperature, this information can be readily converted to absorption by means of appropriate conversion curves such as those given in Figures 3-2 through 3-9 in Section 3.1. The principles by which the radiometer performs these measurements are also presented in Appendix VI. The attractiveness of correlative radiometric measurements lies in the fact that a radiometer, working with a pencil-beam antenna, automatically integrates all significant atmospheric absorptive influences, along the transmission path, into a single reading. A low-cost superheterodyne radiometer can provide accurate information on prevailing atmospheric conditions at the rate of at least one sample

per second. This sampling rate is consistent with known atmospheric absorption fluctuation rates.

Since the radiometer output integration time for this application can be of the order of one second, the available minimum detectable temperature sensitivities, based on double-sideband superheterodyne configurations, with IF bandwidths of 100 mc, are as follows:

Operating Frequency (Gc)	Min Detectable Temp. Sensitivity, T(°K)
8	0.2
16	0.5
20	0.5
35	1.5
70	2.0
94	2.0

These sensitivities will be adequate for the propagation measurements program.

The radiometers to be used in the propagation experiments are integrated into the ground facility receivers, in that they share the same antenna and r-f head with the communications receiver. The design of these radiometers is discussed in Section 7.3. There are two modes of operation for the radiomters: in the first mode, the radiometer makes measurements during satellite tracking while the signal receiver is making basic amplitude and phase measurements; in the second mode, the radiometer is used independently of the received signal to act as an "environment sensor" by background mapping the sky temperature. This would be done during periods immediately preceding and following satellite tracking.

4.3.3 Special Weather Radar Measurements

It appears that weather radar can be modified to provide rainfall rate data as a useful supplement to the radiometer data. Like the radiometers, there would be two modes of operation. In the first mode, the weather radar antenna would follow the millimeter wave antenna during satellite tracking and provide rainfall rate versus slant range while the communications receiver is making basic signal measurements and the radiometer is providing apparent sky temperature. In the second mode, the weather radar antenna would follow the millimeter wave antenna in scanning a sector of the sky and provide a rainfall map while the radiometer is background mapping the sky temperature.

The WSR-58 Weather Radar is one radar which could be modified as a special correlative measurements radar. The present characteristics of the WSR-58 operating in S-band are given in Table 4-I.

TABLE 4-I

S-BAND CHARACTERISTICS OF THE WSR-58 WEATHER RADAR

Antenna Gain	38.5 db
Antenna Beamwidth	1.8 degrees
Antenna Diameter	12.0 feet
Peak Power	500 kilowatts
Pulse Width	0.25 & 4.0 microseconds
Pulse Repitition Freq.	658, 154 pps
Resolution	4 mm/hr. at 250 nmi.
Elevation Scan	-10 degrees to 45 degrees
Azimuth Scan	360 degrees
Display	12 inch and 7 inch PPI Scope and 7 inch A&R Scope

The 7 inch PPI has been specifically designed for photography. Within the field of view of the scope camera are indicators for the following: date, time, station, pulse length, range, elevation angle of the antenna and frame number of the exposure.

Under most circumstances during the collection of propagation data, the WSR-58 should have a resolution of at least 0.1 mm/hr at most of the slant ranges of interest.

It should be noted that rainfall rate resolution of any radar is a statistical process with a Rayleigh distribution mean. Thus it may be treated as random noise with a numerical value of 5.58 db $-10 \log n$, where n is the number of pulses integrated. The limit of the resolution capability of the radar is a function of the resolvable cross-section, which in turn, is a function of the antenna beamwidth, pulse length, and ground clutter return.

An interesting feature of the WSR-58 is the existing provision for rapidly interchanging the RF heads to provide C and X-band coverage as well as at S-band. More attention will be given to the utility of weather radar as a special correlative sensor before specific recommendations are made.

BLANK PAGE

5. FORMULATION OF EXPERIMENTS

The general ground rules that were observed when formulating the experimental approach were to:

a) design reliable space qualified payload equipment with no requirements for major component development.

b) assume that medium altitude (6000 nmi) and synchronous altitude satellites will be available as the space terminals for the experimental links.

c) consider operation at any frequency from 8 to 100 Gc, or specific frequencies at 8, 16, 20, 35, 70 and 94 Gc.

d) design the spacecraft electronics in modular form with each unit not to exceed 15 pounds in weight and 15 watts in peak power consumption.

e) make maximum use of existing or planned millimeter wave experimental ground facilities.

This section of the report discusses the desirability of using medium altitude and synchronous altitude satellites with a specific recommendation that the initial propagation experiment be conducted with a payload at medium altitude. Up-links are compared with down-links, that is, using satellite receivers versus satellite transmitters and the equipment design problems and equipment operational problems involved. The use of down-links are most desirable from an overall viewpoint except in the area of transmitting tube efficiency and reliability.

Implementation of measurement waveforms is presented in answer to Section 4.1 which suggested three types of waveforms - AM, PAM and

PAM/FM - in terms of their propagation measurement value. For the initial experiment, the AM waveform is recommended.

Another problem is the frequency stabilization of transmitters and receiver local oscillators. Several methods are discussed and the Pound stabilizing loop is favored most, especially in the satellite terminal.

A survey of millimeter sources completes this section on formulation experiments. Millimeter wave generation is the most critical factor in the payload design. It becomes readily apparent that a satisfactory propagation experiment could not be designed under the 15 watt restriction on payload unit peak prime power. It is recommended that this restriction be eased with greater attention given to duty cycle on a daily, weekly and monthly basis and its compatibility with the needs of the other missions.

5.1 Candidate Satellite Evaluation

The categories of spacecraft considered are:

a) medium altitude (6000 nmi), gravity gradient oriented and inclined 28.5 degrees

b) earth synchronous, gravity gradient oriented and stationary

c) earth synchronous, spin stabilized and stationary

The information in this quarterly report can be used in the consideration of other satellites should they become identified. Appendix VII gives general orbital characteristics to show how the 6000 nmi and synchronous orbits are related to those at other altitudes. Appendix VIII contains the basic 6000 nmi and synchronous orbital data used to evaluate the above satellites.

Figure 5-1 shows the zero degree elevation coverage contours for a 6000 nmi satellite for ground terminals located near Los Angeles, California; Austin, Texas; Washington, D. C. ; Boston, Massachusetts; and Ottawa, Canada. The Ottawa location has been included to accommodate Canada's Defense Research Telecommunication Establishment (DRTE) in any planning they might have for participation in this program. Coverage contours at other elevation angles are given in Figures 6-1 through 6-5 in Section 6. These coverage diagrams clearly indicate the flexibility of a medium altitude orbit.

Figures 5-2 and 5-3 give elevation angle versus synchronous satellite longitude for the same geographic locations. These curves clearly indicate the limitations of a synchronous orbit for any given fixed position.

The medium altitude satellite is recommended for the initial propagation experiment. The behavior of the millimeter channel with varying elevation angle is important because the minimum useful horizon for a given radiated power, channel bandwidth, and receiver sensitivity, is a key factor in the design of useful space-earth communication links. By the same analytical methods used in Section 3. 3, the data collected with a medium altitude satellite can be directly applied or extrapolated to the design of communications systems using satellites at other altitudes.

The angular elevation rate of the medium altitude satellite is slow enough (no faster than . 025 degrees per second at 6000 nmi) to permit ample viewing time per pass with sufficient data samples per degree of elevation. On the other hand, the elevation angular rate is fast enough to complete a full elevation profile before significant weather changes can occur. Elevation coverage from the horizon to 30 degrees can take place well within an hour on many of the orbital passes. As the coverage diagrams indicate, the altitude of this satellite is sufficiently high to permit simultaneous observation by many ground stations for two hours or more.

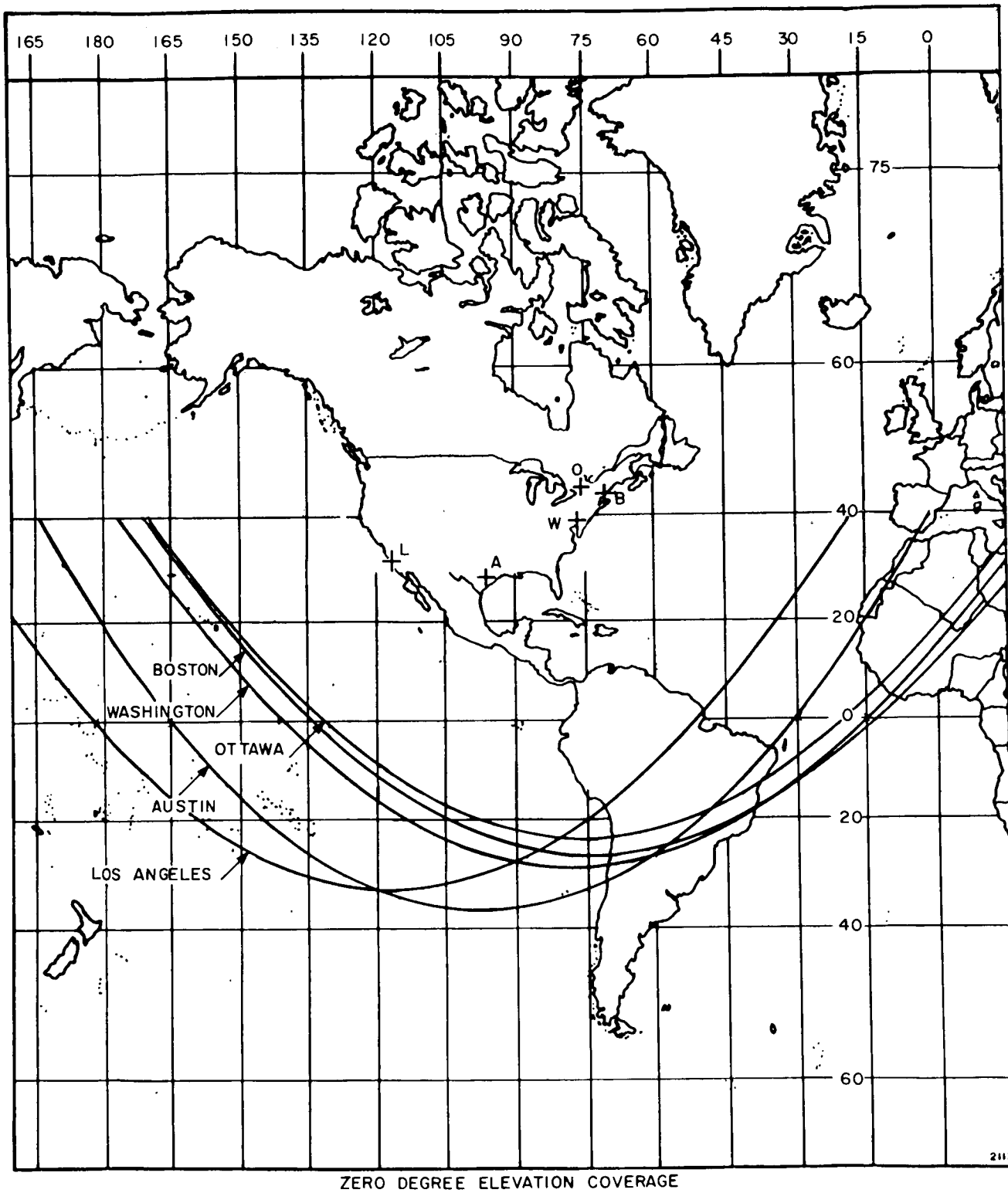

ZERO DEGREE ELEVATION COVERAGE
CONTOURS FOR A 6180 N. SATELLTE

Figure 5-1. Zero Degree Elevation Coverage Contours for a 6000 nmi Satellite

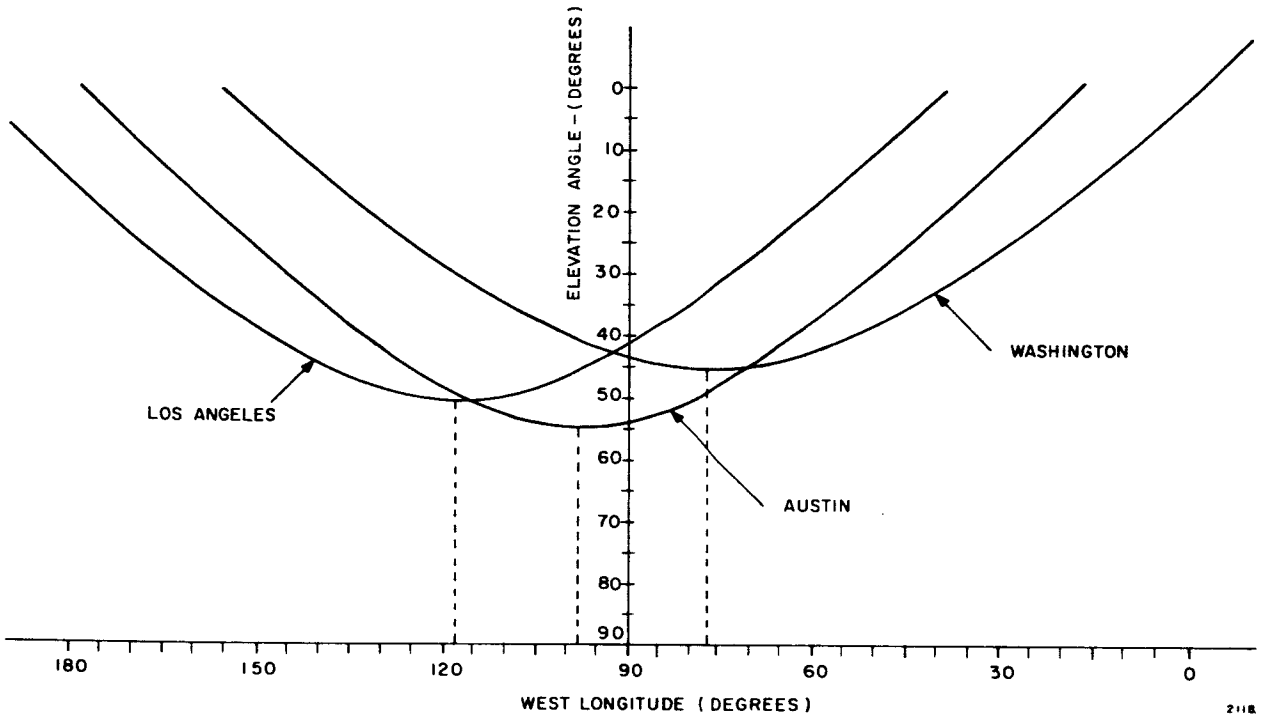

Figure 5-2. Zenith Angle vs Synchronous Satellite Longitude for Los Angeles, Austin, and Washington

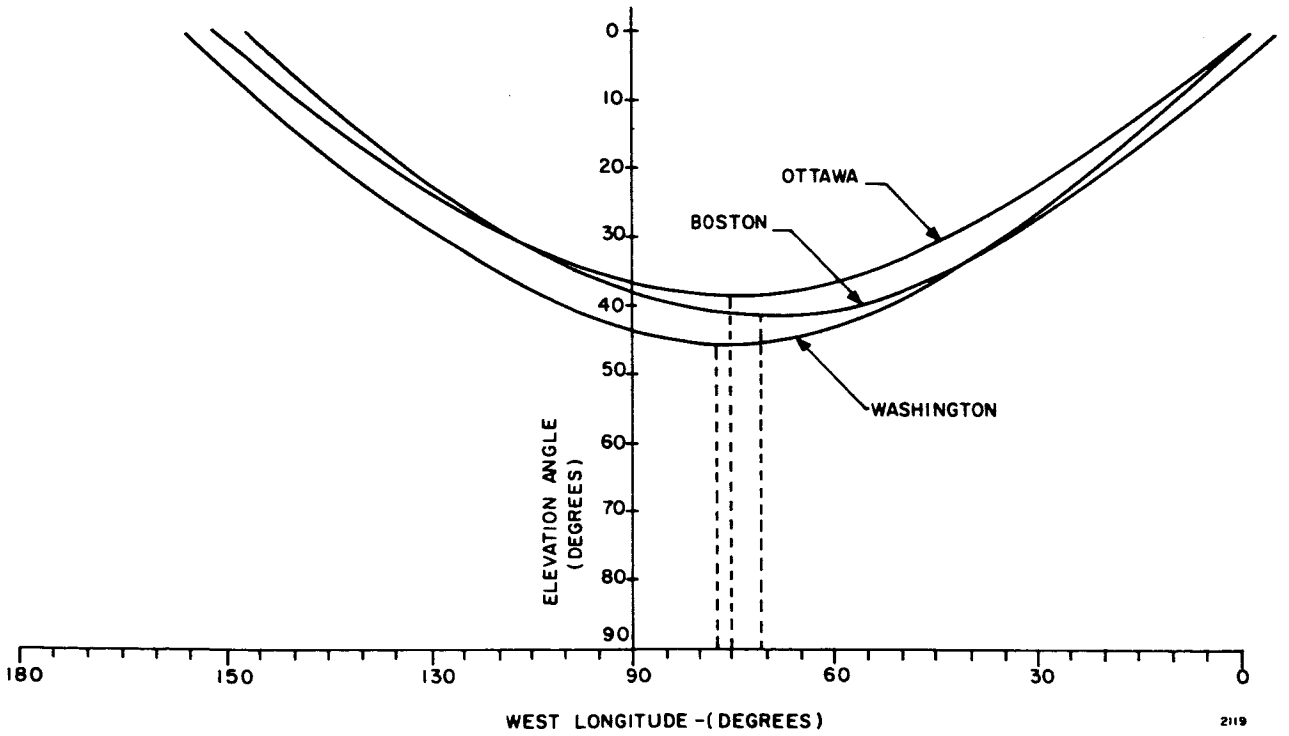

Figure 5-3. Zenith Angle vs Synchronous Satellite Longitude for Washington, Boston and Ottawa

A one-year viewing time profile was developed to: 1) estimate the number of satellite passes available to a ground station during any interval of time; 2) estimate the amount of viewing time per pass; and 3) estimate the total operational time on the satellite payload which is required to service all the ground stations during a given pass. The results of this profile, which is presented in Appendix IX, show that the available viewing time is abundant, ranging from 35 passes (165 - 200 minutes per pass) every 13 days for Austin, Texas, to 31 passes (130 - 180 minutes per pass) every 13 days for Ottawa, Canada. For the same period of time, the maximum payload operational time ranges from 180 - 340 minutes for each of the 35 passes. This mission profile data is helpful in planning the data collection schedule for a one-year propagation program.

As mentioned in the summary, synchronous stationary satellites are less desirable as a space platform for basic scientific propagation experiments. The position of the satellite is critical in that the right combination of elevation angles from two or more existing ground stations is required. The stationary satellites, however, are more attractive from an operational standpoint in that no modifications are required in the antenna pointing systems and also that no accurate prediction of orbital parameters is necessary.

5.2 Up-Links versus Down-Links

Down-links are most desirable when conducting propagation experiments. Up-links should be considered only if the down-link transmitter proves to be a problem. Two-way links using a satellite transponder are of little value because no additional propagation data is provided at the expense of the more complex payload.

The most important reason for wanting to use a down-link is that it requires less coordination and less modification on the part of the existing millimeter facilities. If properly instrumented with an automatic tracking system or a programmed tracking system, these facilities can receive the test waveforms and make propagation measurements with little or no coordination with GSFC except to obtain satellite ephemeris data. Several stations can make measurements simultaneously without interfering with one another.

Furthermore, acquisition and tracking is much more difficult with an up-link because a closed loop is required to confirm that the transmitted signal is being properly received. A closed loop would require that each ground facility be equipped to receive a beacon signal or a telemetry signal from the satellite which indicates that the transmit beam is properly pointed.

One objection to the down-link is the power consumption of the space transmitter. However, a good receiver local oscillator consumes almost as much power and, since it must be on longer than the transmitter in order to handle each ground station individually, it is doubtful whether the satellite receiver really provides an advantage in prime power. The up-link just does not provide the necessary flexibility in scheduling propagation data collection with the other experiments being performed with the satellite.

Finally, down-links are more desirable because simultaneous measurements with multiple feed antennas and dual reflector antennas are possible, thus allowing measurement of wavefront tilt and spatial decorrelation.

As mentioned in the summary, the recommended experiment consists of a 35 Gc down-link and a 94 Gc up-link. The 94 Gc up-link was recommended because of the development problems that would be associated with a long life 94 Gc satellite transmitter in the time scale assumed. The 94

Gc up-link is somewhat attractive because of the ground transmitter development presently underway for the Aerospace facility and because of the fact that the 94 Gc satellite receiver local oscillator signal can be derived from the 35 Gc transmitter output at little expense in performance.

5.3 Implementation of Measurements Waveforms

As indicated in Section 4-1 of this report, three types of test waveforms are considered: an AM waveform with two sidebands, a PAM waveform, which is a time quantized pulse amplitude modulated waveform, and a PAM/FM test waveform which involves a pulse amplitude modulation waveform on a frequency modulated carrier. This section of the report deals with the implementation of these proposed waveforms.

5.3.1 AM Test Waveform

First consider AM waveforms which utilize two sidebands equally spaced about the carrier. This particular waveform lends itself readily to implementation in that it does allow the utilization of a stabilized millimeter source as the carrier, and through the utilization of an inguide shunt-mounted semiconductor modulator, the sideband energy is introduced onto the stable carrier. It is felt, at this time, that this particular approach is realistic and within the state-of-the-art, requiring a minimum amount of development work for implementation, when a reasonable transmitter power level is considered. This holds for frequencies from 10 through 35 Gc. This shunt type of modulation does allow the introduction of modulating signals ranging from dc on through approximately 25 to 50 megacycles. The upper limiting capability of these shunt modulators is somewhat determined by the incident RF power which is being modulated. This is to say that the upper frequency limit of modulation is inversely proportional to the power being modulated. Above this frequency range, namely from

8 millimeters to 3 millimeters, a major development program in the semiconductor material and the type of modulation techniques would be required. This modulation approach can be implemented with approximately a 20 db on-off ratio which is equivalent to an approximate index of modulation of 80 percent. This modulation index would prove to be most adequate for the evaluation of the communication channel. The limiting factors in the generation of this modulation index are the engineering trade-offs between insertion loss I_L and isolation Iso, namely the switching ratio Iso:I_L of the modulator. Hence, if more than 80 percent modulation was required, this would be accompanied by a greater loss in carrier power due to I_L.

5.3.2 PAM Test Waveform

The second mdoulation to be considered is that of a PAM waveform. The implementation of this test waveform is very similar to that discussed in Section 5.3.1 of this report in that an RF line modulation would be used. The major difference is that the modulation signals will now become a pulse train, and the output would be RF pulses which have a coherent stable characteristic. In Section 4.1.2 of this report it is suggested that a 10 nanosecond pulse will be used with a one to two nanosecond rise time. This type of modulation can best be accomplished at a power level below 100 mw and at a wavelength below 8 mm. Since this technique does require the utilization of a duty factor, this approach of RF line modulation yields a reduction in average power which is proportional to the duty of the waveform generator. Therefore, it is felt that this modulated signal be followed by a coherent pulse amplifier such as a TWT, Pulse Klystron Amplifier, and/or other devices. This would allow for boosting the peak power output to obtain an average power level which would provide adequate signal-to-noise ratio in the channelized receiver. This problem of generating peak power in coherent millimeter devices cannot be solved without a development in the RF source capability. This fact will become more evident in

Section 5.4. It shows dramatically the limitations that are evident in today's millimeter source technology. Namely, the only devices capable of peak power equal to average power are found in the magnetron family and those are duty limited and provide only non-coherent signals, which would pose major problems in obtaining narrow-band predetection bandwidths.

5.3.3 PAM/FM Test Waveform

Finally, the third mode of modulation, namely the pulse amplitude FM test waveform can be implemented most readily through the utilization of a low power pulse amplitude FM signal generator followed by a final driver RF amplifier, such as TWT's and/or RF distributed amplifier techniques. Once again, the argument as presented in the preceding paragraph, as it relates to peak and average power devices, is applicable to this type of operation. Hence, the implementation of this system would be through the utilization of a low power FM oscillator followed by an RF line modulator whose output is fed directly to a high power transmitter amplifier device. Through the implementation of this technique, it is felt that this will more closely simulate an actual PAM/FM communication system, in that direct control of the PAM and direct control of the FM signals may be independent and may provide a coherent source for the purposes of implementing a channelized receiver.

5.3.4 Conclusions

When the proposed implementation of each of the presented waveforms is considered and applied directly to the implementation of such hardware, within the confines of satellite and space environments, the most readily implemented of the three test waveforms at wavelengths below 8 millimeters is the AM waveform which requires a true RF shunt modulator. This waveform will fulfill the purposes of generating equally spaced

sideband energies which may be processed through receivers to determine the phase stability of the communications channels and the relative amplitude stabilities of the two sidebands. Hence, it is felt that this approach is implementable for systems on a time schedule compatible with a one to two-year flight hardware program. For time schedules of greater periods, that is, two to four years, implementing the other waveforms can be considered for installation and utilization in a space vehicle.

5.4 Survey of Millimeter Sources

By way of demonstrating feasibility of the proposed experiments, the RF component survey was concentrated on the definition of RF sources, since millimeter wave generation is deemed the most critical factor in the payload design. This survey represents the present state-of-the-art availability and also includes projections of presently active development programs and proposed programs.

5.4.1 Tabulation of Sources

Investigation of the high power devices (by definition, those capable of delivering one watt or more of CW RF output power) in the 16 to 100 GC frequency range was made. A tabulation of these oscillator and amplifier devices is given in Tables 5-I and 5-II. Figures 5-4 and 5-5 show in bargraph form the power output available as a function of frequency. Specifications on some tubes with power outputs below one watt have also been examined since the possibility exists of using these tubes in proposed experiments. In addition to this, solid state sources have been investigated.

The bargraphs show that, as of this date, there is a scarcity of high power generators in this frequency spectrum. If it is desired that an experiment be conducted at a frequency where a device exists, then the

TABLE 5-I

TABULATION OF HIGH POWER MILLIMETER OSCILLATOR DEVICES

Company	Type No.	Power (watts)	Freq. Range (Gc)	Structure	Tuning
Eimac	X1149	1.5	12.4-18	KLR	MT
Sperry	SOU4040	1.0	13.3-17.5	KL2	FF
Sperry	SOU403	1.0	16.395-16.405	KL2	FF
Eimac	X1119	1.0	15.5-18	KLR	MT
Sylv.-Micro	BWM4280	70.0	14.9-18.1	BWTM	VT
Watkins-Johnson	WJ205	10.0	15.0-18.0	BWT	VT
Sperry	SOU4041	1.0	17.5	KL2	FF
Varian	VA513	1.0	17.75	KL2	FF
Elliot	12TFK2	8.0	21-25	KLF	MT
Litton	L3631	8.0	21-25	KLF	MT
Elliot	12FK1	10.0	21-25	KLF	FF
Litton	L3630	10.0	21-25	KLF	FF
St. Tel. and Cable	7747	10.0	26.5-40	BWT	VT
ITT	F2904	1.0	28.33	KLR	EM
OK1	KC31A	7.0	30-32	KL2	FF
OK1	34LV10	10.0	33.2-34.8	KLF	MT
Litton	L3659	5.0	32-37	KLF	MT
Elliot	8TFK2	10.0	33-37	KLF	MT
Litton	L3628	10.0	33-37	KLF	MT
Elliot	8FK1	15.0	33-37	KLF	FF
Litton	L3629	15.0	33-37	KLF	FF
Elliot	8FK14	30.0	34-36	KLF	FF
Litton	L3713	30.0	34-36	KLF	FF

TABLE 5-I (Cont)

Company	Type No.	Power (watts)	Freq. Range (Gc)	Structure	Tuning
Elliot	8FK15	5.0	34-36	KLF	FF
Litton	L3736	50.0	34-36	KLF	FF
ITT	F2900	1.0	33-38	KLR	FF
Watkins-Johnson	WJ282	1000.0	35.2-36.2	TWT	
Siemans	RRW040	15.0	32-40	BWT	EM
CSF	C080	20.0	39-41	BWT	VT
ITT	F2907	1.0	45-50	KLR	EM
Elliot	6FK1	1.0	48-52	KLF	FF
Elliot	6TFK2	1.0	48-52	KLF	MT
Litton	L3693	1.0	48-52	KLF	MT
OKI	50LV10(D)	5.0	49.2-50.8	KLF	MT
Litton	L3640	1.0*	48-52	KLF	FF
Hughes	381H	5.0	51-56	BWT	VT
Hughes	810H	10.0	51-56	KL	VT
OKI	KC55B	12.0	53-57	KL2	FF
Hughes	181H	15.0	54-56	BWT	VT
CSF	C040B	20.0	68.25-71-75	BWT	MT
Hughes	182H	1.0	90-99	BWT	VT
Hughes	183H(D)	10.0	94-98	BWT	VT
Hughes	811H(D)	5.0	90-99	KL	VT

*Stated 5.0 watts in Microwave Data Book

(D) Denotes development not complete

TABLE 5-I (Cont)

SYMBOLS	
Structure	Tuning
KLR - Reflex Klystron	MT - Mechanically Tuned
KL2 - 2 Cavity Klystron	FF - Fixed Frequency
KL5 - 5 Cavity Klystron	
KLF - Floating Drift Tube Klystron	VT - Voltage Tunable
KL - Distributed Interaction Klystron	
TWT - Traveling Wave Tube	EM - Electromechanically Tuned
BWT - Backward Wave Tube	
BWTM - Backward Wave Tube "M" Type	
CFA - Crossed Field Amplifier	

TABLE 5-II

TABULATION OF HIGH POWER MILLIMETER AMPLIFIER DEVICES

Company	Type No.	Power (watts)	Freq. Range (Gc)	Structure	Gain	C. F.
Microwave Elect.	M2405A	1.0	12.4-18.0	TWT	30 db	15.2
Microwave Elect.	M2405B	1.0	12.4-18.0	TWT	30 db	15.2
Microwave Elect.	M2405F	1.0	12.4-18.0	TWT	30 db	15.2
Microwave Elect.	M2405BB	2.0	12.4-18.0	TWT	30 db	15.2
Microwave Elect.	M2405E	2.0	12.4-18.0	TWT	30 db	15.2
Microwave Elect.	M5046	3.0	12.4-18.0	TWT	30 db	15.2

TABLE 5-II (Cont)

Company	Type No.	Power (watts)	Freq. Range (Gc)	Structure	Gain	C. F.
Microwave Elect.	M2405	4.0	12.4-18.0	TWT	30 db	15.2
Varian	VA619G	10.0	12.4-18.0	TWT	35 db	15.2
Sperry	SAU211	8.0	12.6-18.0	KL2	6 db	15.3
Varian	VA882A	1000.0	15.36	KL5	30 db	15.36
Microwave Elect.	M2405G	1.0	12.0-18.0	TWT	30 db	16.0
Microwave Elect.	M2405BA	2.0	14.0-18.0	TWT	30 db	16.0
G. E.	ZM5183	10.0	14.0-18.0	TWT	30 db	16.0
Litton	L3909	350.0	14.5-17.5	CFA	20 db	16.0
G. E.	ZM5184	1000.0	14.0-18.0	TWT	30 db	16.0
Watkins-Johnson	WJ266	1000.0	34.77-35.23	TWT	13 db	35.0
Hughes	812H	150.0	52-55	TWT	12 db	53.5
Hughes	813H	1000.0	54.5-55.5	TWT	20 dbq	55
Hughes	814H	100.0	90-99	TWT	15 dbq	94.5

inherent disadvantage of that particular device must be accepted, unless development of new devices or modification of existing devices is contemplated. Between 35 and 100 Gc the devices are, in general, relatively large, heavy, and require multiple power supplies. To help understand the parameters of the devices, specifications on a tube in each family are discussed. The particular type selected as an example does not imply that this device is preferred in any way over other types.

The quantity and quality of the data available on Hughes Aircraft Company's devices has the tendency to bias this survey in that direction. Unfortunately, similar data on other types is not readily

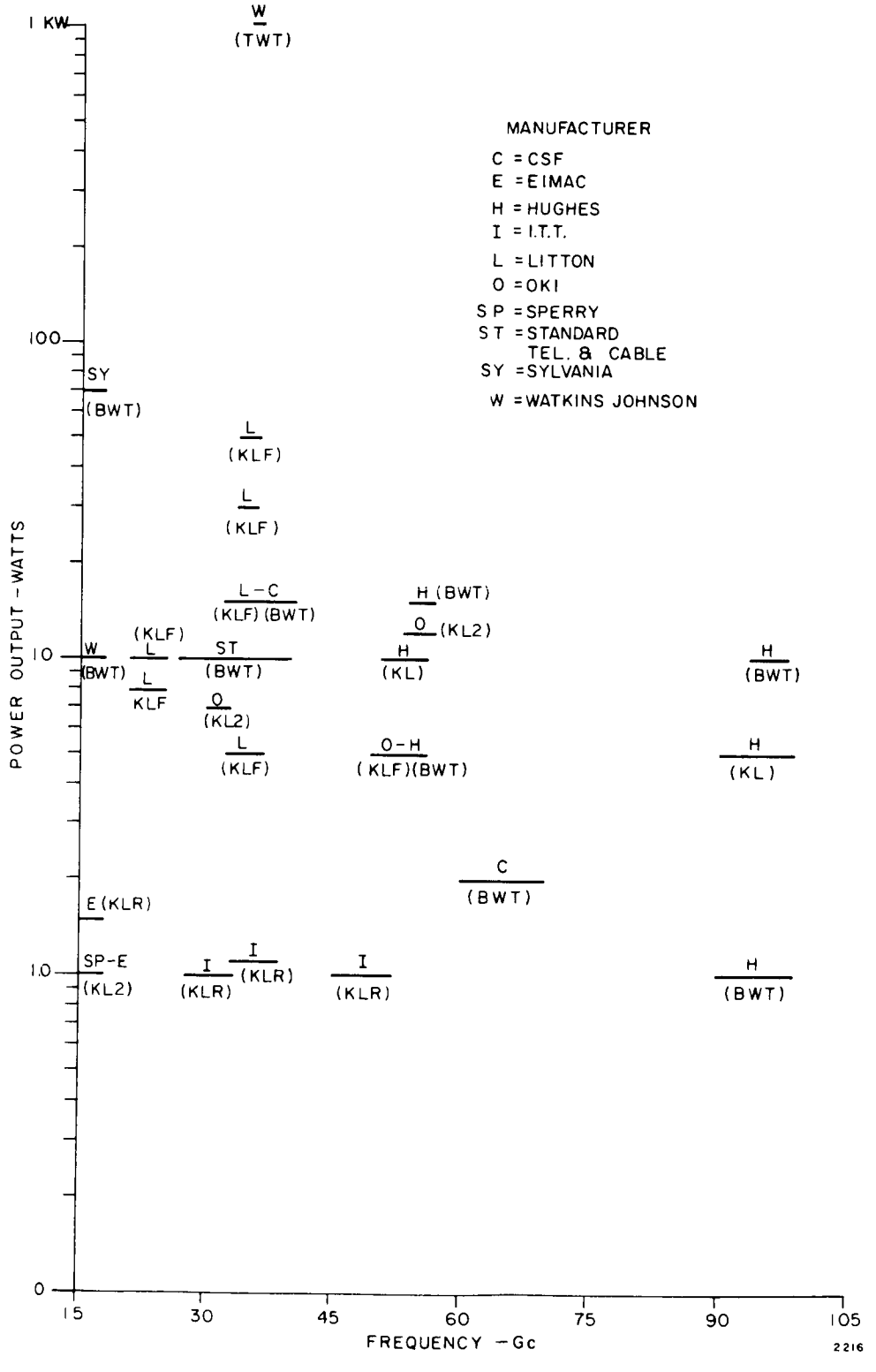

Figure 5-4. CW Power Output vs Frequency for High Power Millimeter Amplifiers

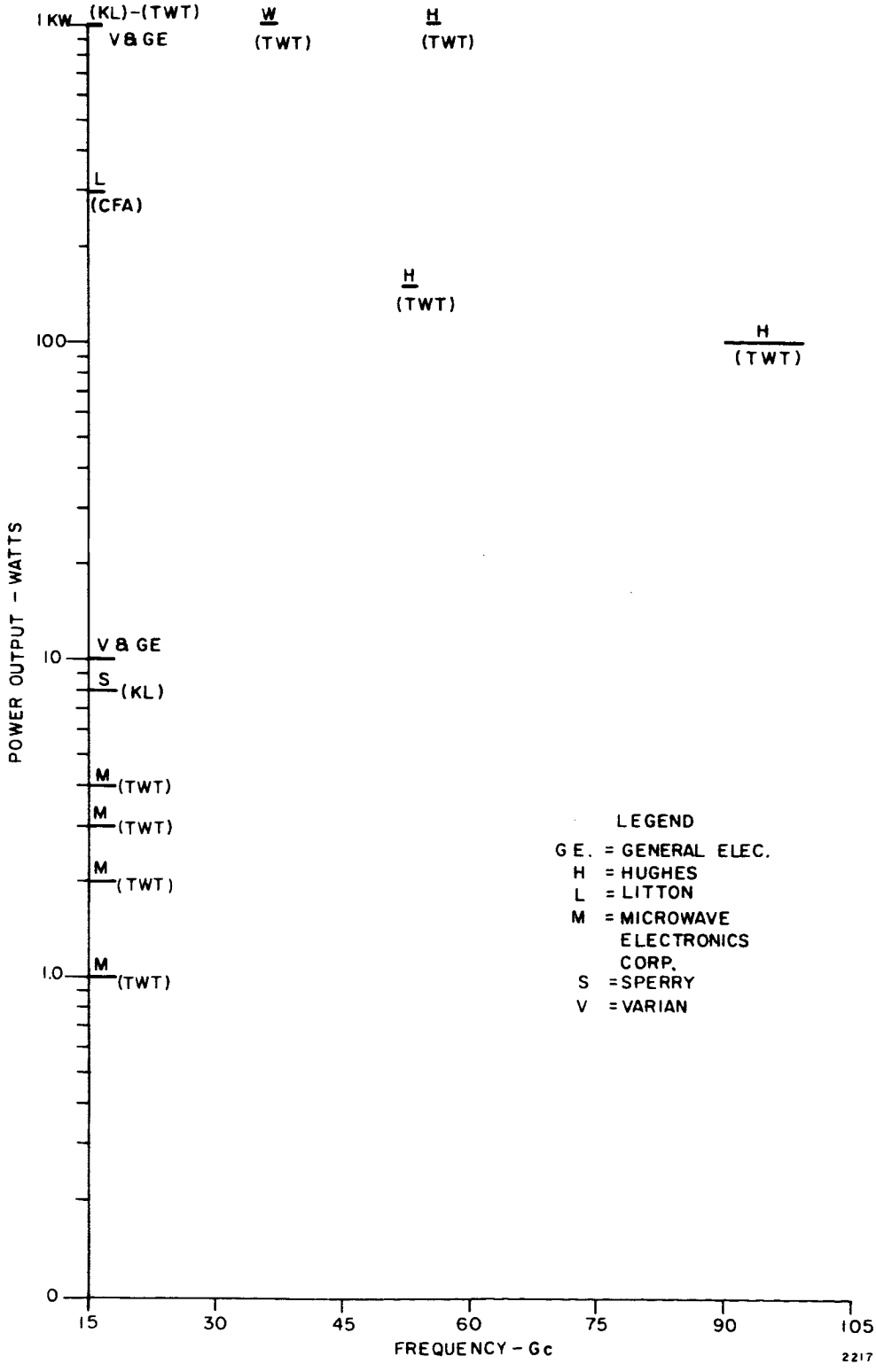

Figure 5-5. CW Power Output vs Frequency for High Power Millimeter Amplifiers

available. Further investigation on these other types will be made to determine the feasibility of utilizing them in satellite terminal applications.

5.4.2 Explanation of Tube Types

Two basic types of interaction are used in conventional high frequency generators, namely linear beam interaction and crossed field interaction. The linear beam type employs a straight beam; magnets are used merely as an accessory to help focus this linear beam. The other is the crossed field family, in which the electrons travel in cycloidal trajectories caused by passing through a magnetic field perpendicular to the electric field. Both of these major classes have many subdivisions, which differ mainly in the form of the RF circuit that interacts with the electron beam. Linear beam types discussed in this survey are shown in Table 5-III, and the crossed field devices are shown in Table 5-IV.

TABLE 5-III
LINEAR BEAM INTERACTION DEVICES

Device	Use	RF Circuit Wave
Klystron	Oscillator Amplifier	Standing (Cavity)
Laddertron	Oscillator	Standing (Cavity)
O-BWO (O-Carcinotron)	Oscillator	Backward (Delay Line)
Traveling Wave Tube	Amplifier	Forward (Delay Line)

TABLE 5-IV
CROSSED FIELD INTERACTION DEVICES

Device	Use	Cathode	RF Circuit Wave
M-BWO (M-Carcinotron)	Oscillator	Injected Beam	Backward
Crossed Field Amplifier	Amplifier	Injected Beam	Forward

The Reflex Klystron

The reflex klystron utilizes a single tuned-cavity and a single interaction gap. The electron beam from the cathode is accelerated by a positive voltage from the cavity region. It is velocity modulated by RF voltage while passing the cavity gap and the shift region is terminated by the repeller. The negative potential on the repeller causes the electrons to turn around and pass the gap a second time, but in the opposite direction. If the electrodes are properly designed the electrons are prevented from returning a third time. The faster electrons approach closer to the repeller and hence require longer to return to the gap. They may arrive at the gap at the same time as other slower electrons which left the gap at a later time during the first transit. Bunches of electrons may thus be formed.

If the repeller is now adjusted in such a way that the electron bunch returns just when the RF field is in its retarding cycle, that is, when the transit angle is $\theta = (\eta - 1/4)\pi$, energy will be delivered to the RF field of the cavity by the electron beam.

The Two Cavity Klystron

The two cavity klystron consists of an electron gun (cathode), two cavities separated by a drift tube, and a collector. As an amplifier,

RF energy is fed into the first cavity and removed from the second cavity. Because of the small dimensions of the cavities and the drift tube in millimeter wave klystrons, the cavities are an integral part of the vacuum envelope rather than external to it.

In operation, an electron beam of time-constant current density enters the gap of the input cavity. Initially, all electrons of the beam have the same velocity. When the electrons are exposed to the RF field across the first gap, which varies with time, they are accelerated or retarded depending on the time at which they enter the gap; that is the beam is velocity modulated while passing the first gap. In the field drift region between the cavities, the beam becomes density-modulated with time since some electrons travel faster than others and even pass some of the slower ones. The bunched beam now enters the second gap which is a predetermined distance from the first gap, and induces a current which in turn results in RF voltage, the amplitude of which depends to a large extent on the Q of the cavity. Hence there is voltage amplifications as well as power amplification. Finally the electron beam is accumulated by the collector. By providing proper feedback, the two cavity klystron amplifier can be made into an oscillator.

Floating Drift Tube Klystron

The floating drift tube klystron differs from the standard two cavity klystron in that the two cavities are tightly coupled so that there is essentially one cavity which is a distinct advantage in fabrication and tuning, but still retains the higher efficiency of the two cavity klystron relative to the reflex klystron.

Traveling Wave Tubes

In the traveling wave tube, an electron beam is emitted from a cathode and accelerated toward the collector end of the tube. The electrons

of the beam are surrounded by an RF wave with a strong field component in the direction of the beam travel. If the velocities of the beam and the wave are nearly the same, interaction takes place. A delay line is used to slow the RF wave to the velocity of practical beams. A helix is commonly used to accomplish this function.

The electron beam is injected into the helix and maintained over the length of the line by a focussing system. The small RF signal is coupled into the delay line at the gun end and the amplified signal is extracted at the collector end of the delay line. The electron beam is velocity modulated and eventually becomes density modulated, or launched by the interaction of the RF wave. The continuous action results in a growing wave so that the tube amplifies.

Because of the high degree of coupling between the input and output of the TWT, the device can easily develop oscillations. To avoid this, reflections at both ends of the RF circuit must be kept to a minimum. In addition, further decoupling between the input and output is attained by attenuating the delay line. The helix is by no means the only suitable slow wave structure. Many other types have been used to accomplish this action.

O-Type Backward Wave Oscillators

These tubes are members of the traveling wave tube family. They differ only in that they use a fundamental or space harmonic with phase and group velocity of different signs. The first BWO's were nothing but traveling wave tubes. These tubes are made up of an electron gun, a slow wave structure (delay line), a collector and an RF output port. The RF energy is led out at the gun end of the delay line and the far end of the line is terminated at the collector in its characteristic impedance. The velocity of the electron beam is synchronized with the phase velocity of the slow wave structure. The energy exchange is much the same as that in

a TWT, except that the electrons and the RF energy are traveling in opposite directions. Thus, a feedback loop is formed by the beam and the line and oscillations start if the beam current exceeds a certain level.

One of the unique features of the BWO is that of purely electronic tuning. The oscillator can be tuned over a range of frequencies by varying the beam-voltage.

The Laddertron

This device is an intermediate between the reflex klystron and the O-type BWO and utilizes the basic concepts of both. An explanation of the construction is contained in the discussion of the OKI devices.

5.4.3 Specifications on Tubes

5.4.3.1 Comments on Hughes Company Millimeter Devices

This company has concentrated on high power capability in the millimeter region and does not manufacture low power devices. These devices exhibit relatively high efficiencies as quoted by the manufacturer as between 20 and 30 percent. However, examination of the tentative data shows a more pessimistic efficiency rating, and is affected by operating parameters. At present, these are primarily laboratory devices and/or ground terminal devices, in that a complex power supply system is required, consisting of four different supplies plus a vac-ion power supply. All of these voltages are in the kilovolt or tens of kilovolt region with the exception of the filament supply.

It is felt that the power supply design presents no major problem areas. Power supply efficiencies in the order of 75 to 85 percent at these high voltage, high power levels have been made.

The Hughes Laboratory is equipped with adequate facilities to perform cycling tests, filament testing and space environmental testing programs. The laboratory feels that with a concentrated effort, they could develop a qualified transmitter which would weigh no more than 15 pounds utilizing a doughnut type of magnet structure, to conserve on power and weight.

Life testing has been limited, but Hughes Company has quoted the operation of a device at 6500 hours. The cathode design has a theoretical limit of 10,000 to 20,000 hours.

Hughes Company recommends a Distributed Interaction Klystron as the best choice for space implementation because it has slightly higher efficiency and possesses the ability to be more readily adaptable to the doughnut type of magnet structure.

The major problem foreseen with this device in a space environment, is the required collector cooling. Methods of evaporative cooling, and/or heat sinking, might be considered. Closed loop heat exchanger techniques are also feasible.

Hughes Company feels that devices from 8 millimeters to 3 millimeters could be built for space applications and would require approximately six months for the first breadboard, serially followed by six months for a prototype, followed by approximately one year of environmental testing and checking, to assure reliability and the capability of performing in a space environment. In parallel with the tubes development the three power supplies required for the tubes operation would be developed, tested and evaluated.

With the effort, Hughes Company could provide a two to three year development program resulting in a flight worthy, tested and

qualified transmitter package, including power supplies which would be capable of delivering 10 to 100 watts of CW RF power.

Type 381H Backward-Wave Oscillator Tentative Data

Description

The tube type 381H is a Backward-Wave Oscillator capable of a CW output power of more than 5 w over the frequency range of 51 to 55 Gc. The output frequency is determined by the cathode voltage in the range of about 6 to 10 kv. The output power is determined by the beam current which can be adjusted independent of the operating frequency. High efficiency is obtained by the substantial depression of the collector potential below the circuit potential. A permanent magnet is used to focus the electron beam and the collector is air-cooled. An integral ion pump is included to insure long life.

Mounting Position

Any

Connectors

RF	UG-385/U Waveguide
DC	Flying Leads

Mechanical (Maximum Overall)

Length	13-1/4 in.
Width	12-7/8 in.
Height	4 in.
Weight	40 lb.
Cooling Air Flow (sea level)	
Collector	5 cfm at about 6 in. H_2O
Envelope	natural convection

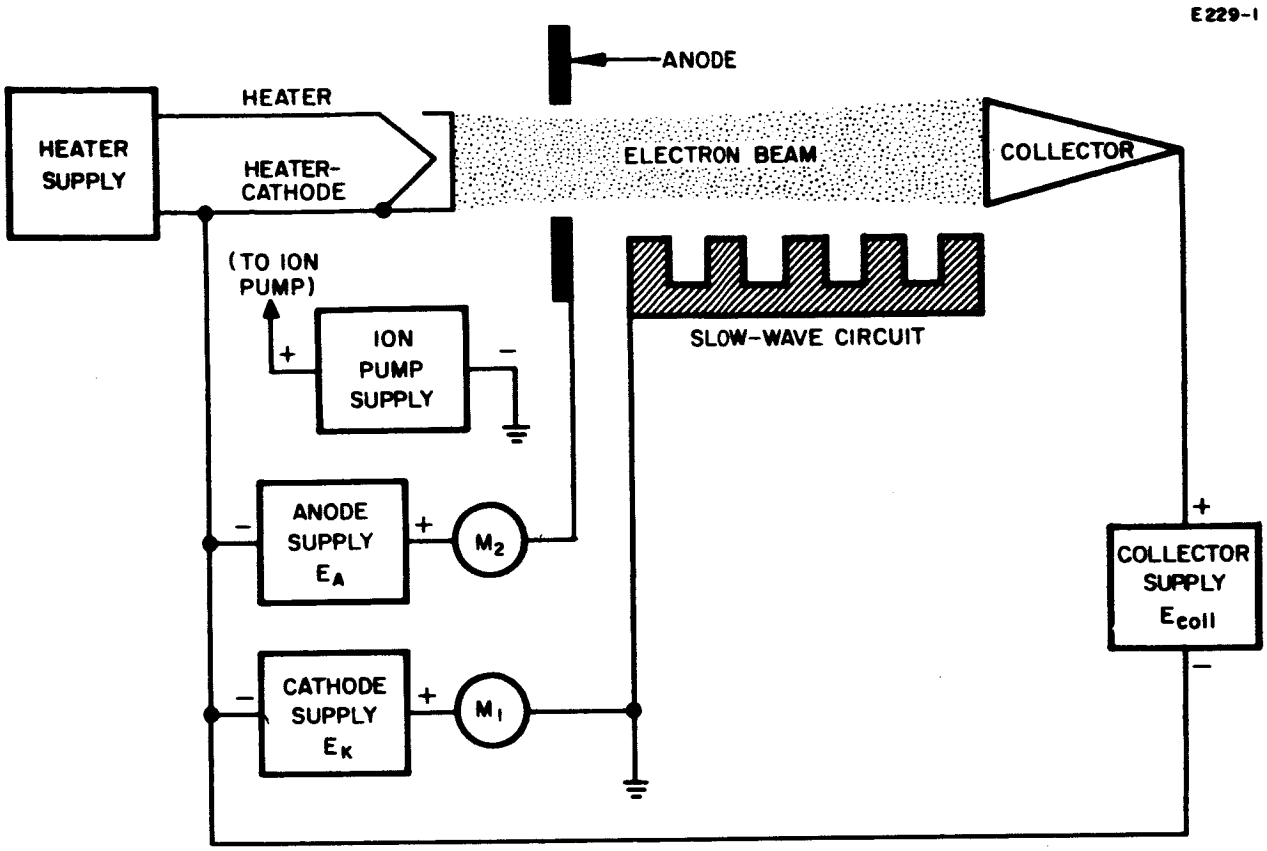

M_1 = Slow-Wave Circuit Current Meter

M_2 = Anode Current Meter

NOTE: The permanent magnet is at ground potential. The gun end metal tube envelope is at anode potential and is isolated from the magnet assembly. Due care must be exercised for personnel safety. In general, a common isolation transformer can be used to power the heater, anode, and collector power supplies. Air to the collector must be supplied via an insulated duct. A suitable relay should be provided in the slow-wave circuit connection to remove the anode voltage if the slow wave circuit current exceeds 10 mA.

Figure 5-6. Type 810H and 381H Oscillator Power Supply Operating Circuits

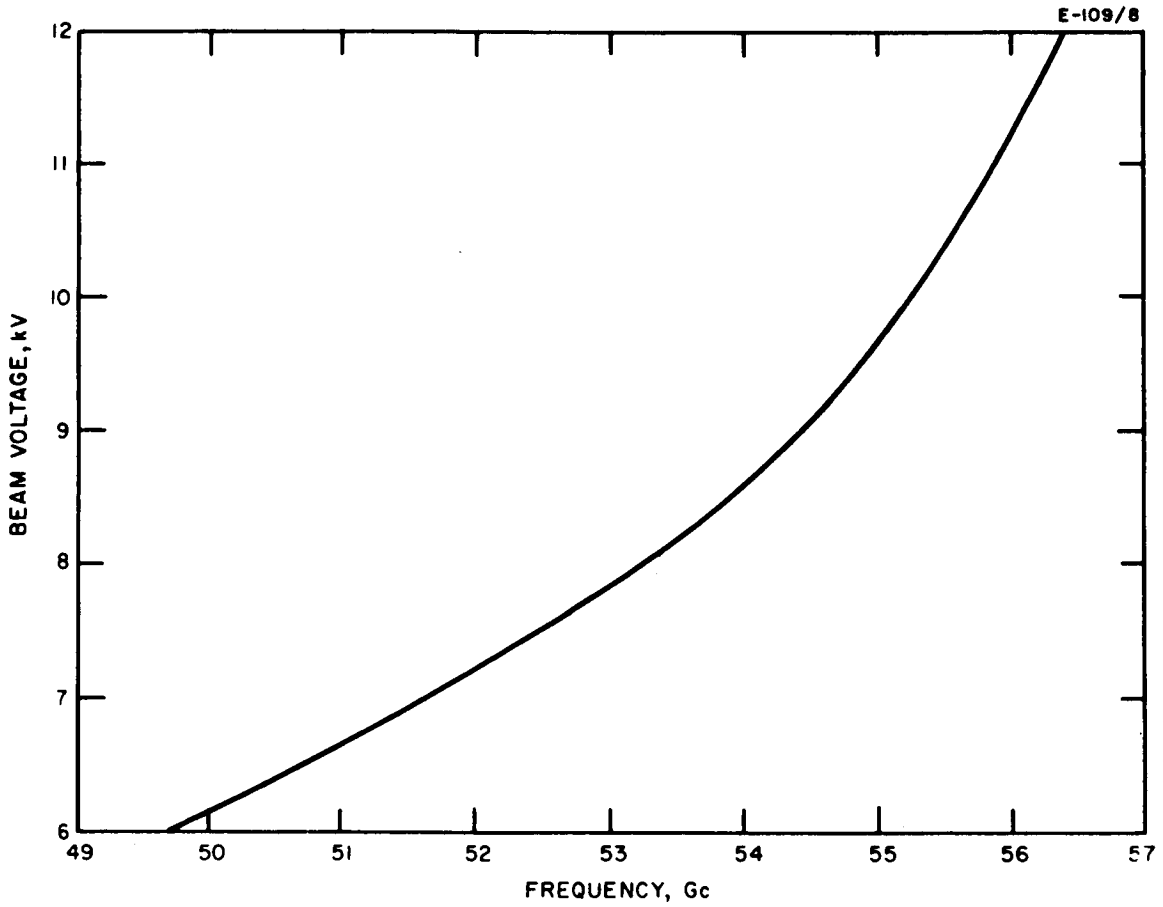

Figure 5-7. Typical Tuning Characteristics of the Type 381H Oscillator Tube

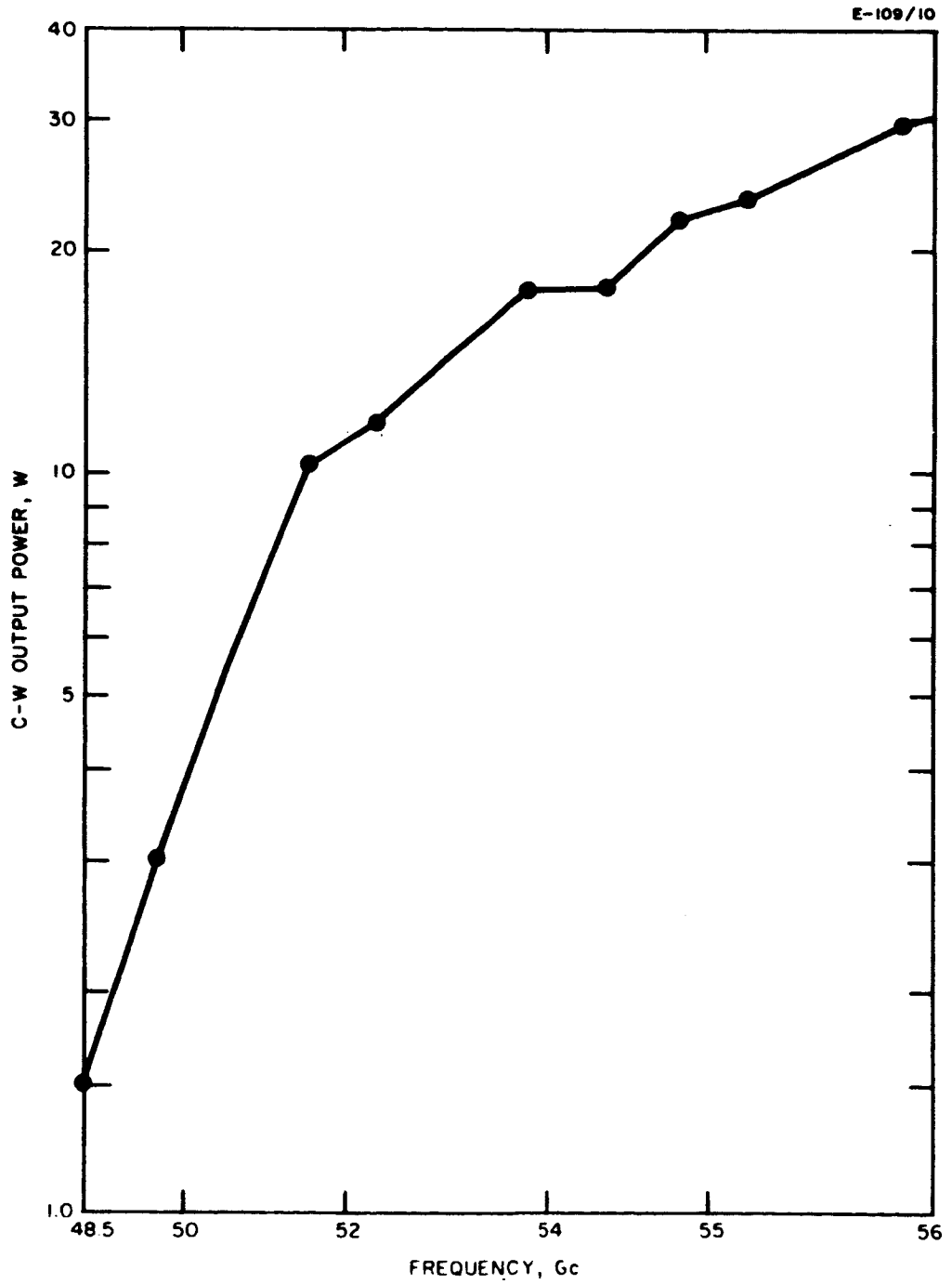

Figure 5-8. Typical Power Output Characteristics of the Type 381H Oscillator Tube

Electrical (Typical)

Heater Voltage	2.6 v, ac or dc
Heater Current	3.2 a, ac or dc
Collector Voltage (wrt cathode)	2.0 kv, dc
Collector Current	50 ma, dc
Anode Voltage (wrt cathode)	6.5 kv, dc
Anode Current	0.2 ma, dc
Cathode Voltage (wrt ground)	6 to 10 kv, dc
Tube Body Voltage	0
Tube Body Current	5 ma, dc
Ion Pump Voltage	3.5 kv, dc
Ion Pump Current	1 mu a, dc
Duty	100%
RF Power Output (min)	5w
Frequency Output	51 to 55 Gc
Tuning Slope (approx.)	1 mc/v

Type 381H Application Notes

Frequency Stability

The Type 381H provides an output signal with a very stable frequency. In general, the frequency stability is determined by the quality of the power supplies used with the tube. The cathode supply requires the best regulation but fortunately supplies only a few milliamperes of current. As seen from the tuning curve, the output frequency will vary about 1 kc per 1 mv of ripple in this supply. This corresponds to a regulation of 10^{-7} to hold the frequency constant to the order of 1 kc. The anode power supply is about 16 times less sensitive in producing a frequency change. This supply must be regulated to about 2.5×10^{-5} to limit the frequency change to 1 kc. The output frequency change is inversely proportional to the change in anode

voltage. This dependence is opposite to the characteristics of the cathode power supply and affords the possibility of cancellation of frequency shift by adjustment of the ripple phase and amplitude of the two power supplies. The collector supply plays no part in the RF operation of the tube and can be essentially unregulated. The tube requires about 30 minutes under operating conditions to become thermally stable. During this time the frequency will drift 20 mc and then be stable ± 1 mc due to thermal conditions. For best results the heater should be operated with a dc supply.

The 381H can be used as an extremely stable millimeter-wave source by locking the tube with a Pound discriminator circuit and a Fabry-Perot resonator. The Q of such a resonator can be easily about 100,000. In such an arrangement the tube is stable to at least one part in 10^7.

Spurious Output at Rated Conditions

The FM noise output of the 381H is down more than 30 db from the carrier power level at ± 6 kc. At ± 10 mc the noise output power is down more than 70 db.

The integrated AM and FM noise generated by the tube is as follows:

Spectrum Region from Carrier, Mc.	Max. Spectrum Power per Megacycle Bandwidth
± 5	-20 dBm
± 10	-30
± 15	-35
± 20	-35
± 40	-30
± 60	-40
± 80	-35
100	-40

FM to AM Conversion at Rated Conditions

The slope of the power output versus frequency curve is such that a 1 Mc change in operating frequency will produce less than a 0.1 dB change in output power.

Type 810H Distributed Interaction Klystron, Tentative Data

Description

The tube 810H is a distributed interaction klystron capable of a CW power output of more than 10 w over the frequency range of 51 to 55 Gc. The output frequency is determined by the cathode voltage in the range of 7 to 10kv and the resonant modes of the klystron cavity. The output power is determined by the beam current. High efficiency is obtained by the substantial depression of the collector potential below the circuit potential. A permanent magnet is used to focus the electron beam and the collector is air-cooled. An integral ion pump is included to insure long life.

Mounting Position

Any

Connections

RF	UG-385/U Waveguide
DC	Flying Leads

Mechanical (Maximum Overall)

Length	11 in.
Width	9 in.
Height	5 in.
Weight	10 lb.

Cooling Air Flow (sea level)

Collector	5 cfm at about 6 in. H_2O
Envelope	natural convection

Electrical (Typical)

Heater Voltage	2.6 v, ac or dc
Heater Current	3.2 a, ac or dc
Collector Voltage (wrt cathode)	2.0 kv, dc
Collector Current	60 ma, dc
Anode Voltage (wrt cathode)	7.2 kv, dc
Anode Current	0.5 ma, dc
Cathode Voltage (wrt ground)	7 to 10 kv, dc
Tube Body Voltage	0
Tube Body Current	10 ma, dc
Ion Pump Voltage	3.5 kv, dc
Ion Pump Current	1 μ A, dc
Duty	100%
RF Power Output (min)	10w
Frequency Output	51 to 55 Gc (not continuous)
Tuning Slope (approx.)	60 kc/v

Type HAV-1 Traveling Wave Amplifier, Tentative Data

Description

Tube type HAV-1 is a CW forward wave amplifier operating over the range of 49-58 Gc. (Serial numbers below 12 are single-structure tubes; those above are severed-circuit tubes featuring decoupled input and output slow-wave structures). These amplifiers have small signal gains of 10-15 db for the single-circuit tubes and 18-22 db for the severed tubes. Large signal output power is 100-150 watts for the former group, and 80-110 watts

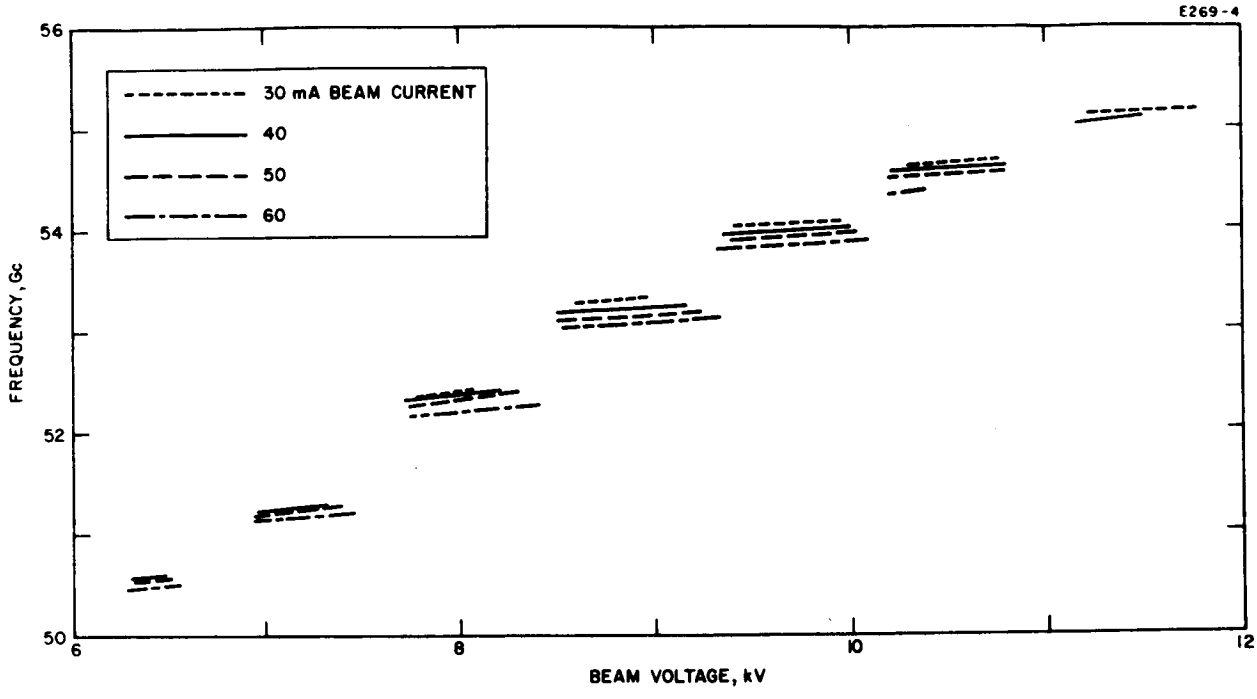

Figure 5-9. Typical Tuning Characteristics of the Type 810H Oscillator Tube

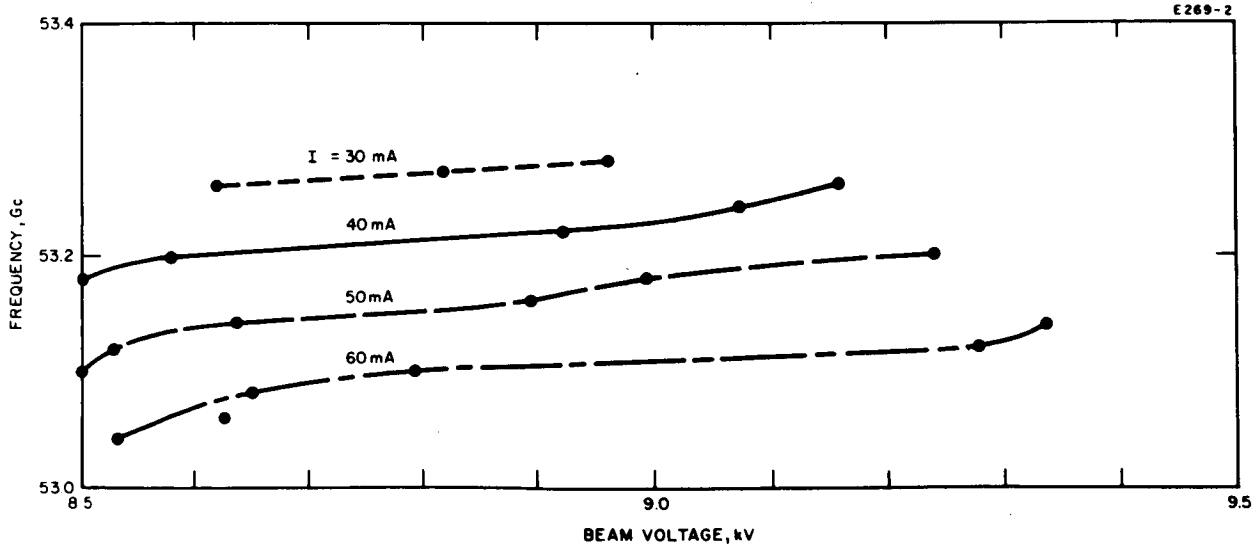

Figure 5-10. Detailed Tuning Characteristic of a Single Mode

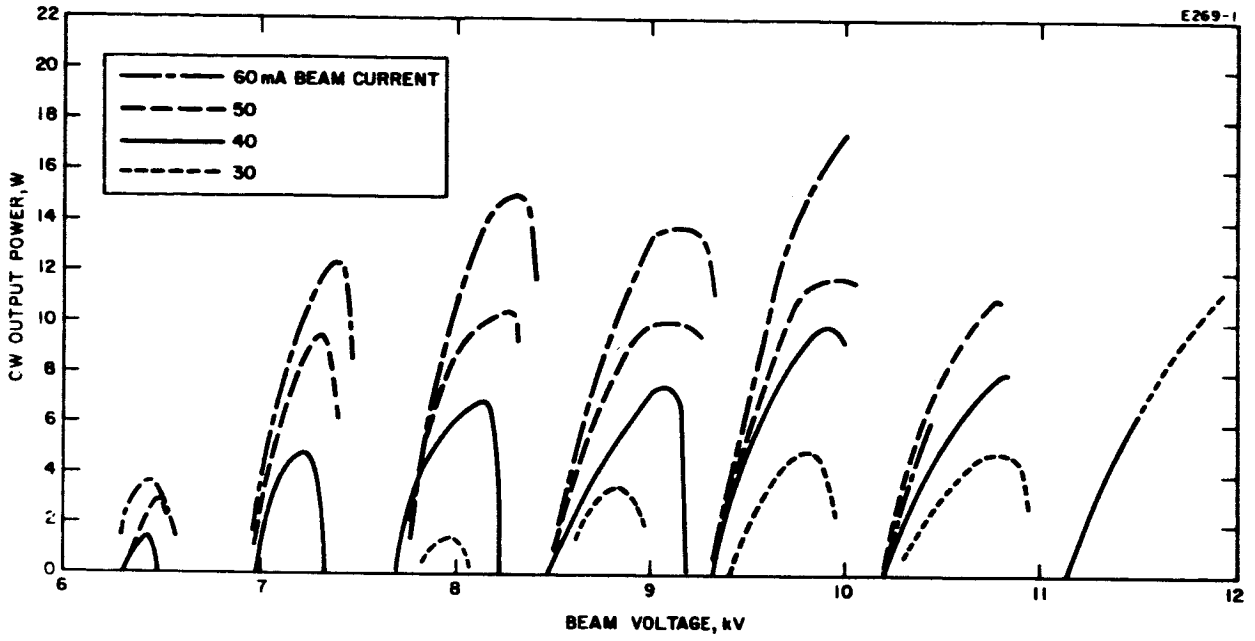

Figure 5-11. Typical Power Output Characteristics of the Type 810H Oscillator Tube

for the latter. High efficiency is obtained by a substantial depression of the collector potential below circuit potential. As a result of the reduced collector dissipation, only forced air is required to cool the collector radiator. An appendage ion pump is included as an integral part of the tube, resulting in extended tube life due to high-vacuum operation. The tube is designed for operation in a permanent magnet for focusing. It can also operate in a solenoid; numbers above 12 require a solenoid.

Mounting Position

Any

Connectors

RF	Input and output WR 15 waveguide with UG 385/U flanges.
DC	Flexible Leads

Mechanical Considerations (Maximum Overall)

Length	15 in.
Width	4 in.
Height	10 in. (length of permanent magnet)
Weight	17 lb., including magnet
Cooling Air Flow:	
Collector	50 cfm free air
Envelope and Magnet	Natural convection
Solenoid Cooling Water	1 gpm at approx. 50 psi.

Typical Operating Conditions

	Serial Below 12	Serial Above 12
Heater Voltage, ac or dc	3.2 v	3.2 v
Heater Current, ac or dc	3.2 a	3.2 a
Cathode Voltage, wrt tube body	-12 kv	-12 kv
Body Current	6 ma	6 ma
Collector Voltage, wrt cathode	+ 4 kv	+ 4 kv
Collector Current	125 ma	125 ma
Appendage Pump Voltage	3 kv	3 kv
Appendage Pump Current	1 μ a	1 μ a
Frequency Range	49-58 Gc	49-58 Gc
RF Output Power	100-150 w	80-110 w
Small Signal Gain	10-15 db	18-22 db
Duty	100%	100%

	Serial Below 12	Serial Above 12
Focusing Field	3000 gauss	3000 gauss
Solenoid Voltage	--	12.5 amp
Solenoid Current	--	200 volt

5.4.3.2 Comments on the Elliot-Litton Devices

The devices, although not quite as large as the Hughes family of tubes, share many of the same disadvantages in regards to use in a satellite environment. Efficiencies run in the order of three percent, but only two voltages excluding the heaters are required by these devices as compared to the Hughes tubes.

Since water cooling is recommended by the manufacturer, a closed loop heat exchanger or some other form of cooling would be required. This is the only major problem area. The power supply problem is similar to that of the Hughes tubes.

In regards to weight, investigation should be conducted to determine the feasibility of utilizing the doughnut type magnet structure instead of the present E shaped heavier magnets used on these tubes.

L-3628 Millimeter Wave Tubes

Floating Drift Tube Klystron Oscillator
8 mm, 10 Watts Power Output

This high power floating drift tube klystron oscillator operating in the millimeter frequency range has been designed by Elliott-Litton, Ltd. The floating drift tube construction gives the effect of a single cavity tube with the working efficiency of a two cavity klystron. Special advantages are

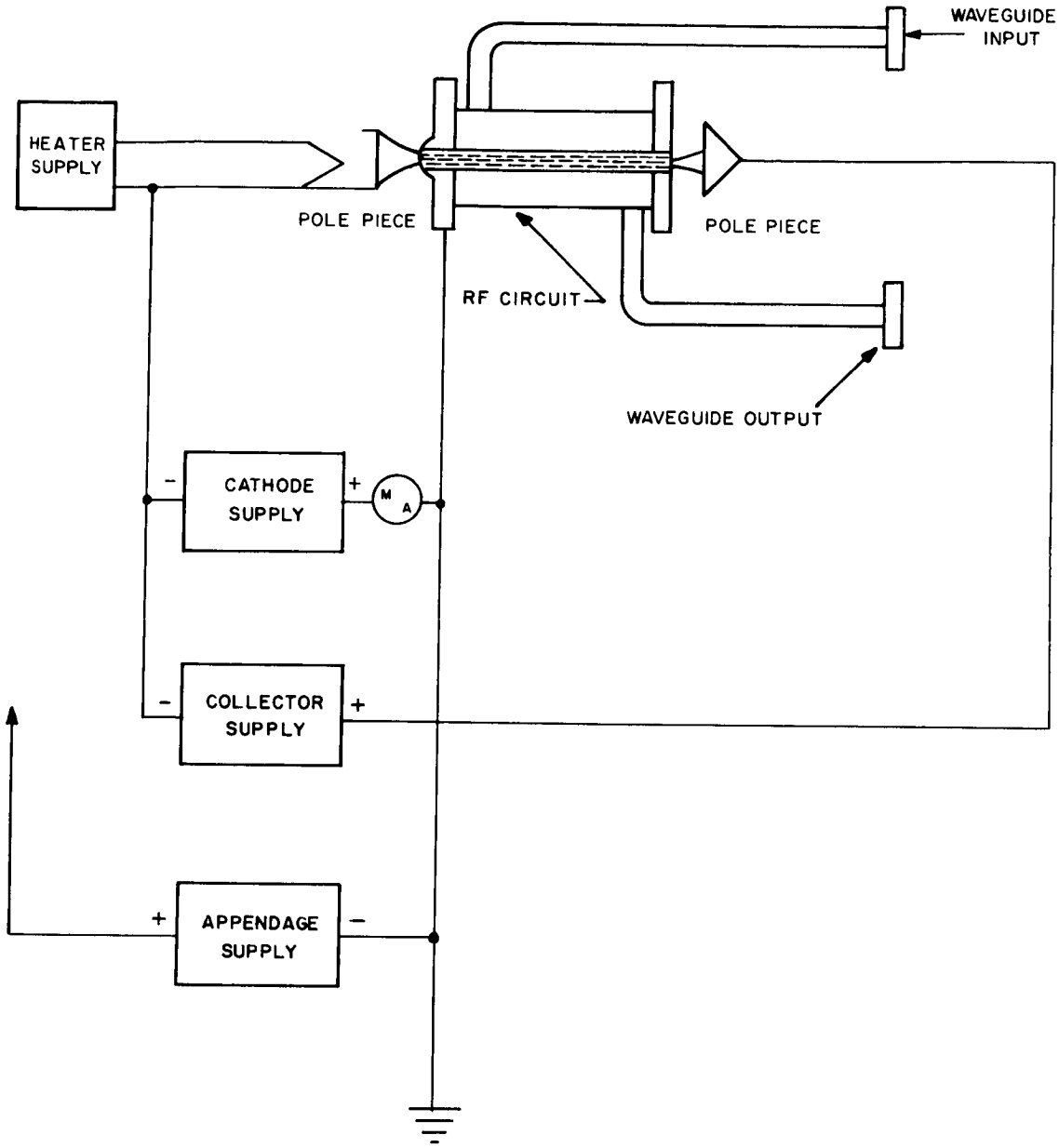

NOTE: The magnet or solenoid is at ground potential. The collector and cathode ends of the tube are at high potential and isolated from the magnet. Due care must be exercised for personnel safety. In general, a common isolation transformer can be used for heater and collector supplies. A suitable overcurrent protection device should be provided to remove cathode voltage when cathode-body current exceeds 7 mA.

Figure 5-12. Type HAV-1 Power Supply Circuits

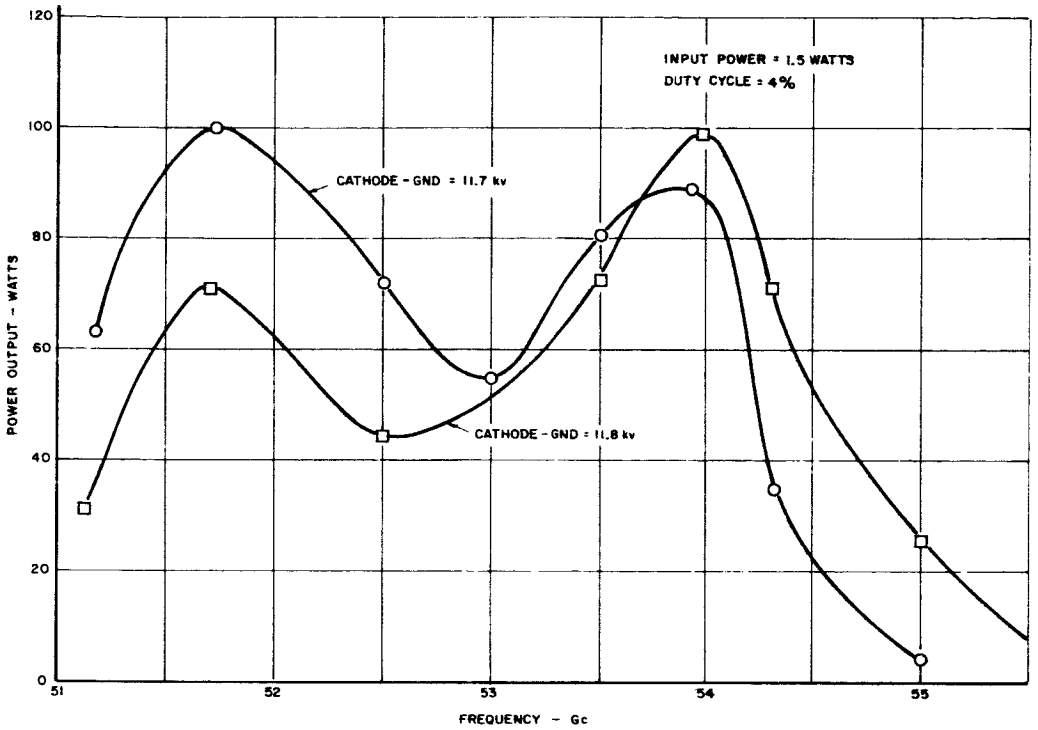

Figure 5-13. Power Output for HAV-1.15

freedom from hysteresis and an increase in operation stability. Low noise characteristics and improved cathode durability result in long life and reliability.

Performance Characteristics

Center Frequency	35 ± 2 Gc
Tuning Range	1600 mc
Power Output	(Min.) 10 w
Duty	CW

Typical Operating Conditions

Heater Voltage	6.3 v
Heater Current	2.0 a

Cathode Voltage	3.6 kvdc
Cathode Current	135 ma
Focus Electrode (Rel. to Cathode)	-750 v
Resonator Current	40 ma

Maximum Ratings

Heater Voltage	7.0 v
Cathode Voltage	4.0 kv
Cathode Current	150 ma
Focus Electrode (Rel. to Cathode)	-1000 v
Resonator Current	45 ma
Reflected Power	50 w

Mechanical Characteristics

Dimensions	See Figure 5-14
Weight	10 lbs.
Cooling	Water
Mounting Position	Any
Waveguide Output	Mates with RG-96/U

*Recommended water flow 0.25 gallon per minute corresponding to an inlet-outlet pressure differential of 3 pounds per square inch. After five minute warm up, drift due to change of ambient temperature from 20°C to 70°C is less than 2 megacycles providing water temperature is kept constant. With changing water temperature frequency drops approximately 1 megacycle per degree centigrade rise.

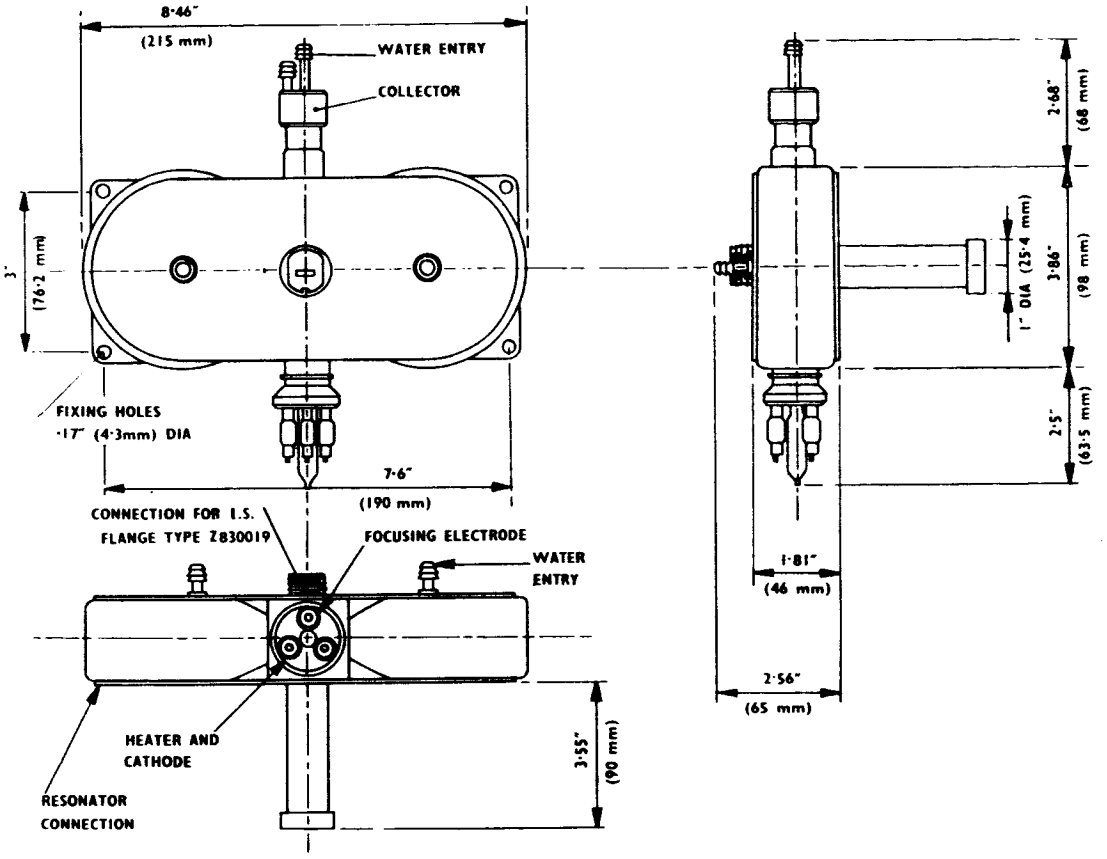

Figure 5-14. L-3628 Millimeter Wave Tube Outline Drawing

5.4.3.3 Comments on CSF and Warnecke Millimeter Devices

These tubes, at present, are laboratory and/or ground terminal devices. Efficiencies run in the order of three percent maximum. They are large and heavy devices and require multiple power supplies. An available capabilities report on the Warnecke Electron Tubes Company does not show the facilities to develop or test a device for satellite environment. However, the company may have access to such facilities outside of their own laboratory. Such data on CSF is not available at present.

The cooling problem applies to these tubes in much the same way as for any of the previously mentioned types. Investigation and development would be required to implement the use of these tubes in a satellite.

CSF Carcinotrons

These tubes, typical of the Backward Wave Oscillators marketed by CSF of France and Warnecke of the United States, are designed to cover the 39-41 Gc range and the 68 to 71 Gc range. Other frequencies outside the spectrums of concern in the proposed experiments are also generated by this family of devices. The 39-41 Gc device is an M-type cross-field BWO while the 68 to 71 Gc device is a Millman or Vane type BWO.

The CM-08 is cooled by forced air and the CO-40 is liquid cooled. The tubes are focussed by permanent magnets and specially designed for very high signal to noise ratio. The minimum fundamental to FM spurious noise between 0.1 to 7 mc from the carrier is 30 db. The minimum signal-to-AM noise ratio between 0.1 and 30 mc from the carrier is 130 db per cycle. All tubes are rugged and can withstand 10 to 50 cps vibration with max. acceleration of 10 g's.

	CM-08	CO-40
Band (Gc)	31-37	60-72
Heater Voltage (v)	4-6	6.0-7.5
Max. Heater Current (a)	2.4	2.2
Max. Cathode to Grid G1 Voltage (v)	0	-200
Cathode K to Anode A1 Voltage (v)	0-1800	0-3000
Max. Anode A1 Current (ma)	2	65
Cathode K to Line A2 Voltage (v)	1000-3500	3000-6000
Max. Line A2 Current (ma)	250	100

	CM-08	CO-40
Max. Cathode K Current (ma)		100
RF Output Connector	WG-RG 96/U Flange UG 381/U	WG-RG 98/U Flange UG 385/U
Power Connecting Base		Flying Leads
Approx. Weight (lbs.)	18	35
Minimum RF Output Power	15 w/CW	2 w-15 w

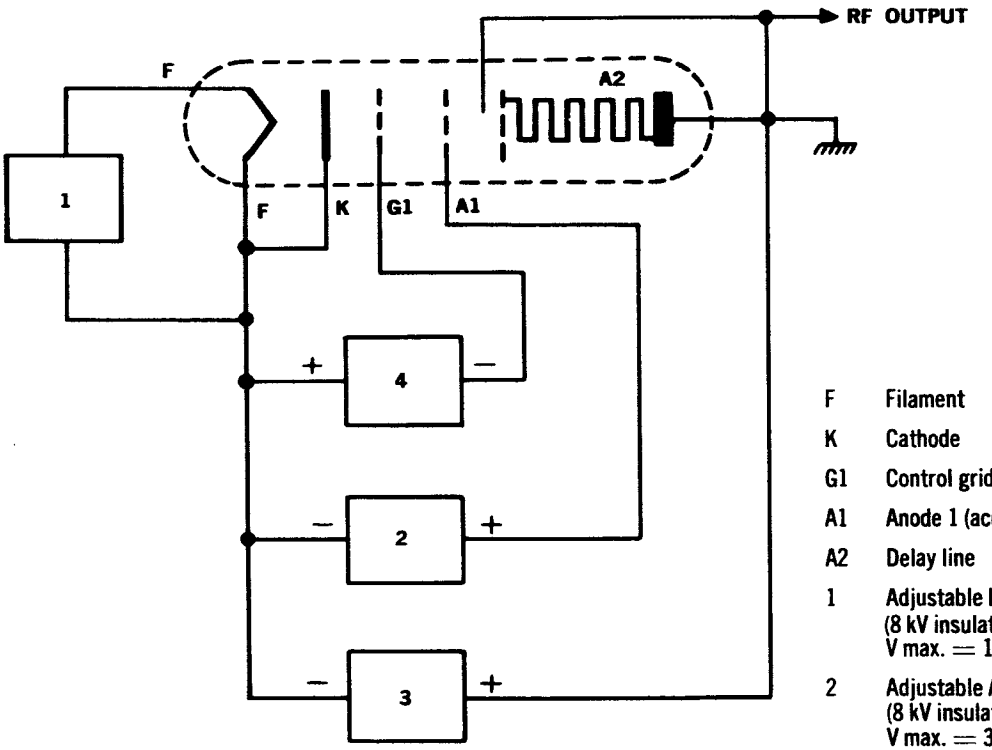

F Filament
K Cathode
G1 Control grid
A1 Anode 1 (accelerator)
A2 Delay line
1 Adjustable heater supply, preferably D.C., (8 kV insulation)
V max. = 10V I max. = 3A
2 Adjustable Anode A1 D.C. supply (8 kV insulation)
V max. = 3000V, I max. = ± 10mA
3 Adjustable Delay Line A2 D.C. supply
V min. = 2000V V max. = 6500V
I max. = 100 mA (COE 40)
80 mA (COE 20-1)
4 Adjustable control Grid G1 D.C. supply (8 kV insulation)
V min. = 0 V max. = −200 volts
I max. = 10mA

NOTE: The cathode is internally connected to one of the heater terminals.

Figure 5-15. Typical Carcinotron Circuit Diagram

AVERAGE CHARACTERISTICS

CARCINOTRON COE 40

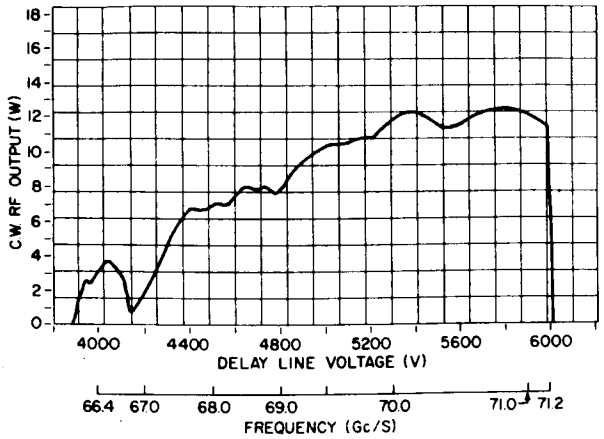

CARCINOTRON COE 20-1

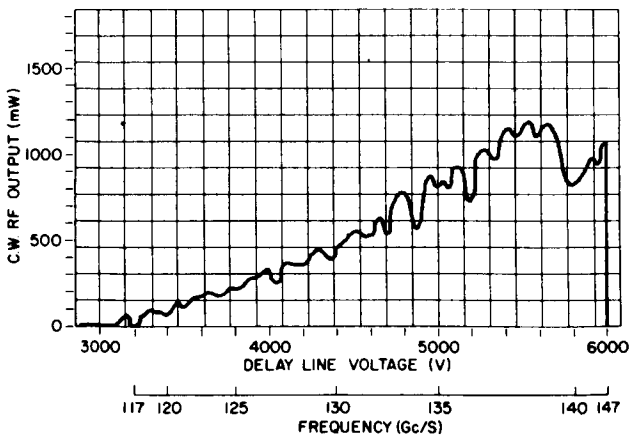

PHYSICAL LAYOUT

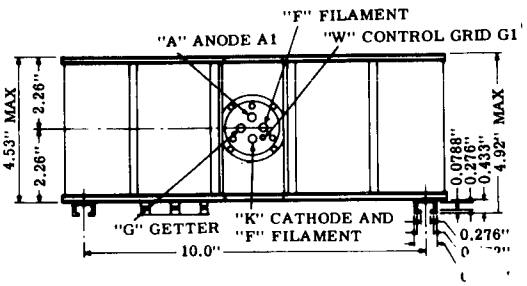

	COE 40	COE 20-1
WAVEGUIDE	RG 98/U	RG 138/U
GUIDE FLANGE	UG 385/U	UG 387/U

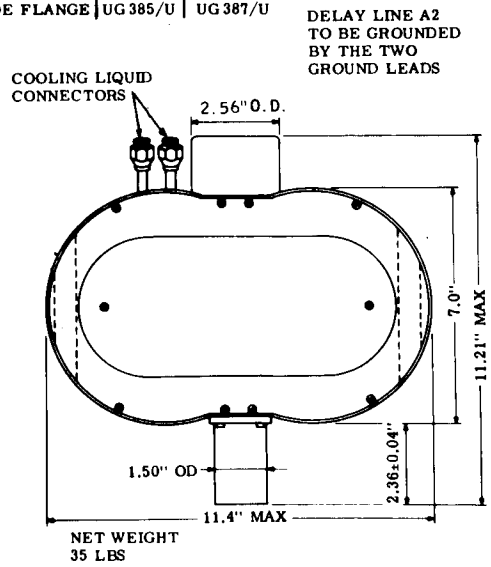

Figure 5-16. Carcinotron Average Characteristics and Physical Layout

5.4.3.4 Comments on OKI Millimeter Devices

OKI manufactures two types of high power millimeter oscillators. The "Laddertron", a type of floating drift tube klystron, and the second type, a two cavity klystron. The Laddertrons are similar to the Elliot-Litton devices and cover approximately the same spectrum while the two cavity klystrons operate in the 50 Gc range which is the lower end of the operating range of the Hughes Company devices.

These tubes are also laboratory and/or ground terminal devices. They share the same problems in general with all of the high power millimeter tubes. Since water cooling is required for operation of these tubes, the same effort will be required to obtain a solution to this problem if the device is to be operated in a satellite environment.

Life data is not available at this time.

Model 34LV10 OKI Electric Industry

General

The "Laddertron" is a tunable, flat-beam, single cavity, multi-gap klystron that has many superior features and characteristics as a high-power millimeter wave oscillator.

The 34LV10 is of mechanical tuning type, ranging from 33.2 Gc to 34.8 Gc and the output at 34 Gc is 10 watts approximately.

Features

High output power.
Higher efficiency as compared with other Klystrons.
Operation at lower voltage.

Broad range for mechanical tuning.

Broad range for electronic tuning.

Capable of frequency modulation by control electrode voltage.

Specifications

Mechanical Data

Output Connector:	Waveguide RG-96/U Flange UG-599/U
Base Connections:	Refer to Figure 5-17
Mounting:	Any position Magnetic materials should be kept away from the magnet by more than 10 cm.
Weight:	13 kg. approx.
Dimensions:	282 mm x 246 mm x 147 mm. approx. (Refer to Figure 5-17)
Cooling:	Water cooling required Minimum water flow at 20° to be more than 0.5 liters per minute.

Electrical Data

Maximum rating:

Heater Voltage	5.7-6.9v
Heater Current	1-2.0a
Resonator Voltage	2100v max.
Cathode Current	140 ma max.
Control Electrode Voltage	-50 -500v
Frequency Range	33.2-34.8 Gc
Output Power	3 watts min.

Warming up Time	150 sec. min.
Load VSWR	1.5 max.
Series resistance connected with cathode	20 k max.
Temperature at outflow of cooling water	35°C

Typical Operating Data

Heater Voltage	6.3v
Frequency	34000 mc
Resonator Voltage	1900v
Cathode Current	120 ma
Control Electrode Voltage	-200v
Output Power	10w
Electronic tuning range	*(1) 20 mc
	**(2) 40 mc
Modulation Sensitivity	*(1) 0.2 mc/vc
	**(2) 0.4 mc/vw
Cooling Water Flow	1 ℓ/min.

*(1) Defined as the frequency difference between the half power points of the maximum power output and is obtained by the variation of the resonator voltage alone. (Refer to Figure 5-17)

**(2) Defined as the frequency difference between the half power points of the maximum power output and is obtained by the variation of the control electrode voltage using the reference circuit in Figure 5-17.

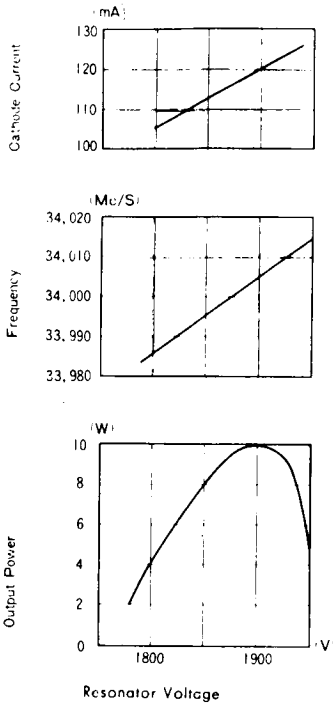

Typical operating data

With mechanical tuning fixed at a certain position, the circuit with which FIG. 1 is obtained by changing the beam voltage is shown in Fig. 2 (at R 0).

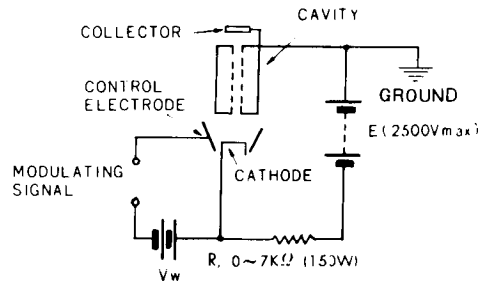

Electrical connections

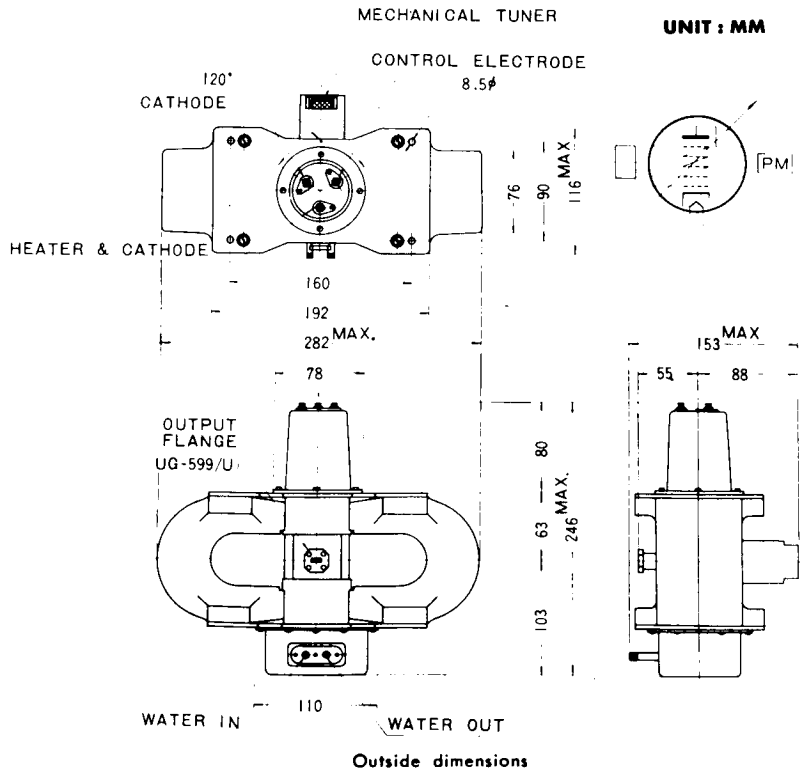

Outside dimensions

Figure 5-17. 34 kmc Laddertron Outline Drawing, Electrical Connections and Operating Data

Caution: 1. Do not turn on the switch of the power supply to the resonator without applying the water cooling.

2. Much care should be taken not to give any shock to the tuning mechanism.

5.4.3.5 Comments on I. T. T. Millimeter Devices

Operating in the one watt area, the I. T. T. reflex klystron is a small light weight device. At present, this device has been operated at a power level of one watt to 45 Gc. Efficiencies for this device run about two percent. For stable frequency operation, the use of a blower is recommended. Further investigation of this parameter would have to be made and adequate cooling methods implemented for use in a space craft.

It is felt that adaptation of this device to a satellite environment would be relatively easy.

I. T. T. Millimeter Devices

The reflex klystron, operating at a semi-fixed frequency, utilizes an external tuner. By removing the tunable element from the path off the direct beam, the design is greatly simplified according to the manufacturer.

Tube Characteristics and Performance

The design according to the manufacturer is applicable to the range of 18-100 Gc by only adjusting the cavity, output waveguide and window dimensions. As of this date, one watt has been obtained up to 45 Gc, but tubes have been made throughout the 18 to 110 Gc range to ascertain suitability of design.

Frequency in Gc	Power in Watts
23	2.7
35	2.4
45	1.0
70	0.5
110	0.01

The tuning characteristics of tubes operated at 35 Gc are shown in Figure 5-18.

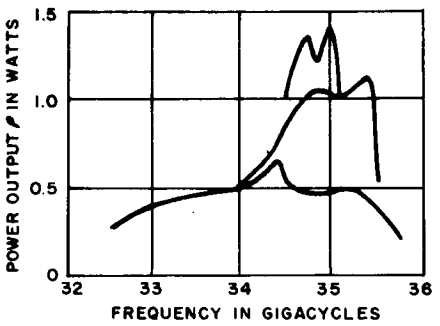

Figure 5-18. Typical Tuning Characteristics of I. T. T. 35 Gc Tubes

The three curves result from adjusting the coupling between the klystron and the external tuning cavities and indicate the balance obtainable between power output and tuning range. At 35 Gc, the frequency stability is stated at ± .25 mc representing a dimensional variation in the cavity interaction gap of about 50 atomic layers.

For the externally tuned klystron, a temperature coefficient of 1 mc per degree up to 60° C has been obtained. A high order of modulation

linearity from 0.5 to 1 percent, expressed as the change in slope over a bandwidth of 10 mc has also been realized. Alternatively the measured level of harmonic distortion produced by the nonlinearity gives bandwidths of the order of 10 mc at a second harmonic level of -70 db.

The tube output appears in circular waveguide, and the transition to rectangular guide is incorporated in the external tuner. Cooling fins are provided to enable a small blower to maintain the body temperature at a few degrees above ambient. Convection cooling is adequate for all applications, except those demanding the highest frequency stability.

Life testing on several tubes is being conducted. By November 1963, one tube had reached 4200 hours without appreciable change in characteristics. The tungsten dispenser-type cathode being used is moderately loaded at 1.6 amperes per square centimeter. Cathode manufacturers currently talked in terms of 70,000 hours of life at 2.5 amperes per square centimeter.

Typical Operating Conditions

Parameter	Unit of Measurement	Rating
Cathode Voltage	Volts	-2000
Grid Voltage - (with respect to cathode)	Volts	-50
Outer Reflector Voltage (with respect to cathode)	Volts	-700
Inner Reflector Voltage (with respect to outer reflector)	Volts	-60
Peak Output Power	Watts	1.5
Min. output Power over tuning range of 2 per cent	Watts	1
Center Frequency	Gc	35

Electronic Tuning

Reflector Mode	Peak Power in Watts	Bandwidth in mc at Half Power Points
3 3/4	2.18	82
4 3/4	.960	220
5 3/4	.270	550

Conclusion on I. T. T. Devices

The information stated above, was primarily obtained from an article in the December 1964 issue of the Microwave Journal. The results are peak performance realized in the laboratory. The manufacturer is much less optimistic in stating the specifications for purchasing reasons. As an example, a tube contained in the family of these devices will yield the following parameters on a production basis:

Type	F-2900
Frequency Gc	33-40
Typical Power Output	1100 mw
Min. Power Output	1000 mw
Elec. Tuning Range	35 mc
Beam Voltage Typical	2kv
Beam Current Typical	40 ma
Reflector Voltage Volts	-25 to -1kv
Focusing Grid Voltage	0 to -200v
Heater	V 6.3v I 1.2a
Mounting Position	Any

5.4.3.6 Devices Below One Watt

Of the many millimeter tubes with power output of less than one watt, the following were selected: Raytheon's QKK 996 and Varian's VA-239. Both of these devices have been designed for space environment and are ruggedized, compact, light weight, reflex klystrons. The specifications are as follows:

	QKK-996*	VA-239
Frequency Range Gc	34-35.6	34-35.6
Minimum Output Power	300 mw	400 mw
Typical Output Power	Not Listed	600 mw
Mech. Tuning Range	1600 mc	Fixed Freq.
Elect. Tuning Range	Not Listed	75 mc
Filament Voltage	6.3 v	6.3 v
Filament Current	0.9 a	1.25 a
Beam Voltage	900 v	2500
Beam Current	75 ma	25 ma
Repeller Voltage	-150 to -350	-200 to -600
Max. Shell Temp.	200°C	200°C
Input Base	Flying leads	Flying leads
Output Flange	UG-599/U	UG-599/U
Output Waveguide	RG-96/U	RG-96/U
Mounting Position	Any	Any
Altitude	Any	Any
Cooling	Conduction	Conduction
Vibration	10 g 10~to 1 kc max. dev. = 1 mc p-p	10 g 10~to 1 kc max dev. = 1 mc

*Under Development

5.4.3.7 Solid State Multipliers and RF Sources

The solid state RF source in most cases takes the form of a crystal stabilized transistor oscillator followed by a varactor frequency multiplier chain. It is now possible to obtain tenths of watts of RF power by this method at X-band and one company claims a tenth of a watt at 33 Gc using the varactor multiplier technique. Other solid state microwave oscillators using tunnel diodes, transistors (directly), varactors (directly, as a parametric oscillator), molecular-atomic and piezo electric crystal frequency standards and other microwave parametric resonant devices are also available but not discussed in this report. Table 5-V shows some available types from 10 Gc up.

Noise (Short Term Stability)

Measurement data on a two cavity klystron compared with a solid state source showed the klystron to have an order of magnitude less FM noise in a 1 kc bandwidth. As the 1 kc bandpass was moved away from the carrier, the klystron noise decreased and the solid state unit's noise increased. The AM noise in a 1 kc bandwidth measured between 2 kc and 100 kc from the carrier was always 2 to 6 db less for the klystron. Passive stabilization (a high Q cavity at the output of the klystron) decreased the klystron FM noise by two orders of magnitude and the AM noise decreased by three db under the above conditions.

Frequency Stability (Long Term)

The stated frequency stability of the solid state devices of $\pm 1 \times 10^{-6}$ is achieved by placing the crystal oscillator and buffer in an oven which limits the temperature excursion to one or two degrees. Two cavity klystrons will have a long-term stability of better than 50 ppm if their operating temperature is kept constant to within $\pm 1\,^{\circ}C$.

TABLE 5-V

SOLID STATE MICROWAVE SOURCES FROM 10 Gc UP

Type	Manufacturer	Output Freq. (Gc)	Max. DC Input Power Required (watts)	Max. Spurious Harmonics (db)	Freq. Stability Long Term with Oven	Min. Power Output (mw)	Status
MA-8606	Microwave Assoc.	8.5–10	43.36	-30	$\pm 1 \times 10^{-6}$	150	Production
MA-8607	" "	8.5-10	14.56	-30	$\pm 1 \times 10^{-6}$	10	"
MA-8614	" "	10.0-12.4	43.36	-30	$\pm 1 \times 10^{-6}$	75	"
MA-8601	" "	12.75-14.5	43.36	-30	$\pm 1 \times 10^{-6}$	75	"
MA-8232	" "	12.75-14.5	14.56	-30	$\pm 1 \times 10^{-6}$	5	"
MA-8233	" "	14.5-16.5	14.56	-30	$\pm 1 \times 10^{-6}$	3	"
MA-8619	" "	32.0-36.0	43.36	-30	$\pm 1 \times 10^{-6}$	3	"
D91U2	Sperry	13.25	49.0	-30	$\pm 1 \times 10^{-6}$	500	"
D91U1	"	17.5	49.0	-30	$\pm 1 \times 10^{-6}$	300	"
R-601	Raytheon	10.225-10.525	25	-60	$\pm 1 \times 10^{-6}$	75	"
SMX3127	West. Microwave Lab., Inc.	9.8-10.2	3.9	Not Listed	$\pm 1 \times 10^{-6}$	2	"
SMX3131	" "	10.5-11.2	5.4	"	$\pm 1 \times 10^{-6}$	5	"
SMX3135	" "	12-12.4	5.4	"	$\pm 1 \times 10^{-6}$	1	"
--	Sylvania	33	None (requires 200 mw RF input)	Not Listed	--	100	Developmental 3X Multiplier

Vibration

Tests made on a solid state L-band source shaken with 1/2 g from 5 cps to 2 kc showed peak deviations gradually increasing from about 20 cps at low vibrating frequencies to 50 cps at 2 kc. A large number of resonances, which seemed to come from the crystal itself were observed. Full scale readings for these tests was one kc deviation, and this was exceeded at five or six frequencies between 920 cps and 2 kc.

Reflex klystrons, unfortunately exhibit resonances in the 2-100 kc region when vibrated at frequencies between 10 cycles and 2 kc. A number of two cavity klystrons have been tested under vibration; these tubes do not exhibit resonances unless shaken directly at the resonant frequency. These tubes exceeded the 1 kc deviation at only three points.

Efficiencies

Klystrons run the range from a fraction of a per cent to as high as 20 percent depending on the frequency and power output. Klystrons are available at the one watt level at 35 Gc having an efficiency of two per-cent. The Sperry D91U2 listed, has an efficiency of about one per cent for 500 mw at 13 Gc.

Bandwidth

At present, varactor-chain bandwidth is a serious problem. Present state-of-the-art is about one to two per cent at X-band. When these bandwidths are required, efficiency is markedly reduced. Improvements are expected in this area.

Stress, Reliability, and Life

There exist circumstances in which the reliability of solid state sources is questionable. As an example, an X-band source producing

100 to 400 mw uses three to five power amplifier stages between the crystal oscillator and the VHF output point. The final VHF stage most likely consists of two transistors in parallel, operating near or at their maximum ratings. The impedance match from the output VHF stage to the first varactor stage is extremely critical and should environmental stresses for example, distort a coil, the transistors could easily be destroyed. In addition, the four varactor frequency multipliers (assuming X 128) would have input and/or output filtering stage, some double or triple tuned and three of the multipliers would utilize idler circuits. All varactor stages would be required to deliver state-of-the-art efficiency and the input stage would be operating near its maximum power rating. From this viewpoint, this device would probably be inferior to a klystron. In an application where long term life is required, it may be more advisable to use a low power klystron with a proven MTBF in excess of two to one above the life requirements.

Size and Weight

There seems to be little trade-off in this respect. A typical X-band solid state source required eighty cubic inches. With better packaging this could probably be reduced to fifty cubic inches. A VA508 klystron packaged with its own regulated, filtered power supply would occupy fifty to sixty cubic inches. Both units would weigh three to five pounds.

Conclusions

The choice of using a solid state source or a klystron in a given application should be made objectively without being trapped by the current cliches of "solid-state reliability and compactness". A careful study of the system requirements should be made before specifying the type of device.

5.5 Stabilization of Receiver Local Oscillators and Transmitters

This section discusses a family of frequency control methods through the implementation of stabilization loop techniques in RF sources and presents the transfer equations which allow for the proper selection of the optimum loop closure for a given device. The selected loop is dependent on the control parameters and types of RF source under consideration in the utilization of different loop techniques that allow for either frequency locking or phase locking of RF sources. Note that these loops are generally applicable as transmitter stabilizers or local oscillator AFC lock subsystems.

5.5.1 IF Discriminator Loop Frequency Control

The basic control system may be described by the simple block diagram shown in Figure 5-19. Given a block diagram, it is convenient

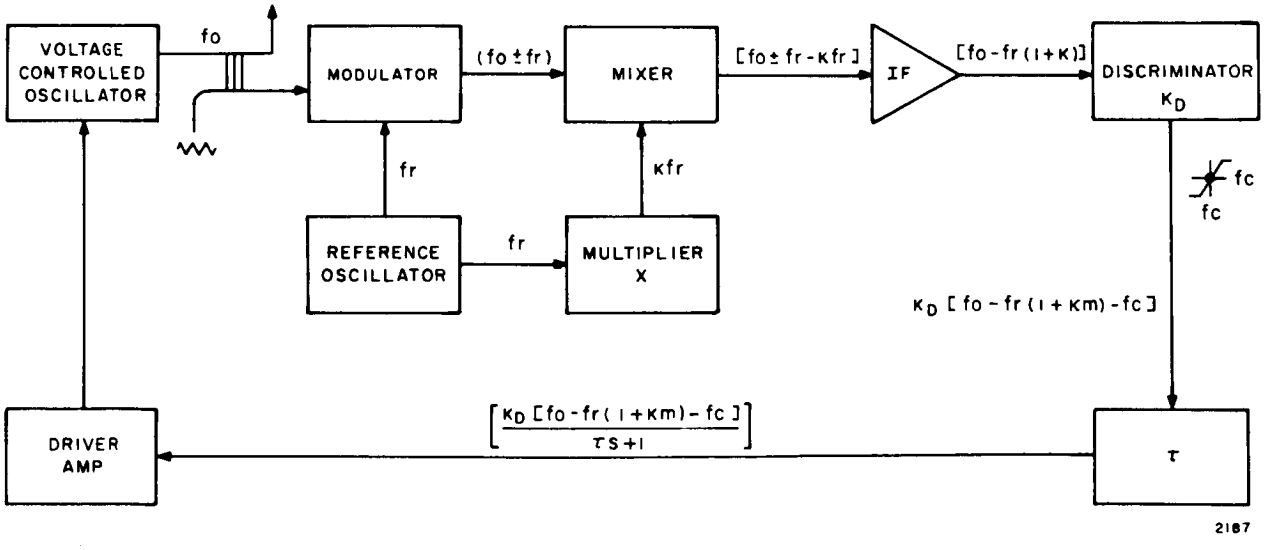

Figure 5-19. IF Discriminator Frequency Lock Loop

to write the equivalent signal flow graph. The value of the signal at various points in the block diagram is stipulated in Figure 5-19.

From Figure 5-19:

$$f_o(s) = \frac{K_1 K_D \left[f_o(s) - f_R(s)(1 + K_M) - f_c(s) \right]}{\tau S + 1} \tag{5-1}$$

$$f_o(s) \left[1 - \frac{K_1 K_D}{\tau S + 1} \right] = - \frac{K_1 K_D \left[f_R(s)(1 + K_M) + f_c(s) \right]}{\tau S + 1} \tag{5-2}$$

$$f_o(s) = - \frac{K_1 K_D \left[f_R(s)(1 + K_M) + f_c(s) \right]}{\tau S + 1 - K_1 K_D} \tag{5-3}$$

The transfer function of the loop is a function of two control variables; namely f_R (the frequency of the reference oscillator), and f_c (the crossover frequency of the linear discriminator). The two transfer functions of interest are:

$$\frac{f_o(s)}{f_r(s)} = - \frac{K_1 K_D (1 + K)}{\tau S + 1 - K_1 K_D} \tag{5-4a}$$

$$\frac{f_o(s)}{f_c(s)} = - \frac{K_1 K_D}{\tau S + 1 - K_1 K_D} \tag{5-4b}$$

The transient performance of a feedback control system is analyzed by determining the time it takes for a loop to reach the final value. Assume the loop is open, thus f_o is independent of f_r. When the loop is closed it appears to the controlled variable f_o as a step displacement of the reference variable f_r. From Equation (5-4a) for a step input of F_r,

$$f_o(s) = - \frac{K_1 K_D (1 + K) F_r}{S \left[\tau S + 1 - K_1 K_D \right]} \tag{5-5}$$

By partial fraction expansion

$$f_o(s) = -\frac{\frac{K_1 K_D (1+K) F_r}{1 - K_1 K_D}}{S} + \frac{\frac{K_1 K_D (1+K) F_r}{1 - K_1 K_D}}{S + \frac{1 - K_1 K_D}{\tau}} \qquad (5\text{-}6)$$

Taking the inverse Laplace Transform yields

$$f_o(t) = -\frac{K_1 K_D (1+K)}{1 - K_1 K_D} F_r + \frac{K_1 K_D (1+K) F_r}{1 - K_1 K_D} e^{-\frac{(1 - K_1 K_D) t}{\tau}}$$

$$= \frac{K_1 K_D}{1 - K_1 K_D} (1+K) F_r \left[e^{-\frac{(1 - K_1 K_D) t}{\tau}} - 1 \right]$$

System Stability

The system is stable if the exponential term is damped, or if

$$\frac{1 - K_1 K_D}{\tau} > 0$$

$$K_1 K_D < 1$$

Steady State Error

As t approaches ∞ the output frequency $f_o(t)$ approaches

$$f_o(t) = -\frac{K_1 K_D}{1 - K_1 K_D} (1+K) F_r$$

$$t \to \infty$$

Assume we wanted the desired output frequency to approach $(1 + K) F_r$, then the error between what is desired and what is achieved is (defined as e_{ss}, error steady state):

$$e_{ss} = (1 + K) F_r - f_o(t)$$

$$t \to \infty$$

$$= (1 + K) F_r + \frac{K_1 K_D}{1 - K_1 K_D} (1 + K) F_r$$

Simplifying yields

$$e_{ss} = \frac{1}{1 - K_1 K_D} (1 + K) F_r$$

Summary: What has been obtained is that for a step change in the controls variable f_r the system observes a control variable $(1 + K) f_r$. This is intuitively satisfying as the reference frequency is multiplied by the constant K.

When a step change is made in the variable f_r the output frequency f_o apporaches the value $(1 + K) f_r$ with an error of

$$e_{ss} = \frac{1}{1 - K_1 K_D} (1 + K) f_r$$

The time it takes the output f_o to reach the final value is the time required for the exponential term $e^{-\frac{(1-K_1 K_D)}{\tau} t}$ to decay.

The response of the system could have been obtained if the various principles and techniques utilized in the analysis and design of feedback or automatic control systems had been employed. This approach will be taken here, as it is simpler and gives a better "insight" into the system.

From Equation (5-4a) an equivalent block diagram can be obtained

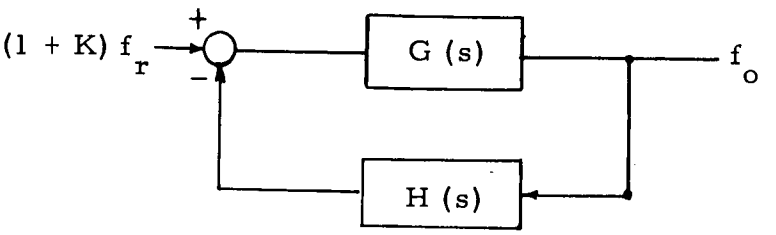

$$G(s) = - \frac{K_1 K_D}{\tau S + 1}$$

$$H(s) = 1$$

Stability

On a root locus plot one pole at $s = -1/\tau$, and one zero at $s = \infty$

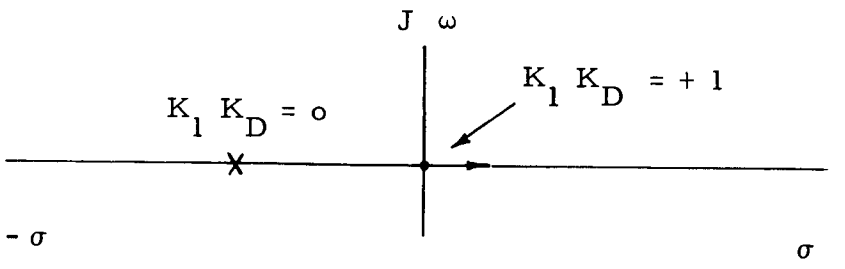

Intersection of root loci with imaginary axis when gain $K_1 K_D = -1$

Type of System

Zero order system

$$K_p = \lim_{s \to o} G(s)$$

$$= - K_1 K_D$$

Positional Error

$$e_{ss} = \frac{\text{control variable}}{1 + K_p}$$

$$e_{ss} = \frac{(1 + K) F_r}{1 + K_p}$$

$$e_{ss} = \frac{(1 + K) F_r}{1 - K_1 K_D}$$

5.5.2 Multiplier Phase Lock Loop

The basic control system may be described by the simple block diagram shown in Figure 5-20. Given a block diagram it is convenient to write the equivalent signal flow graph. The value of the signal at various points in the block diagram is stipulated in Figure 5-20. From Figure 5-20

$$f_o(s) = \frac{K_1 K_\phi \left[f_o(s) - (1 + K) f_r(s) \right]}{s (\tau s + 1)} \qquad (5\text{-}5)$$

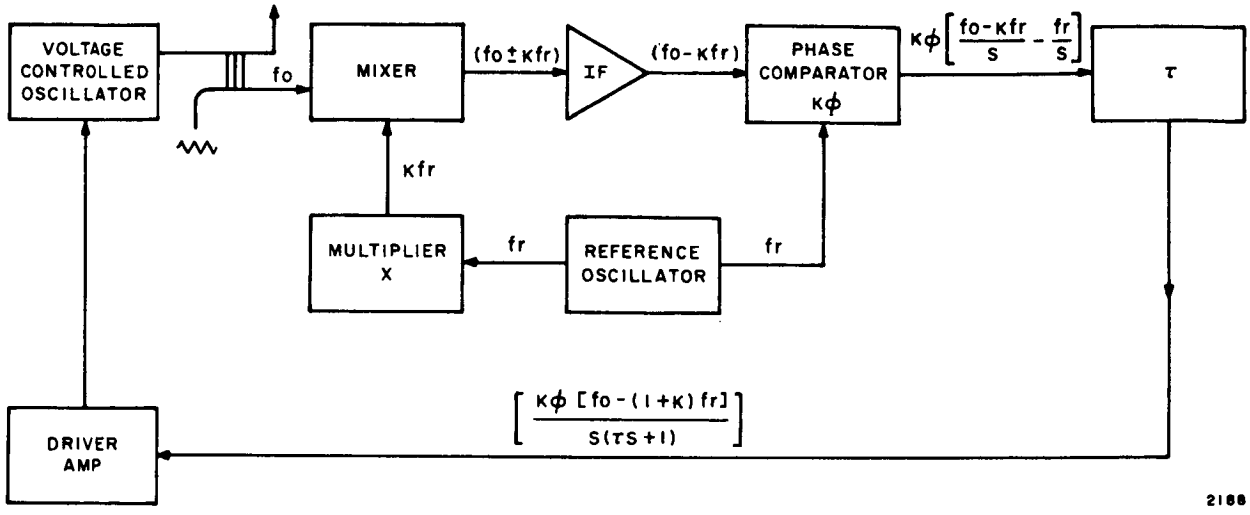

Figure 5-20. Multiplier Phase Lock Loop

Simplifying yields

$$\frac{f_o(s)}{f_r(s)} = \frac{-\dfrac{K_1 K_\phi (1+K)}{s(\tau s+1)}}{1-\dfrac{K_1 K_\phi}{s(\tau s+1)}} \qquad (5\text{-}6)$$

From the equation (5-6) the equivalent block diagram is

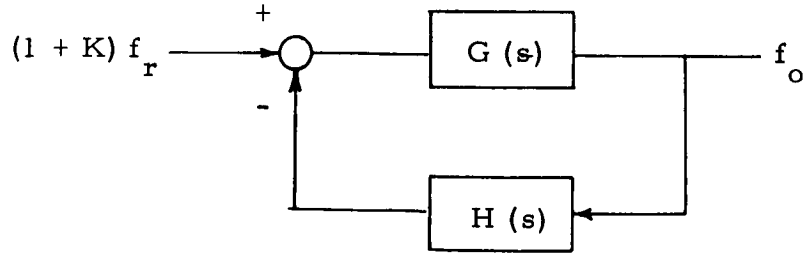

$$H(s) = 1$$

$$G(s) = -\frac{K_1 K_\phi}{s(\tau s+1)}$$

Type of System

A first order system thus a zero position error.

$$K_p = S \quad o = \infty$$

$$K_v = S\,G(s) = -K_1 K_\phi$$

$$s \rightarrow o$$

Stability

Root locus plot

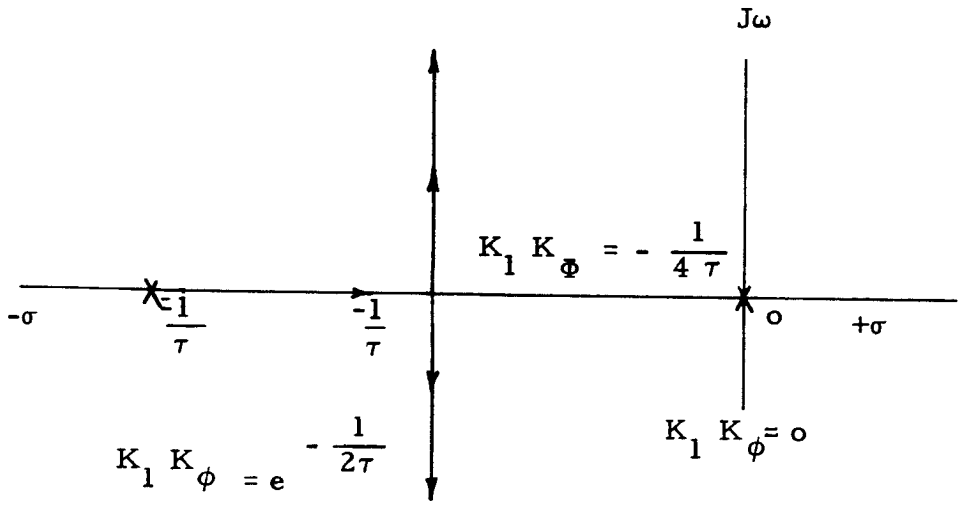

5.5.3 Modulated Phase Lock Loop

The basic control system may be described by the simple block diagram shown in Figure 5-21. Given a block diagram it is convenient to write the equivalent signal flow graph. The value of the signal at various points in the block diagram is stipulated in Figure 5-21. For analysis purposes, it is convenient to let the IF strip pass the upper sideband. It can be shown that either sideband yields the same result.

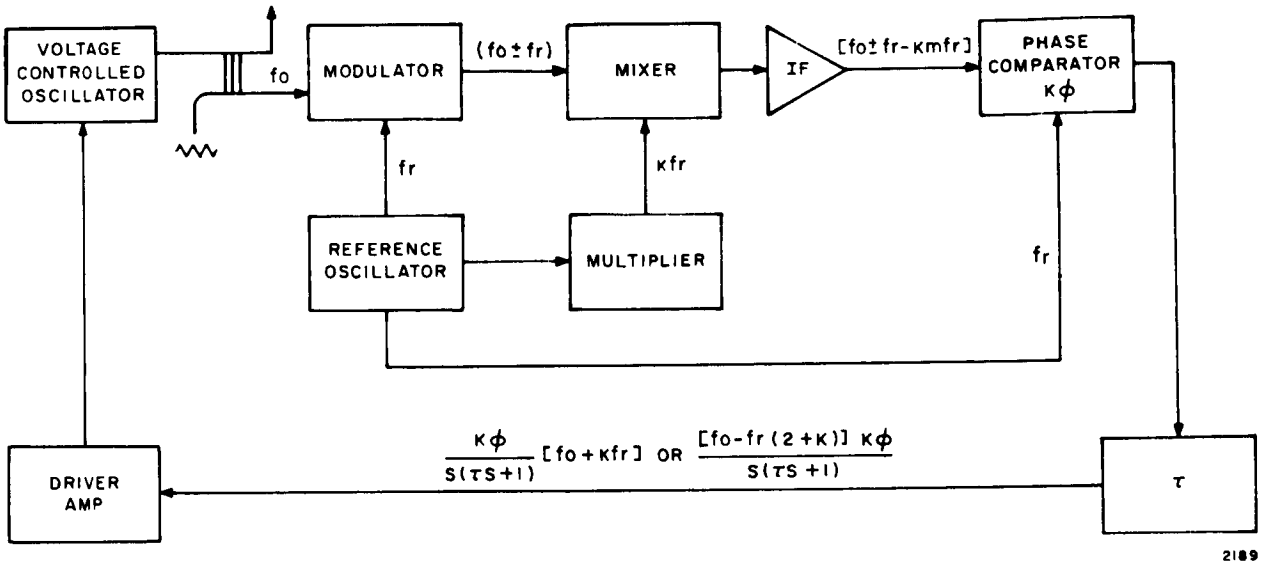

Figure 5-21. Modulated Phase Lock Loop

From Figure 5-21 using the upper sideband:

$$f_o(s) = \frac{K_1 K_\phi \left[f_o(s) + K f_r(s) \right]}{S(\tau S + 1)} \tag{5-7}$$

Simplifying

$$\frac{f_o(s)}{K f_r(s)} = \frac{K_1 K_\phi}{S(\tau S + 1) - K_1 K_\phi} \tag{5-8}$$

From Equation (5-8) an equivalent block diagram

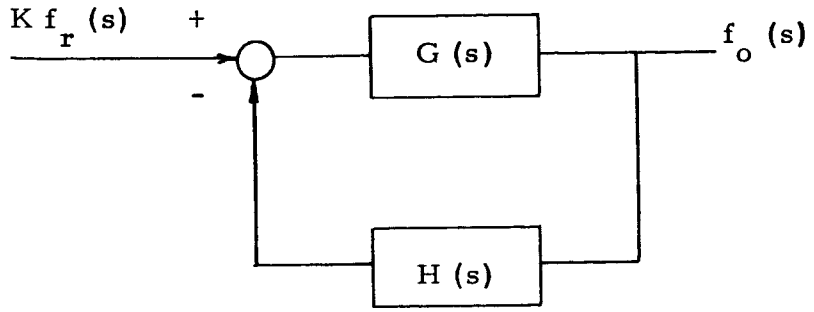

$$G(s) = \frac{K_1 \quad K_\phi}{S(\tau S + 1)}$$

$$H(s) = -1$$

Type of System

A first order system, thus a zero position error

$$K_p = \infty$$

$$K_v = K_1 K_\phi$$

Stability

Root Loci Plot

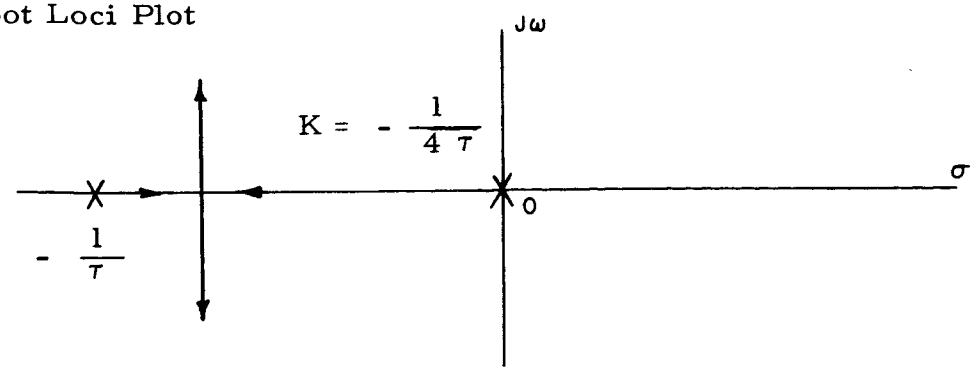

5.5.4 Multiplier Control Technique (Figure 5-22)

$$f_o(s) = K f_r(s) \tag{5-9}$$

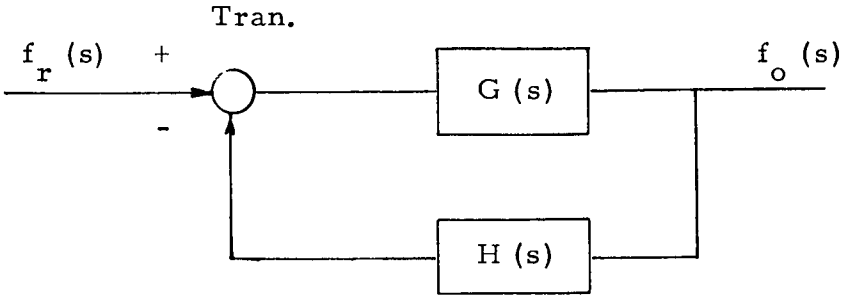

$$G(s) = K$$

$$H(s) = o$$

No feedback a free running loop.

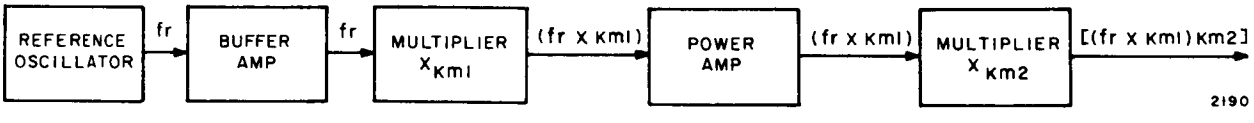

Figure 5-22. Multiplier Chain

5.5.5 Injector Lock Control (Figure 5-23)

$$f_o(s) = K_1 K f_r(s) \tag{5-10}$$

$$\frac{f_o(s)}{f_r(s)} = K_1 K \tag{5-11}$$

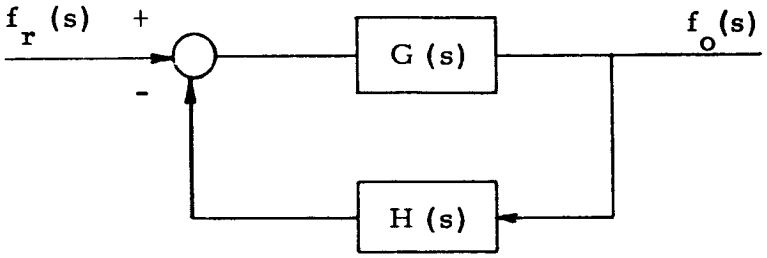

$$G(s) = K_1 K$$
$$H(s) = o$$

Free running loop with no feedback.

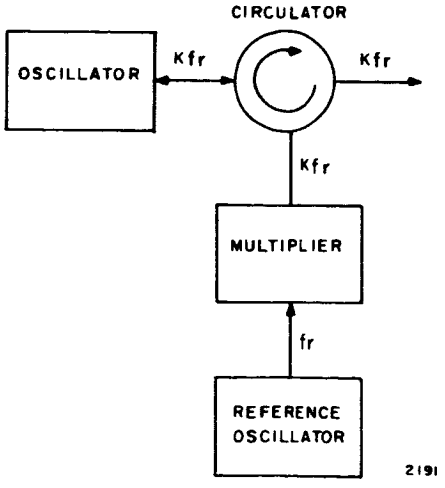

Figure 5-23. Injector Lock Technique

5.5.6 Pilot Modulated Phase Loop

If the IF strip passes the upper sideband of the balanced mixer there is no error signal generated by the phase comparitor. The control loop is "free running".

If the IF strip passes the lower sideband then from Figure 5-24

$$f_o(s) = -\frac{K_1 K_\phi 2 f_r(s)}{S(\tau S + 1)} \tag{5-12}$$

or

$$\frac{f_o(s)}{f_r(s)} = \frac{-K_1 K_\phi 2}{S(\tau S + 1)} \tag{5-13}$$

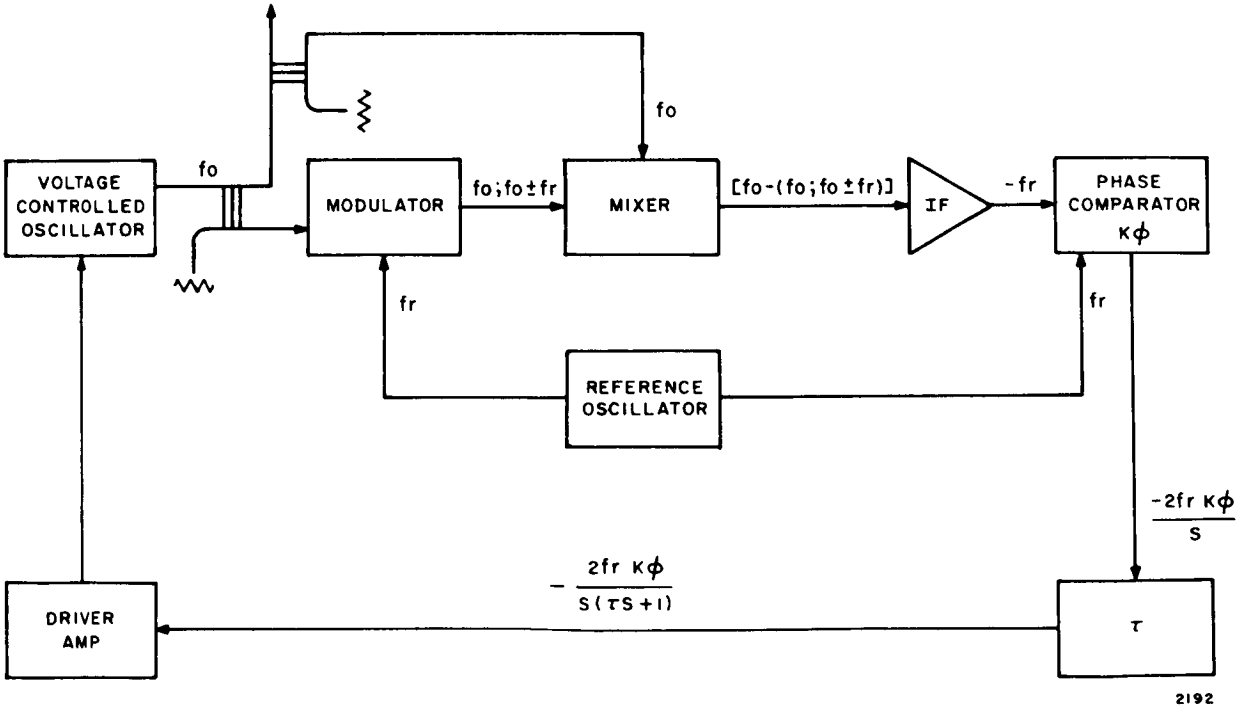

Figure 5-24. Pilot Modulated Phase Loop

An equivalent block diagram is

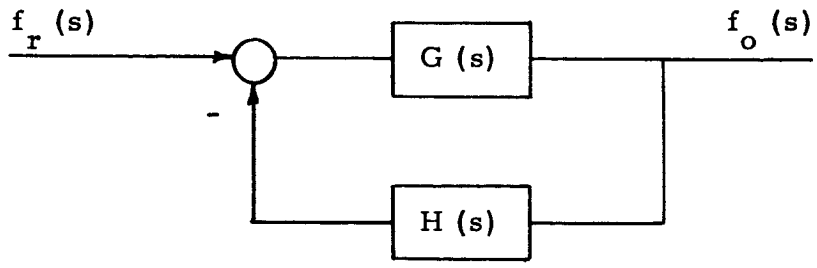

$$G(s) = \frac{-2 K_1 K_\phi}{S(\tau S + 1)}$$

$$H(s) = o$$

A free running loop with no feedback.

5.5.7 Double Phase Lock Loop

The basic control system may be described by the simple block diagram shown in Figure 5-25. Given a block diagram, it is convenient to write the equivalent signal flow graph. The value of the signal at various points in the block diagram is stipulated in Figure 5-25.

$$f_o(s) = \frac{K_1 K_{\phi 1} K_{\phi 2} K_2 \left[f_o(s) - (1 + K) f_r(s)\right]}{S^2 (\tau_1 S + 1)(\tau_2 S + 1)}$$

$$- \frac{K_1 K_{\phi 2} f_r(s)}{K_D S (\tau_2 S + 1)} \qquad (5\text{-}14)$$

or

$$f_o(s)\left[1 - \frac{K_1 K_{\phi 1} K_{\phi 2} K_2}{S^2(\tau_1 S+1)(\tau_2 S+1)}\right] = -f_r(s) K_1 K_{\phi 2}$$

$$\left[\frac{1}{K_D S(\tau_2 S+1)} + \frac{K_2 K_{\phi 1}(1+K)}{S^2(\tau_1 S+1)(\tau_2 S+1)}\right] \qquad (5\text{-}15)$$

$$f_o(s)\left[1 - \frac{K_1 K_{\phi 1} K_{\phi 2} K_2}{S^2(\tau_1 S+1)(\tau_2 S+1)}\right] =$$

$$- \frac{f_r(s) K_1 K_{\phi 2}}{K_D S^2(\tau_1 S+1)(\tau_2 S+1)}$$

$$\left[(\tau_1 S+1) S + K_D K_2 K_{\varphi 1}(1+K)\right] \qquad (5\text{-}16)$$

$$\frac{f_o(s)}{f_r(s)} = -\frac{K_1 K_{\phi 2}\left[S(\tau_1 S+1) + (1+K) K_D K_2 K_{\varphi 1}\right]}{K_D S^2(\tau_1 S+1)(\tau_2 S+1) - K_1 K_2 K_D K_{\phi 1} K_{\varphi 2}} \qquad (5\text{-}17)$$

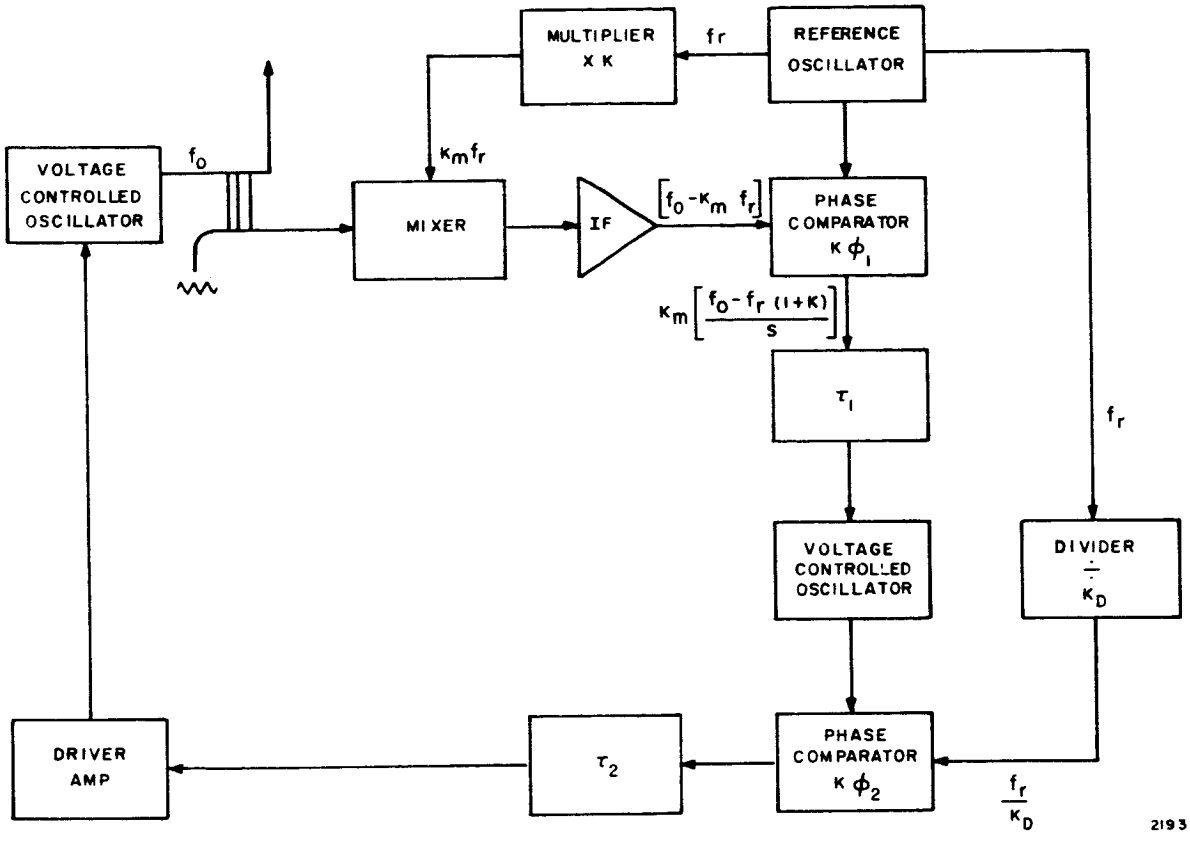

Figure 5-25. Double Phase Lock Loop

Or a simplified block diagram

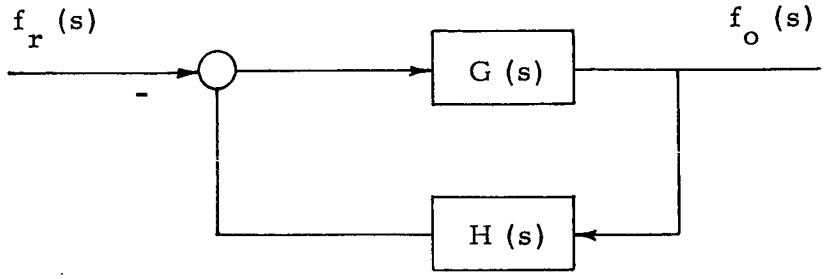

$$G(s) = -\frac{K_1 K_{\phi 2}\left[S(\tau_1 S + 1) + (1 + K) K_D K_2 K_{\phi 1}\right]}{K_D S^2 (\tau_1 S + 1)(\tau_2 S + 1)}$$

$$H(s) = \frac{K_2 K_D K_{\phi 1}}{S(\tau_1 S + 1) + (1 + K) K_{D2} K_2 K_{\phi 1}}$$

Type of System

Second Order System. Zero position error and zero velocity error.

$$K_p = \infty$$

$$K_v = \infty$$

$$K_a = -(1 + K) K_1 K_2 K_{\phi 1} K_{\phi 2}$$

Stability Root Loci Plot

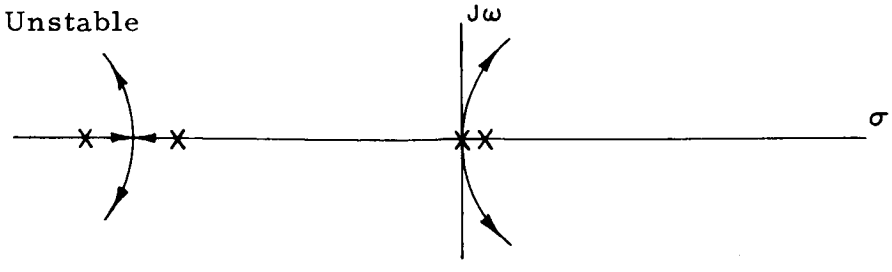

5.5.8 The Pound DC Stabilizing Loop

Figure 5-26 is a microwave implementation of the IF Discrimination Loop shown in Figure 5-19. This loop, the Pound stabilizer, has been used very successfully for the purpose of microwave spectoscopy as the primary standard of this field. Hence, the following is an examination of the Pound loop and its implementation mechanisms.

The Pound discriminator, one of the earliest microwave frequency stabilizing systems, consists of two magic-T waveguide hybrids, a high-Q cavity, and two crystal mounts. One of the magic-T's is used to isolate the input signal from the detector that receives the reflected power from the discriminator T. The input power is applied to arm 3 of the input T, and arm 1 drives the discriminator T. Arm 2 is terminated in a matched load. The crystal detector for reflected power on arm 4 receives only half the transmitted power. In order to achieve the balanced-discriminator

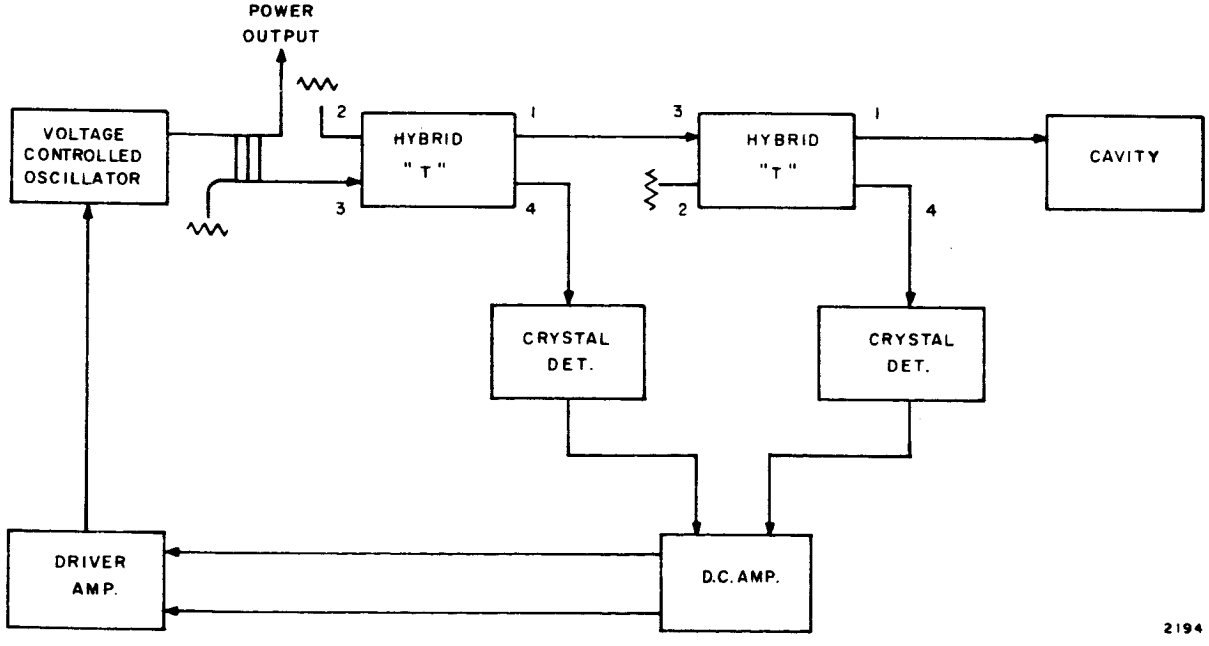

Figure 5-26. Pound Discriminator Lock Loop

action, the output voltage or input power to the detector on arm 4 of the discriminator T, must be attenuated to half the value.

The differential equation describing the voltage-frequency action of this discriminator is given by:

$$\frac{dv}{df} = D P_o \frac{Q_o}{f_o} \frac{4\alpha}{(1+\alpha)^2}$$

where,

D = the detector sensitivity in volts per unit power input

P_o = the microwave power applied to the discriminator

Q_o = the unloaded Q of the cavity

f_o = the resonant frequency of the cavity

$\alpha = \delta_1/\delta_o$, where δ_o = decrement of the unloaded cavity and,

δ_1 = the change in decrement when the cavity is coupled to a matched waveguide.

For optimum sensitivity, α should be equal to unity.

5.5.9 Summary

As shown in this section of the report, many similar loops are possible and in some cases the math readily indicates the loop closure to be unstable and/or conditionally stable. The selection of a stabilizing or AFC loop for transmitter or receiver operation will be made such that, when satellite operation is considered, a minimum number of components should be used to insure maximum reliability. This statement stands, assuming all parts have the same reliability. This, it is felt, can be true if all

components other than the millimeter components are considered. Hence, as can be seen from the previous section, the loop which contains the least number of standard nonmillimeter-wave components is the Pound stabilizer. This loop also has the same number of active millimeter components and/or less than most others. For this reason, it is felt desirable to utilize this approach for a space vehicle type of transmitter stabilizer. The critical item in this loop is the cavity reference which would be required to be temperature stable and maintain its high Q operation.

BLANK PAGE

6. GROUND FACILITIES EVALUATION

This section of the report evaluates the presently available millimeter facilities within the Continental United States plus a new facility being established at Goddard Space Flight Center. These facilities and their geographic location are listed in Table 6-I.

TABLE 6-I

GROUND FACILITY GEOGRAPHICAL CHARACTERISTICS

Facility	Area	Latitude °N	Longitude °W	Altitude-Ft
Aerospace	El Segundo, Calif.	33.9	118.4	157
U. of Texas	Austin, Texas	30.5	97.7	600
GSFC	Greenbelt, Md.	39.7	76.8	220
AFCRL	Waltham, Mass.	42.4	71.2	478
Lincoln	Lexington, Mass.	42.5	71.3	250
Haystack	Tyngsboro, Mass.	42.7	71.4	

The data presented in this section, accumulated during the first study phase of this contract, has been derived from reports published on the facilities and through direct communications with the personnel associated with each of these facilities. In particular, this section reviews the evaluation of the task of integrating these presently instrumented facilities into a millimeter communications experiment. This section of the report also lists the series of characteristics of each of the facilities and notes the deficiencies of each of the facilities as they relate to their ability to perform in this millimeter communications experiment.

As a point of general interest, it can be noted that the facilities presented here do represent an excellent cross-section of engineering technology in the assembly of each of these facilities. This statement is exemplified in the fact that there are four basically different and unique approaches to the fabrication of high-precision parabolic reflectors. In addition, this cross-section of technology is shown most drastically in the invar honeycomb construction technique utilized by the University of Texas in direct contrast with the machined aluminum panel technique utilized by Aerospace Corporation. Further comparison can be drawn with the Lincoln Laboratory spun-cast technique and finally a fourth fabrication technique utilizing a machined foamed plastic surface with two radii pendulous routing. All of these techniques have been utilized successfully for the fabrication of high precision parabolic reflectors.

In addition, several mount configurations and several servo drive configurations have been implemented and tested, namely, the differential torque drive technique utilized by the University of Texas, the hydraulic servo constant displacement type of drive implemented on the Aerospace facility, and the more conventional torque drive utilized by the AFCRL facilities.

As will be noted in the body of this section, each of these facilities has been evaluated as a site and performance measurements have been conducted on the gain, efficiency and antenna patterns, all in the millimeter regions. In addition, pointing accuracies and dynamic tracking accuracies have been checked primarily through the utilization of celestial body radio astronomy. Hence, it is felt that the designers of future millimeter facilities will have at their disposal many design curves and techniques which have been implemented and tested and, therefore, may be directly compared on a cost effectiveness basis. This, therefore, should allow a most excellent trade-off analysis to be performed which would allow the communications designer to choose the most efficient design and fabrication techniques for utilization in a massive communications network.

By way of summary, Tables 6-II and 6-III have been included to compare various characteristics of the facilities. Figure 6-1 has been prepared to show antenna gain versus wavelength for each facility.

TABLE 6-II

GROUND FACILITY ANTENNA SYSTEM CHARACTERISTICS

Facility	Type of Mount	Type of Antenna	Antenna Diameter
Aerospace	Equatorial	Cassegrain	15
U. of Texas	Equatorial	Feed at Focus	16
GSFC	Azimuth-Elevation	Cassegrain	15
AFCRL	Azimuth-Elevation	Cassegrain	29
Lincoln	Azimuth-Elevation	Degenerate Cassegrain	28
Haystack	Azimuth-Elevation	Cassegrain	120

TABLE 6-III

MAXIMUM ELEVATION AND MAXIMUM ANGULAR VELOCITY WITH A 6000 NMI SATELLITE INCLINED 28.5 DEGREES

Facility	Maximum Elevation Angle Degrees	Maximum Velocity - Deg./Sec.	
		Satellite Orbit	Mount Capacity
Aerospace	81	.03 H-A	3.00 H-A
U. of Texas	88	.03 H-A	0.07 H-A
GSFC	74	.09 Az	4.00 Az
AFCRL	68	.07 Az	1.80 Az
Lincoln	68	.07 Az	0.07 Az
Haystack	68	.07 Az	2.50 Az

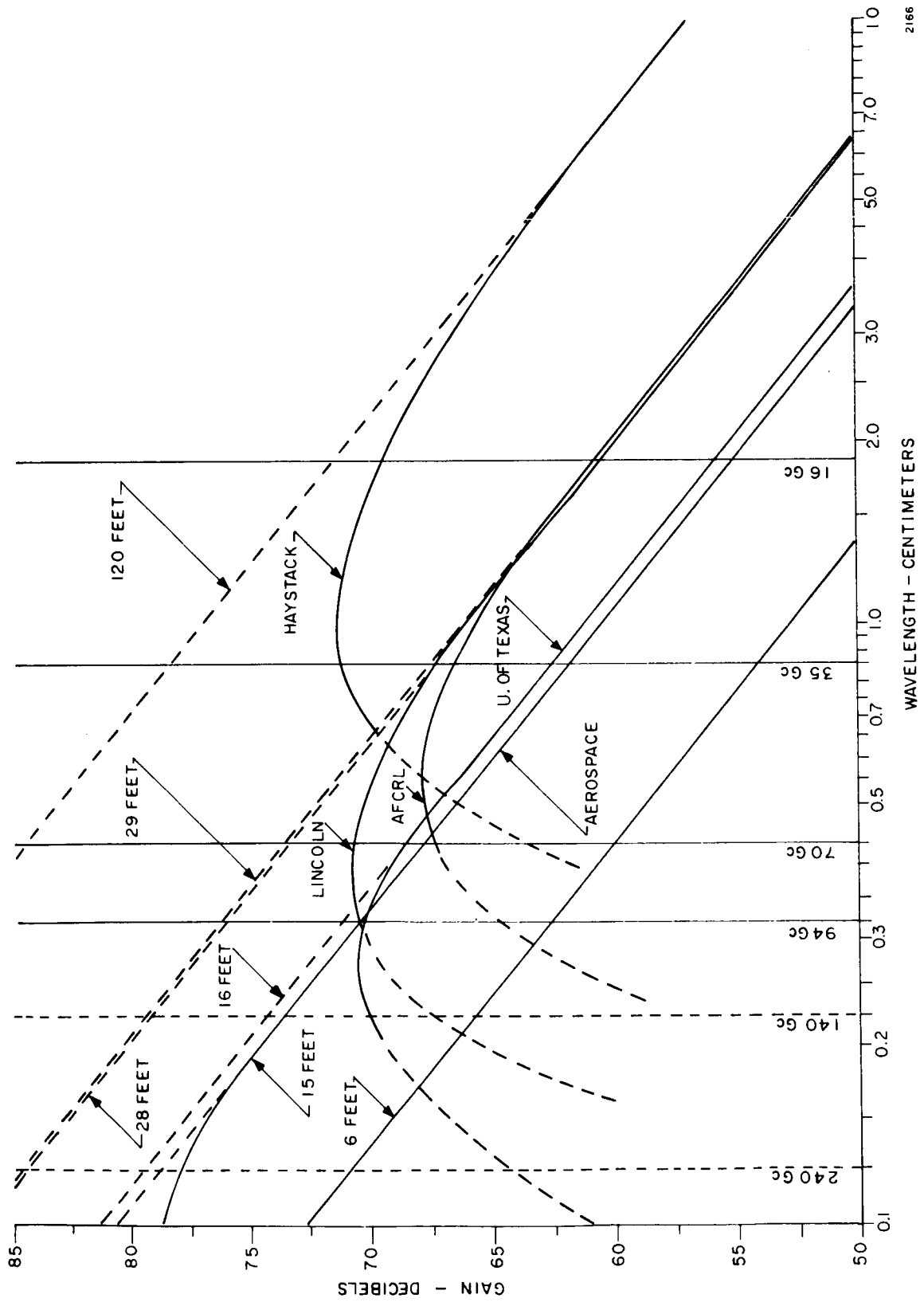

Figure 6-1. Antenna Gain at Ground Station Facilities

6.1 Millimeter Facilities and Capabilities

6.1.1 Aerospace Corporation

The Aerospace facility (References 42 and 43) was established to investigate the suitability of millimeter wavelength systems for space and missile applications involving, in particular, the practicality of constructing and operating a large aperture ground based antenna with tracking capabilities at a sea level site. The antenna has been operating with a 3.2 millimeter radiometer since December 1963, and performance has also been evaluated in operation as a radio telescope. Primary emphasis was given to measurements made during the lunar eclipse of 30 December 1963, and radiometric data is being taken on the earths' atmosphere, the sun, the moon, and Venus.

Research programs on the use of the spectrum between 10 mm and 1 mm have been undertaken by this facility, and work has been done at 3.2 mm under the auspices of the Air Force Ballistic Systems and Space Systems Divisions to explore the technical and economic feasibility of using the millimeter spectrum for cummunications and radar.

The original program plan formulated at the facility was as follows:

1. Exploration of practical uses of the millimeter spectrum using millimeter components in such a manner that the requirements of the system would be similar to those placed on radar and communications equipment.
2. Investigate the ability to fabricate a relatively large antenna with exceptionally fine beamwidths and extremely fine tolerances on pointing accuracy and boresight stability, since this would determine the practicality of millimeter systems.

3. Gather basic propagation data.
4. Provide a millimeter instrument to fill the important spectrum gap in radio astronomy observations with the associated unusual resolution capability of such an instrument.

It was felt that the proper approach was to build and operate a millimeter radio telescope, but with sufficient control and dynamic capability to permit subsequent tracking of near-earth satellites in communications and radar experiments. By this approach, the critical factors of large antenna design and cost was explored and, at the same time, immediate investigation into receiver type components was started and usefully employed. All of the pointing control, mechanical stability, alignment, calibration, and feed design problems were investigated.

A steerable 15 foot diameter parabolic antenna with surface tolerances adequate for efficient operation up to 1 mm was purchased along with an equatorial mount and servo system. This was installed on the roof of the Aerospace R&D Center in El Segundo, California. At the same time, digital data processing equipment was purchased and installed in the control penthouse at the same facility along with the remaining required support equipment.

The Space Radio Systems Facility consists of five basic elements:

1. A large aperture antenna supported by an equatorial mount and tower.
2. A hydraulic servo system capable of high pointing accuracy over a wide dynamic range of tracking rates.
3. A digital data processing unit which is adequate to perform the functions of ephemeris computations, servo control, and data reduction.

4. Radiometric receivers and calibration equipment.
5. Boresighting capability to accomplish accurate alignment between the mechanical axis of the reflector and the multiple r-f feed patterns.

Table 6-IV shows the condensed specifications (Reference 43) on the Aerospace Corporation's antenna. The antenna tower assembly is secured to the top of four building columns which pass from the ground base through the roof slabs. The stability of these support members has been measured and found adequate to support an antenna of high pointing accuracy.

TABLE 6-IV
CONDENSED SPECIFICATIONS OF THE AEROSPACE MILLIMETER WAVE FACILITY

Item	Specifications
APERTURE (Circular)	
Configuration	Cassegrainian
Magnification Factor	14.29
Effective Focal Length (with feed at paraboloid vertex)	777.06 in. (19.737 m)
Diameter	15 ft (4.57 m) D/λ = 1436 at λ = 3.2 mm (94 Gc) D/λ = 3660 at λ = 1.25 mm (240 Gc)
F/D of Parabola	0.3
Material	Machined aluminum reflector and subreflector with an aluminum backup structure
Shape	Paraboloidal reflector with hyperbolic subreflector
Beamwidth (HP)	3 arc min at 3.2 mm (94 Gc)* 2 arc min at 2.2 mm (140 Gc) 1.2 arc min at 1.2 mm (240 Gc)

*Measured values

TABLE 6-IV (Cont)

Item	Specifications
Gain	70.5 db ± 0.5 db at 3.2 mm (94 Gc)* 73 db at 2.2 mm (140 Gc) 78 db at 1.2 mm (240 Gc)
Aperture Efficiency	55.5% ± 10% (94 Gc)*
Feed Configuration	On-axis plus multiple off-axis feed. Variable polarization capability
Polarization	Parallel to declination axis
Operating Wavelength Interval	8 to 1 mm (35 to 300 Gc)
Contour Deviations from a True Parabola at Zenith Attitude	0.0018 in. rms (λ/16 at 410 Gc)
Contour Deviations** from a True Parabola at Zenith Angles Less Than 60 Degrees (Normal Observing Attitudes)	0.0031 in. rms (λ/16 at 238 Gc)
Contour Deviations** from a True Parabola for Horizon Coverage	0.0036 in. rms (λ/16 at 205 Gc)
Special Features	Dew prevention by thermal heating of reflecting surfaces. Paint on reflecting surfaces for scattering of infrared wavelengths
MOUNT AND SERVO	
Mount Type	Equatorial
Servo Drive	Hydraulic
Control Capability	Automatic programmed tracking (closed loop digital servo)

*Measured values

**The deviations from a true parabola are valid for all conditions of sunlight and operating wind loads.

TABLE 6-IV (Cont)

Item	Specifications
Pointing Accuracy*	< 20 arc sec, overall system
Tracking Rates*	0.001 deg/sec (1/4 sidereal rate) to 3.0 deg/sec (low altitude satellite tracking rate)
Slew Rate*	3 deg per sec
Acceleration Rate*	5 deg per sec^2
ENVIRONMENTAL (Operational)	
Wind	20 mph winds
Weather Protection of Antenna	None
SITE DESCRIPTION	
Ocean Proximity	2.8 mi from ocean
Site Coordinates	Latitude 33° 54' 49.45" north Longitude 118° 22' 35.60" west Mean elevation of reflector 157 ft

* Measured values

The antenna assembly made up of a 15 foot diameter parabolic reflector and a hyperbolic sub-reflector supported by a tetrapod structure made up the cassegrain assembly. Final parabolic contour was achieved by the precision milling of welded preformed aluminum gores. Deviations from a true parabola as shown in Table 6-IV are .0018 inch rms when the antenna points to the zenith. The combined effect of normal operating angles which are less than 60 degrees from the zenith, solar illumination, and 20 mph winds is to raise the deviation to .0031 in. rms and .010 in. peak. At a λ of 1 mm the reflector rms error amounts to .08 λ.

Two six inch holes bored through the parabolic reflector accommodate a boresight telescope and a television camera. The TV camera has a field of view of approximately 40 arc minutes.

Seismometers are used to measure building tilt and show movements of about 20 arc seconds during the day, due to thermal heating. Building movements attributable to such factors as trains, road traffic, air conditioning machinery and wind, did not exceed 0.1 arc second as shown on the seismometers.

Ephemeris data stored on magnetic tape are compared in the digital data processor with shaft-angle encoder outputs, and analog information is generated to actuate the hydraulic servo drive motors.

A type 920 digital data processor accepts inputs on atmospheric pressure, temperature, tilt north-south, tilt east-west, humidity, wind velocity, wind direction, rainfall rate, and radiometer or receiver signal. The computer provides coded pulse trains to operate calibration switches for radiometers and receivers, real-time processing of receiver outputs, and computes and displays data such as right ascension, hour angle, declination, and sidereal time. Simultaneous handling of input, output and compute functions is performed.

The data processor has a 24 bit word length, a multiply time of 32 microseconds and a 4000 word memory capacity. Four magnetic tape units with 200 bits per inch packing density are provided.

Hour angle and declination axis are both encoded into 20 bit binary numbers with a peak error of less than 5 arc seconds, and at a sampling rate of 10 kc.

The SRSF boresight station is located on San Pedro Peak near Palos Verdes and includes a direct line, tone command, remote control capability. This station uses a two foot parabolic antenna and operates at 94 Gc using a klystron RF source. The antenna has 53 db gain and a 3 db beamwidth of 20 arc minutes. The E-field polarization is continuously variable through 360 degrees.

Power supplies are highly regulated and all important operational parameters are automatically monitored. To aid in optical acquisition, a 1200 watt light assembly is used at the boresight station.

Aerospace is experimenting with a 12 mile, 94 Gc television link between San Pedro Peak and the El Segundo facility. They are receiving signals from one of the Los Angeles commercial stations, via standard TV receiver and then relaying the program over the 94 Gc link.

The measurement of signal loss during a rain storm is another interesting problem being worked on at Aerospace. The question of percentage loss of signal due to attenuation of the water film on the antenna and the attenuation due to absorption by the atmosphere. Experiments are being designed to study this problem.

By the summer of 1965, Aerospace expects installation of a 100 watt, 94 Gc transmitter.

At present, the Aerospace facility has one deficiency in that it does not have built-in automatic tracking capabilities. The ephemeris data is introduced via computer with update control available to the operating personnel.

The present 15 ft. facility would find its utilization at frequencies above 94 Gc; therefore, interfacing with the proposed experiment would be

performed via the 94 Gc ground transmitter and a proposed 6 foot 35 Gc, tracking receiver capability. This tracking information could be used to direct the 94 Gc transmitting antenna via the existing computer.

6.1.2 University of Texas

The University of Texas facility is a millimeter wave radio telescope which is installed at the University's field station. The precision 16 foot diameter parabolic antenna was designed for near optimum performance at wavelengths of approximately 4 millimeters and also possesses the capability of slightly degraded performance at 2 millimeters and 1 millimeter. The primary intent of the installation was to survey the surface of the moon which would allow the determination of surface characteristics and atmospheric contents. To date, the primary emphasis of the facility has been on assisting in the selection of the sites for the manned lunar landing. Through the utilization of its very narrow beamwidth, which is a few minutes of arc, it is possible to probe the lunar surface to determine the radiometric temperature variances as a function of frequency.

The utilization of this reflector is accomplished through its attachment to a high resolution equatorial mount. This mount facility is new in design and utilizes a differential torque drive technique to accomplish its high pointing accuracy capabilities. This mount, when coupled to the antenna which is fabricated with invar honeycomb, performs as a well integrated radio astronomy facility. Hence, the actual fabrication of this antenna facility was done through the implementation of an entirely new technique - the assembly of a temperature compensated precision reflector using invar as a major construction material. From the presently available measured data on this facility, it appears that the development and utilization of this technique has proved to be extremely successful.

The actual implementation of measurements hardware at the University of Texas has been primarily in the area of radiometric systems. These particular systems utilize a Dicke type of radiometric receiver with a 10 megacycle predetection bandwidth. These two receiving systems are built in such a manner that, via plug-in receiver heads at the reflector focus position, the frequency of the radiometer may be changed from 35 to 70 Gc.

The future implementation and equipment modifications planned at the facility call for the introduction of 94 and 140 Gc radiometric capability. These will be fabricated to be compatible with the feed-at-focus plug-in technique. As a further extension of the radiometric system capabilities, an increase of the predetection bandwidth to 100 megacycles is planned.

This is one of the few new facilities which utilizes a feed-at-focus primary feed system. It should be noted that for all other facilities under consideration a Cassegrain technique or a modified degenerate Cassegrain technique is utilized for their feed system. Hence, the problems and limitations of introducing equipment at the primary focus of this main reflector are best exemplified by the basic weight limitations imposed by the structure. A feed weight of less than 40 pounds must be maintained in order to preserve surface and prime focus accuracy over the entire elevation operation of the main reflector. This inherent system limitation indicates the lack of adaptability for which this type of system lends itself; the difficulties of instrumenting a high power millimeter transmitter at the prime focus of this particular facility cannot be overcome.

In no way does the weight limitation affect the ability of the site to perform as a receiver terminal as described in Section 7. It is felt that the critical interfacing between IF's and post IF's may well be accomplished by a long length of cable which would allow for the remote location, the larger and more bulky signal processing equipment, utilized by the ground terminal in a main receiver rack.

A second limitation to the site facility is related directly to the site's inability to perform during foul weather conditions. This ground base facility is housed within an observatory type dome which allows true fair weather operations without the adverse effects of radomes. The proposed solution to this particular problem could well be accomplished through the implementation of a thin film membrane radome material installed over the observatory dome window; this would provide adequate protection for all weather operation of the facility.

The next area of prime concern in utilizing this facility is the relatively slow slew and track rate capability. In view of the primary mission of the facility having been established as a radiometric observatory, the slew and track capabilities have been tailor-made for celestial body observations. This has produced a system which is limited in its ability to perform on higher angular velocity targets such as 6000 mile satellites. Its capability in the hour angle axis is better than that of the declination axis because in celestial work the hour angle is the working axis of the radio observatory. It is felt that through the utilization of the present differential torque drive a higher slew and track rate may be accomplished if a relaxation of the dynamic pointing accuracy can be tolerated.

The mount limitation is aggravated by the inability of the site to perform a programmed acquisition sector scan mode of operation. Presently the facility does not possess the capability of performing differential scan type servo action. This would be a necessary requirement in the extension of the site's facilities for work in the millimeter propagation experiment.

In summary, it is felt that the University of Texas facility, as presently assembled, provides a receiver aperture capable of receiving millimeter waves, but the primary limitations of the facility are those associated with its servo and acquisition capabilities which would require maximum attention if this site is to be utilized.

6.1.3 Air Force Cambridge Research Laboratories

The following information has been derived primarily through direct interview with the personnel at the facility. At present no documented report has been published on the facility, although one is expected in the near future. This facility consists primarily of a precision millimeter parabolic antenna system coupled to a high precision elevation over azimuth mount. This system is presently under evaluation to determine contractor's compliance to specifications. To date mechanical measurements have been completed and electrical performance of the facility is being evaluated through the utilization of its boresite facility located on Nobscot Hill in Sudbury. The electrical performance parameters are being checked at 35 Gc with primary emphasis being placed on antenna beam pattern and antenna gain via the technique of integrated beam pattern gain measurements. Also being implemented is a standard gain horn antenna gain measurements technique. As shown from the summary tables in the previous section, the system servo capabilities, namely, its elevation and azimuth mount drive rates, are well within those required for the performance of satellite track. The facility has the capability of approximately two degrees per second in each axis and is programmable by an eighteen bit digital code computer interface.

The previously described antenna system and associated mount assembly is presently assembled, uses a Cassegrain feed system, and is primarily instrumented for 35 Gc operation. This mode of operation, when coupled with the 29 foot antenna, generates 4.2 minutes of arc (.07 degrees) antenna beam and is expected to yield 66.7 db antenna gain at 35 Gc. This is comparable to a 45 percent efficiency at this frequency.

Presently the AFCRL facility is planning a superhetrodyne radiometric receiving system at 35 Gc, which will incorporate a low noise RF amplifier as the front end, namely, a maser amplifier which should allow

antenna temperatures of approximately 20 degrees K to be realized with this system. The RF bandwidth capability of the maser front end is expected to be approximately 20 to 25 megacycles. This will then be coupled to a conventional superhetrodyne converter, whose output will be directly interfaced with conventional Dicke type radiometric mode of operation. This radiometric receiver and maser assembly is expected to be assembled within the year. In addition to this planned facility, AFCRL possesses a 1 kilowatt CW capability at 16 Gc, which is intended to be utilized on the antenna facility primarily as a radar-astronomy instrument. This facility is expected to have the standard meteorological sensors for temperature, pressure, humidity and precipitation rate. This facility is being assembled primarily for radio astronomy and radar astronomy type of operation at K_u- and K_a-band, and is expected to be in full operation within the next two years.

This facility presently exhibits some deficiencies in being able to participate in the propagation experiment. These deficiencies are primarily in the area of its ability to track a source at millimeter frequencies and at present there are no plans to introduce a loop switch or monopulse technique. The personnel associated with the facility indicate their desire to participate in the planned experiments and would consider the instrumentation of the facility to allow its interface with the experiment. As seen to date, other problems associated with the utilization of the facility would be the difficulties associated with the environmental conditions found at the instrument compartment in the rear of the reflector. The basic instrument compartment is located behind the primary feed in the Cassegrain feed system, which allows the introduction of the RF components without the utilization of rotary joints and other complex RF plumbing techniques. This compartment possesses adequate volume, but presents problems in access and ability to perform system installation rapidly and conveniently. Therefore, it is felt that a parallel front end receiver package would be required in this

compartment which would allow, via the utilization of RF line switching, switch-over from their low noise maser operation to a more conventional superheteodyne receiver approach for use in the communications experiment. The introduction of a quadra-horn feed system into this Cassegrain approach is being utilized which lends itself readily to this kind of modification.

In summary, it is felt that the AFCRL 29 foot facility presents a real possibility of being implemented into a millimeter communications experiment, and would be capable of performing either an active track mode or a programmed track mode for a 35 Gc experiment. The site's ability to perform above this frequency, it is felt, should be evaluated at a later time once the present measurements of the facility have been completed and its true capability determined. It shall also be noted at this point that the AFCRL facility is an exposed facility, in that no protective radome is utilized. This leads to some operational problems during severe winter conditions, in that no antenna surface heating is introduced to allow for the removal of snow accumulated in the reflector. This method of operation would prove to be interesting during the winter season because a true evaluation of the potential of a totally exposed facility without radome protection could be made especially with water and snow on the dish surface.

6.1.4 Lincoln Laboratory

Actually, Lincoln Laboratory possesses two millimeter facilities. Namely, the 28 foot spun cast precision system (References 44 and 45) located at the Laboratory itself and the Haystack 120 foot radar installation (Reference 46). The 28 foot facility has been in existence for several years and has performed as a radio astronomy observatory both for the pure radiometric mode and as a radar astronomy instrument. This facility is limited by the mount's capability to perform satellite track missions since it utilizes a gun mount which has limited elevation and azimuth drive capability.

This type of mount system, when coupled to the existing servo-drive capabilities, is limited in stiffness and in track rate, such that it would be most difficult to perform a track and acquisition mode on a 6000 mile satellite.

The ability to introduce a tracking capability to the facility is somewhat limited due to its primary feed system, that of utilizing a degenerate Cassegrain technique. This type of primary feed would require the development of a single horn mode selector monopulse receiver system. If such a feed were implemented, the drive capability of the mount would still limit the usefulness of the facility.

The instrumentation available to the 28 foot facility includes a phase-locked klystron 10 watt transmitter capability which has allowed radar work to be performed at 35 Gc. They also have a superheteodyne 35 Gc Dicke type radiometer. This radiometric system has 100 megacycles of pre-detection bandwidth and may be tuned ± 2 Gc from its center frequency. This system has a receiver noise figure of 10 db on a single channel and utilizes a dual receiver channel from the output of a four port Faraday rotator Dicke switch. This dual receiver approach allows for a direct comparison between independent communications paths. This inherent capability of two receivers would allow the introduction of a lobe switch tracking technique to be readily implemented with a minimum of additional hardware required except for the basic limitation of being unable to introduce a lobe switch horn complex in the degenerate Cassegrain primary feed system.

Additional planned equipment for this 28 foot antenna system is the 1 kilowatt TWT operating at 35 Gc. This device is planned as a direct installation which will allow the improvement in signal-to-noise ratio when moon backscatter investigations are being performed. The date for the availability of this particular system has not yet been firmly established, although this capability is expected to exist within the year.

The Haystack facility was assembled as a radar research instrument and was primarily developed to prove the feasibility of, and obtaining design technology for, the fabrication of large precision parabolic antenna structures to introduce high resolution high precision mount capabilities to the radar field. The system has been fabricated and mechanically tested and electrical tests are presently being initiated. The actual operation of this large radar system will be forthcoming within the next year.

The facility has a 120 foot parabolic receiving aperture capable of operating from 1 to 10 Gc. Note that the lower limit of frequency of 1 Gc is dictated by the present space frame radome of the facility. The upper frequency of 10 Gc is that which was initially specified in the procurement of the facility. As shown in Figure 6-1, it is expected that reasonable operation at 35 Gc will be accomplished and that antenna gains in the order of 71 db will be realized with corresponding reduction in overall antenna efficiency.

The facility is planned to be evaluated within the ensuing year at frequencies up to 35 Gc through the utilization of radiometric techniques. Through the instrumentation of a radiometer it is expected that an evaluation of the antenna's capabilities at these frequencies will be performed. The radiometric experiment will also allow operation as a radio astronomy facility at 35 Gc.

Among other things the facility will be utilized as a 10 Gc radar system having a capability of 100 kilowatts CW.

The site is intended to be utilized as an extension of the Westford work and will perform directly in conjunction with the Westford radar system. The design of the facility has allowed for the introduction of varied experiments through the utilization of plug-in room techniques which are located to the rear of the prime feed in the Cassegrain feed system. This

approach will prove to be most satisfactory and a conversion of the facility from one mode of operation to an entirely different mode can be done within one hour.

This facility would prove to be most interesting as a ground terminal receiver for the proposed millimeter communication experiments because it would allow the evaluation of extremely large aperture antennas for millimeter systems. It is felt, that this facility would be best utilized in conjunction with the previously described AFCRL millimeter facility. For the satellites that are presently considered in the study, the facility has no mechanical limitations which directly conflict with the requirements of the vehicle. It can either be programmed to track the satellites using ephemeris data or it can be slaved to the Millstone Hill Radar which can skin-track the satellites. It is anticipated that a minimum of difficulty will be encountered in the utilization of this facility in the communications work.

6.1.5 Goddard Space Flight Center Facility

A millimeter wave experimental ground facility is in the process of being implemented at the Goddard Space Flight Center in Greenbelt, Md. To date, GSFC has procured a 15 ft. spun-cast millimeter reflector. This parabolic reflector has the ability to perform up to a wavelength of 3 mm. There presently exists a set of specifications describing the high precision servo and mount assembly. Delivery of this mount is expected within one year. In parallel with this procurement, a detailed investigation of possible site locations is being performed and a site location should be selected which will allow for adequate sky coverage and line-of-site vision to the boresight assembly. It is expected that the range of the boresight facility will be in the order of 2.5 to 3.0 miles. This short length of boresight range is due to the lack of elevated terrain in the Greenbelt area.

6.2 Orbital Profiles

Some discussion on orbital profiles was given in Section 5.1 "Candidate Satellite Evaluation." Orbital coverage contours for a 6000 n mile altitude satellite are presented here in Figures 6-2 through 6-6 for elevation angles of 0°, 10° and 20°. The areas of Los Angeles, California; Austin, Texas; Washington, D. C.; Boston, Massachusetts; and Ottawa, Canada are represented. Appendix VIII gives more detailed characteristics for medium altitude orbits.

6.3 Meteorological and Geographical Profiles

This section is a description of the geographical and meteorological characteristics (Reference 1) of the area in which facilities under consideration for participation in the proposed millimeter experiments are located. Some characteristics have already been given in Section 3.1. Figure 6-7 is a comparison of the monthly mean precipitation for each of the areas to be discussed.

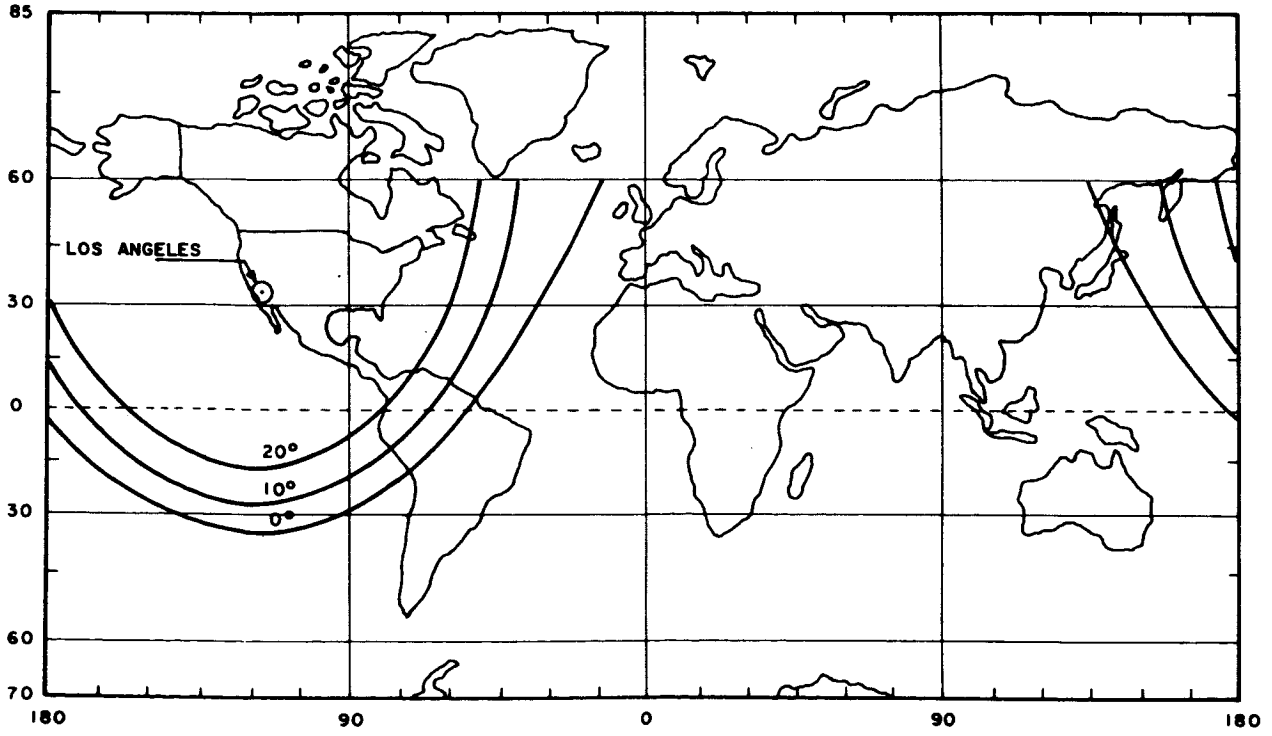

Figure 6-2. Coverage Contours for Los Angeles Area on 6000 nmi Satellites

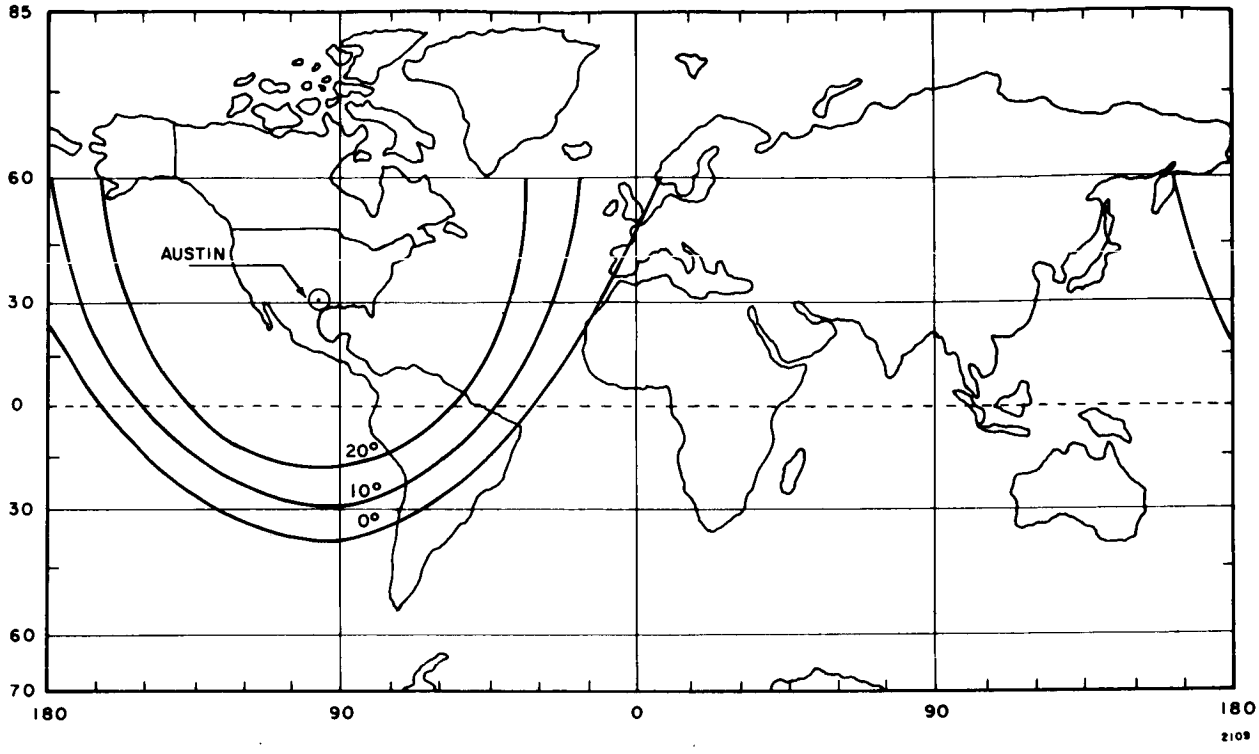

Figure 6-3. Coverage Contours for Austin Area on 6000 nmi Satellites

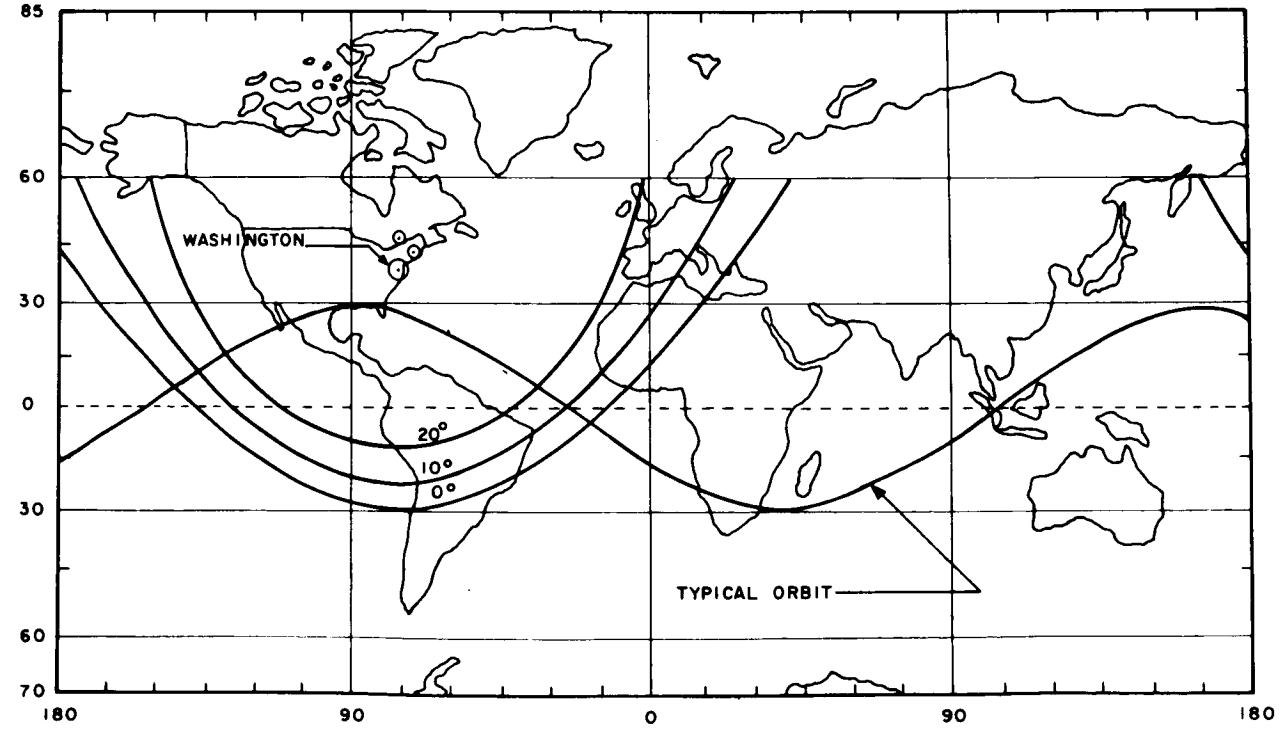

Figure 6-4. Coverage Contours for Washington Area on 6000 nmi Satellites

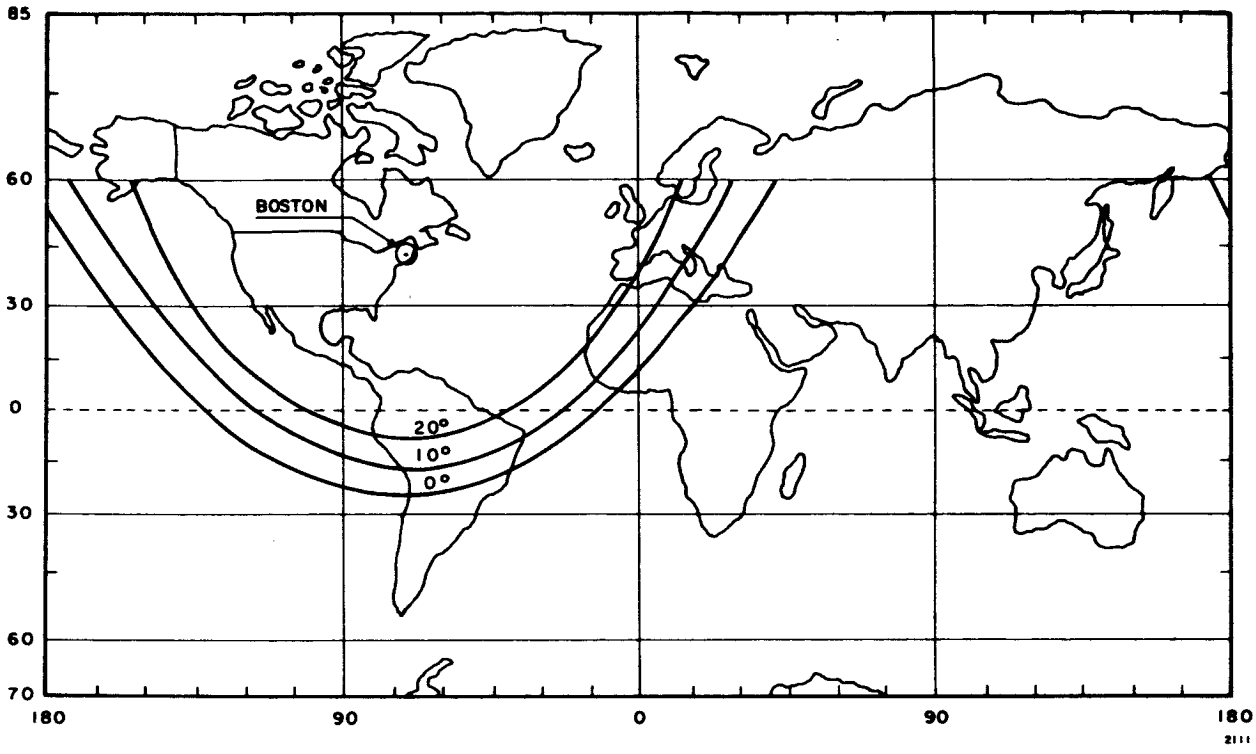

Figure 6-5. Coverage Contours for Boston Area on 6000 nmi Satellites

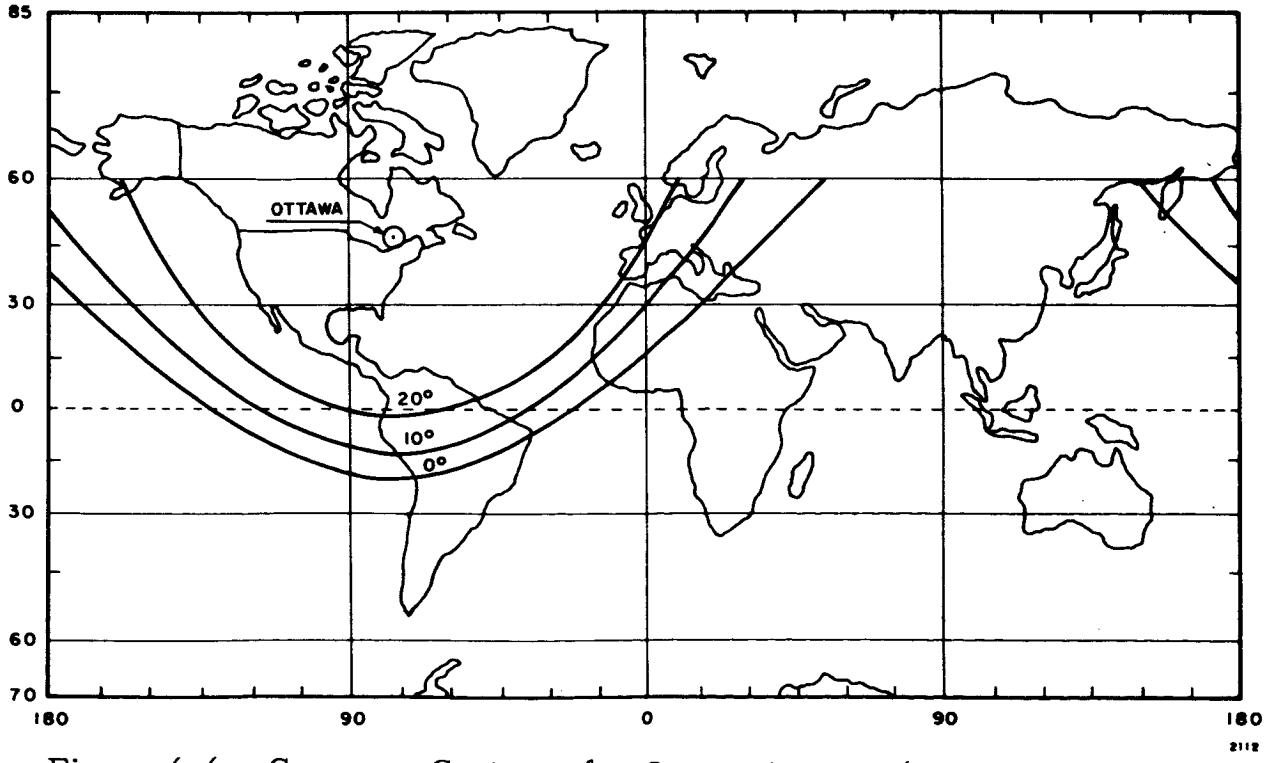

Figure 6-6. Coverage Contours for Ottawa Area on 6000 nmi Satellites

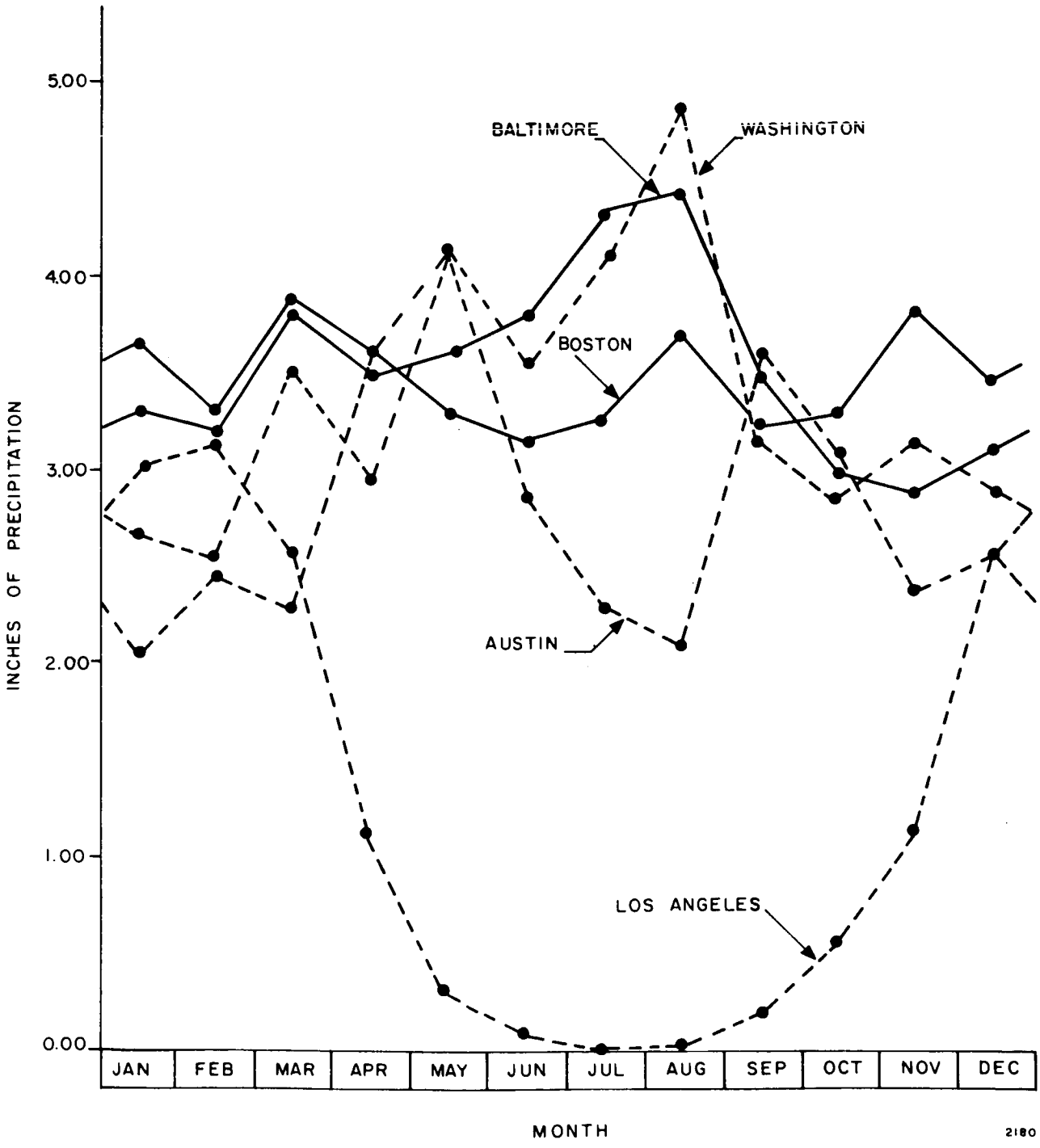

Figure 6-7. Mean Monthly Precipitation

6.3.1 Aerospace

The Aerospace Corporation Space Radio Systems Facility (SRSF) is located on the roof of the two-story Building F at the Aerospace Research and Development Center in El Segundo, California. This "sea level" site in the Metropolitan area of Los Angeles is very near the Pacific Ocean. The boresight station for this 15 foot antenna facility is located on San Pedro Peak (1100 feet altitude) in the Palos Verdes Hills, a distance of eleven nautical miles to the south.

The climate of Los Angeles is normally pleasant and mild through the year. The Pacific Ocean is the primary moderating influence but coastal mountain ranges lying along the north and east sides of the Los Angeles coastal basin act as a buffer against extremes of summer heat and winter cold occurring in desert and plateau regions in the interior. A variable balance between mild sea breezes and either hot or cold winds from the interior results in some variety in weather conditions but temperature and humidity are usually well within the limits of human comfort. An important, and somewhat unusual aspect of the climate of the Los Angeles metropolitan area is the pronounced difference in temperature, humidity, cloudiness, fog, rain, and sunshine over fairly short distances.

These differences are closely related to the distance from, and elevation above, the Pacific Ocean. Both high and low temperatures become more extreme and the average relative humidity becomes lower as one goes inland. On the coast and in the lower coastal plain average daily temperature ranges are about 15° in summer and 20° in winter. Relative humidity is frequently high near the coast but during periods of high temperatures the relative humidity is usually below normal so that discomfort is rare except for infrequent periods when high temperatures and high humidities occur together.

Like other Pacific Coast areas most rainfall comes during the winter with nearly 85 percent of the annual total occurring from November through March, while summers are practically rainless. As in many semiarid regions there is a marked variability in monthly and seasonal totals. Annual precipitation may range from less than a third of the normal value to nearly three times normal while some customarily rainy months may be either completely rainless or receive from three to four times the average for the month. Precipitation generally increases with distance from the ocean from a yearly total of around 12 inches in coastal sections to the south of the city up to over 20 inches in foothill areas. Thunderstorms are infrequent.

Prevailing winds are from the west during the spring, summer, and early autumn with northeasterly wind predominating the remainder of the year. Average wind speeds are rather low. At times the lack of air movement combined with a frequent and persistent temperature inversion is associated with concentrations of air pollution in the Los Angeles coastal basin and some adjacent areas. Sunshine, fog, and clouds depend a great deal on topography and distance from the ocean. Low clouds are common at night and in the morning along the coast during spring and summer. Light fog may accompany the usual night and morning low clouds but dense fog is more likely to occur during night and early morning hours of the winter months.

6.3.2 University of Texas

The radio telescope facility operated by the Electrical Engineering Research Laboratory of the University of Texas is located at the University of Texas field station just outside of Austin, Texas. The boresight station for this 16 foot antenna facility is installed in a University tower in the city nearly 7 miles away.

Austin, the capital city of Texas, is located on the Colorado River where the stream crosses the Balcones Escarpment from the Edwards Plateau. Elevations within the city vary from 400 feet to 700 feet above sea level. The climate is influenced by the nearness of the Gulf of Mexico which is the source of the maritime tropical air mass which moves over Austin with the prevailing south winds. However, surges of polar air in winter account for the frequent north winds experienced during December, January and February.

The normal annual temperature is 68.3 degrees. During winter the daily range in temperature is from about 60 degrees to about 40 degrees but wide variations from these figures and sudden changes occur as cold polar air replaces warm tropical air and vice versa. Daily range in temperature in summer averages from 74 in the early morning to 94 in the afternoons.

Annual rainfall has varied from 65 inches to as little as 11 inches, but the normal annual rainfall is 32.58 inches. Seventy percent of the years have totaled rainfall between 24 and 44 inches. Prolonged dry spells do occur and all months of the year have seen little or no rain. There is no pronounced dry and wet season and rainfall is fairly well distributed throughout the year with a May normal of 3.71 inches and an August normal of 1.94 inches.

The mean number of days with temperature below 32 degrees is 19 per year. These usually occur from late November to mid-March.

On the average, 133 days are cloudy each year, 113 days are partly cloudy, and 119 days are clear. An average has 81 days with measurable precipitation, with 40 days having thunderstorms. Destructive winds are infrequent and occur in connection with thundersqualls. Gulf hurricanes offer no threat of wind damage this far from the coast.

6.3.3 Goddard Space Flight Center (GSFC)

Goddard Space Flight Center is located near Greenbelt, Maryland on the Baltimore-Washington Parkway about 10 miles from downtown Washington. Since GSFC is only 23 miles from the center of Baltimore, climatological summaries for both cities are given.

Washington lies at the western edge of the Middle Atlantic coastal plain, about 50 miles east of the Blue Ridge Mountains and 35 miles west of Chesapeake Bay at the junction of the Potomac and Anacostia Rivers. Elevations range from a few feet above sea level to about 400 feet in parts of the northwest section of the city.

Summers are warm and humid and winters mild; generally pleasant weather prevails in the spring and autumn. The coldest weather occurs in late January and early February. The warmest weather occurs late in July. There are no well pronounced wet and dry seasons. Thunderstorms, during the summer months, often bring sudden and heavy rain showers and may be attended by damaging winds, hail, or lightning. Tropical disturbances occasionally, during their northward passage, influence Washington's weather mainly with high winds and heavy rainfall, but extensive damage from this cause is rare. Mean annual snowfall is 16.4 inches and snow accumulations of more than 10 inches are relatively rare.

Records of the past 20 years show the average date of the last freezing temperature in the spring to be March 29 and the latest, April 16. The average date of the first freezing temperature in the fall is November 10 and the earliest, October 21.

The Baltimore area lies about midway between the rigorous climate of the North and the mild South and adjacent to the modifying influences of the Chesapeake Bay and Atlantic Ocean to the east and the Appalachian

Mountains to the west. Since Baltimore is near the path of most systems of low barometric pressure which move across the country, changes in wind direction are frequent and are the cause of the changeable character of the weather. However, the overall effect of the mountains to the west and the Bay and Ocean to the east is to produce a more equable climate compared with other continental locations at the same latitude. While hot, humid, muggy periods of weather are not uncommon during the warmer months, they are frequently attended by afternoon or evening thundershowers or breezes which provide some relief from the uncomfortable conditions.

Rainfall distribution throughout the year is rather uniform. Severe drought during the growing season is infrequent. Rainfall during the growing season occurs principally in the form of thundershowers, and rainfall totals during these months vary appreciably, depending on the number of thundershowers which occur largely by chance in a given locality. Although annual precipitation totals have been within 5 inches of the 44. 21 inch normal almost one-half of the time, the annual amounts have varied from 62. 35 inches in 1889 to 21. 55 inches in 1930.

6. 3. 4 Air Force Cambridge Research Laboratories (AFCRL) and Lincoln Laboratory

The AFCRL facility is situated 20 miles inland from Boston on Prospect Hill beside Route 128 in Waltham, Massachusetts. The 478 foot elevation of Prospect Hill permits excellent coverage near the horizon in all directions. The boresight station for this 29 foot antenna facility is located on Nobscot Hill in Sudbury, Massachusetts, which is about 10 miles west of Prospect Hill.

The Lincoln Laboratory 28 foot antenna radio telescope facility is located on the roof of the main laboratory building at L. G. Hanscom Air Force Base in Bedford, Massachusetts. Hanscom AFB is about 25 miles

west of Boston. The boresight station for this facility is located in Billerica, Massachusetts 5 nautical miles away. Its elevation above sea level is 350 feet.

The Lincoln Laboratory 120 foot research facility for space communications, radar and radio astronomy is located at Tyngsboro, Massachusetts. The installation, which is named Haystack Experimental Facility is located approximately 30 miles northwest of Boston and about one-half mile from the Millstone Hill radar.

Three important influences are responsible for the main features of Boston's climate. First, the latitude (42° N) places the city in the zone of prevailing west to east atmospheric flow in which are encompassed the northward and southward movements of large bodies of air from tropical and polar regions. This results in variety and changeability of the weather elements. Secondly, Boston is situated on or near several tracks frequently followed by systems of low air pressure. The consequent fluctuations from fair to cloudy or stormy conditions reinforce the influence of the first factor, while also assuring a rather dependable precipitation supply. The third factor, Boston's east-coast location, is a moderating factor effecting temperature extremes of winter and summer.

Hot summer afternoons are frequently relieved by the locally celebrated "sea-breeze", as air flows inland from the cool water surface to displace the warm westerly current. This refreshing east wind is more commonly experienced along the shore than in the interior of the city or the western suburbs. In winter, under appropriate conditions, the severity of cold waves is reduced by the nearness of the then relatively warm water. The average date of the last occurrence of freezing temperature in spring is April 8. The average date of the first occurrence of freezing temperature in autumn is November 7. In suburban areas, especially away from

the coast, these dates are later in spring and earlier in autumn by up to one month in the more susceptible localities.

Boston has no dry season. For most years the longest run of days with no measurable precipitation does not extend much more than two weeks. This may occur at any time of year. Most growing seasons have several shorter dry spells during which irrigation for high-value crops may be useful.

Much of the rainfall from June to September comes from showers and thunderstorms. During the rest of the year, low pressure systems pass more or less regularly and produce precipitation on an average of roughly one day in three. Coastal storms, or "northeasters", are prolific producers of rain and snow. The main snow season extends from December through March. The average number of days with four inches or more of snowfall is four per season, and days with seven inches or more come about twice per season. Periods when the ground is bare or nearly bare of snow may occur at any time in the winter.

Relative humidity has been known to fall as low as 8%, but such desert dryness is very rare. Heavy fog occurs on an average of about two days per month with its prevalence increasing eastward from the interior of Boston Bay to the open waters beyond.

Although winds of 32 m. p. h. or higher may be expected on at least one day in every month of the year, gales are both more common and more severe in winter.

BLANK PAGE

SECTION 7. RECOMMENDED EXPERIMENT EQUIPMENT

This section of the report deals with the proposed implementation of space flight hardware and ground facility modifications which would be needed in the recommended one-year propagation measurements program outlined in the summary. The proposed program satisfies the basic measurements requirements and uses a basic measurement waveform which can be readily implemented. In view of the existing and planned experimental millimeter wave facilities, the proposed experiments would make the best use of all the available equipment capabilities and, therefore, provide the best propagation data for the funds and payload space expended.

It is proposed that a 35 Gc satellite transmitter be utilized, which transmits a single AM double-sideband waveform with a variable modulation frequency to several ground stations simultaneously. In addition, it is proposed that a 94 Gc receiver be carried aboard the satellite in order to receive an AM double-sideband waveform from a transmitter such as the one being developed for the Aerospace facility.

At this point, it is desirable to restate a few of the many considerations which have led to the selection of this experiment. First and foremost, the availability of flight qualified hardware grossly limits the introduction of more sophisticated and/or higher frequency devices to be carried in the vehicle as transmitter sources, although it is well acknowledged that a transmitter source in the vehicle does present the most useful of all experimental approaches.

Secondly, as will be seen in Section 7-1, the 35 Gc transmitter power capabilities will range from a minimum useful radiated RF power of 200 milliwatts up to approximately 2 watts of RF power. These factors may again be considered as trade-offs depending upon the time of the experiment, namely, a schedule of development which can be allowed for generation of a useful experiment for a particular satellite payload.

As will be noted, tubes are available which possess the capability of providing a suitable RF source which has been missile and/or flight tested, hence will provide the greatest factor of confidence in the system.

A third major consideration in the selection of this experiment has been the availability of ground facilities and their ability to adequately interface with a communications experiment. It is most apparent that all sites presently available have been established and are presently utilizing radiometric systems as their main operational mode. In examining their capabilities, it is evident that, in order to achieve meaningful experimental data, a thorough site evaluation is necessary. This requires data on the facilities' operational capabilities at the frequencies at which the experiment is to be performed. The selection of a 35 Gc satellite transmitter was made primarily on the basis that all of the existing sites except Aerospace are presently performing at 35 Gc. Radiometric measurements have been made with these antenna facilities, either on extended targets or point sources, which have allowed them to perform sufficient antenna calibration and beam pattern measurements. Also, for the most part, all of these facilities have boresight facility measurements on their antenna and have established gain figures of antennas and pointing accuracy capabilities.

Hence, for the above listed reasons, it was deemed most advisable that a 35 Gc experiment be performed which allows the utilization of the

University of Texas, Lincoln Laboratory and AFCRL antenna facilities and could also include the recently developed Haystack facility as a possible receiver site for the evaluation of a large antenna aperture. Also, in conjunction with the vehicles transmitter capabilities, and with the presently planned 94 Gc transmitter capability at the Aerospace Corporation, it will be shown that the ability to piggy-back a 94 Gc receiver on the 35 Gc transmitter in the satellite does not grossly penalize the weight and power consumption of the payload. It is proposed that this be accomplished through the utilization of a third harmonic mixer and an X-band IF technique which will allow the reception of 94 Gc signals. It is felt that this technique of utilizing a receiver in the spacecraft most readily interfaces with the Aerospace facility.

In conversation, it has become evident that the Air Force, namely the Aerospace facility, is not planning to descend into the millimeter region below 94 Gc. Any plans for the application of frequencies below 94 Gc would be associated with a smaller six-foot reflector system, presently being prepared for use at 35 Gc. For this reason, and since they are presently instrumenting a one-hundred watt transmitter capability, the trade-offs for introducing a receiver within the spacecraft will yield a completely independent channel characterization capability to the experiment. It is also suggested that the Goddard Space Flight Center consider as part of its ground facility, a similar 94 Gc transmitter capability. This would provide an independent channel characterization capability totally under the control of NASA.

7.1 35 Gc Satellite Transmitter

The 35 Gc satellite tranmitter, shown as part of Figure 7-1 is considered to be the greatest power consuming device aboard the satellite, and thus will receive prime emphasis. Although certain devices, such

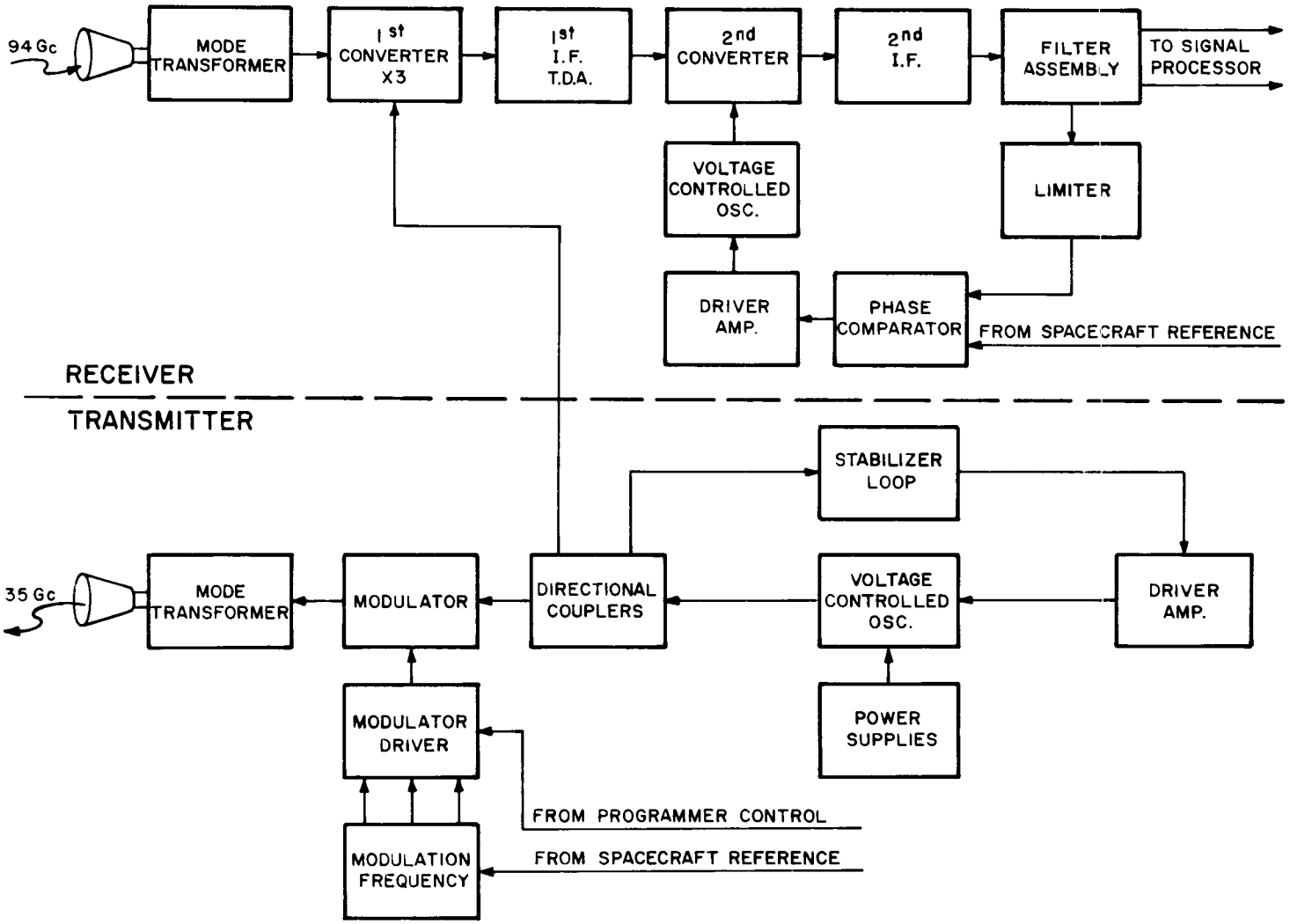

Figure 7-1. Proposed Satellite Transmitting and Receiving System

as the dual-cavity klystron designed by Dr. El Hefni of Bell Laboratories exhibit efficiencies up to 80 percent, these devices are still in the category of laboratory curios. Typical efficiencies of 0.1 to 1.0 percent for off-the-shelf items are more realistic. It should be noted that as the efficiency of the device is increased the prime power supplies decrease proportionately in size and weight. There are presently available two types of klystron oscillators capable of supplying 2 watts and 200 milliwatts respectively.

The efficiency of these two devices varies by almost an order of magnitude. This is due to the fact that as higher power outputs are attained, the standby power, such as filament power becomes less significant in the accumulative prime power required. This continues to be the case as greater and greater RF power is generated.

The possiblility of introducing a two-watt transmitter is within the state-of-the-art if one is willing to supply prime power in excess of 250 watts. To supply the minimum useful output of 200 milliwatts with present-day tubes, about 80 watts of prime power must be supplied.

The calculation represented by Table 7-I is the reference point from which typical performance of a 35 Gc down-link is derived. The satellite is directly over the ground terminal and the complete absence of an atmosphere is assumed. A 50 degree satellite antenna beam was chosen because the earth subtends an angle of 43 degrees at 6000 nmi altitude. The 37 db signal-to-noise ratio represents a 2-watt unmodulated carrier.

Table 7-II shows the effects on signal-to-noise for an unmodulated carrier, an AM double sideband modulated carrier, and one of the AM sidebands for antenna sizes of 6, 15, 30 and 120 feet.

TABLE 7-I

SIGNAL ANALYSIS FOR 35 Gc DOWN LINK

Free Space Attenuation $= \left[\frac{4\pi R}{\lambda}\right]^2$ R = 6000 nmi.	204.4 db	(-)
Propagation Loss [2] (zero loss is used as a reference)	0.0 db	(-)
Satellite Antenna Gain (50° beam)	10.5 db	(+)
Ground Antenna Gain (15 feet, 55% efficiency)	61.9 db	(+)
Noise Density ($KT = 12.7 \times 10^{-23}$, T = 9200°K, NF = 15 db)	-189.0 dbw	(+)
Effective Receiver Bandwidth (100 cps)	20.0 db	(-)
Transmitter Power (2 watts)	3.0 dbw	(+)
Polarization Loss (transmit circular, receive linear)	3.0 db	(-)
Signal-to-Noise Ratio (carrier alone)	37.0 db	

TABLE 7-II

REFERENCE CHART FOR 2 WATT 35 Gc DOWN LINK PERFORMANCE FOR VARIOUS ANTENNAS

Antenna Size (feet)-55%	6	15[1]	30[2]	120[3]
Ground Antenna Gain (db)	53.9	61.9	67.9	71.0
Signal-to-noise ratio (db)				
(a) Unmodulated Carrier	29.0	37.0	43.0	45.1
(b) Modulated Carrier	26.0	34.0	40.0	42.1
(c) Each Sideband	23.0	31.0	37.0	39.1
Margin (db)				
(a) Unmodulated Carrier Lock-on	19.0	27.0	33.0	35.1
(b) Modulated Carrier Lock-on	16.0	24.0	30.0	32.1
(c) Unmodulated Carrier Un-Lock	26.0	34.0	40.0	42.1
(d) Modulated Carrier Un-Lock	23.0	31.0	37.0	39.1

(1) Gain for GSFC antenna Gain for University of Texas antenna is 62.8 db.

(2) Gain for AFCRL antenna is 66.7 db. Gain for Lincoln antenna is 67.5 db.

(3) Gain for Haystack antenna

In determining receiver lock-on margin, it is first considered that a 10 db signal-to-noise ratio is required for the receiver to lock-on. The remaining signal above this required minimum is called margin in db. For example, the 15 foot receiving antenna case has a 37.0 db signal-to-noise ratio for an unmodulated carrier. With a 10 db signal-to-noise ratio required to lock-on, the margin becomes 27.0 db. Table 7-II also shows S/N ratio and signal margin at which the receiver will unlock after acquisition. For a 200 milliwatt 35 Gc transmitter subtract 10 db from all of the S/N ratios and signal margins.

The performance of a 2 watt 35 Gc down link is best illustrated in Figure 7-2. Taking the reference margins established in Table 7-II, an atmosphere and the other variations associated with elevation angle are now introduced into the analysis. For one of the three weather models represented with either unmodulated carrier lock-on or modulated carrier unlock and a given antenna size and elevation angle, the signal margin is shown in Figure 7-2 as the difference between the appropriate relative signal loss curve and the appropriate horizontal line.

This performance chart only shows the effects of atmospheric attenuation, satellite antenna beam shape loss and relative free space attenuation. Signal fading due to multipathing, which will occur at the lower elevation angles, must be absorbed by the signal margins shown. Atmospheric attenuation versus elevation angle was taken from Figure 3-3 in Section 3.1 where the typical weather models were derived. The rain attenuation curve represents a rainfall rate which occurs about 0.5 percent of the time in all geographic areas of interest. Beam shape loss and relative free space attenuation were taken from curves given in Appendix VIII.

Another performance chart for a 200 milliwatt 35 Gc down-link is given in Figure 7-3. As an example, for the rainy weather model given,

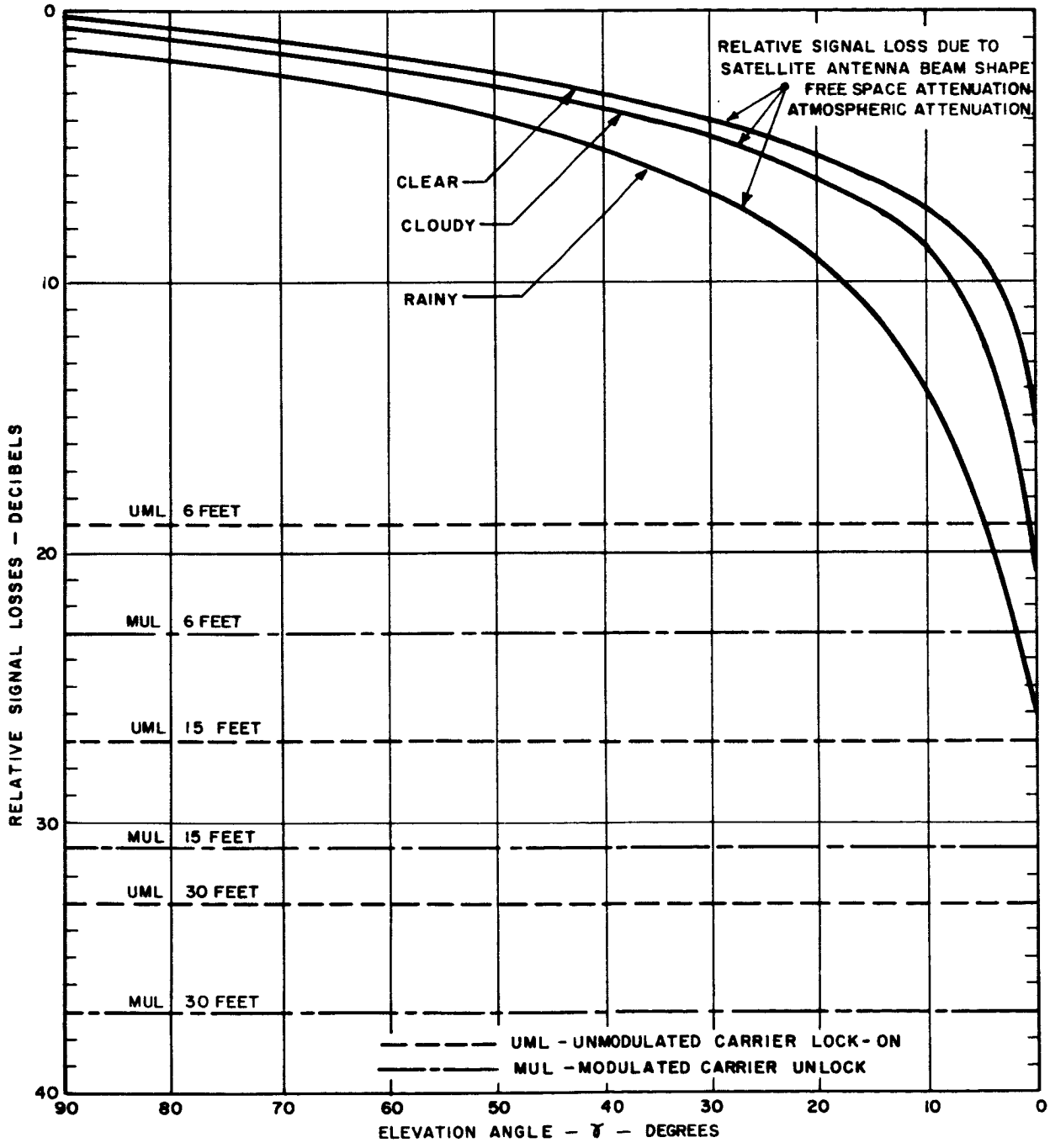

Figure 7-2. 35 Gc Down Link Performance Chart for a 2w Transmitter on a 6000 nmi Satellite

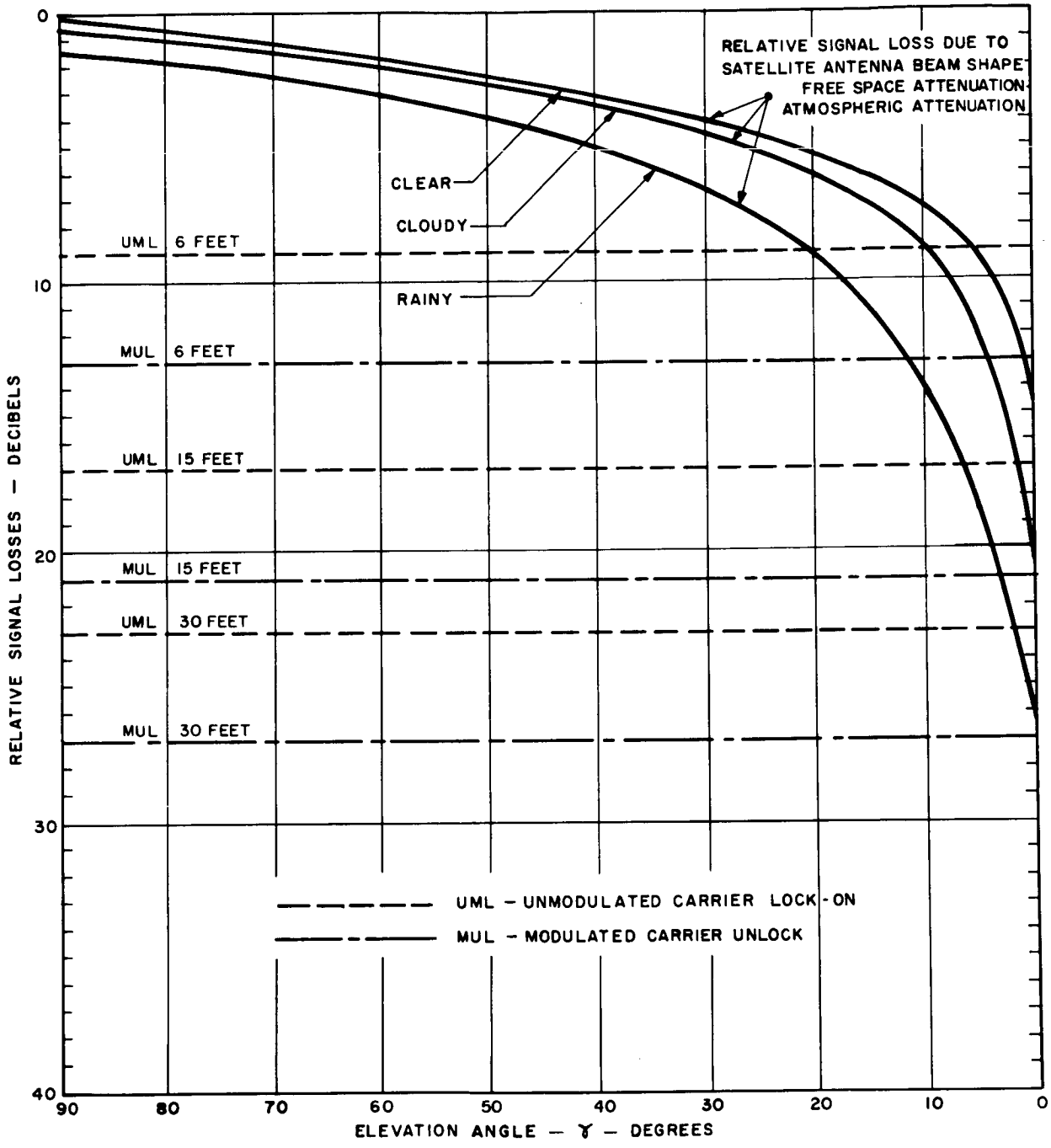

Figure 7-3. 35 Gc Down Link Performance Chart for a 200mw Transmitter on a 6000 nmi Satellite

a 35 Gc receiver with a 15 foot antenna could lock onto an unmodulated carrier at 10 degrees elevation with 3 db of fading. This same receiver would later lose lock on a modulated carrier at 8 degrees elevation with 5 db of fading. The conclusion is, therefore, that a radiated power of 200 milliwatts is not always sufficient to probe the atmosphere at low elevation angles. A radiated power of 2 watts is much more desirable for this reason.

For this report the design of a 200 milliwatt transmitter is presented because of the specified prime power restrictions and because it possibly represents the minimum useful experiment. Higher power designs will be discussed in subsequent reports. Referring to the 35 Gc transmitter in the block diagram of Figure 7-1, the total losses in the various coupling elements have been estimated conservatively to be a maximum of 3 db. Thus, the source must be capable of delivering a minimum of 400 mw of microwave power. It is furthermore desirable to employ as the transmitter a device which has been derated as far as its power output is concerned, and ruggedized for missile applications.

One possibility is the all dielectric Raytheon QKK-996. This klystron has been derated from an output of about 1 watt to 300 milliwatts. It is felt that no serious problem exists in operating this device at 400 milliwatts output power. Another possible device is the Varian VA-239 reflex klystron with an output power of 400 milliwatts minimum, and typically 600 mw. This tube has been designed for extreme environments in airborne applications.

The prime power required for the QKK-996 is 77 watts and slightly less for the Varian tube. The transmitting tube will be stabilized in frequency utilizing an AFC loop as described in Section 5.5. The sampled power is derived from a directional coupler with a coupling coefficient of

about 20 db and an insertion loss not exceeding 0.5 db. The transmitted power, meanwhile, is applied to the input of a second directional coupler. Here, approximately 2 to 4 milliwatts is coupled out and applied as the local oscillator drive to the 94 Gc receiver harmonic mixer. The output of this directional coupler is fed to a semiconductor AM shunt modulator. The insertion loss of the modulator is estimated at a maximum of 1.5 db.

The RF carrier is modulated at three independent modulation frequencies, i.e., 10 kc, 10 mc, and 50 mc. The change in modulation frequency is performed in a step manner and need not be done excessively fast as the propagation path of a 6000 mile altitude satellite will not change at a fast rate. The modulating signals are derived from the spacecraft reference and divided down to the proper frequencies. These frequencies are selectable either through a ground command or a simple, slow commutating switch aboard the satellite.

The modulator itself consists very simply of a varactor diode located in a shunt configuration in a $\lambda/4$ length of waveguide. One side of the diode is at DC ground, while the other side is attached to a TNC connector center conductor via an RF bypass network. The drive power required is quite small, certainly below 100 milliwatts. Thus, the modulator driver need not be very elaborate. A transistor buffer amplifier followed by an emitter follower ought to suffice. The modulated RF is now applied to the antenna subsystem through a short length of waveguide. The antenna will be circularly polarized and preceded by a mode transformer in order to make polarization measurements at the ground terminal, and to minimize signal perturbations due to the vehicle attitude changes.

Table 7-III is a tabulation of the weight, volume, and power consumed by the 35 Gc transmitter.

TABLE 7-III

35 Gc TRANSMITTER VOLUME, WEIGHT AND POWER

ITEM	Volume (inches)	WEIGHT (lb)	POWER (watts)
Power Supply	112	12.0	80
RF Source	2	0.4	included in above
AFC Loop and Power Supply	6	1.0	1
Dir. Coupler (no. 1)	1	0.5	0
Dir. Coupler (no. 2)	1	0.5	0
AM Modulator	0.5	0.3	0
Mod. Driver and Power Supply	2.0	0.5	2
Ant. (Horn)	--	0.2	0
TOTAL	124.5	15.8	83

7.2 94 Gc Satellite Receiver

As previously described in this section, the proposed satellite receiver will make use of a portion of the on-board generated RF energy from the unmodulated transmitter carrier. Through the implementation of this technique, the receiver's overall prime power consumption is drastically reduced. As an example, it would require approximately 60 to 80 watts prime power to generate the necessary local oscillator signal for the

first converter. However, in the proposed implementation, the satellite 94 Gc receiver utilizes the previously generated 35 Gc signal as its first converter signal, and through the use of a third harmonic converter receiver operation is feasible at the expense of 6 watts or less. The proposed receiver and its interface with the transmitter is shown in Figure 7-1.

The 94 Gc signal is received by the antenna subsystem which is circularly polarized in order to minimize the effects of the vehicle's change in attitude, tending to degrade the signal amplitude. Once the signal has been collected by the antenna, it is fed to a mode filter which converts the circularly polarized signal into a linearly polarized signal for processing by the receiving subsystem. The first element encountered is the harmonic mixer where the signal is converted into the first IF. This first converter derives its local oscillator drive from the 35 Gc transmitter by means of a directional coupler. The third harmonic is generated in the nonlinear mixer diode and is used as the down converting signal in order to derive the X-band IF signal. It should be noted that this technique is not beyond the present state-of-the-art, considering the millimeter and submillimter work being done by many in the field and, in particular, the capabilities of Raytheon's Santa Barbara Operation to utilize their wafer diodes as harmonic mixer elements for receiving systems in the millimeter and submillimeter regions. The X-band IF system consists of a tunnel diode amplifier which requires minimum power, yet provides adequate amplification to minimize the effects of the second stage noise figure. Considering that both of these devices represent state-of-the-art technology, this approach becomes quite practical.

The first IF is now followed by the second mixer which converts the X-band signal to a second intermediate frequency at approximately 200 megacycles with an instantaneous bandwidth of approximately 100

megacycles.. The output of this IF is then fed directly to a triplexing device which, through high pass, low pass, and bandpass filtering, allows the selection of the carrier and its two associated sidebands. At this point the carrier filter output is utilized for closing the loop of the phase locked AFC system. This is accomplished by means of tuned narrow band amplifiers and limiters in order to provide the error signal for the phase comparator which drives the VCO. This VCO is a solid state, X-band oscillator which is tuned to the proper frequency in order to correct for doppler and other frequency shifts inherent in the communications channel. This loop will be provided with an automatic sweep acquisition circuit which sweeps the VCO until a lock signal is derived from the phase comparator, and will also contain an override signal to prevent the VCO from locking onto one of the sidebands associated with the carrier. The following sections will describe in more detail how these two signals, namely, the sweep and lock-on override signal, are derived from the signal processor.

Table 7-IV provides a reasonable weight, size, and power estimate of this particular receiver system. As can be seen from the tabulation, the totals for the instrumentation of this receiver within the satellite package burdens the overall package payload by a very small amount.

A reference calculation for a 94 Gc up-link is represented by Table 7-V. As in the case for the 35 Gc down-link, the satellite is directly overhead. Signal-to-noise ratios and signal margin estimates are indicated when a ten watt ground transmitter, and a 25 db receiver noise figure are considered. It is considered that both of these numbers are conservative estimates of the system's operational capabilities, in that a 100 watt ground transmitter is considered practical and is presently being implemented by the Aerospace Corporation. The receiver noise figure for the satellite might even be reduced to the order of 20 db for this

TABLE 7-IV

ESTIMATED WEIGHT, SIZE AND POWER FOR
94 Gc SATELLITE RECEIVER

Subsystem	Weight/lbs.	Size/in.^{3}	Power/watts
Antenna (Horn)	0.1		0
Mode (Transistor)	0.1		0
First Converter	0.2	4	0
First I. F.	0.2	6	0.1
Second Converter and I. F. plus Filters	0.2	12	0.1
Second LO and AFC	0.2	12	5.0
Misc.	0.5	4	0.5
TOTALS	1.5 lbs.	38 in.^{3}	5.7^w

TABLE 7-V

SIGNAL ANALYSIS FOR 94 Gc PROPAGATION EXPERIMENT

6000 n. mile Satellite Receiver in Satellite		
Free Space Attenuation (6000 n. m.)	213.0 db	(-)
Propagation Loss (assume no atmosphere)	0.0 db	(-)
Satellite Antenna Gain (50° beam)	10.5 db	(+)
Ground Antenna Gain (15', 55% efficiency)	70.5 db	(+)
Noise Density ($KT = 1.3 \times 10^{-18}$, T = 95,000°K, NF = 25 db)	-179.0 dbw	(+)
Effective Receiver Bandwidth (200 cps = $\sqrt{2 \times 2\text{ kc} \times 10\text{ cps}}$	23.0 db	(-)
Transmitter Power (10 watts)	10.0 dbw	(+)
Polarization Loss (transmit linear, receive circular)	3.0 db	(-)
Signal-to-noise Ratio (carrier alone)	31.0 db	
(modulated carrier)	28.0 db	
(each sideband)	25.0 db	
Margin: (a) Unmodulated Carrier Lock-On	21.0 db	
(b) Modulated Carrier Lock-On	18.0 db	
(c) Unmodulated Carrier Un-Lock	28.0 db	
(d) Modulated Carrier Un-Lock	25.0 db	

type of broad-band IF converter. As a point of interest, the major difficulty in reducing the noise figure of the receiver is the improvement of the conversion efficiency of the mixer and reduction of the second stage noise figure of the IF amplifier.

A performance chart for the 10 watt 94 Gc up-link with a 15 foot antenna is given in Figure 7-4. In conclusion, an extra 10 db in transmitter power and a lower noise figure would be most desirable for probing the atmosphere at the lower elevation angles.

7.3 35 Gc Ground Receiver

This section of the report deals with the implementation of the ground terminal receiver for the recommended satellite package. This ground terminal receiver will incorporate the capability of performing radiometric measurements in the band of interest and will include the capabilities of a channelized communications receiver function. This proposed ground terminal receiver is shown in Figure 7-5. As seen from this block diagram, the receiver is composed of three major subsystems: a communication receiver, a radiometric receiver and a common RF receiver head.

The radiometric receiver subsystem provides the capability to perform a radiometric measurement either referred to the reference load or to a lobe switched horn. The reference load type of measurement would be used during times when pure radiometric work was being performed such as background mapping of sky temperatures while the lobe switching technique would be utilized during the actual tracking of the satellite. These measurements would be in reality the delta temperature references referred to pre-calibrations of the radiometers. When the system is operating as a pure radiometer, the feed horns on the main

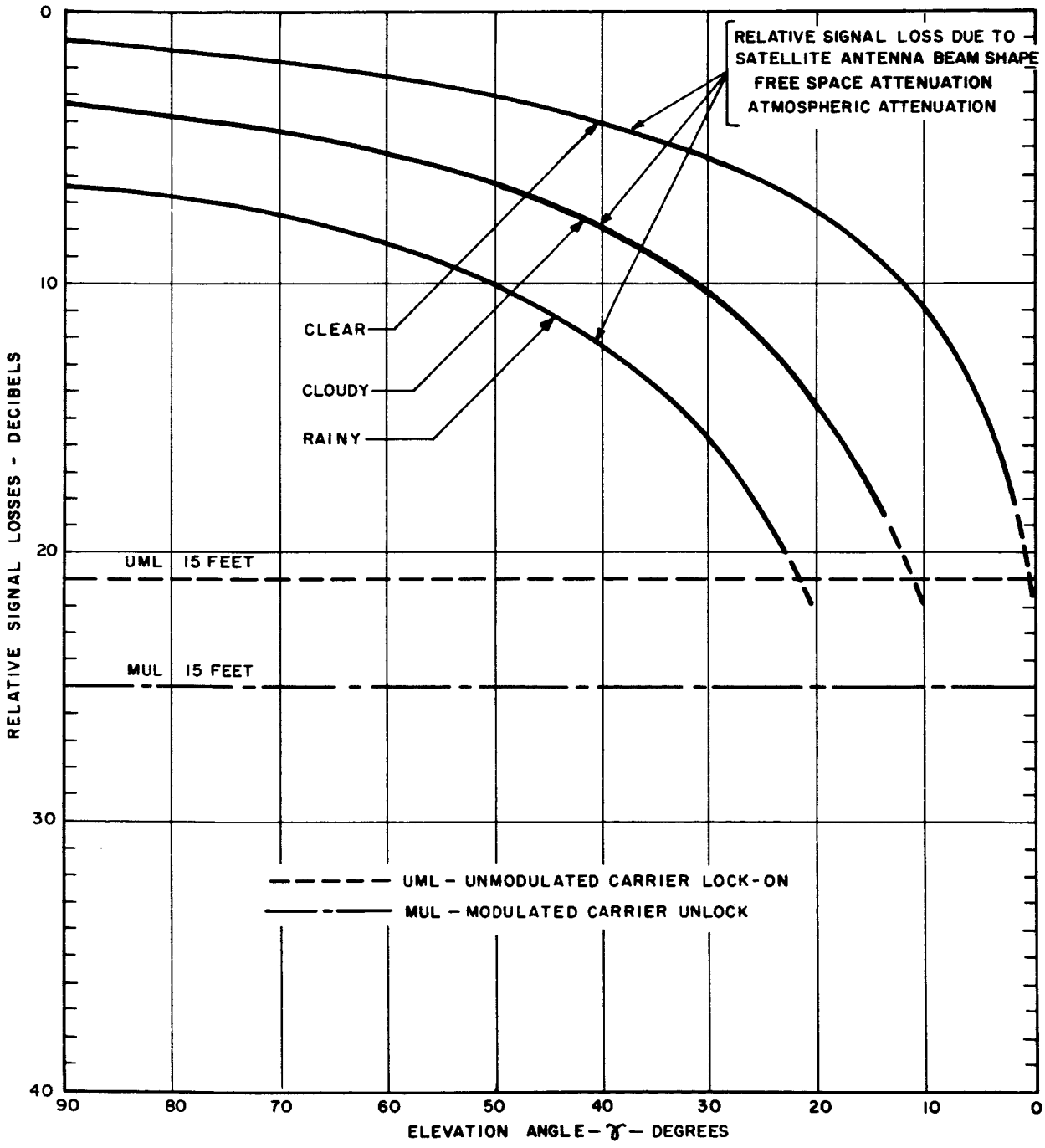

Figure 7-4. 94 Gc Up Link Performance Chart for a 10 w Transmitter and a 6000 nmi Satellite Receiver

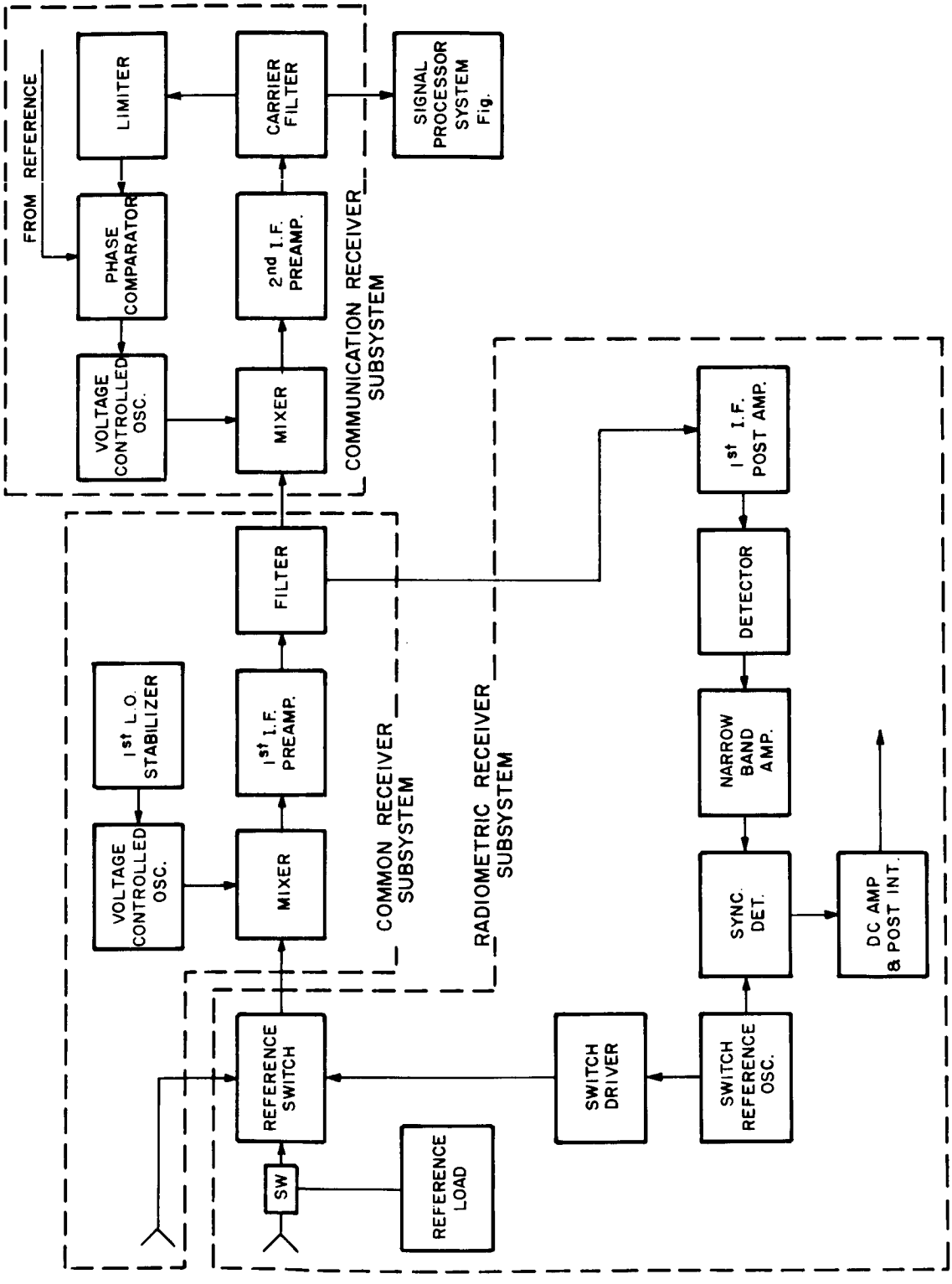

Figure 7-5. Proposed Ground Terminal Receiver

antenna assembly supply the unknown signal to the reference switch while the other port of the switch is supplied with a reference load temperature which will be known and calibrated. The output of the reference switch is then fed to the first converter and then to the broadband first IF pre-amplifier section which, in this proposed receiver, would be a tunnel diode amplifier or TWT operating in the C- or X-band region. Its instantaneous bandwidth would be approximately 500 to 700 megacycles. The output of this pre-amplifier is then fed to a filter system which selects the intelligence bandwidth to be employed by the communications receiver. The unused bandwidth of the preamplifier which is then passed on to the first IF post amplifier in the radiometric section, would be in the order of 400 to 600 megacycles. A square law detector is introduced in order to amplitude detect the signal before going through a narrow band amplifier and into the synchronous detector where the reference switch frequency is removed. The output of the synchronous detector provides a dc voltage to a post detection integration network, the resulting output of which is a measure of the noise power contained in the main antenna relative to the calibrated reference band.

Simultaneous operation of the radiometric and communication subsystems is made possible by the filter after the first IF amplifier. During this mode of operation the radiometric lobe switching technique will be implemented which will allow antenna temperature measurement as the satellite is tracked across the celestial sphere. The communication signal is fed to the second converter whose local oscillator signal is provided by a voltage controlled oscillator in a phase lock loop. The communication receiver will provide the outputs required for the signal processor system described in Section 7.5.

7.4 94 Gc Ground Transmitter

This section of the report deals with the requirments and capabilities of the ground transmitter operating at 94 Gc which would interface with the satellite receiver described in Section 7.2. As indicated in Section 7.2, the signal power analysis is based on a 10 watt transmitter as the minimum capability. However, serious consideration should be given to a 100 watt capability.

This transmitter can take the form of a low power driver such as klystron or distributed interaction klystron devices which can be amplitude modulated via a shunt modulation technique, as previously described in Section 7.1. This, then would be followed by a final driver amplifier which would transmit 10 to 100 watts of RF power. This final driver amplifier could readily take the form of the presently developed Hughes TWT type of coherent millimeter amplifier.

This type of operation would prove to be most efficient in that the final driver stages may be operated in a saturated mode to optimize the power output of the last driver stage and minimize amplitude fluctuations due to the previously introduced AM technique. Hence, it is felt that this general philosophy would lend itself readily to solving the problems of generating high levels of millimeter power for ground based installations. Further detail on this particular approach would, by necessity, require a more detailed investigation into the actual operating characteristics of the final driver stages and its associated hardware.

This information, it is felt, will be available within the near future, due to the actual experience of the Hughes and Aerospace test and evaluation programs on these high power millimeter transmitter sources. Therefore, it is proposed that a continuing exchange of information with these two

groups be such that the latest and most up to date information with regard to these devices is introduced into the final design document of this study.

7.5 Satellite and Ground Signal Processors

This section discusses the possible configuration of a signal processor which would handle the AM double sideband modulation approach as previously discussed in Sections 4.1.1 and 5.3.1. A detailed block diagram of the signal processor as presently conceived is given in Figure 7-6. The signal processing system contains three basic elements: the sideband selector and delta doppler corrector, the amplitude processor which derives the amplitudes of the upper and lower sidebands, and the signal phase processor which performs a relative phase comparison of the two sidebands.

7.5.1 Sideband Selection and Delta Doppler Correction

This section of the signal processor interfaces directly with either phase lock receiver described in Sections 7.2 and 7.3. The input to the signal processor derives its signal from the output of the receiver and then performs upper and lower sideband separation with high pass and low pass filters. These two filters are each followed by a converter stage that will allow for the cancellation of delta dopplers which are the residual left on the sidebands due to their frequency separations from the phase locked carrier signal. This is performed by injecting a local oscillator signal equal to the center frequency of communication IF receiver and tuning the buffer amplifier in the upper sideband channel to select the lower conversion product of the mixer and tuning the buffer amplifier in the lower sideband channel to select the upper conversion product of the mixer. The sideband information is now at one frequency. Each buffer amplifier is then followed by another converter stage which

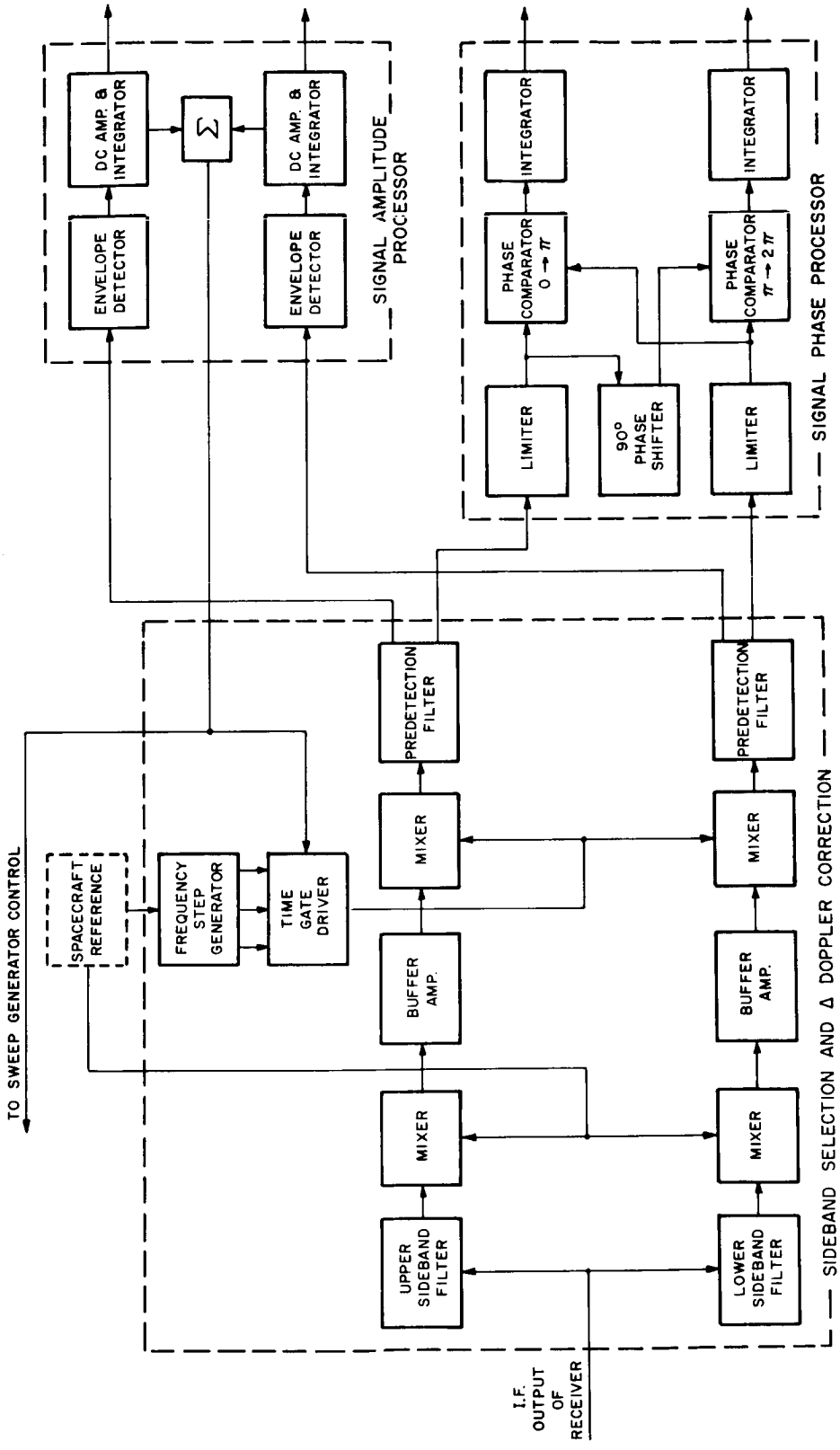

Figure 7-6. Signal Processing System

translates its sideband signals down to the center frequency of a good predetection filter for improvement in S/N ratio.

7.5.2 Signal Amplitude Processor

In this particular subsystem, the relative amplitudes of the upper and lower sidebands are processed, via envelope detection and dc amplification and integration. This section, as shown on the block diagram, interfaces directly with the predetection outputs. The output of these dc amplifiers and integraters is either fed directly to telemetry for ground transmission in the case of satellite, or recorded directly at the ground terminal for computer processing. Also included with the package is the summation of the two relative amplitudes such that a sweep control generator signal is provided. This summation is also provided as a lock-on thresholding device to the time gate generator which selects the proper frequency steps to be provided for the second converter in the sideband selector and delta doppler corrector.

7.5.3 Signal Phase Processor

In this subsection of the signal processing system, the signals are received and processed through tuned hard limiter circuits which provide in-phase and quadrature signals for processing through dual phase comparators. This provides an output from 0 to 360 degrees of phase information. The output of the phase comparator is integrated and buffer amplified such that direct interfacing with the telemetry link is provided for the spacecraft and direct interfacing with the tape recorder is provided for the ground terminal.

7.6 Breadboarding of Key Items

This section of the report deals with the key areas of concern for the proposed satellite experiment. The following two sub-sections give a listing of priority items which should be implemented in such a way that these design developments are available to the millimeter experiment designer prior to final commitment of final package design. These design development areas will require a time period of six months to one year to perform adequate evaluation of the proposed design approaches.

The best possible means of properly evaluating these key items is by constructing breadboard models and/or purchase of certain items whose performance specifications may be in doubt or improved upon by a better understanding of their performance.

7.6.1 Transmitter Breadboarding

Insofar as the 35 Gc transmitter is concerned, three items fall under this category. First and foremost, the Pound discriminator should be built and thoroughly evaluated. This item is of the greatest importance for the following reasons:

1. The ultimate sensitivity is achieved when the receiver bandwidth is narrowed to 1 cps. Anything approaching this can only be obtained if the transmitter is stable to within this bandwidth. It is, therefore, well worthwhile to experimentally determine the best achievable stability without a major development program.
2. This form of microwave discriminator, although tried and true, has not been materially improved since its early use. With the advent of improved semiconductor diodes, klystrons, and low-noise dc amplifiers, it

should be possible by means of good design techniques, to improve the overall capability of the Pound discriminator.

The second key item in the transmitter is the shunt modulator. For this particular application, a modulation depth of 20 db or better is desirable. This feature by itself is not very difficult to achieve. The important point is that this modulation range must occur simultaneously with a very low insertion loss. The presently allocated insertion loss is 1.5 db for the modulator. Certainly this must not be exceeded, and, if possible, lowered to less than 1 db.

Two types of shunt modulators will be evaluated - the reflective type and the absorption type. The implementation of the reflective type is closest to present-day capabilities, but would require the introduction of low-loss millimeter wave isolation to prevent the reflected energy from reaching the stabilized transmitter source and any frequency converters supplied by this source.

The shunt modulator, therefore, should ideally be an absorption type of modulator. The desirability of this feature is the fact that when the modulator is in the non-transit bias position, all the non-transmitted energy will be absorbed. The only presently available true absorbing semiconductor modulator is the PIN diode. Therefore, the operation of a PIN diode modulator at 35 Gc must be throughtly investigated and documented. The main evaluation of this device would be to determine the actual change in match due to a change in the percent modulation. This, then, would be compared with a reflective model coupled to an isolator.

To this end, two, or possibly three suitable modulators will be purchased and tested. On the basis of these results, a decision will be made as to the most suitable unit. As part of this work, any required modifications will be made.

The following are some typical manufacturers of diode modulators including some of the performance specifications.

Manufacturer	Insertion Loss (db)	Modulation Range (db)	Max. Req. Power
Philco	1.5	20	50-60 mw
Somerset Radiation	4	60	1 w
Microwave Associates	3	30	100 mw
Hewett Packard	Not high enough in freq.	--	-------
Microwave Technology Inc.	less than 1.0	20	100 mw

The third critical item is the choice of the power supply. This unit must be capable of withstanding high g forces during launch and remain highly stable with a minimal change in the output levels. Power supplies of the SCR type are generally in use in space applications, but are usually tailor-made for any specific experiment. A thorough search of manufacturers literature would be made, circuit diagrams will be examined, and specifications will be scrutinized in order to arrive at the best choice.

7.6.2 Receiver Breadboarding

Three items in the receiver require early and special attention. The establishment of a firm foundation of knowledge and skill in these areas is somewhat lacking, as a general rule, and the best solution to problems of this nature is the construction of, and experimentation with, actual hardware.

The first of these key items is the harmonic mixer which receives signals at 94 Gc and uses the 35 Gc transmitter power for the local oscillator drive, thus delivering an IF signal at X-band. The loss and noise figure of this mixer has, of course, a direct relation to the sensitivity of the receiver and methods should be determined to optimize this sensitivity. For instance, it may be possible to obtain an improved performance by means of a small, external diode bias. This bias would certainly improve the IF impedance with respect to that of the tunnel diode IF amplifier input, another crucial item.

The next key item is the IF amplifier itself. The stability, impedance match and lowest available noise figure must be firmly established. A shortcoming of the tunnel diode amplifier, namely its limited dynamic range, will be carefully studied and suitable technology applied to overcome this shortcoming. Low-pass filtering techniques will be employed to avoid diode burnout due to dc transients.

Thirdly, the phase-lock loop must be scrutinized in minute detail. The S/N ratio values required for lock and unlock are still theoretical postulates. Thus, it is essential that a loop be constructed and various levels of signals plus noise be injected into the loop in order to gain a firm feel for the possible improvements in this unit.

In order to retrieve the upper and lower sidebands of the 94 Gc signal, it is, of course, necessary to maintain a stability in the satellite, comparable to that of the ground terminal transmitter. Considering that hardly any restrictions are imposed on the size, weight and volume of the ground equipment, it is expected that the transmitted signal will be stable indeed. Thus, an extremely tight loop is required and should be given early attention.

8. PROGRAM FOR NEXT PERIOD

For the most part the program for the remaining five months will follow that which is specified in the Program Definition Document. Specifically, the work to be accomplished shall include the following major items.

8.1 Basic Data Format

Develop the basic data format required to determine the data processing requirements for translating raw communication signal data and raw correlative data, collected during the propagation experiments, to the form required for the millimeter wave propagation data handbooks.

8.2 Millimeter wave Propagation Data Handbook

Make an outline of the propagation data handbook which should be the major result of the millimeter communication propagation program. The handbook should contain a theoretical section on propagation of millimeter waves, a presentation of basic data collected during the propagation program, and a performance evaluation of certain key modulations inferred from this basic data.

8.3 Descriptive Bibliography

Write a descriptive bibliography of reports related to this experiment design study. It should include such technical areas as theory of millimeter wave propagation, millimeter wave communication system technology, millimeter wave components, and existing experimental millimeter wave ground facilities.

8.4 Correlative Measurements

Investigate further the usefulness of weather radar as a correlative tool to be used in conjunction with other meteorological and radiometric devices.

8.5 Implementation of Measurement Waveforms

Describe the millimeter transmitters and receivers required to implement the PAM and PAM/FM measurement waveforms and describe the magnitude of the required development effort in time and cost.

8.6 Ground Facilities Evaluation

Describe how each facility can track or be modified to track a 6000 nautical mile satellite. Specify the interfaces between the existing equipment and the experimental equipment recommended in Section 7. Define characteristics of each site so that specific performance evaluation can be calculated in the general form presented in Section 7.

8.7 Experiment Concepts

Describe a 16 Gc satellite transmitter which could work with the 35 Gc transmitter/94 Gc receiver package recommended in Section 7, in terms of system performance, components required and prime power - weight-volume estimates.

Describe the 94 Gc satellite transmitter, particularly the development effort required, which could replace the 94 Gc receiver recommended in Section 7.

In the event that medium altitude satellites are considered to be unavailable for the initial experiments, develop concepts based on the use of synchronous satellites.

8.8 Equipment Design

Perform the equipment design task specified in the Program Definition Document. The equipment recommended in Section 7 shall be submitted to design at the schematic block diagram level. The 35 Gc satellite transmitter design shall include two alternates: the 200-milliwatt output and the 2-watt output.

8.9 Data Processing Requirements

Describe the data processing requirements as specified in the Program Definition Document. Also include a very careful account of how satellite orbits will be determined, and how the ephemeris data should be distributed to the ground millimeter facilities.

BLANK PAGE

9. BIBLIOGRAPHY

(1) "Local Climatological Data with Comparative Data", Weather Bureau, U. S. Dept. of Commerce, 1963.

(2) "Rainfall Frequency Atlas of U. S. for Durations from 30 minutes to 24 hours and Return Periods from One to 100 Years", Technical Paper 40, Weather Bureau, U. S. Department of Commerce.

(3) MIT Radiation Laboratory Series, Volume 13, 1948.

(4) "Model Precipitation Distributions", E. Kessler III and David Atlas Aero/Space Engineering, Dec. 1959, pp 36-40.

(5) "Handbook of Geophysics for U. S. Air Force Designers", Air Force Cambridge Research Labs, Chapter 6.

(6) "Losses Due to Rain on Radomes and Antenna Reflecting Surfaces: IEEE Transactions on Antennas and Propagation", B. C. Blevis, January, 1965.

(7) "Dielectric Behavior of Water at Microwave Frequencies", E. H. Grant, T. J. Buchanan, and H. F. Cook, Journal of Chemical Physics, Volume 26, January, 1957.

(8) "Theory of the Reflection and Transmission of Electromagnetic Waves By Dielectric Materials", H. Leaderman and L. A. Turner, in "Radar Scanners and Radomes", MIT Radiation Laboratory Series, Volume 26, 1948.

(9) "Effects of Rain or Transmission Performance of a Satellite Communications System", D. Gibble, IEEE International Convention, March, 1964.

(10) "An Analysis of Time Variations in Tropospheric Refractive Index and Apparent Radio Path Length", M. C. Thompson, H. B. Janes, and R. W. Kirkpatrick, J. Geophys Res., Volume 65, January, 1960, pp. 193-201.

(11) "Reasons for the Failure of Radio Interferometers to Achieve their Expected Accuracy", D. K. Barton, Proc. IEEE, Volume 51, No. 4, April 1963, pp. 626-27. (See also pp. 485-90 in "Radar System Analysis", Prentice-Hall, Inc., 1964).

(12) "Errors Inducted by the Atmosphere in Microwave Range Measurements H. B. Janes and M. C. Thompson, Radio Science (Sec. D of NBS Journal of Research), Volume 68D, No. 11, pp. 1229-1235, November, 1964.

(13) "Report of the Ad Hoc Panel on Electromagnetic Propagation", David Barton (Editor), ACAFSC 103, 1962.

(14) "Radar System Analysis", David Barton, Prentice-Hall, Chapter 15, 1964.

(15) "Climatic Charts and Data of the Radio Refractive Index for the United States and the World", B. R. Bean, J. D. Horn, and A. M. Ozanich, NBS Monograph 22, 1960.

(16) "A Survey of the Techniques for Measuring the Radio Refractive Index", McGavin, NSB Technical Note 99, May, 1962.

(17) "Frequency Correlation of Line-of-Sight Signal Scintillations", R. B. Muchmore and A. D. Wheelon, IEEE Trans. Antennas and Propagation, Jan., 1963, pp. 46-51.

(18) "Radiation and Propagation of Telemetry Signals During Hypersonic Re-entry", E. Langberg, K. Baldwin, and J. Yos, IRE Proceedings of the National Symposium on Telemetering - 1958.

(19) "Electromagnetic Properties of High-Temperature Air", M. P. Bachynski, T. W. Johnston, L. R. Shkarofsy, Proc. IRE, Volume 48, March, 1960, pp. 347-356.

(20) "Antenna Noise Temperature in Plasma Environment", M. P. Bachynski, L. P. French, G. G. Cloutier, Proc. IRE, Volume 49, December, 1961, p. 1848.

(21) "Free Path Formulas for the Electronic Conductivity of a Weakly Ionized Gas in the Presence of a Uniform and Constant Magnetic Field and a Sinusoidal Electric Field", L. G. H. Huxley, Aus. J. Phys., Volume 10, 1957, pp. 240-245.

(22) "Plasma Physics of Shock Fronts", M. P. Bachynski, L. P. Shkarofsky, T. W. Johnston, Res. Labs., RCA Victor Co., Ltd., Montreal, Can. RCA RES. Depts. No. 7-801-3; June, 1959.

(23) "Electronic and Ionic Phenomena", H. S. W. Massey and E. H. S. Burhop, Oxford University Press, New York, N.Y., 1952.

(24) "Transparent Phenomena in a Completely Ionized Gas", L. Spitzer and R. Harm, Phys. Rev., Volume 89, 1953, pp. 977-981.

(25) "Electrical Conductivity of Thermally Ionized Air Produced in a Shock Tube", L. Lamb and S. C. Lin, J. Appl. Phys., Volume 28, July, 1957, pp. 754-759.

(26) "Various Thermodynamic Properties of Air", A. R. Hochstim and R. J. Arave, Convair, San Diego, California, Report No. ZPH-004, June, 1957

(27) "High-Frequency Breakdown in Air at High Altitudes", A. D. MacDonald, Proc. IRE, Volume 47, March, 1959, pp. 436-441.

(28) "RF Breakdown Conditions in the Presence of the Plasma Sheath", R. F. Whitmer, "Electromagnetic Effects of Re-Entry", selected papers from the symposium on Communications and Detection, Boston, December, 195 Published by the Pergamon Press, 1961.

(29) "Voltage Breakdown of Antennas at High Altitude", W. E. Scharfman and T. Morita, Proc. IRE, Volume 48, November, 1960, pp. 1881-1887.

(30) "A Millimeter Communications Propagation Study", BR-3011, June 8, 196

(31) "Synthesis of an Arbitrary Bank of Filters by Means of a Time-Variable Network", E. Brookner, IRE Conv. Record, Part 2, 1961, pp. 221-235.

(32) "Characterization and Measurement of Time-and-Frequency Spread Chann R. G. Gallager, Technical Report, Lincoln Laboratory, April 30, 1964.

(33) "Variation of Bandwidth with Modulation Index in Frequency Modulation", M. S. Corrington, IRE, October, 1947, p. 1013.

(34) "Physics Review", R. G. Bergmann, Volume 70, 1946.

(35) "A Statistical Survey of Atmospheric Index-of-Refraction Variation", C. M. Crain et al, IRE Trans. Antennas and Propagation, October, 1953, pp. 43-46.

(36) "Error Probabilities for Binary Symmetric Ideal Reception through Nonselective Slow Fading and Noise", G. L. Turin, IRE, September, 1958, pp. 1603-1619.

(37) "Error Probabilities for Rician Fading Multichannel Reception of Binary and N-ary Signals", W. C. Lindsey, IEEE Trans. on Information Theory, October, 1964, pp. 339-350.

(38) "Error Probabilities for Random Multichannel Reception of N-ary Signals", W. C. Lindsey, (Original Version of Reference 6).

(39) "Digital Troposcatter Transmission and Modulation Theory", E. D. Sunde, The Bell System Technical Journal, January, 1964, pp. 143-153.

(40) "Intermodulation Distortion in Analog FM Troposcatter Systems", The Bell System Technical Journal, January, 1964, Part 2, pp. 399-435.

(41) "Low Cost Digital System Records Weather Data", F. T. Goldwater, Electronics, January 10, 1964.

(42) "Research on the Suitability of Millimeter Wavelength Systems for Space Application", B. J. DuWaldt, WESCON, 1964.

(43) "Research and Experimentation on Space Applications of Millimeter Waves", H. E. King, Aerospace Corporation, BSD and SSD, Contract AF 04(695)-269, October, 1964.

(44) "Experimental Evaluation of a 1000-Wavelength Antenna", W. D. Fitzgerald, V. L. Lynn, and K. J. Keeping, NEREM Record, 1962.

(45) "Radar Observation of the Moon at 8.6 mm Wavelength", V. L. Lynn, M. D. Sohigian, and E. A. Crocker, Lincoln Laboratory, Technical Report 331, October 8, 1964.

(46) "The Haystack Experimental Facility", H. G. Weiss, Lincoln Laboratory, Technical Report 365, September 15, 1964.

(47) "Factors Affecting Earth-Satellite Millimeter Wavelength Communications", A. W. Straiton and C. W. Tolbert, IEEE Transactions on Microwave Theory and Techniques, September, 1963.

(48) "The Microwave Spectrum of Oxygen in the Earth's Atmosphere", A. E. Lilley and M. L. Meeks, Journal of Geophysical Research, Volume 68, No. 6, March 15, 1963.

(49) "An Estimate of Influence of the Atmosphere on Airborne Reconnaissanc Radar Performance", T. F. Rogers, AFCRL, January, 1953.

(50) "The Microwave Properties of Precipitation Particles", K. L. S. Gunn, and T. W. R. East, Quarterly of the Journal of the Royal Meteorologica Society, 80, October, 1954.

(51) "A Method for the Determination of High-Altitude Water-Vapor Abundance from Ground-Based Microwave Observations", A. H. Barrett, V. K. Chung, Geophysical Research, Vol. 67, No. 11, October, 1962.

(52) "Propagation of Short Radio Waves", Radiation Laboratory Series, Volume 13, Page 682.

(53) "Channel Characteristics=Time-Invariant Dispersive Channels", T. Kailath, Lectures On Communications System Theory, Edited by E. Baghdady, McGraw Hill, 1961.

(54) "Statistical Theory Applied to Communication Through Multipath Disturbances", R. Price, Lincoln Laboratory, Tech. Report No. 34, September, 1953.

(55) "Sampling Models for Linear Time Variance Filters", T. Kailath, Technical Report 352, MIT, May, 1959.

(56) "Measurement of Power Spectra", R. B. Blackman and J. W. Tubey, Bell System Tech. Jour., 1958.

(57) "Effects of Tropospheric Refraction in Earth-Space Links", K. A. Norton, XIVth General Assembly of URSI, Japan, September, 1963.

(58) "On the Shape of Collision Broadening Lines", J. H. Von Vleck and V. F. Wiesskopf, Review of Modern Physics, Volume 17, April - July, 1945.

(59) "Statistical Survey of Atmospheric Refraction Variation", C. M. Crain, A. W. Straiton, and L. E. Von Rosenberg, IRE Trans. on Antennas and Propagation, October, 1953.

(60) "Telstar Communications Tests", R. W. Hatch, S. B. Bennett, and T. P. Kinzer, Bell System Tech. Jour., June, 1963.

(61) "Electromagnetic Theory", T. Jordan, McGraw Hill.

APPENDIX I

MILLIMETER WAVE ATTENUATION DUE TO WATER VAPOR, RAIN AND OXYGEN

In the millimeter wave region of the spectrum, the atmosphere produces attenuation through resonance absorption of its constituent gases. This attenuation is determined principally by oxygen and water vapor. Prominent water vapor peaks occur at 22 Gc, 184 Gc, and 324 Gc, and there are approximately 150 water lines in the submillimeter region. A cluster of oxygen lines occurs at both 60 Gc and 118 Gc. Figure I-1 shows the water vapor attenuation at sea level and four altitudes above sea level (Reference 47). Figure I-2 indicates the horizontal attenuation and Figure I-3 indicates the vertical opacity of the atmosphere due to its oxygen content (Reference 48).

Millimeter wave signals are subject to attenuation from fog, rainfall, snowfall, and the melting layer or "bright band". Theoretical models of rainfall attenuation based on experimental data indicate that attenuation per unit length is directly proportional to rainfall rate. Attenuations for various rates of rainfall in the microwave and millimeter-wave region are shown in Figure I-4. Attenuation for clouds and fogs are shown in Figure I-5 (References 49 and 50).

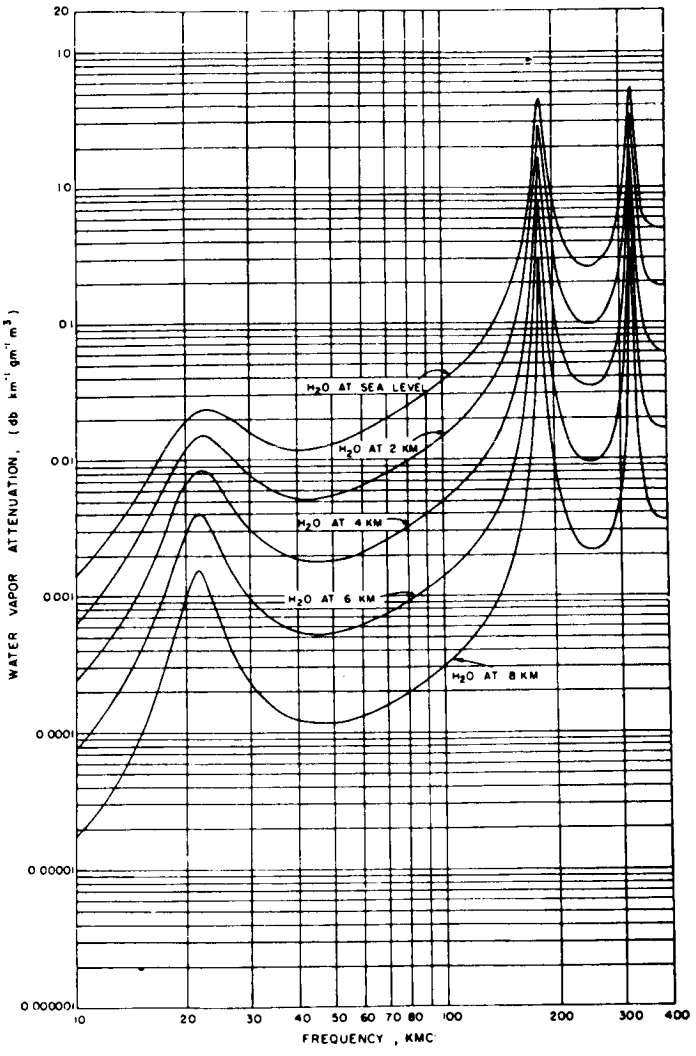

Figure I-1. Attenuation Due to Water Vapor at Five Elevations

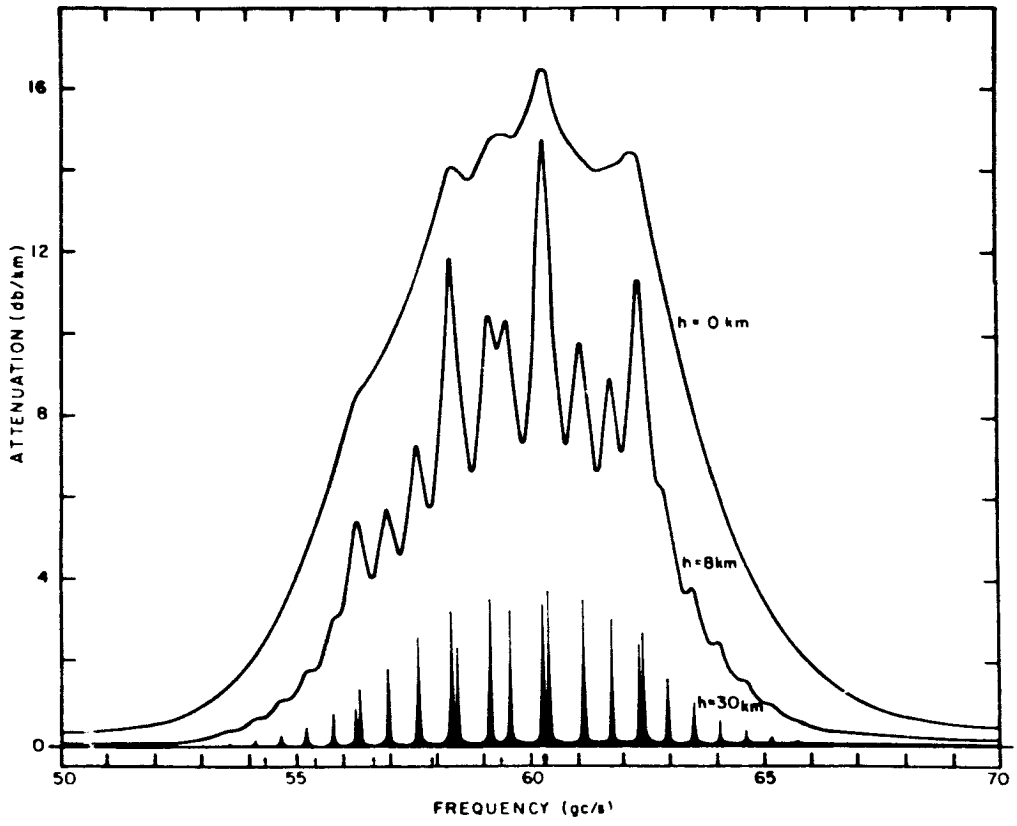

Figure I-2. Horizontal Attenuation Due to Oxygen

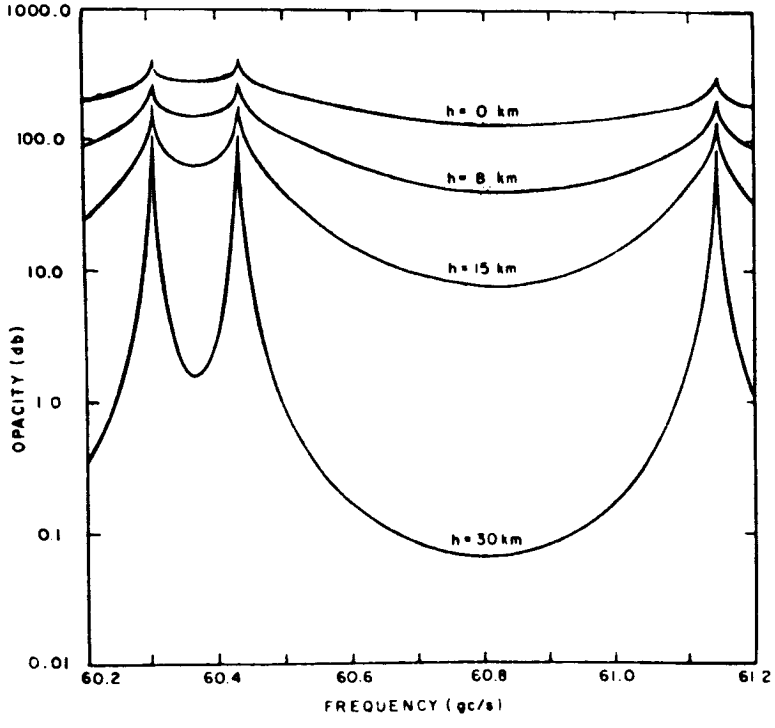

Figure I-3. Vertical Opacity Due to Oxygen

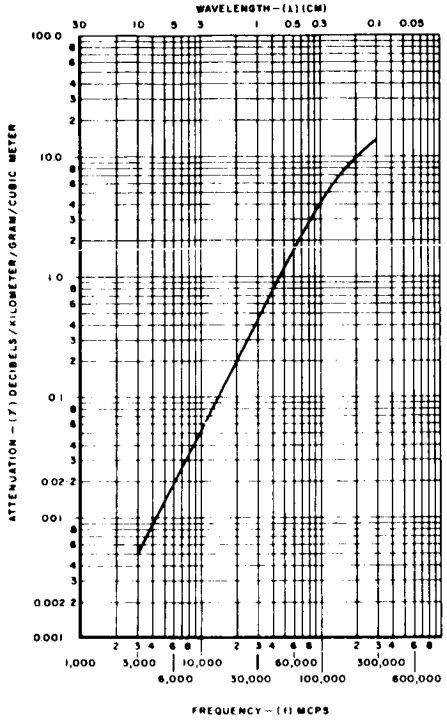

Figure I-4. Rainfall Attenuation vs Frequency for Various Precipitation Rates

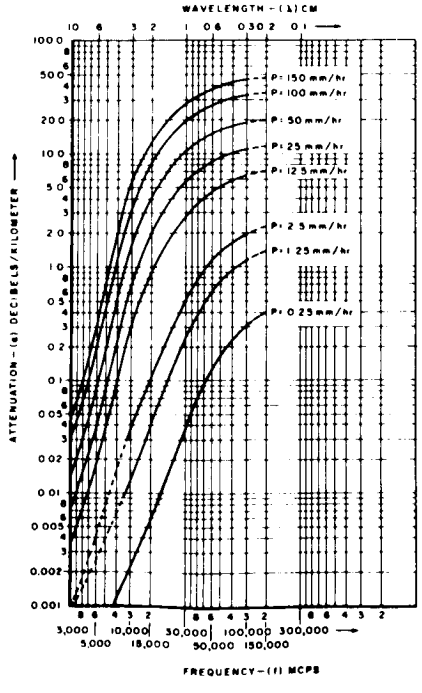

Figure I-5. Attenuation Due to Clouds of Fog

APPENDIX II

DIGITAL COMPUTER PROGRAM FOR CALCULATION OF APPARENT SKY TEMPERATURE AND ATMOSPHERIC TRANSMISSION FACTOR

The apparent temperature of a body as received by an antenna at an altitude H above the surface of the Earth and a nadir angle ϕ, may be expressed as follows:

$$T_H = \tau \left[\epsilon T + (1 - \epsilon)T_{S\phi}\right] + T_R', \ ^oK \text{ (for specular reflector)} \qquad \text{(II-1)}$$

$$T_H = \tau \left[\epsilon T + (1 - \epsilon) T_S\right] + T_R', \ ^oK \text{ (for a diffuse reflector)}$$

where τ is the atmospheric transmission factor; ϵ is the emissivity of the body; T is the thermometric temperature of the body, ^oK; $T_{S\phi}$ is the apparent sky temperature at zenith angle ϕ, ^oK; T_S is the average apparent sky temperature, ^oK; T_R' is the radiated apparent temperature of the atmosphere between the body and the antenna.

The purpose of this discussion is to show the exact expressions for several of the factors appearing in Equation (II-1).

For an upward-looking radiometer, the received apparent temperature will be equal to $T_{S\phi}$ unless a target such as an airplane, a satellite, or a star happens to be in the antenna beam.

In addition to target detection, a radiometer can be used to determine certain characteristics of the atmosphere. It will be shown below that the measurable quantities τ and $T_{S\phi}$ are dependent on air temperature, relative humidity, air pressure, water vapor content, and rainfall rate. By judicious selection of operating frequency, information about these factors can be obtained from radiometric measurements.

The development of this formulation is an extension of published reports (References 48 and 51) and is based on the Van Vleck-Weisskopf theory of molecular absorption. From Reference 51, Equation (II-2) gives the

transmission factor for the atmosphere from the ground up to altitude h_i, and Equation (II-3) gives the apparent sky temperature at a zenith angle ϕ.

$$\tau_i = 0.23 \sum_{j=0}^{i} \alpha_j \Delta x_j \qquad \text{(II-2)}$$

$$T_{S\phi} = \sum_{j=0}^{n} T_i \left(1 - e^{-0.23 \alpha_j \Delta x_j}\right) e^{-(\tau_{j-1})}, \ ^oK \qquad \text{(II-3)}$$

where α is an absorption coefficient to be defined later; Δx is incremental slant range, meters $x = -R \cos\phi + \sqrt{R^2 \cos^2\phi + 2Rh + h^2}$, meters; R is radius of Earth, meters; h is altitude, meters; ϕ is angle away from the vertical, degrees; and T_i is thermometric temperature at altitude h_i, ^oK.

It should be noted from the definition of x that the curvature of the earth has been considered in this formulation.

The absorption coefficient, α , is a function of frequency, atmospheric constituents, and atmospheric temperature. It can be expressed (in db/km) as a sum of four separate coefficients.

$$\alpha = \gamma_1 + \gamma_2 + C_1 + C_2, \text{ db/km} \qquad \text{(II-4)}$$

where γ_1 is the absorption coefficient of oxygen; γ_2 is the absorption coefficient of uncondensed water vapor; C_1 is the absorption coefficient of clouds or fog; and C_2 is the absorption coefficient of rain.

Average apparent sky temperature is given by Equation (II-5).

$$T_S = \frac{1}{\pi} \int_o^{2\pi} \int_o^{\pi/2} T_{S\phi} \sin\phi \cos\phi \, d\phi \, d\theta \qquad \text{(II-5)}$$

where θ is the azimuth angle.

If sky conditions are constant over the range of azimuth angles, Equation (II-5) simplifies to

$$T_S = 2 \int_o^{\pi/2} T_{S\phi} \sin\phi \cos\phi \, d\phi, \ ^oK \qquad \text{(II-6)}$$

From Reference 48, Equation (II-7) gives the absorption coefficient of oxygen:

$$\gamma_1 = 2.6742 \times 10^{-9} P_i T_i^{-3} \nu^2 \sum_{N=1}^{2d+1} \left\{ \left[\frac{\Delta\nu_1}{(\nu_{N+} - \nu)^2 + \Delta\nu_1^2} + \frac{\Delta\nu_1}{(\nu_{N+} + \nu)^2 + \Delta\nu_1^2} \right] \left[\frac{N(2N+3)}{N+1} \right] + \left[\frac{\Delta\nu_1}{(\nu_{N-} - \nu)^2 + \Delta\nu_1^2} + \frac{\Delta\nu_1}{(\nu_{N-} + \nu)^2 + \Delta\nu_1^2} \right] \left[\frac{(N+1)(2N-1)}{N} \right] + \left[\frac{\Delta\nu_1}{\nu^2 + \Delta\nu_1^2} \right] \left[\frac{2(N^2+N+1)(2N+1)}{N(N+1)} \right] \right\}$$

$$\exp \left[-2.0684 \, N(N+1)/T_i \right] \quad \text{db/km} \qquad \text{(II-7)}$$

From Reference 51, Equation (II-8) gives the absorption coefficient of uncondensed water vapor.

$$\gamma_2 = (4.56 \times 10^{-23}) \left(\frac{M\nu^2}{T_i^{3/2}}\right) \left\{ \frac{e^{-\frac{644}{T_i}}}{T} \left[\frac{\Delta\nu_2}{(\nu - \nu_o)^2 + \Delta\nu_2^2} + \frac{\Delta\nu_2}{(\nu + \nu_o)^2 + \Delta\nu_2^2} \right] + (7.238 \times 10^{-24})(\Delta\nu_2) \right\} \text{ .db/km} \qquad \text{(II-8)}$$

where:

d	= 1 to 22
P_i	= pressure at altitude h_i, mm of Hg
T_i	= temperature at altitude h_i, ^oK
ν	= frequency, cps
ν_o	= 22.235 Gc = 22.235×10^9 cps
ν_{N+} and ν_{N-}	= transition frequencies listed on page 1684 of Reference 48
M	= water content = $me^{-\frac{h_i}{1.5}}$, h_i is altitude in kilometers
m	= $\frac{0.979 \times 10^{19}\rho}{T_i}$
$\Delta\nu_1$	= $aP_i \left[0.21 + 0.78B\right] \left(\frac{300}{T_i}\right)^{0.85}$
a	= 1.95 mc = 1.95×10^6 cps
B	= 0.25 for $h_i < H_1$ ($P_i < 267$ mm of Hg) = $0.25 + 0.5\,(h_i - H_1)/H_2 - H_1)$ for $H_1 \leq h_i \leq H_2$ = 0.75 for $h_i > H_2$ ($P_i < 19$ mm of Hg)

$$\Delta\nu_2 = 2.62 \times 10^9 \frac{P_i/760}{(T_i/318)^{0.625}} \left[1 + 0.0046\rho\right] \text{, cps}$$

ρ = density of water vapor, grams/meter^3

The absorption coefficients C_1 and C_2 are found from the water vapor content and rainfall rate from the desired weather model and are converted to db/km by referring to a chart or graph such as is given in Reference 52. The values given in Reference 52 include the effect of scattering of electromagnetic energy by water drops according to the probability distribution of drop sizes.

BLANK PAGE

APPENDIX III

A GENERAL MATHEMATICAL MODEL FOR A COMMUNICATION CHANNEL

Introduction

A systematic procedure for evaluating performance capabilities and limitations of communication links is best initiated by formulating a mathematical model of the channel itself. A general model for a communications channel, represents the physical processes associated with propagation effects on a communication channel in order to provide an understanding of the basic physics involved. The optimum waveforms for determining the characteristics of such a channel model are then presented.

It must be emphasized, however, that an experimental measurements approach based on this model would clearly not be the most effective nor expedient method for two reasons. First, it is not clear that it is feasible to carry out measurements of the properties of the channel to the degree of fineness necessary in such a model. Second the complexity of the descriptive relationship of the processes may not permit exact solution, and mathematical approximation that may have to be made might compromise the validity of results to such an extent where it becomes necessary to carry out an experimental program for their substantiation anyway. It is better therefore to employ a semi-empirical phenomenological model whose parameters can be adjusted on the basis of experimental measurements which describes the propagation effects directly.

Mathematical Model

To obtain the form of this model, consider the most general type of communications channel. It will be comprised of many paths through which the signal can propagate from the transmitter to the receiver as shown in Figure III-1. These paths will have different delay times. One can group together the paths which have nearly the same delay to within some $\Delta\tau$. Thus, the ith path is made up of a set of sub-paths whose delays are all

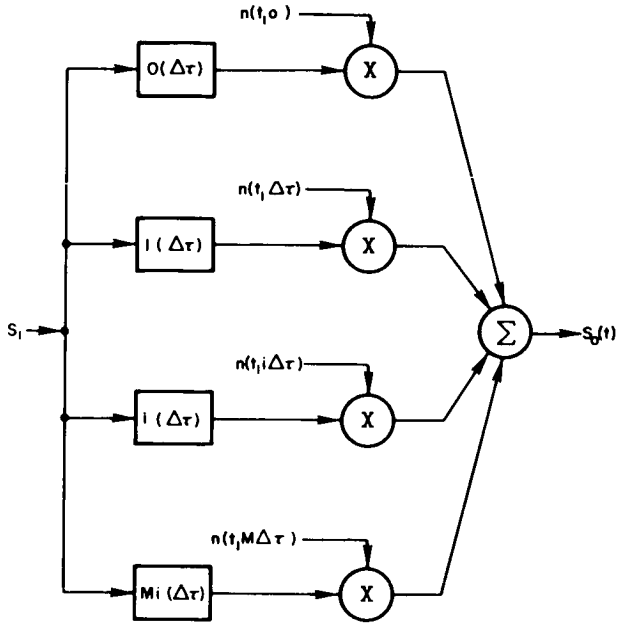

Figure III-1 - Communication Channel Model

within $\Delta\tau$ of each other. The signal propagating through this ith path will thus be composed of the sum of delayed versions of the transmitted signal. In a communications channel, the values of the subdelays vary in a random manner. As a result, the signal received from the ith delayed channel will be composed of the sum of vectors having arbitrary phases which vary randomly and will consequently introduce fading onto the signal from the ith channel. This fading or scintillation is generally Rayleigh distributed. Figure III-1 characterizes such a communication channel in terms of a delay line network. The noise voltage $n_i(t)$ multiplying the signals of the ith channel introduces the fading or, equivalently, the scintillation of the signal. These noise voltages could be independent or dependent. In this model, it is assumed that there are delay paths having delays from 0 to T in steps of $\Delta\tau$. If one of the delay paths did not actually exist, the modulation voltage would be zero.

The model given in Figure III-1 represents the general form of any

time-variable stochastic network (Reference 53). The communications channel, represented by the model given in Figure III-1, is regarded as a time-variable stochastic network. This model characterizes a communications channel having flat fading (which occurs for any narrow band communications channel) and one having frequency selective fading (References 39 and 54). The above model, however, does not take into account the variations of the path with frequency, that is, a system having frequency dispersion. Nor does it take into account the possibility that the scintillation may depend on the signal frequency and also on the delay path. To extend the above model to include frequency dispersion and the possibility of a dependence of the scintillation on frequency, each path of the model shown in Figure III-1 should include a bank of narrow band filters followed by noise modulators and a summer as shown in Figure III-2.

Other characteristics of the communications channel of interest which are not included in the above model are the dependence of the received

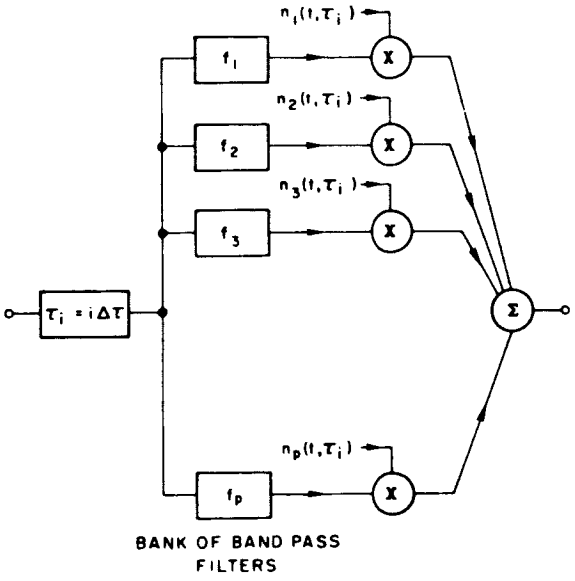

Figure III-2 - Model for ith Delay Path

signal on the antenna's:

1) Spatial location
2) Pointing angle
3) Polarization

As shall be shown later, these factors are the bases of diversity techniques for compensating the degradation due to the presence of multiple channels in the communications path.

On the basis of the above model, it can be established that certain specific data must be derived, based on measurements, to fully characterize the channel with regard to its influence on signal propagation. These will be discussed in the following Section.

Waveform Requirements

From the general discussion above, the optimum signal for determining the characteristics of the communications channel is seen to be one which indicates the number of paths, the delay τ_i of each path and the auto-correlation function or equivalently the power spectral density function of the scintillation introduced into the signal by each path. This problem is similar to the radar problem in which one desires to measure range and doppler velocity simultaneously. Accordingly, as in the radar case, the optimum signal for obtaining the channel characteristics is generally a signal having a noise-like structure (Reference 55). That this is indeed the case as shown by the following simple mathematical proof.

Assume that a signal s(t) is transmitted and that the scintillation introduced by the ith path is $n(t, \tau_i)$. Then the received signal will be given by:

$$S_o(t) = \sum_{i=1}^{m} n(t, \tau_i)\, S_1(t - \tau_i) \qquad \text{(III-1)}$$

The above can be approximated by an integral to give:

$$S_o(t) = \int_o^T n(t, \lambda)\, S_1(t - \lambda)\, d\lambda \qquad \text{(III-2)}$$

Using the above expression, the mean-square-value of the voltage at the output of a filter which receives the transmitted signal can be determined. Specifically, the mean-square output is observed at a time τ at the output of a matched filter which is tuned to a frequency shifted up from the carrier frequency of the transmitted signal by a small ν. That is:

$$\phi_R(\tau, \nu) = \int_{-\infty}^{\infty} \int_{-\infty}^{\infty} \Phi(f,\lambda) \; |X(\tau - \lambda, \nu - f)|^2 \, df \, d\lambda \qquad \text{(III-3)}$$

Where $\Phi(f,\lambda)$ is the power spectral density of the scintillation introduced onto the signal by the ith delayed path. That is:

$$\Phi(f,\lambda) = \int_{-\infty}^{\infty} \phi(t', \lambda) \exp(-j 2\pi f t') \, dt' \qquad \text{(III-4)}$$

$X(\tau, \nu)$ is the ambiguity functions for the transmitted signal. That is:

$$X(\tau, \nu) = \int_{-\infty}^{\infty} S_1(t) \, S_1^*(t - \nu) \exp(j 2\pi \nu t) \, dt \qquad \text{(III-5)}$$

For the case where the signal is noise-like in structure, the ambiguity function for the transmitted signal is approximately a two-dimensional delta function. That is:

$$X(\tau, \nu) = \delta(\tau) \; \delta(\nu) \qquad \text{(III-6)}$$

substituting Equation (III-4) into (III-3) yields:

$$\phi_R(\tau, \nu) = \Phi(\tau, \nu) \qquad \text{(III-7)}$$

Hence, the mean-square output observed at time τ at the output of a matched filter tuned to a frequency doppler shifted by ν away from that of the transmitted signal, gives the power spectral density for the delayed path having a delay of τ at the frequency ν. Moreover, a bank of such filters tuned to all possible frequencies of interest would give the power spectral density of the scintillation for all delay paths. The relationship for estimating the power spectral density of the scintillation for each path where the ambiguity function cannot be assumed to be a two-dimensional delta function is given by:

$$\Phi(f, \lambda) = \int_{-\infty}^{\infty} \int_{-\infty}^{\infty} \frac{\Phi_R(n, \lambda)}{|X(\lambda, n)|^2} \exp(j 2\pi n \tau + j 2\pi \lambda f)\, dn\, d\lambda \qquad \text{(III-8)}$$

where:

$$\Phi_R(n, \lambda) = \int_{-\infty}^{\infty} \int_{-\infty}^{\infty} \phi_R(\tau, \nu) \exp(-j 2\pi n \tau - j 2\pi \nu \lambda)\, d\tau\, d\nu \qquad \text{(III-9)}$$

Signals having a simple rectangular structure are suggested. Such signals have certain capabilities and limitations in measuring channel characteristics.

First, consider the transmission of a single narrow pulse which has a width less than $\Delta\tau$. This signal will enable one to determine the number of multipaths and delays of each multipath. However, it will not permit the determination of the spectrum of the scintillation introduced by each path. To obtain the power spectral density of the scintillation introduced by each path, a train of such pulses having equal spacings between them could be used if certain conditions are met. In particular, these conditions are: the spacing between pulses must be greater than the difference in the delay between the shortest delay path and the longest delay path and, at the same time, the bandwidth of the scintillation must be less than one over the spacing between samples. The first requirement permits unambiguous resolution of the different delay paths. The second requirement allows the unambiguous measurement of the scintillation spectrum since the sampling rate is higher than the bandwidth of the scintillation. If these conditions cannot be met, that is, if the reciprocal of the bandwidth of the scintillation is greater than the maximum difference in delay then the ambiguities will not be resolved in the determination of the scintillation spectrum of unambiguous path resolution is to be obtained. Assuming conditions are met and the above signals are used, the pulses would be processed coherently in the receiver.

BLANK PAGE

APPENDIX IV

DATA REDUCTION AND ANALYSIS

The actual processing of data can be performed by off-the-shelf equipment. The important consideration is that in the planning study, this data processing equipment must be specified in detail so that its procurement or lease becomes an integral part of the experiment design package.

Labor for data processing and analysis will be specified in the planning study results.

Data to be used in the final description of the propagating medium will come from three principal sources. They are:

a) Satellite position data from a satellite tracking facility.
b) Amplitude and phase data either telemetered from spacecraft receivers or extracted from ground receivers.
c) Meteorological and radiometric data from correlative sensors.

Proper emphasis must be placed upon correlative sensors and correlative data processing. It does little good to determine atmospheric absorption, atmospheric noise, selective frequency fading and channel capacity unless we accurately classify the meteorological conditions existing during each measurement period and determine the probability of recurrence of each class of conditions during the annual cycle. Good correlative data will allow prediction of propagation effects for many future ground terminal locations from data taken with a few ground terminals.

Three phases of data processing will be considered for the experiments. They are:

a) Real-time on-site data processing which will be useful for operational monitoring and last minute changes in test schedule during the satellite pass or measurement interval.

b) Non-real time on-site data processing which is necessary for short range test schedule planning for the subsequent satellite passes or measurement intervals.

c) Non-real time off-site data processing performed by existing contractor and/or government computer facilities required to develop the final data in statistical form and infer from these statistics the performance of various modulation systems.

An extensive quantity of data will result from the experimental program and considerable thought must be given early to the problem of processing the data into final system design and evaluation format. Based on a preliminary analysis of the problem the following points could be made regarding the computations to be performed and the form in which the data will be presented.

The attenuation of the channel as a function of time of day, month of the year, year, weather conditions, elevation angle, and location will be presented. Figure IV-1 shows a typical plot of the long-term variation of

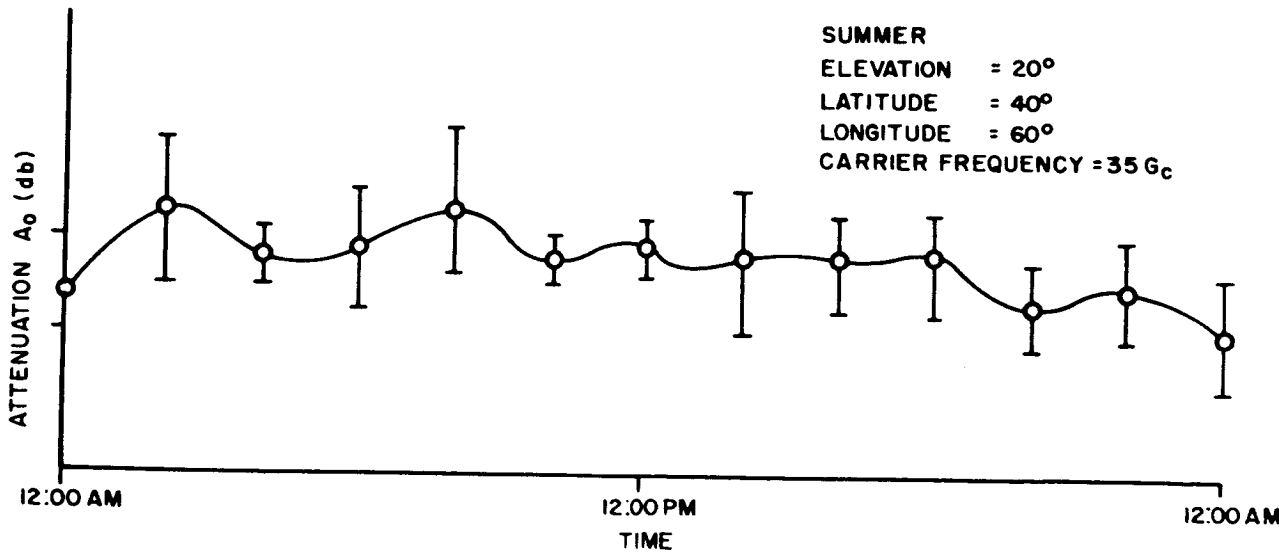

Figure IV-1 - Atmospheric Attenuation as a Function of Time of Day

attenuation for a 24-hour period. The plot is given for a particular elevation angle, θ, a particular day, a particular frequency and a particular location. The circled points represent 15 minute medians of the attenuation or equivalently of the received carrier amplitude, A_o, (intervals other than 15-minutes, such as hourly, might be chosen). The bars indicate the rms deviation of A_o for the 15 minutes of samples. Such a curve will be presented for each carrier frequency used, for about 5 elevation angles, for 2 times of day (noon and night), for typical days chosen for winter, autumn, spring and summer, and for several locations. Similar curves will be given showing the variations over a month and over a year period. Finally, several curves will be given to show the dependence of A_o as a function of frequency and elevation angle. Results will be given for clear weather and inclement weather.

In order to make such time plots useful for prediction of system performance, the data will be transformed into statistical form, giving the probability that the attenuation will be less than a specified amount for various percentages of the time for various geographical locations, times of day and elevation angles. This involves first computing the probability density function of the measured quantity from the time plots. This yields curves typified by that given in Figure IV-2. From these curves then may be plotted probability distribution function as illustrated in Figure IV-3.

To illustrate the process of raw data extraction from the signal waveform, the use of a carrier and pair of sidebands is assumed. The difference in the amplitude of the sidebands from the carrier signal will be presented in a manner similar to that given for the carrier amplitude, A_o. The difference between the amplitude of the carrier signal and the upper sideband Δf_1 is designated as ΔA_1 while the difference between the carrier amplitude and the lower sideband Δf_2 is represented by ΔA_2. Figure IV-4 shows a typical form of a plot of ΔA_1 versus elevation angle. These plots are also to be converted to probability distribution function format.

A similar process will be applied to the sampling autocorrelation coefficient between the amplitudes of the carrier frequency and the

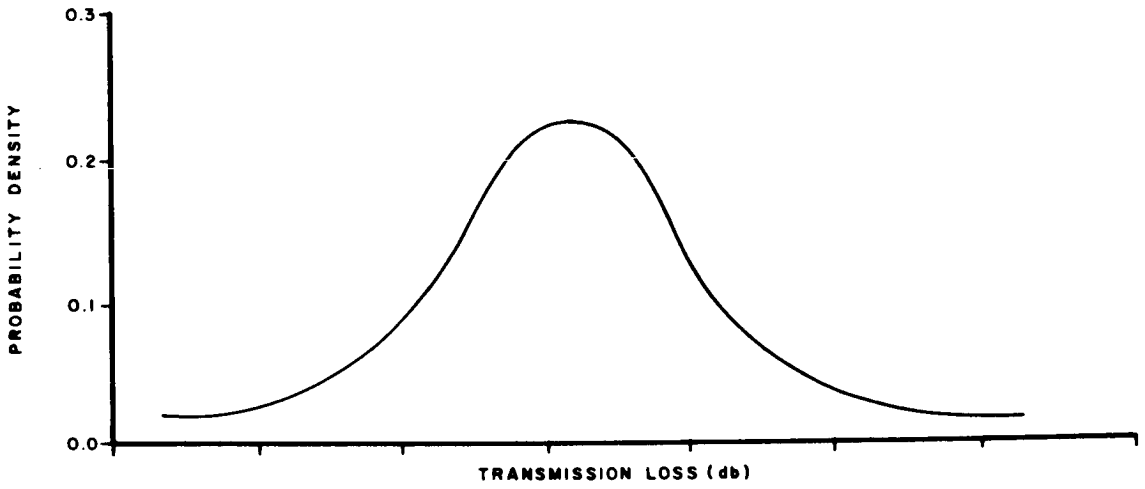

Figure IV-2 - Typical Probability Density Function of Fifteen Minute Median Transmission Loss

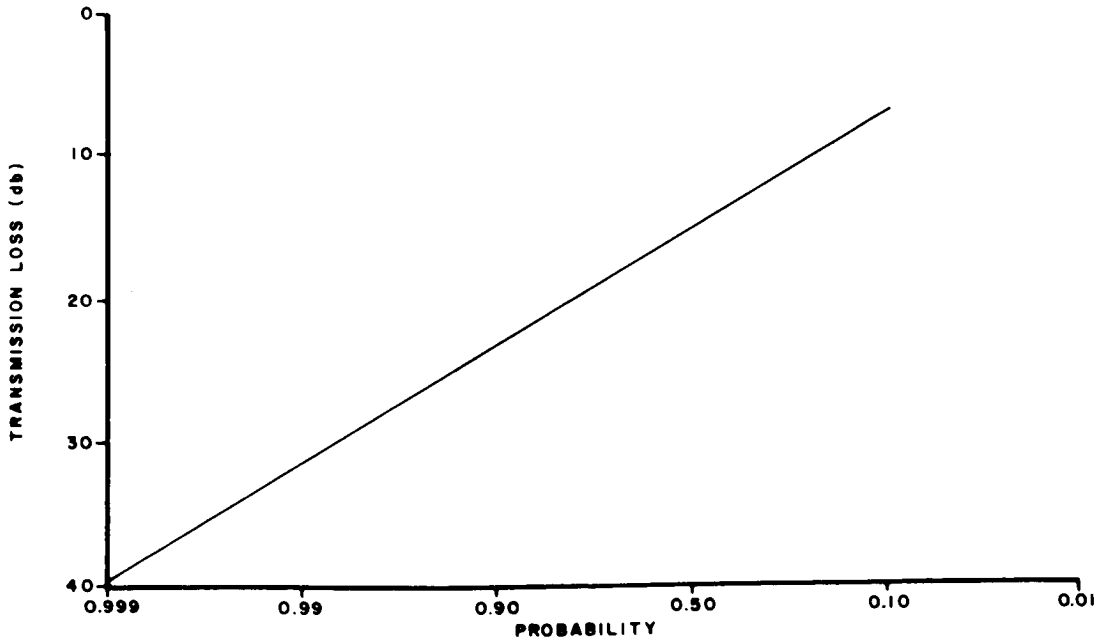

Figure IV-3 - Probability That Fifteen Minute Transmission Loss will not Exceed Ordinate Value

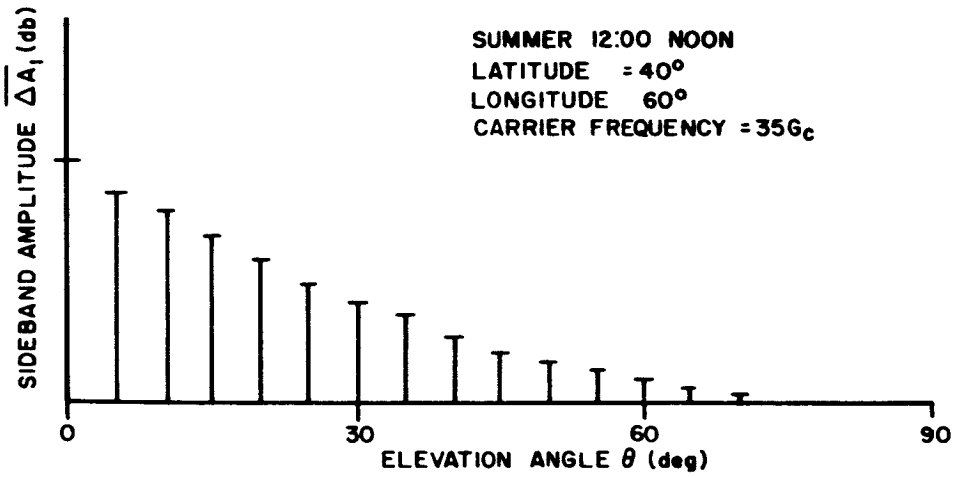

Figure IV-4 - Typical Sideband Amplitude Variation with Elevation Angle

sidebands. The sampling autocorrelation coefficient between the amplitude of the carrier and that of the sideband Δf_1 away is given by

$$\gamma_{o1} = \frac{\overline{(A_{oi} - \bar{A}_{oi})(A_{1i} - \bar{A}_{1i})}}{\bar{A}_{oi}\,\bar{A}_{1i}} \qquad \text{(IV-1)}$$

where A_{oi} and A_{1i} are the amplitude of the received voltage measured at time t_i for the carrier and the upper sideband. The expression for the lower sideband is similar to Equation (IV-1). Both short and long time averages will be used in computing the sample autocorrelation coefficient.

The bar indicates ensemble averages.

Curves similar to those that would be presented for the attenuation will be given for the time to achieve signal independence. The procedure outlined by Blackman and Tukey (Reference 56) will be used to compute the sample spectrum of the fading and presented in the form of curves similar to those given by Thompson et al (Reference 57). Also, curves like those derived for the attenuation will also be obtained for the phase shift of the sidebands. The configurations are capable of providing the data for this derivation in that it gives the difference between the phase shift introduced onto the upper sideband and that introduced onto the lower sideband. Introducing a frequency discriminator provides a unique means for directly obtaining a measure of the sum of those phase shifts relative to the carrier. This can be seen from the following consideration.

For an amplitude modulated waveform, which is the waveform being proposed, phase distortion will show itself as the introduction of frequency modulation onto the signal. The transmitted signal can be represented as

$$s(t) = A_o \cos 2\pi f_o t + A_1 \cos (2\pi \Delta f_1 t) \cos 2\pi f_o t \qquad \text{(IV-2)}$$

Assume a phase shift θ_{-1} for the lower sideband and a phase shift θ_{+1} for the upper sideband both measured relative to the carrier frequency phase shift. Then these phase distortions which show themselves as an FM modulation having a frequency deviation of approximately

$$\frac{A_1 (\theta_{-1} + \theta_{+1}) \Delta f}{A_o} \qquad \text{(IV-3)}$$

The signal-to-noise ratio for the FM component is approximately given by

$$X_{FM} = \frac{A_1(\theta_{-1} + \theta_{+1})}{A_o} \quad X_o \qquad \text{(IV-4)}$$

where X_o is the signal-to-noise ratio for the carrier of the signal. Hence, if $X_o = 35$ and $\theta_{-1} + \theta_{+1} = 10$ degrees and $A_1/A_0 = 1/2$, then $X_{FM} = 3$.

All measured variations in the delay time and attenuation of the communications channel will be correlated to the variations in the index of refraction simultaneously obtained from measurements with a refractometer at the ground station. In addition the attenuation that is measured will be related to the observed meteorological conditions by the use of the Van Vleck-Weisskopf Equation (Reference 58).

The next step in the data processing consists of combining the desired probability distribution functions of the measured attenuation and additive noise to compute, for each type of system considered, the corresponding output signal-to-noise probability distribution function. Typically, the output of this step has a form as depicted in Figure IV-5. This format gives the percentage of time a specified signal-to-noise level will be exceeded.

At this point similar distributions may also be derived for the dispersive multipath time delay effects and fading bandwidths of random frequency variations (that is, A and r respectively as previously described). In turn, these three probability distributions, in conjunction with system characterization curves for binary PM and FM systems, can then yield the probability distribution function for the error rate performance of the system. This error-rate distribution function represents the final format of the system evaluation data for this propagation channel and typically might have the form shown in Figure IV-6. Thus the performance capacity and reliability of the system over the channel is completely specified in this format.

Although two particular primary systems (a PM and FM system) has been used here to illustrate methodology, a similar procedure can be developed and carried out for all systems of interest, both digital and analog. During the design phases of the experimentation planning program,

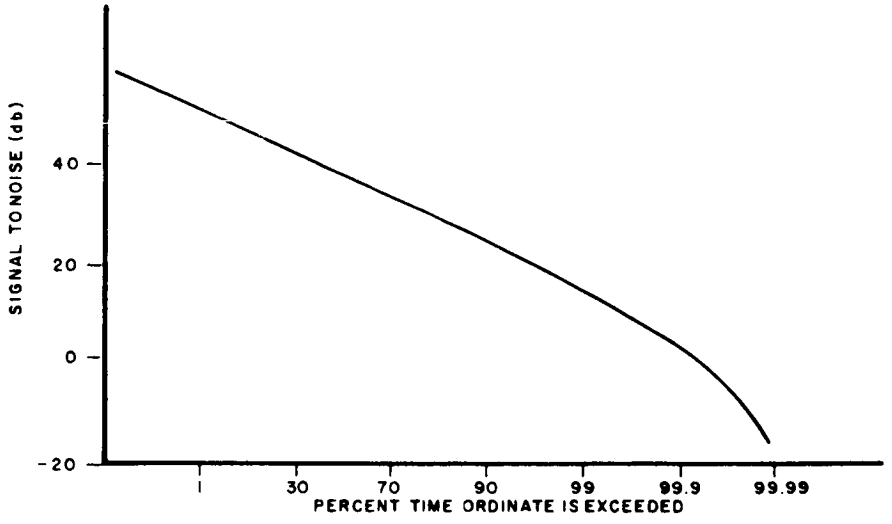

Figure IV-5 - Typical Probability Distribution Function of Signal-to-Noise Ratio

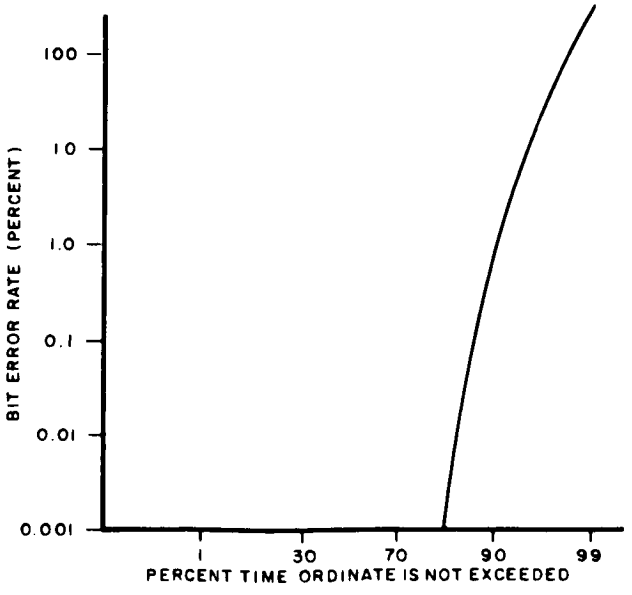

Figure IV-6 - Typical Performance Curve for Binary PM or FM Systems

detailed consideration will be given to the associated tasks of processing, reduction, and transformation of the expected data. Potential interaction problems so identified, between the actual experiments themselves and the handling of the ensuing data, will permit, as necessary, early reformulation of experimentation designs. This would insure that the experimentation program is both efficacious in terms of providing data on the important channel characteristics and optimum from a cost-effectiveness standpoint.

BLANK PAGE

APPENDIX V

AMPLITUDE FADING IN SPACE-EARTH COMMUNICATION CHANNELS

Amplitude Fading

Amplitude fading arises from a number of factors. These are:

1. Variations in the water vapor content in the atmosphere.
2. Atmospheric turbulence.
3. Direct and reflected wave interference.

Variations in the water vapor give rise to slow variations in signal amplitude. The variations are diurnal in nature, although more rapid fluctuation can occur due to the passing of clouds across the communications path and the occurrence of rain, snow or hail.

Atmospheric turbulence gives rise to multipathing in the communications channel. This results from the stochastic-temporal variations of the index of refraction in the atmosphere in the presence of turbulence. Experimental data indicate that the decorrelation distance for the index of refraction is of the order of 100 to 200 feet (Reference 57). Furthermore, the frequency components of the spectrum of these fluctuations are usually 10 cps or less (Reference 59). Hence, the frequency of the fading should be 10 cps or less. Moreover, the Telstar data (Reference 60). which used a 6 mc carrier, indicated a frequency rate for the fading of 1/2 cps for an elevation angle of 4 degrees or less.

The fluctuation due to the interference of the direct and reflected wave will occur at low elevation angles and is identical to the interference experienced in ground wave propagation (Reference 61). Moreover, the

fluctuation due to turbulence also occurs at low elevation. The experiment to be performed will determine how deep the fluctuations are and the fluctuation rate as a function of elevation angle, geographical location and weather conditions.

An analysis of the degree of fading due to inhomogeneities in the troposphere has been carried out by Bergmann (Reference 34). He considered the problem solely as one in geometrical optics, neglecting the diffraction effects and assuming that the variation of the index of refraction is isotropic in space. His analysis indicates that the rms intensity fluctuation in db on a one-way path is given by:

$$E_{rms} = 0.0785\, R^{3/2} \sqrt{r_o\, (\nabla^2 n)^2} \qquad \text{(V-1)}$$

where R is the range, r_o is the patch size of the inhomogeneities, ∇^2 is the Laplacian of the refracted index, and the averaging is to be taken over all space.

For propagation vertically through the troposhere, the width of the region in which the inhomogeneities lie is about 10,000 yards. The size of the inhomogeneities is about 40 yards and the peak deviation in the index of refraction is about 10^{-5} (Reference 34). Using these values, one finds that the rms intensity fluctuation (that is, the fading) is only about 0.05 db. For low elevation angles, however, the length of the path over which the inhomogeneities may lie might be of the order of 60,000 yards for the earth-satellite channel. For this value of R, one finds from Equation (V-1) that the intensity of the scintillation is about 0.8 db. Hence, as one might expect, there will be greater scintillation at low elevation angles which will diminish rapidly toward the zenith.

(Measurements recently made at Aerospace at 94 Gc indicate rms fluctuation having considerably larger values than that indicated here. Values of 10 db depth of fading were obtained for a 20,000 yard path.)

BLANK PAGE

APPENDIX VI

THE CONCEPT OF TEMPERATURE AND THE PRINCIPLES OF OPERATION OF THE RADIOMETER

The Concept of Temperature

In order to properly appreciate the sensitivity of the radiometer, it must be expressed in terms of absolute temperature, rather than the more familiar field strength and power terminology.

The power available from a matched resistor is given by the Johnson noise power expression;

$$P = KT\ \Delta F \tag{VI-1}$$

where, K = Boltzmann's constant; T = the thermometric temperature; and F = the frequency interval over which the measurement is being performed.

The power available from the effective radiation resistance of the antenna, submerged in a thermal bath, has the same form as the Johnson noise power. This is expressed by:

$$P = \frac{AE}{2}\ \Delta F \iint B_o F_N(\theta, \phi)\, d\Omega \tag{VI-2}$$

where A_E = the effective aperture area; F = the frequency interval of observation; $B_o = \frac{2KT}{2}$ = the Rayleigh - Jeans approximation of Planck's radiation law; F_N = the noise figure; (θ, ϕ) = antenna beam parameters; and $d\Omega$ = source parameters. Thus,

$$P = A_E\ \frac{KT\ \Delta Fb}{2} \tag{VI-3}$$

where b = beam area = $\frac{\lambda^2}{A_E}$.

The wavelength dependence of the black body radiation as given in the Rayleigh-Jeans approximation is cancelled out by the wavelength dependence of the aperture cross-section: Thus, a constant output power, independent of frequency, is obtained by an antenna surrounded by a black body.

For radiating sources, smaller than the squared beam angle, the antenna temperature is reduced by the linear ratio of the solid angles.

The concept of temperature is graphically illustrated in Figure VI-1. If, ω = the angular subtention of the source; b = the solid angle subtended by the beam; then $T_A = T_S \frac{\omega}{b}$; where, T_A = the antenna temperature; and T_S = the temperature of the radiating source.

The load comparison radiometer was first used by R. H. Dicke. This receiving system minimizes Gaussian gain fluctuations by modulating the input signal as previously mentioned. The Gaussian receiver noise is minimized by means of postdetection integration (i. e., smoothing).

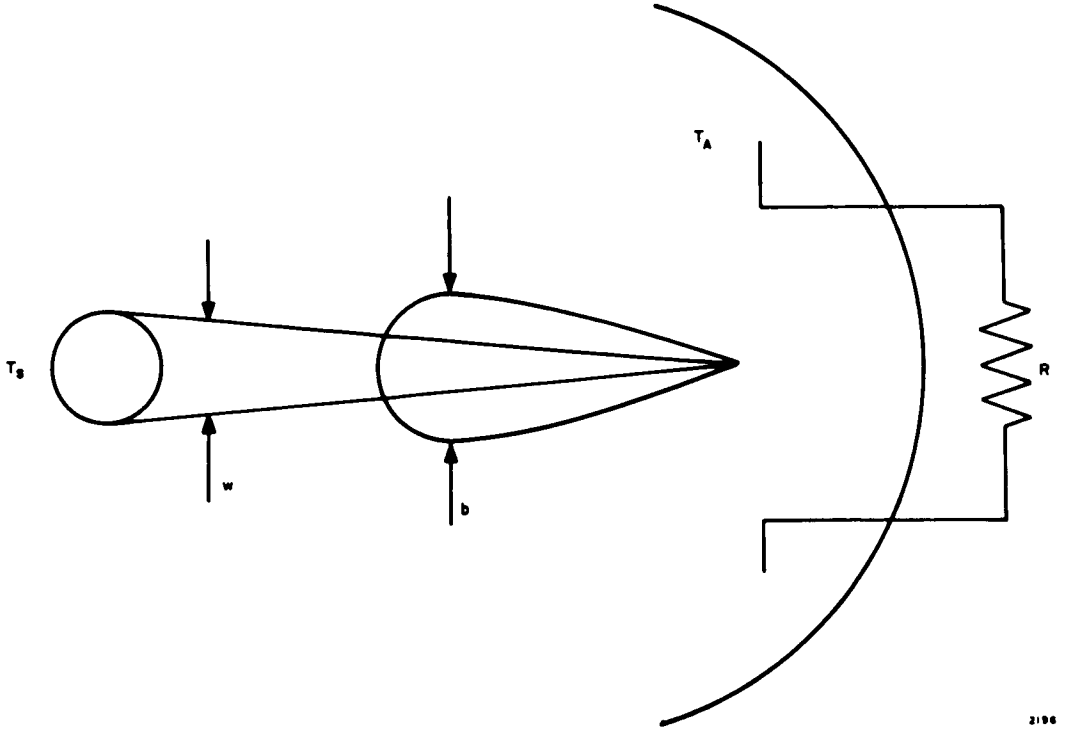

Figure VI-1 - Concept of Antenna Temperatures

For a superheterodyne, load comparison radiometer, the rms sensitivity (ΔT) ^{o}K is given by

$$\Delta T_{rms} = k \left[\frac{(F-1)\, T_o + T_A}{\sqrt{\beta \tau}} \right] \qquad \text{(VI-4)}$$

where, k = a constant dependent on the type of modulation and postdetection filter employed (rarely exceeding a value of 2); $(F-1)\, T_o$ = the receiver noise temperature (^{o}K), (F = receiver noise figure ratio, T_o = the receiver ambient temperature); T_A = the antenna temperature, including line losses, sidelobe contribution etc.; β = the predetection bandwidth; and τ = the postdetection integration interval.

Principles of Operation

A radiometer in it's simplest form is shown in Figure VI-2. It may be considered as consisting of the following functional elements:

1) The Antenna, which acts as the coupling device (and collector), of the electromagnetic energy.

2) The Modulator, which provides the stabilizing modulation of the signal. The modulator "tags" the signal by switching the receiver input alternately between the antenna and a matched termination (that is, reference load). In it's earliest form, the modulator consisted of a length of waveguide, into which was cut a narrow slot, parallel to the direction of wave propagation. A resistive vane was rotated in and out of this slot at some low audio rate, driven by an electric motor. Most modern day modulators are either Faraday rotators (Ferrite switches), or semiconductor diode switches. The choice of modulator involves trade-offs between; size and weight, switching speed and drive power, bandwidth, insertion loss and isolation between the inputs and the output.

3) The amplifier/detector provides the proper amplification and square-law detection at the input signal spectrum as modified by the modulator. The amplifier/detector separates the desired spectrum from

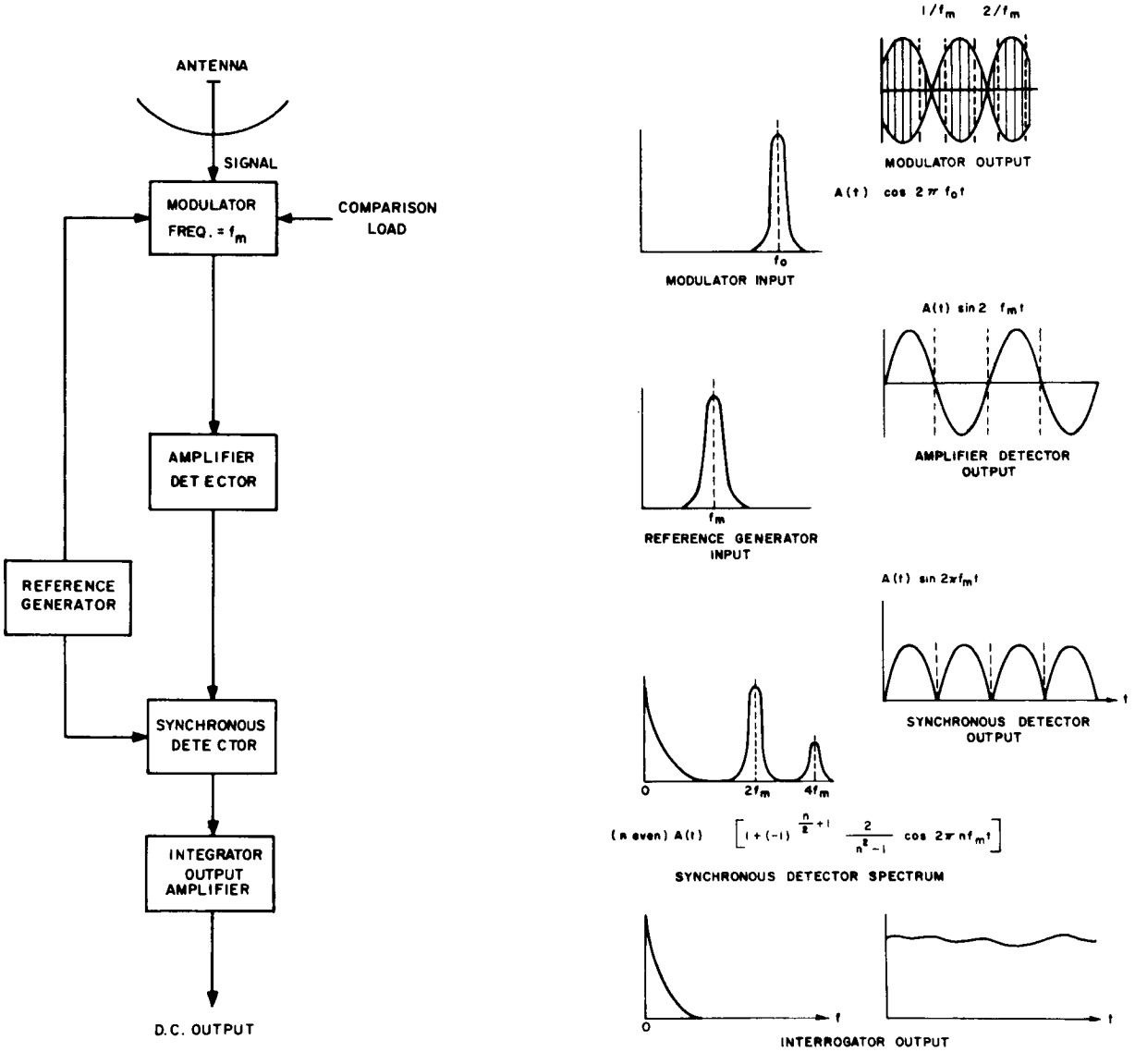

Figure VI-2 - Basic Principles of Radiometric Receivers

unwanted and interfering signals, and presents the desired information in a narrow frequency band, centered at the modulation frequency.

4) The synchronous detector selectively gates the amplifier/detector output signal to provide a DC component which is directly proportional to the magnitude and phase of the modulation applied to the input signal relative to the gating (reference) signal. In this manner, the synchronous detector responds only to the coherent modulation signal, and rejects other, unwanted signals.

5) The integrator/output amplifier reduces the noise fluctuations in the DC output of the synchronous detector, and provides the DC drive required for the recorder.

BLANK PAGE

APPENDIX VII

GENERAL SATELLITE ORBITAL CHARACTERISTICS

Symbols (See Figure VII-1)

r = Earth's radius = 3440 nautical inches
h = satellite altitude - nautical miles
T = orbital period - minutes
γ = elevation angle - degrees
θ = coverage on earth's surface - degrees
α = vision angle - degrees
R_S = slant range - nautical miles
V = satellite velocity - miles/second
V_d = doppler velocity - miles/second.

Formulas

$$T = \frac{(r + h)^{3/2}}{2390} \quad \text{minutes}$$

$$V = \frac{250}{(r + h)^{1/2}} \quad \text{nautical miles per second}$$

$$\text{Maximum } R_S = h^{1/2}(2r + h)^{1/2} \text{ nautical miles}$$

$$\theta = \cos^{-1}\left[\frac{r}{r + h}\cos\gamma\right] - \gamma \text{ degrees}$$

$$\alpha = 2\sin^{-1}\left[\frac{r}{r + h}\right] \text{ degrees}$$

$$\text{Maximum } V_d = V \sin \frac{\alpha}{2} = \frac{250\ r}{(r+h)^{3/2}} \text{ nautical miles per second}$$

Graphs

Figure VII-1	Orbital Characteristics of a Satellite
Figure VII-2	Periods of Circular Orbits
Figure VII-3	Velocity of Circular Orbits
Figure VII-4	Maximum Slant Range vs Satellite Altitude
Figure VII-5	Coverage of Earth's Surface by a Satellite
Figure VII-6	Vision Angle of a Satellite

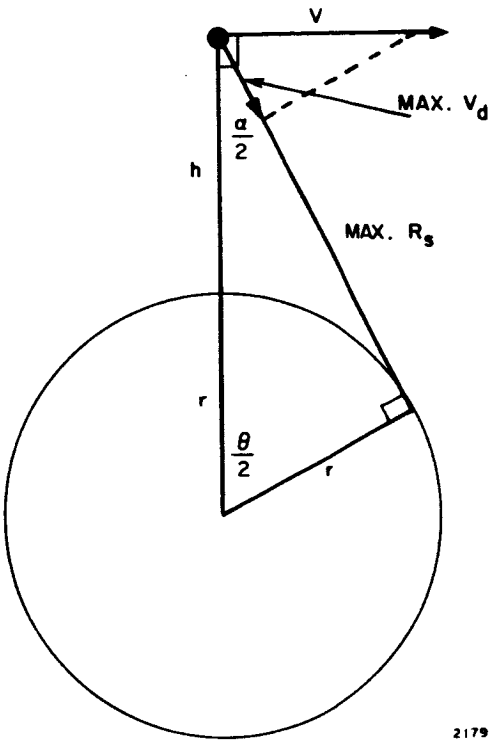

Figure VII-1 - Orbital Characteristics of a Satellite

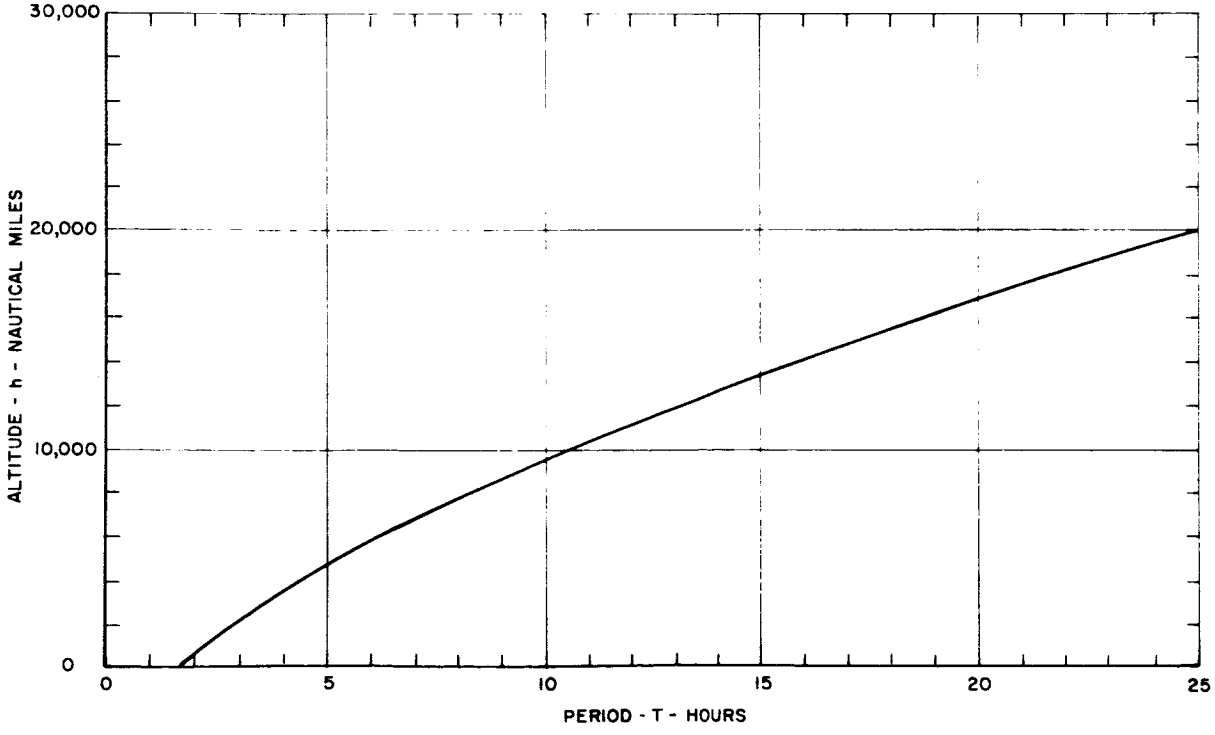

Figure VII-2 - Period of Circular Orbits

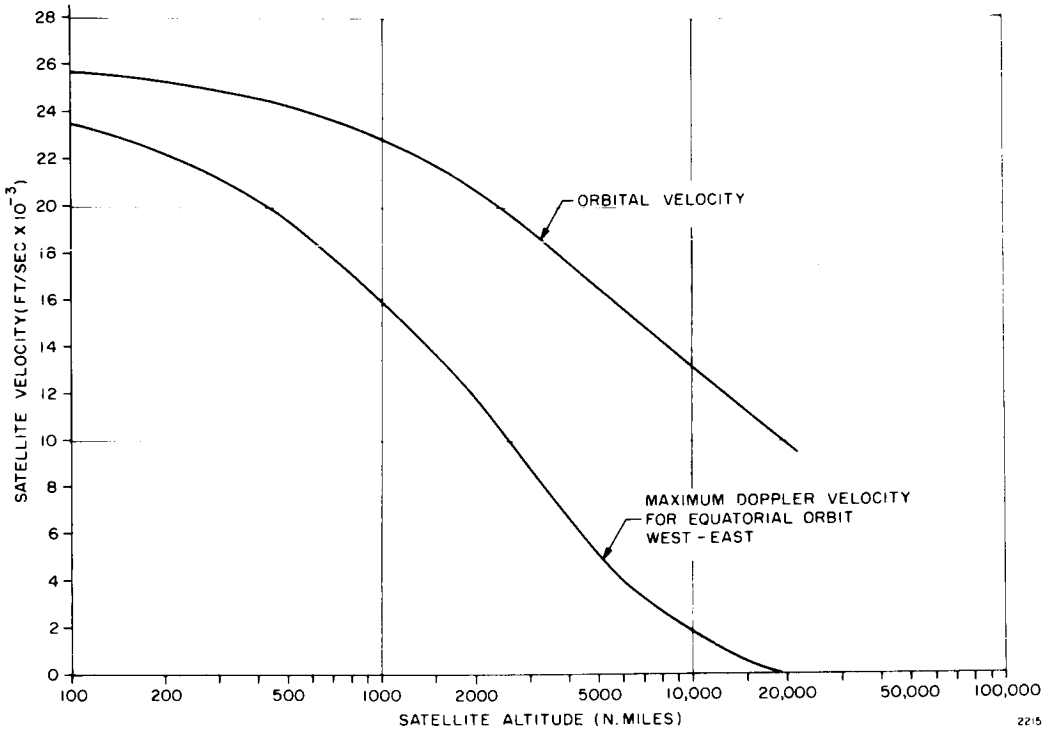

Figure VII-3 - Velocity of Circular Orbits

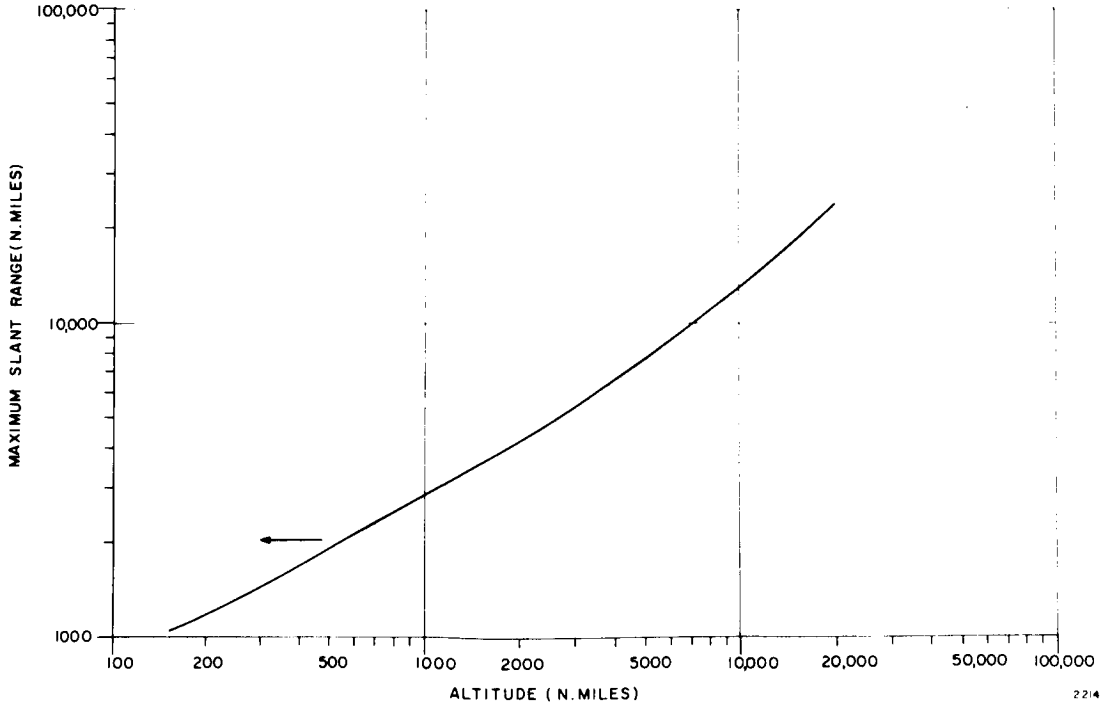

Figure VII-4 - Maximum Slant Range vs Altitude for Circular Orbits

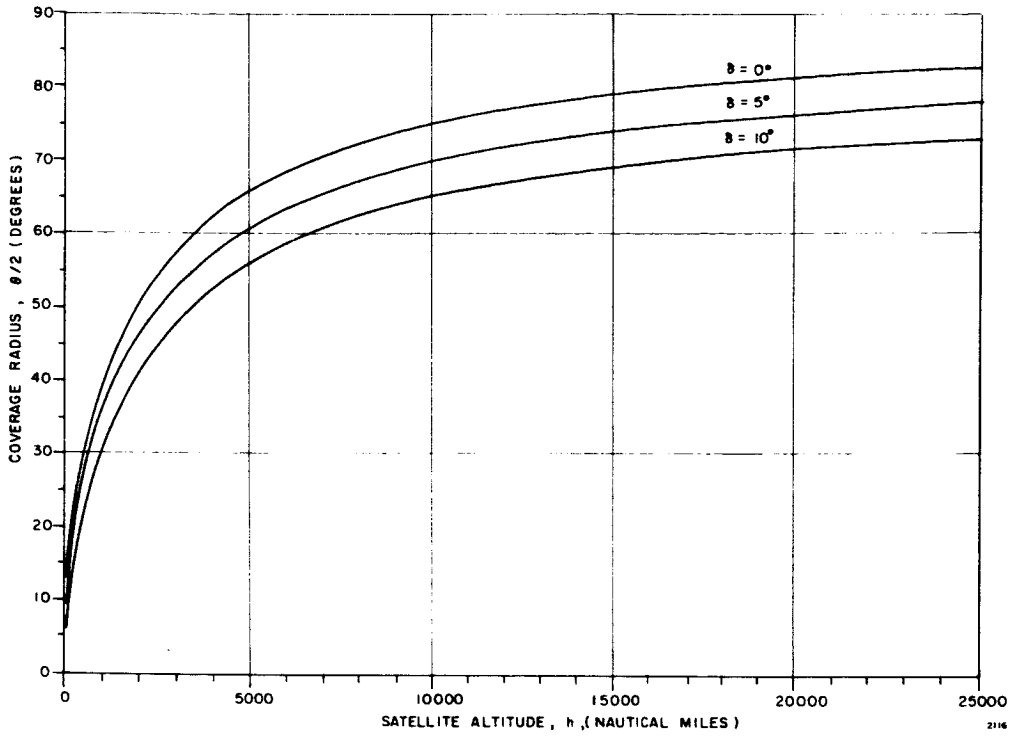

Figure VII-5 - Coverage of Earth's Surface by a Satellite

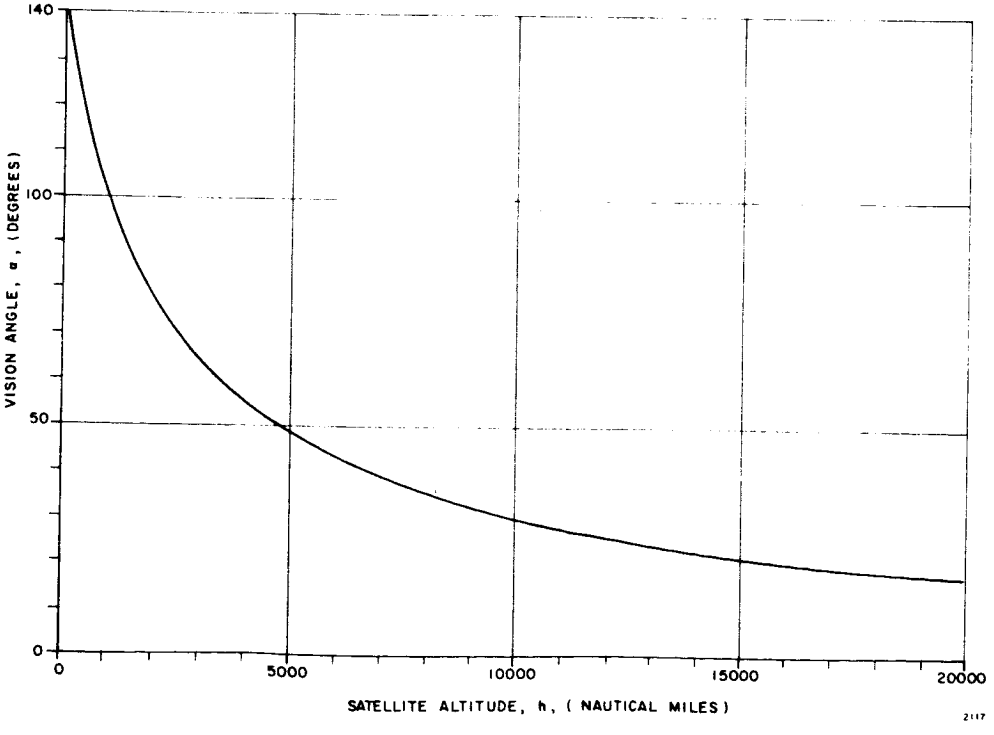

Figure VII-6 - Vision Angle of a Satellite

BLANK PAGE

APPENDIX VIII

SPECIFIC ORBITAL CHARACTERISTICS FOR MEDIUM ALTITUDE AND SYNCHRONOUS ALTITUDE SATELLITES

Figure No.

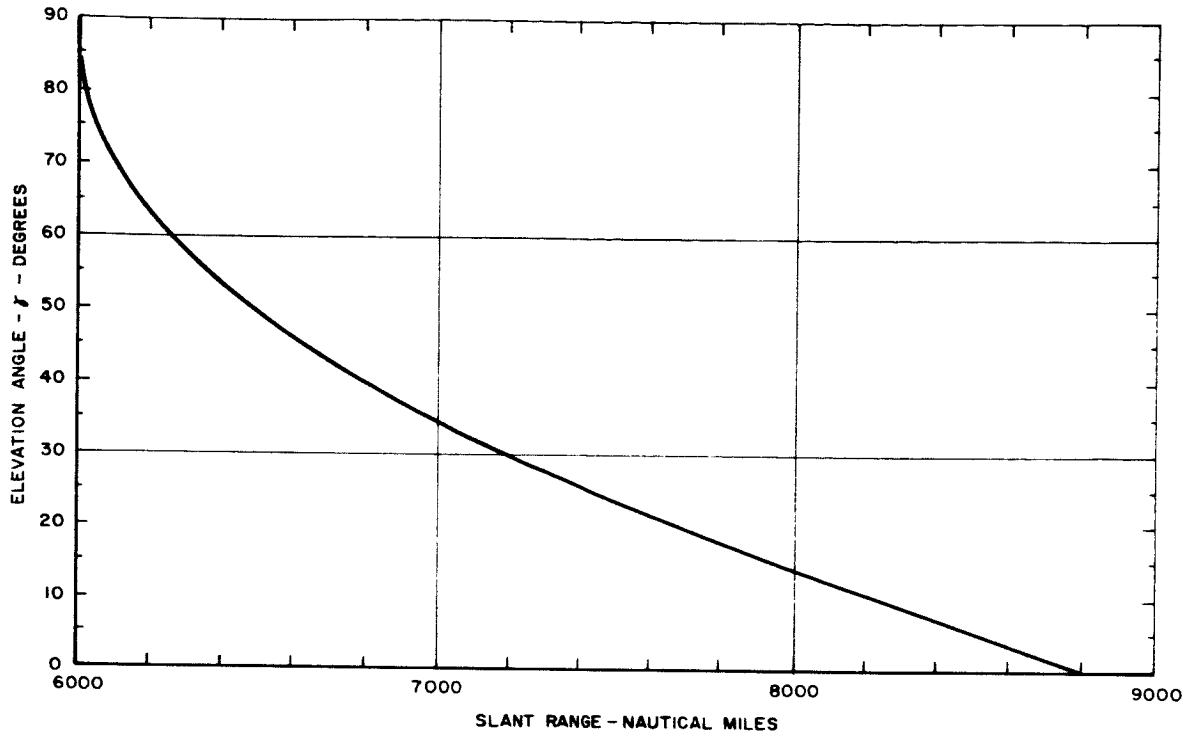

Figure No. VIII-1 Slant Range vs Elevation Angle for a 6000 nmi Satellite

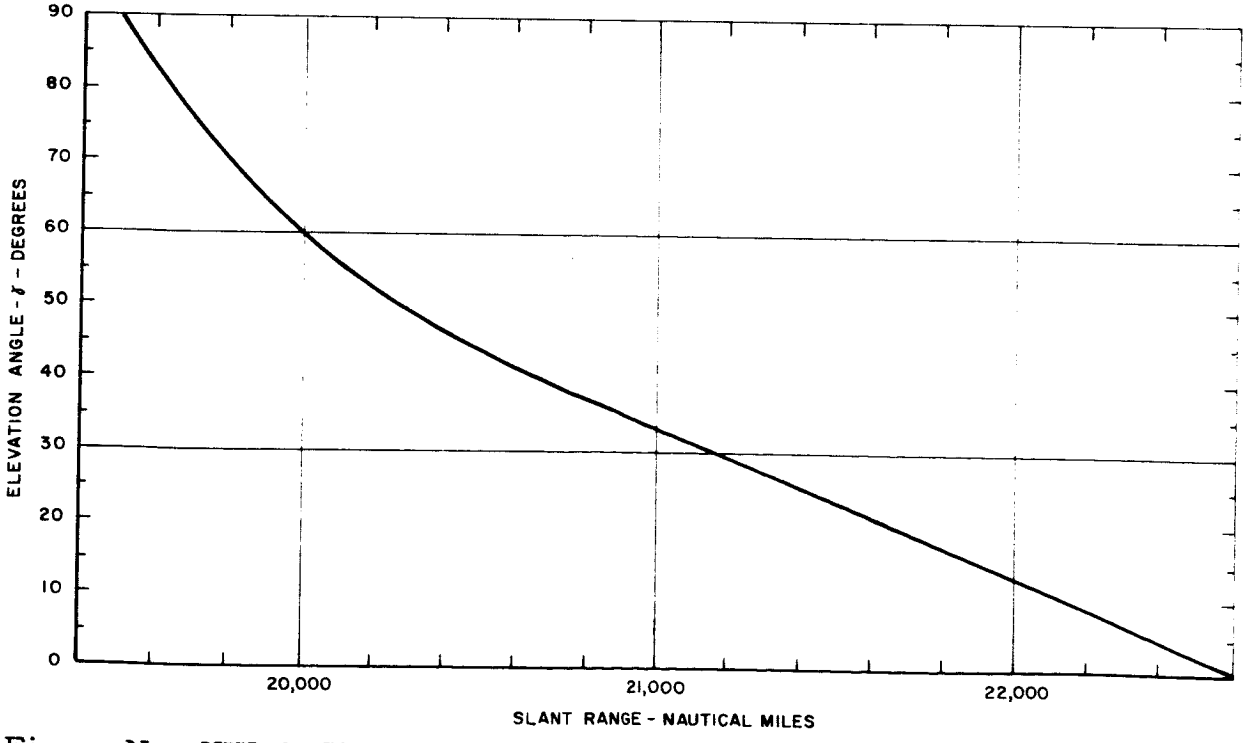

Figure No. VIII-2 Slant Range vs Elevation Angle for a Synchronous Satellite

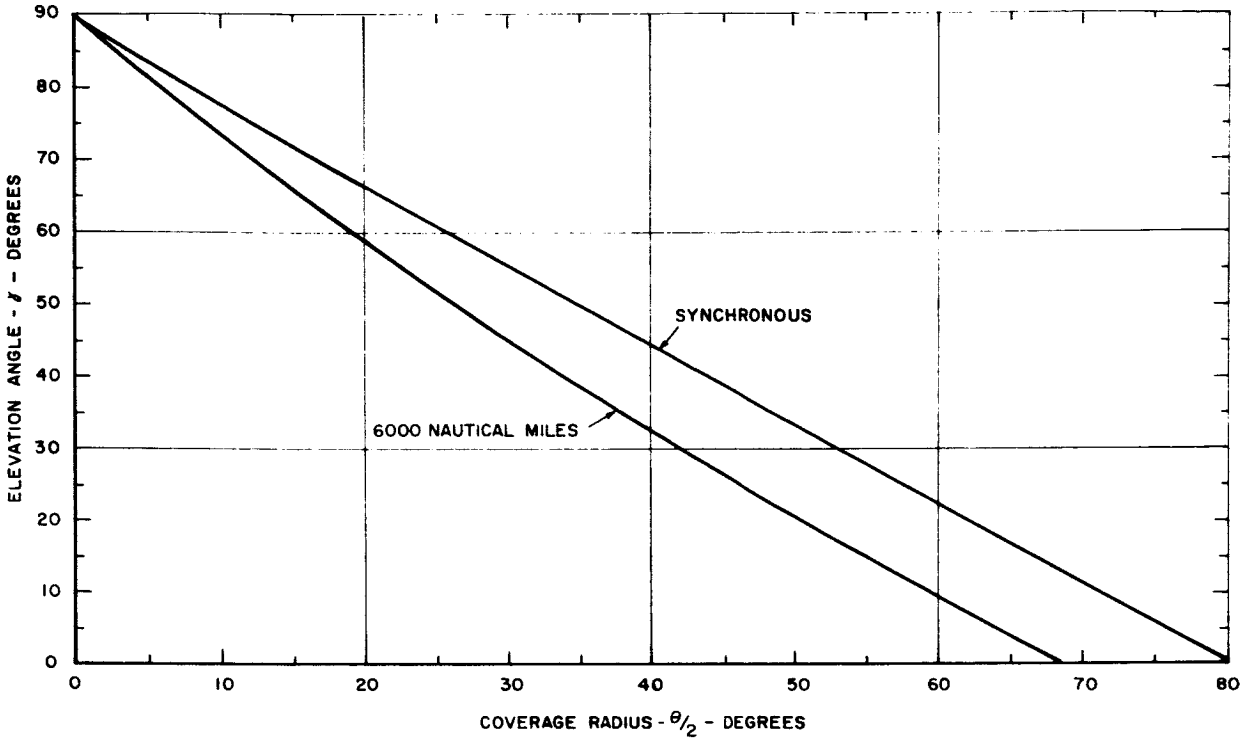

Figure No. VIII-3 Coverage vs Elevation Angle for 6000 nmi and Synchronous Altitude Satellites

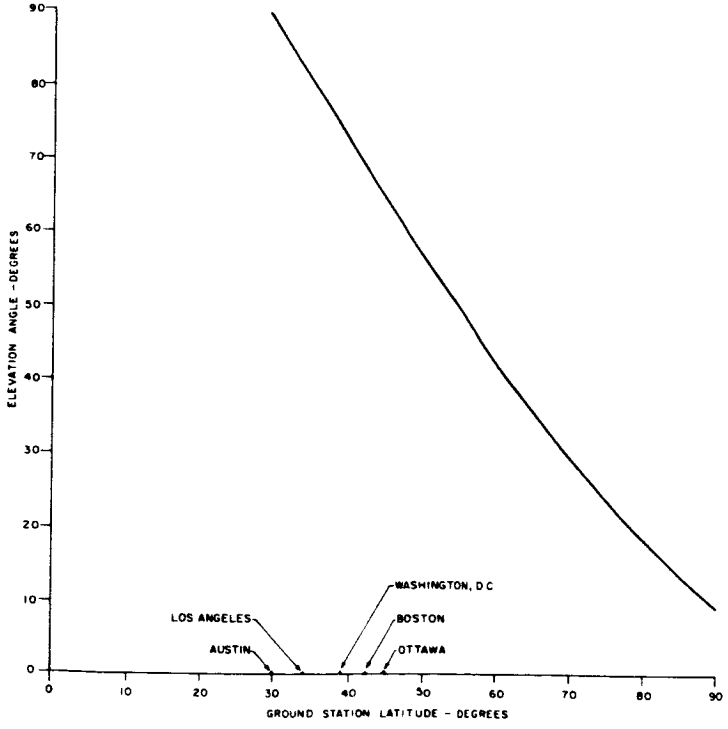

Figure No. VIII-4 Maximum Elevation Angle vs Ground Terminal Latitude for a 6000 nmi Satellite Inclined at 28.5 Degrees

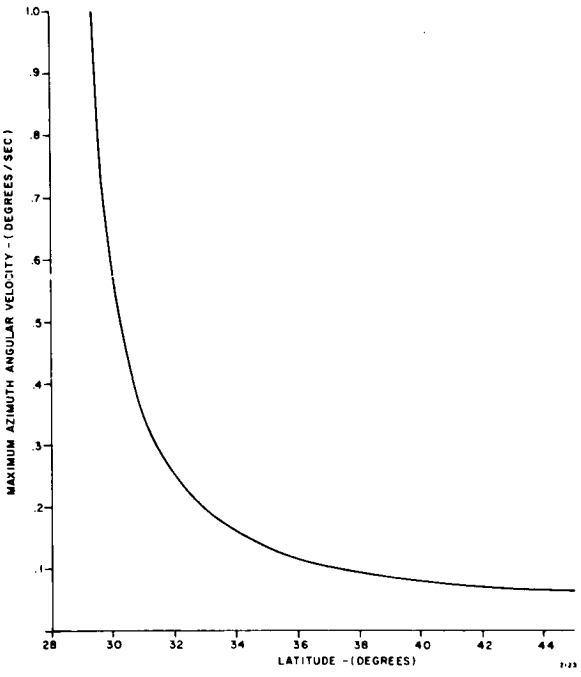

Figure No. VIII-5 Maximum Azimuth Angular Velocity vs Ground Terminal Latitude for a 6000 nmi Satellite Inclined 28.5 Degrees

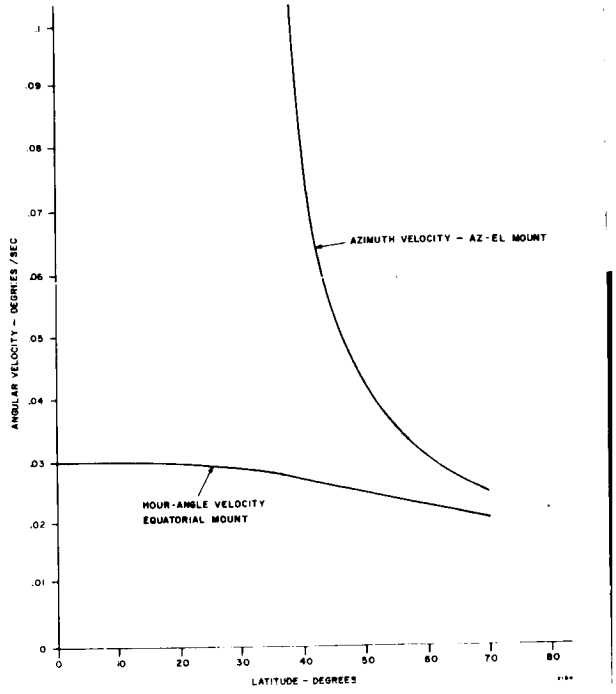

Figure No. VIII-6 Maximum Angular Velocity vs Ground Terminal Latitude (40° - 70°) for a 6000 nmi Satellite Inclined at 28.5 Degrees

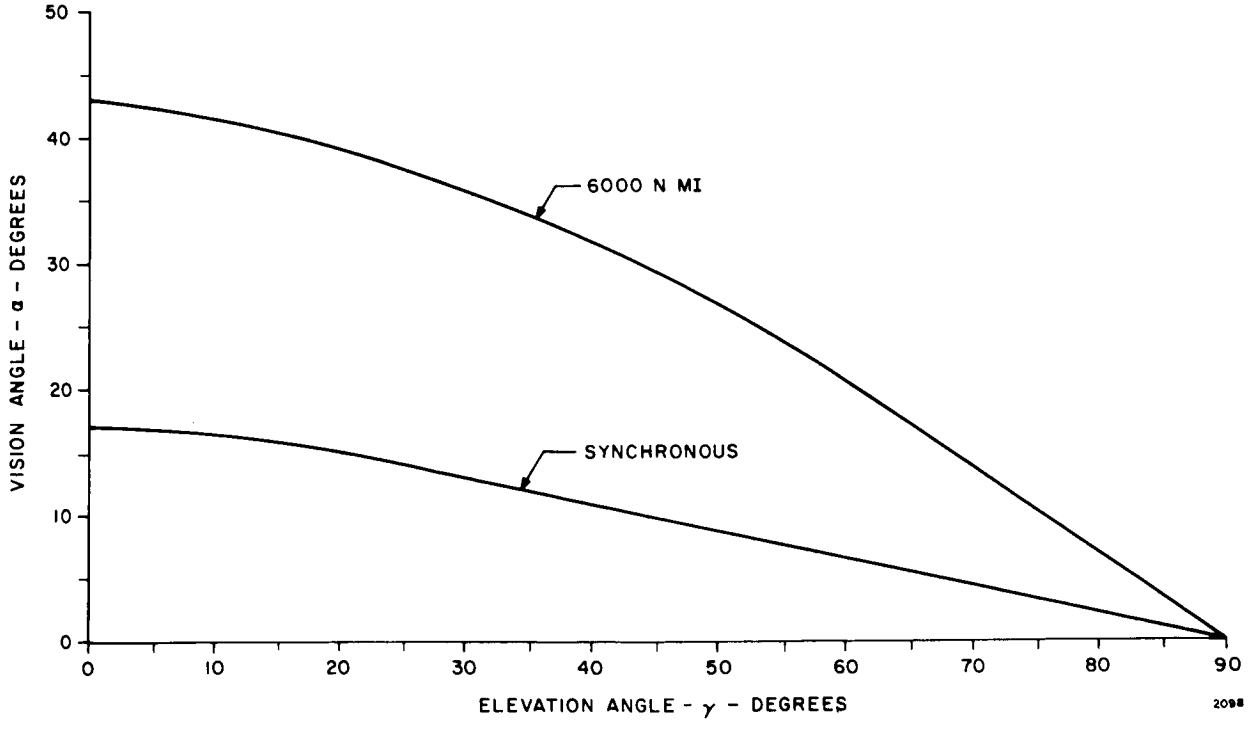

Figure No. VIII-7 Vision Angle vs Elevation Angle for 6000 nmi and Synchronous Altitude Satellites

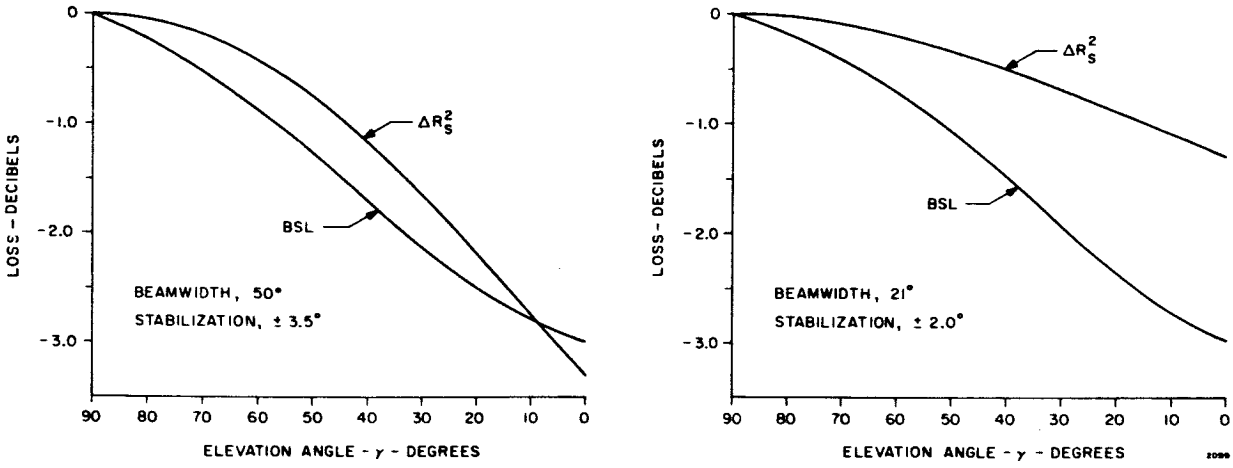

a. 6000 N. MILE SATELLITE

b. SYNCHRONOUS SATELLITE

Figure No. VIII-8 Satellite Antenna Beam Shape Loss and Differential Free Space Loss vs Elevation Angle

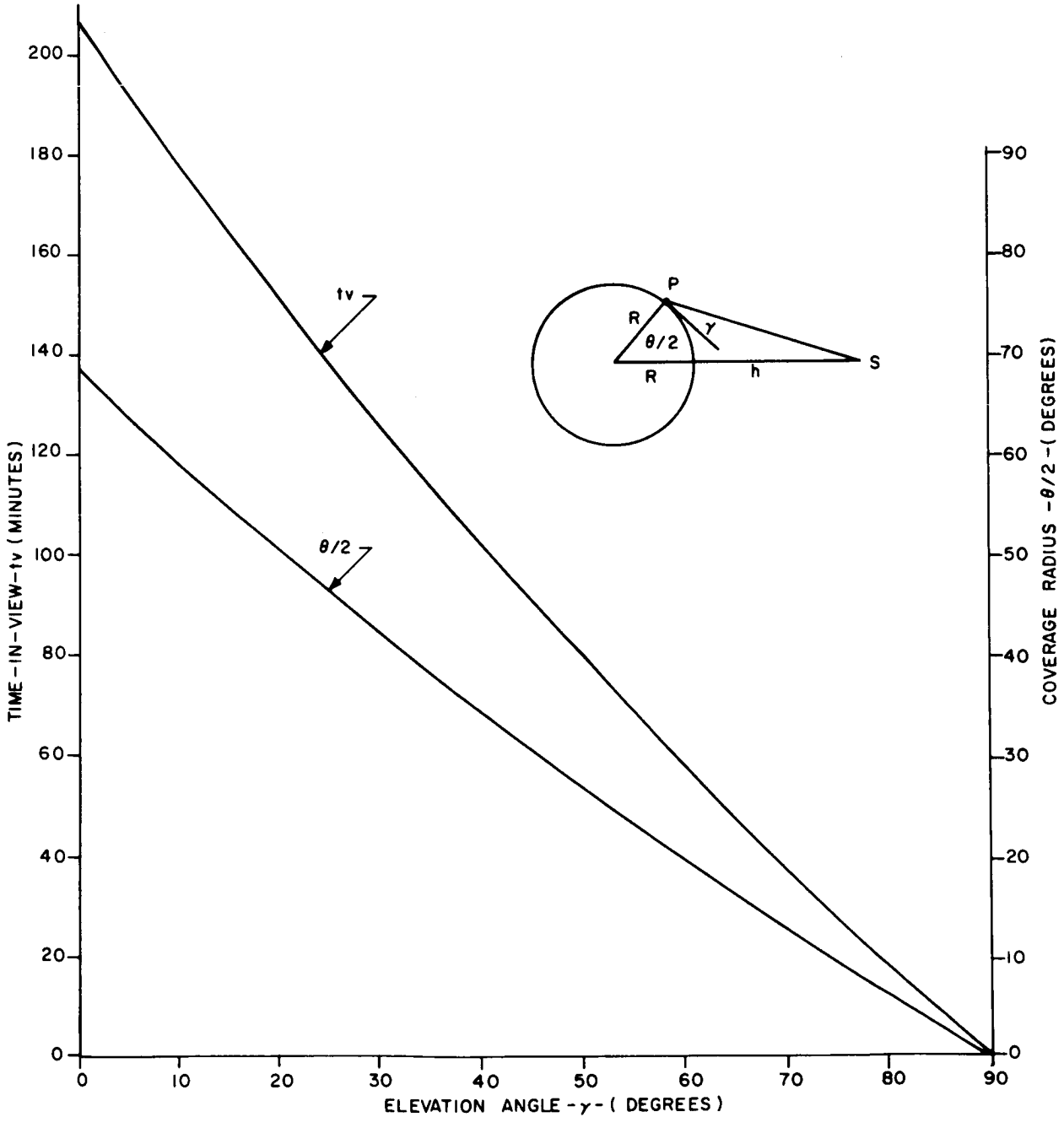

Figure No. VIII-9 Viewing Time and Coverage Radius vs Elevation Angle for 6000 nmi Satellite

APPENDIX IX

VIEWING TIME PROFILES FOR MEDIUM ALTITUDE SATELLITES

A one-year orbital mission profile for a 6180 nautical mile satellite was developed to: (1) estimate the number of satellite passes available to a ground station during any interval of time; (2) estimate the amount of viewing time per pass; and (3) estimate the total operational time on the satellite payload which is required to service all the ground stations during a given pass. This mission profile data is helpful in planning the data collection schedule for a one-year propagation program which must be compatible with the other missions of the ground stations and the other missions of the satellites. In general, the results show that the available viewing time is abundant, ranging from 35 passes (165-200 minutes per pass) every 13 days for Austin, Texas, to 31 passes (130-180 minutes per pass) every 13 days for Ottawa, Canada.

For convenience, a 6180 nautical mile satellite in a circular orbit inclined 28.5 degrees was chosen because it has an orbital period of 6.5 hours giving a 13 day cycle for which the orbit repeats itself in position and time of day. A homogenous spherical Earth was assumed with the nodal point regressing 97.5 degrees longitude with respect to the Earth's surface during each orbital period.

In 13 days, the satellite will have completed 48 orbits and, because of Earth's rotation, the satellite will have completed 35 passes over a given ground station. The viewing time for each pass was measured from 0° horizon to 0° horizon. For an overhead pass, 15 minutes are lost if the minimum useful horizon is increased to 5 degrees in elevation.

The viewing times were measured from zero degree elevation contours for the following ground station locations:

Los Angeles, California
Austin, Texas
Washington, D. C.
Boston, Massachusetts
Ottawa, Canada

These contours are similar to those shown in Figure 5-1, Section 5.1 for a 6000 n. mile satellite. The viewing time for Los Angeles was investigated in detail for the full 13-day-48 orbit cycle. A tabulation of results is given in Table IX-I. Upon completion of the orbital profile for Los Angeles, it was found that reasonable estimates can be made with 12 orbits instead of 48 orbits because of the cyclical manner in which the viewing time behaves. Furthermore, since the altitude of the satellite is so high, orbital coverage varies little for the ground station latitudes of interest. Ottawa (the most northerly location) was the only other location investigated. This gave the range in viewing time for the five ground station locations and an estimate of the total operational time on the satellite payload during each pass over all five stations. Table IX-II is the tabulation of results for 15 passes for a station near Ottawa, and finally, Table IX-III is the estimate of total payload operational time, 15 passes.

TABLE IX-I

ORBITAL MISSION PROFILE
for a
MEDIUM ALTITUDE SATELLITE
Station: Los Angeles, California

Station position: 33.9° N Latitude, 118.4° W Longitude

Satellite position: t = o, 28.5° N Latitude, 75.0° W Longitude

Orbital Pass	Start Time since t = o	Time Visible (min)	Cumulative Time (hrs.)
1	3h 55 m	185	3.1
2	16h 05 m	170	5.9
3	24h 13 m	192	9.1
4	1d 08h 30 m	180	12.1
5	1d 18h 30 m	185	15.2
6	2d 02h 43 m	182	18.2
7	2d 11h 20 m	175	21.1
8	2d 21h 05 m	190	24.3
9	3d 05h 18 m	185	27.4
10	3d 15h 25 m	168	30.1
11	3d 23h 35 m	193	33.4
12	4d 07h 55 m	178	36.4
13	4d 18h 05 m	175	39.3
14	5d 02h 09 m	191	42.5
15	5d 10h 38 m	165	45.2
16	5d 20h 33 m	182	48.3
17	6d 4h 23 m	187	51.4
18	6d 14h 43 m	165	54.1
19	6d 23h 00 m	195	57.4
20	7d 07h 20 m	180	60.4
21	7d 17h 30 m	173	63.3
22	8d 01h 33 m	195	66.5
23	8d 10h 00 m	170	69.3
24	8d 19h 58 m	182	72.4
25	9d 04h 07 m	187	75.5
26	9d 13h 58 m	170	78.3
27	9d 22h 24 m	194	81.6
28	10d 06h 45 m	180	84.6
29	10d 16h 56 m	170	87.4
30	11d 00h 55 m	195	90.6
31	11d 09h 23 m	170	93.5
32	11d 19h 23 m	182	96.5
33	12d 03h 22 m	198	99.8
34	12d 12h 43 m	190	103.0
35	12d 21h 48 m	180	106.0

TABLE IX-II

ORBITAL MISSION PROFILE
for a
MEDIUM ALTITUDE SATELLITE
Station: Ottawa, Canada

Station Position: 45.0 N Latitude, 75.0 W Longitude

Satellite Position: t = o, 28.5° N Latitude, 75.0° W Longitude

Orbital Pass	Start Time since t = o	Time Visible (min)	Cumulative Time (hrs.)
1	6h 32 m	155	2.6
2	17h 10 m	174	5.5
3	24h 55 m	180	8.5
4		0	8.5
5	1d 19h 32 m	178	11.5
6	2d 03h 24 m	176	14.4
7	2d 14h 24 m	150	16.9
8	2d 21h 55 m	182	19.9
9	3d 05h 54 m	161	22.6
10	3d 16h 40 m	170	25.4
11	4d 00h 20 m	182	28.5
12	4d 08h 58 m	40	29.1
13	4d 19h 00 m	176	32.1
14	5d 02h 28 m	176	35.0
15	5d 13h 56 m	138	37.3

TABLE IX-III

MAXIMUM PAYLOAD OPERATIONAL TIME
for a
MEDIUM ALTITUDE SATELLITE

Orbital Pass	Start Time since t = o	Operational Time (Min)	Cumulative Time (hrs.)
1	3h 55 m	210	3.5
2	16h 05 m	250	7.7
3	24h 13 m	240	11.7
4	1d 08h 30 m	190	14.8
5	1d 18h 30 m	240	18.8
6	2d 02h 43 m	220	22.5
7	2d 11h 20 m	340	28.2
8	2d 21h 05 m	240	32.2
9	3d 05h 18 m	210	35.7
10	3d 15h 25 m	250	39.8
11	3d 23h 35 m	240	43.8
12	4d 07h 55 m	190	47.0
13	4d 18h 05 m	240	51.0
14	5d 02h 09 m	220	54.7
15	5d 10h 38 m	340	60.3

BLANK PAGE

APPENDIX X

GAIN AND BEAMWIDTH OF MILLIMETER ANTENNAS

Figure No.

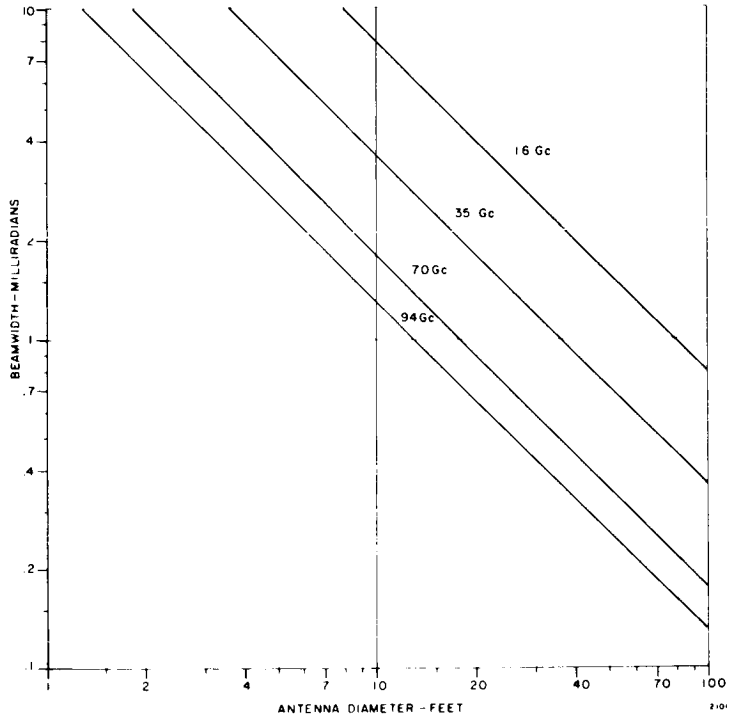

Figure No. X-1 Beamwidth vs Diameter for Large Millimeter Antennas

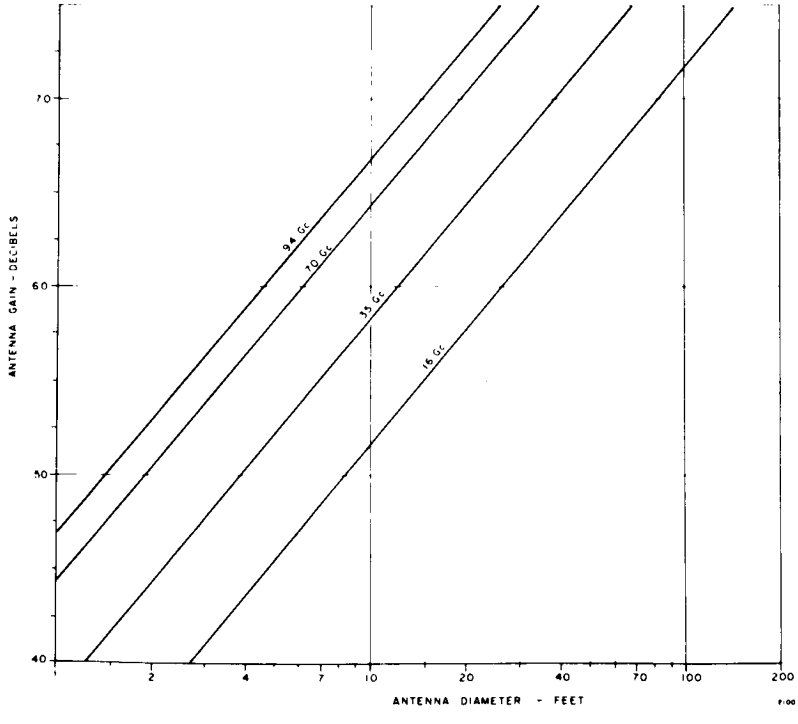

Figure No. X-2 Gain vs Diameter for Large Millimeter Antennas, Efficiency 55 Percent

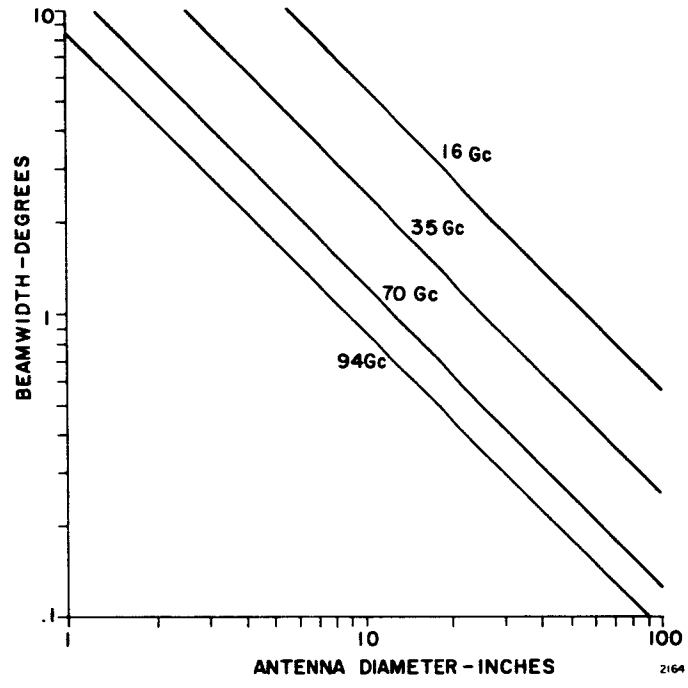

Figure No. X-3 Beamwidth vs Diameter for Small Millimeter Antennas

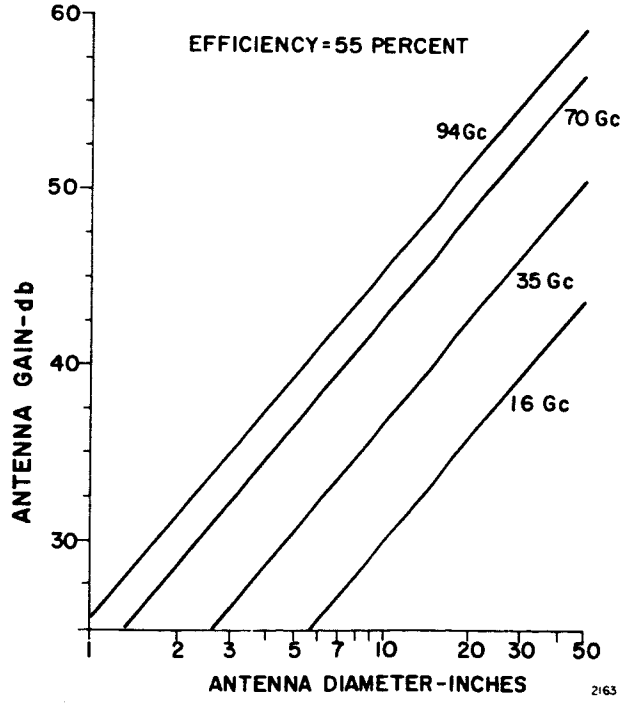

Figure No. X-4 Gain vs Diameter for Small Millimeter Antennas

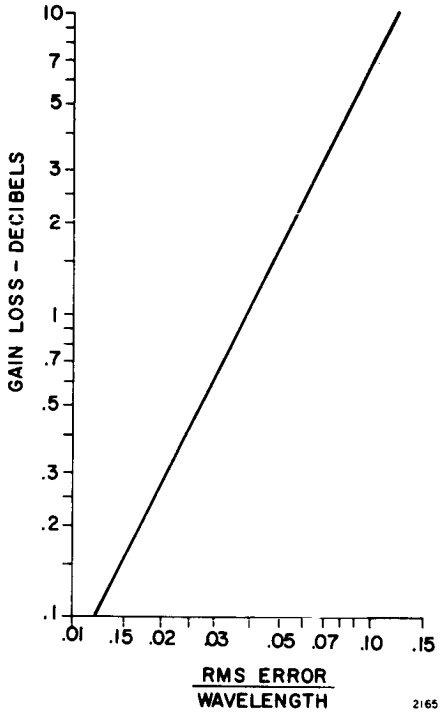

Figure No. X-5 Antenna Gain Loss vs Reflector Surface Errors